Molecular Dynamics Studies of the PKCα-C2 Domain Bound to Mixed Lipid Membranes

BY

Lalit Dubey

M.S. University of Illinois at Chicago, Chicago 2008

THESIS

Submitted as partial fulfillment of the requirements for
The degree of Doctor of Philosophy in Physics in the
Graduate College of the University of
Illinois at Chicago, 2015.

Chicago, Illinois

Defense Committee:

Mark L. Schlossman, Chair and Advisor
Anjum Ansari
Fatemeh Khalili-Araghi
Robert Klie
Wonhwa Cho, Chemistry

"Naïve realism leads to physics, and physics, if true, shows that naïve realism is false. Therefore naïve realism, if true, is false; therefore it is false."

Bertrand Russell

Dedicated to

little-little, prittle-prattle, hanky-panky and nitty-gritty

ACKNOWLEDGEMENTS

"The Moving fingers write, having writ moves on". I would like to thank my thesis advisor Prof. Mark L. Schlossman for his constant support, encouragement, inspiration and for challenging to come up with simulation results as good as experiments! I would like to express my gratitude to our collaborators, Prof. Emad Tajkhorshid and Dr. Y. Zenmei Ohkubo at Urbana campus for their guidance and help. In particular, Zenmei's help in running a simulation on Anton supercomputer is acknowledged. I would also like to express my thanks to my committee members, Prof. Anjum Ansari for introducing me to Biophysics, Prof. Fatemeh Khalili-Araghi for critically reading this thesis and Prof. Wonhwa Cho for insightful comments. I would also like to thank Prof. Robert Klie for agreeing to be in my thesis committee. I thank our group colleague Miroslav Mihaylov (Miro) for his indispensable help in maintaining the clusters and assembling a GPU workstation.

I also remember and acknowledge my not yet forgotten friends for being more than friends in my life.

My first thoughts go to my mother, father and brothers Anurag (zaydee), Vishnu (silbil) and sister Hema for their tireless support and faith on me. I express my deepest appreciation to my wife Prerna for letting me stick to Biophysics and helping and supporting me in all what matters in this world. I fondly remember my son Raghava (*little-little*) for at times plugging out laptop keys and pouring milk etc. on my stuff while he grows with and I continue to work on thesis projects. He and his younger sister Sonakshi (*prittle-prattle*) deserve a loving thank you for letting me do *my work, with my stuff* without bothering for any special attention.

TABLE OF CONTENTS

CHAPTER **PAGE**

TABLE OF CONTENTS (continued)

TABLE OF CONTENTS (continued)

LIST OF FIGURES

FIGURE **PAGE**

LIST OF FIGURES (continued)

LIST OF FIGURES (continued)

LIST OF FIGURES (continued)

LIST OF TABLES

TABLE **PAGE**

LIST OF ABBREVIATIONS

PKC	Protein Kinase C
cPKC	Conventional PKC
PKCα	Protein Kinase Cα
C1 (C1a and C1b)	PKC conserved domain 1
C2	PKC conserved domain 1
PKCα-C2	C2 domain of Protein Kinase Cα
PC	Phosphatidylcholine
PS	Phosphatidylserine
SOPC	1-stearoyl-2-oleoyl-sn-glycero-3-phospho choline
SOPS	1-stearoyl-2-oleoyl-sn-glycero-3-phosphoserine
POPC	1-palmitoyl-2-oleoyl-sn-glycero-3-phosphocholine
POPS	1-palmitoyl-2-oleoyl-sn-glycero-3-phosphoserine
DOPS	1,2-dioleoyl-sn-glycero-3-phospho-L-serine
DCPS	1,2-dicaproyl-sn-phosphatidyl-L-serine
DVPC	divalerylphosphatidylcholine
DVPS	divalerylphosphatidylserine

LIST OF ABBREVIATIONS (continued)

DAG	Diacylglycerol
PIP2	Phosphatidylinositol 4,5-biphosphate
DCE	1,1-dichloroethane
ATP	Adenosine Triphosphate
MD	Molecular Dynamics
HMMM model	Highly Mobile Membrane Mimetic model
FM model	Full Membrane model
NAMD	NAnoscale Molecular Dynamics
VMD	Visual Molecular Dynamics
GROMACS	GROningen MAchine for Chemical Simulations
CHARMM	Chemistry at HARvard Macromolecular Mechanics
CGenFF	CHARMM General Force Field
PBC	Periodic Boundary Conditions
PME	Particle Mesh Ewald
NMR	Nuclear Magnetic Resonance
EPR	Electron Paramagnetic Resonance

LIST OF ABBREVIATIONS (continued)

ATR-IR	Attenuated Total Reflection Infrared
LRC	Lysine Rich Cluster
CBLs	Calcium Binding Loops
COM	Center of Mass
GPU	Graphics Processing Unit

SUMMARY

Signal transduction is one of the key mechanisms through which living cells respond to extracellular as well as intracellular stimuli. Phosphorylation is an essential post translational mechanism through which proteins participate in signaling transduction pathways. Nearly 30% of cellular proteins undergo phosphorylation. Protein kinase (PK) enzymes catalyze phosphorylation in other cellular proteins. In particular, a subfamily of PKs, Protein Kinase C, are implicated in spatial aspects of the signal transduction network. Almost all of spatial signal transduction is mediated by PKCs. In order to perform their unique functions, PKCs localize to specific subcellular regions within cells. Their highly flexible regulatory C1 and C2 domains achieve this localization. Biophysical, biochemical, and crystallographic experiments, as well as computational studies, have addressed the subcellular localization and conformation of PKCs. In spite of several experimental studies to elucidate the membrane bound model of the C2 domain of PKCα (PKCα-C2 domain), there is no definitive view of the bound configuration.

In this thesis, classical Molecular dynamics (MD) simulations are used to study the membrane-bound configuration of PKCα-C2 domain to mixed lipid bilayer membranes composed of 7:3 phosphatidylcholine (PC) and phosphatidylserine (PS). MD simulations that utilized the highly mobile membrane mimetic (HMMM) model, which substitute short-tailed lipids and a region of organic solvent for the full-length 1-stearoyl-2-oleoyl-sn-glycero-3-phospho choline (SOPC) and 1-stearoyl-2-oleoyl-sn-glycero-3-phosphoserine (SOPS) lipids, were compared to long duration simulations that utilized SOPC and SOPS (denoted the Full Membrane, i.e., FM, model). The initial configuration for the simulations consisted of three different orientations guided by experimental results, with the PKCα-C2 domain positioned initially above the membrane, in the bulk water, such that protein-bound Ca^{2+} ions are 6 Å and 14 Å, respectively,

from the membrane surface for the FM and the HMMM models. Though the two lipid models are fundamentally different, they predicted similar membrane bound configurations for the PKCα-C2 domain when the area per lipid was 61 $Å^2$ and 81 $Å^2$ for the FM and HMMM models, respectively. Our results demonstrate that the PKCα-C2 domain has an electrostatic contribution to the membrane binding from residues R249 (in Ca^{2+} binding loop 3), K209 (located on β sheet 4) and bound Ca^{2+} ions. Hydrophobic interactions are also important as a result of membrane binding through consistent dynamical insertion of residue W247 up to the hydrophobic lipid core of the membrane. Moreover, the angle (θ_1, θ_2) which describes the orientation from the membrane normal, is ~ 90°, indicating that the PKCα-C2 domain's beta sheet structure is essentially parallel to the membrane.

We have proposed a membrane bound model of the PKCα-C2 domain whose key features are that residues R249 (from Ca^{2+} binding loop 3) and W247 penetrate into the membrane. Calcium ions bound to the protein are localized to within a mean value of ~ 5 Å from the PO_4^- or COO^- lipid headgroup moieties. The lysine rich cluster (LRC) along with residue K205 that joins strands β3 and β4 of the LRC play a defining role in the membrane bound configuration. Strands β3 and β4 are positioned in a nearly vertical plane, thereby creating an open-faced docking geometry that further exposes the OH-moiety of Y195 and the concave LRC region to binding with other membrane components. Our simulations suggest that larger headgroup lipids, such as phosphatidylinositol 4,5-biphosphate (PIP2) can bind to the LRC region, when PKCα-C2 is in the open-faced configuration, without altering the overall orientation of the protein. Moreover, we have demonstrated that the 3GPE crystal structure of PIP2 inositol ring bound to the lysine rich cluster of the PKCα-C2 domain is not stable in the arrangement suggested by crystallography studies.

Modification of the area per lipid from 81 $Å^2$ to 125 $Å^2$ produces a very different orientation of PKCα-C2 domain. In this case, HMMM model simulations show that the PKCα-C2 domain's β sheet structure is essentially perpendicular to the membrane surface. In this configuration, loop 1 penetrates most deeply into the membrane and residue K205 is far from the membrane with an orientation angle of ~ 30°. These results are consistent with published X-ray reflectivity studies. Our simulation results for different lipid densities may help to reconcile variations in the binding configuration of PKCα-C2 domain reported for different experimental studies.

1 INTRODUCTION

1.1 Background and Motivation

Extensive research is ongoing into the underlying pathways and mechanisms of cellular processes that affect normal physiological functions. This research can lead to therapeutic remedies for their impairment. Eukaryotic cells dynamically coordinate signaling networks of proteins through post-translational modification mechanisms (1). Within the area of signal transduction, protein phosphorylation is a critical part of post-translational modification (2). Reversible phosphorylation regulates many aspects of cell life including metabolism, growth, division, differentiation, motility, organelle trafficking, membrane transport, muscle contraction, immunity, and memory (2-5). Abnormal phosphorylation is a cause or consequence of many diseases like cancer, chronic inflammation, diabetes, rheumatoid arthritis, and stroke (3, 6, 7). Protein phosphorylation (or dephosphorylation) directly affects the function of proteins by enhancing or suppressing their activity, marking them for destruction, allowing them to move from one subcellular compartment to another, enabling protein-protein interactions, and activating or inhibiting enzymes, among other functions (3, 8, 9). It is estimated that 30% of cellular proteins are phosphorylated (10, 11).

Protein kinase enzymes modify other proteins by phosphorylation. Protein kinases catalyze the transfer of the γ-phosphate from adenosine triphosphate (ATP) to specific amino acids like serine (Ser), threonine (Thr) and tyrosine (Tyr) residues in eukaryotes.

Out of 518 human protein kinases, as recognized through their conserved sequence motifs, 478 protein kinases are typical kinases and 40 are atypical. Typical human protein kinases phosphorylate serine or threonine residues (388 kinases) or tyrosine residues (90 kinases) (5, 12). Atypical kinases lack sequence similarity to typical eukaryotic kinases, but still exhibit

biochemical kinase activity. More than 170 unique kinase domain structures from humans (or closely related orthologs) have been determined (13). Protein kinases are one of the largest families of genes in eukaryotes comprising ~ 2% of the human genome and mediate most of the signal transduction in eukaryotic cells (5).

Most eukaryotic protein kinases are structurally similar (14, 15) and share a common mechanism (2). Within all protein kinases, one group of the kinases, protein kinase C (PKC), within the AGC subfamily, (5), has been implicated in the spatial distribution of signals and essential control of higher-level signal organization (16).

The modular architectural structure of the PKC family consists of a conserved catalytic domain and a series of differentially activated regulatory domains (Figure 1A). Within classical kinases, the catalytic domain (~ 250 amino acid long) consists of a small N-terminal lobe of β-sheets and a larger C-terminal lobe of α-helices (2, 17-25). ATP binds in a cleft between the two lobes. When the protein substrate binds along the cleft, a set of conserved residues within the kinase catalytic domain catalyzes the transfer of the terminal γ-phosphate of ATP to the hydroxyl oxygen of the Ser, Thr or Tyr residue of the substrate (Figure 1B) (2).

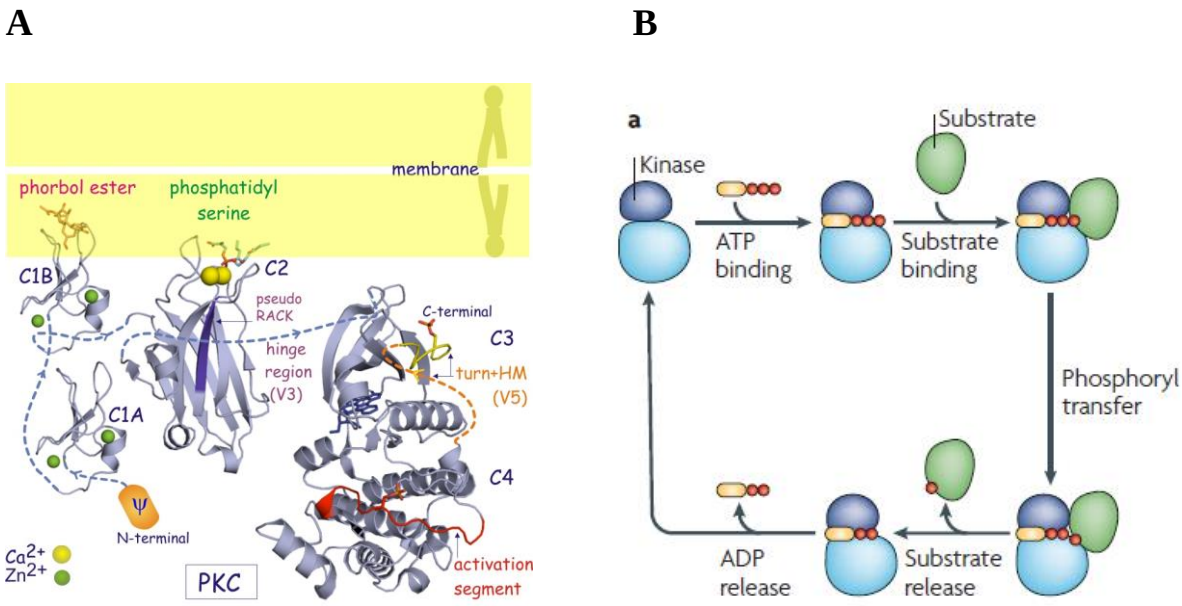

Figure 1: Protein Kinase common fold and mechanism
(A) **Structure of PKC**. Conventional (C2 domain of PKCα (PDB id: 1DSY) and novel (C1 (A+B) domain of PKCδ (PDB id: 1PTR and C3+4 domains of PKCθ (PDB id: 1XJD) isoforms are taken to represent full-length PKC. Regulatory domains, C1 and C2 bind diacylglycerol (or phorbol ester) and phospholipid respectively. C2 domain binding is reinforced by Ca^{2+}. Catalytic domains C3 and C4 are linked to C2 through a hinge region (V3). Adopted from (26).

(B): **Common mechanism of PKC**. Substrate phosphorylation process by a kinase. Beginning at top left and going clockwise, kinase active site is occupied by ATP followed by substrate. The phosphorylation occurs when a γ-phosphate of ATP (red) is transferred to a Ser, Thr or Tyr residue of the substrate. Once phosphorylated, kinase releases the substrate. In the last step, ADP is released from the active site. The order of steps differs for different kinases. For example, some kinases bind to their protein substrates before binding ATP and others release ADP before releasing the protein substrate. The rate-limiting step can also vary between different kinases. Adopted from (2).

The available flexibility of regulatory domains allows PKC activity to be applied with spatial and temporal specificity. This in turn allows PKC activity to be manipulated by membrane

limited secondary messengers, such as the interaction with cytoplasm-side membrane anchored small G-proteins, scaffolds and accessory proteins. As a result of this, the PKC family is centrally involved in the spatial control of signal transduction in cells (16).

Membrane anchoring of the regulatory C2 domain of the classical PKCα (Figure 1A) to the plasma membrane is a crucial event in the activation of PKCα and the subsequent signal cascade. The core issue investigated in this work is the interaction of the regulatory C2 domain of PKCα (PKCα-C2) with the plasma membrane in the presence of secondary messengers like calcium ions (Ca^{2+} ions) and phosphatidylinositol biphosphate (PIP2) through classical Molecular Dynamics (MD) simulations. The academic motivation to study the membrane bound configuration of the PKCα-C2 domain is that several experiments predict different membrane bound configurations of the PKCα-C2 domain, as summarized in Figure 2. We studied this system with MD simulations.

This thesis is arranged in five chapters. Chapter 1 provided background and motivation for this work. A brief description of the basic principles of MD and simulation methods is also included (Section 1.2). Chapter 2 describes the procedures used to model the membrane system and details of the systems simulated in this thesis. Chapter 3 describes the results of simulations on membrane bound configuration of PKCα-C2 domain in a mixed lipid bilayer environment. Along with various other factors, the area per lipid used were ~ 61 $Å^2$ and ~ 81 $Å^2$. Chapter 4 describes the membrane bound configuration of the protein when lipid density was changed to ~ 125 $Å^2$. Lastly, chapter 5 describes the effect of large headgroup lipid PIP2, on the membrane bound configuration of PKCα-C2 domain.

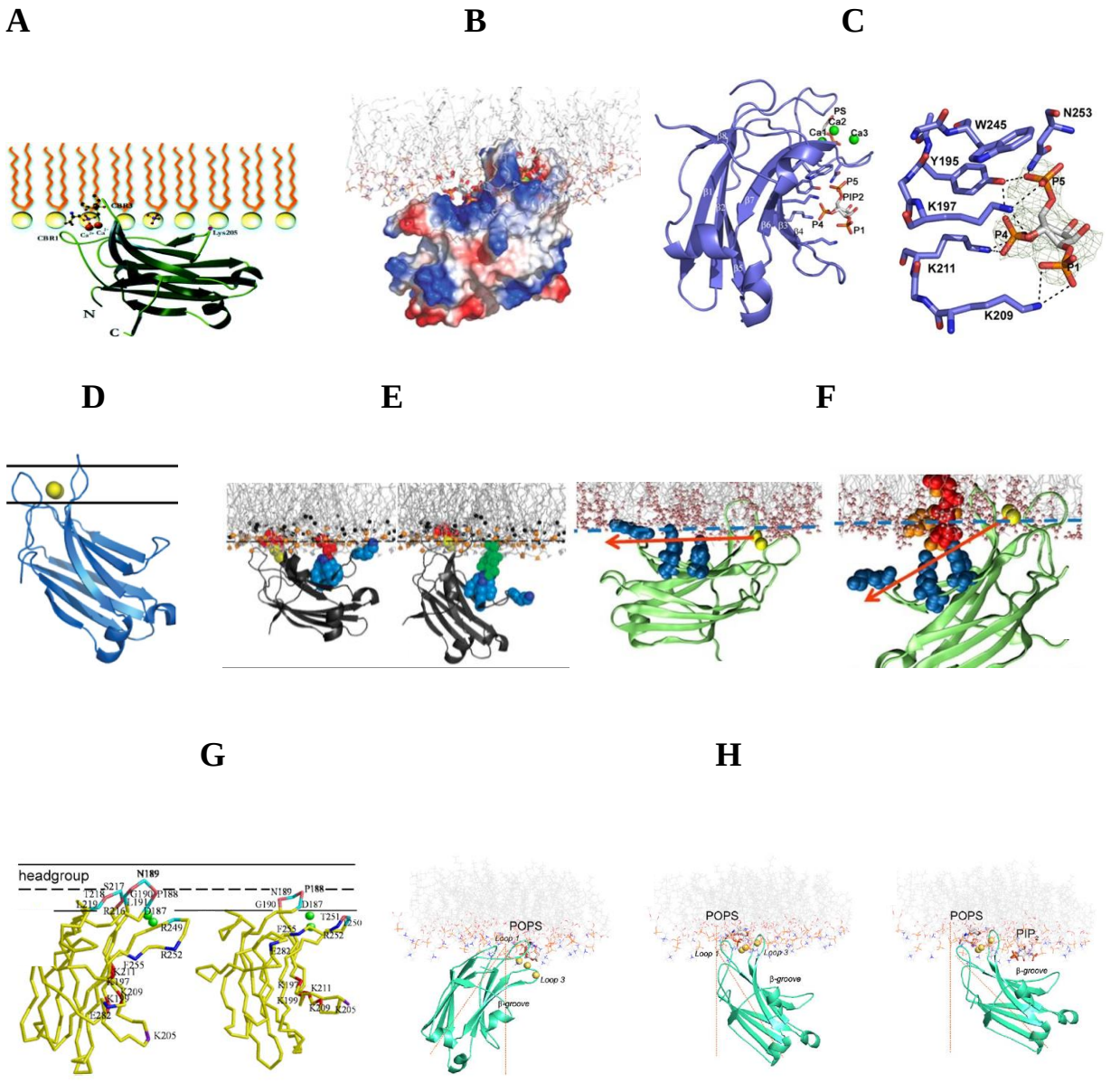

Figure 2: Experimental membrane bound configurations of PKCα-C2 domain The PC/ PS and/ or PIP2 membrane bound models as given by (A), (B) and (C) crystallography (23, 27); (D) and (E) electron paramagnetic resonance (28, 29); (F) MD simulations (30); (G) X-ray reflectivity (31) and (H) attenuated total internal reflection infra-red spectroscopy (32).

1.2 Fundamentals of Molecular Dynamics Simulations

Molecular simulations are computational tools to study the structure, function and dynamics of a physical system. Computer models mirroring real life have become crucial for many advances in the physical sciences. Molecular simulations have been used to study many different biological macromolecular systems (33-35). Molecular simulations require models of the atomic level details of the system components and their interactions. Traditionally, atomic details are obtained from experimental data such as nuclear magnetic resonance (NMR) or X-ray crystallography. The measured spatial arrangement of atoms within molecules, as stored in the protein data bank (www.rcsb.org), are often used as the initial configuration in simulations. In principle, interactions among various atoms in a system are governed by quantum mechanics but calculating such interactions is computationally too expensive. However, for large biological macromolecules, the atomic interactions can be approximated by force fields derived from classical mechanics as obtained through an empirical potential energy function. Using these basic inputs – the initial coordinates and the governing force fields for a biological system – simulations produce snapshots representing an atomic level model of the simulated system.

Molecular dynamics (MD) is a deterministic computational technique in which the time evolution of a system is calculated through numerical integration of the classical Newtonian equations of motion. Newton's 2nd law relates the force (F) on the i^{th} atom of mass m_i to the second derivative of its position r_i,

$$F = m_i \frac{d^2 r_i}{dt^2} = -\nabla V, \qquad (1.1)$$

Where the potential energy function V of the system is given by:

$$V = \sum_{bonds} \frac{k_i^b}{2} (l_i - l_i^{ref})^2 + \sum_{angles} \frac{k_i^a}{2} (\theta_i - \theta_i^{ref})^2 + \sum_{torsions} \frac{V_T}{2} [1 + \cos(n\phi - \gamma)]$$

$$+ \sum_{i=1}^{N-1} \sum_{j=i+1}^{N} \left[4\epsilon_{ij} \left[\left(\frac{\sigma_{ij}}{r_{ij}} \right)^{12} - \left(\frac{\sigma_{ij}}{r_{ij}} \right)^{6} \right] + \frac{q_i q_j}{4\epsilon_0 r_{ij}} \right] \quad (1.2)$$

The first three summations represent the potential energy of the covalently bonded geometry of atoms, viz., bonds between two adjacent atoms, angles formed by three consecutive atoms and dihedral angles of four consecutive atoms. The last summation represents non-bonded potential energy terms that include the Lennard-Jones potential to describe van der Waals and steric interactions, and Coulomb electrostatic interactions for charged particles. Within the Lennard-Jones potential, ϵ is the depth of the potential, σ is the distance at which the inter-particle potential is zero and r is the distance between the two particles. The point charge on each atom is represented by q in the Coulomb term.

Equation (1.1) is used to calculate the force on each particle of the system at a given time. Subsequently, numerical integration produces new positions and new velocities for each particle of the system. New forces are then calculated on each particle of the system in an iterative procedure. To accomplish this iterative protocol, a time integration algorithm is required.

The velocity Verlet integration algorithm is used to update the positions and the velocities of the atoms in time (36, 37). Updated coordinates and velocities are calculated from the current position using Δt as the time step and M is a mass matrix,

$$v_{n+\frac{1}{2}} = v_n + M^{-1} F_n \frac{\Delta t}{2} \quad (1.3)$$

$$r_{n+1} = r_n + v_{n+\frac{1}{2}} \Delta t \quad (1.4)$$

Now, compute

$$F_{n+1} = F(r_{n+1}), \tag{1.5}$$

$$v_{n+1} = v_{n+\frac{1}{2}} + M^{-1} F_{n+1} \frac{\Delta t}{2} \tag{1.6}$$

To start an MD simulation, along with assigning initial atomic coordinates, initial velocities must be assigned to each atom. This is achieved by random assignment of the velocities for each atom through a Maxwell-Boltzmann distribution at the desired temperature (38). In this thesis, MD simulations use the NAnoscale Molecular Dynamics (NAMD) engine (39) in which the required temperature control is implemented through a Langevin thermostat (40). An NPT thermodynamic ensemble (constant Number of particles (N), Pressure (P) and Temperature (T)), is used. Langevin temperature control is combined with pressure control which, in this case, is a modified Nosé-Hoover method where Langevin dynamics is used to control fluctuations in the barostat (41, 42). Furthermore, constant pressure simulations require periodic boundary conditions (PBC) because the pressure is controlled by dynamically adjusting the unit cell size and rescaling all atomic coordinates (except the coordinates of fixed atoms, if any) during the simulation.

Another crucial factor in MD simulations is the integration time step. The actual wall clock time length of a simulation depends upon the integration time step. The highest vibrational frequencies of the molecules ought to govern the integration time step that could be used in a simulation. Hydrogen bonded atomic vibrational frequencies are of the order of 10^{-14} s^{-1} and thus a simulation time step of 1 fs is perfect. However, constraining the hydrogen-oxygen and hydrogen-hydrogen bond lengths in water to a nominal length or angle through the implementation of the SETTLE algorithm (43) and further constraining the bond between hydrogen and the atom to which it is bonded through the SHAKE algorithm (44) creates an opportunity to increase the

integration time step up to 2 fs. Indeed, in all the simulations reported in this thesis, a time step of 2 fs is used.

Another scheme that is implemented in NAMD (39) to increase the speed of the simulations is to calculate the long range electrostatic interactions in Fourier space through the Particle Mesh Ewald (PME) summation (45). Also, a cutoff range modifies long-range van der Waals interactions represented by Lennard-Jones potentials since the magnitude of the interaction is effectively negligible at large distances. A cutoff of 10 - 12 Å is applied in our simulations.

The accuracy of MD simulation results is only as good as the force fields, the associated parameters (equation 1.2), and the efficient sampling of phase space. In general, the empirical potentials and parameters used in this thesis are from Chemistry at HARvard Macromolecular Mechanics (CHARMM) (46-49). We have performed several long simulations as well as short but repetitive simulations to account for efficient sampling of the phase space. A practical way to test the accuracy of the simulation results is to compare and validate a few physical properties of the system directly with experimental results, theoretical results and/or with previous simulation results. Indeed, in this thesis, we compare our simulation results with experimental, theoretical, and previous simulation results.

In general, in this thesis, MD trajectories are generated through NAMD (39) package. Several in house scripts and methods were used to model the systems and analyze the simulation results along with the use of Visual Molecular Dynamics (VMD) (50) and GROMACS (51) utilities.

2 MODELING of MIXED MEMBRANE SYSTEM

2.1 Introduction

Molecular dynamics (MD) simulations are used to investigate the membrane bound configuration of PKCα-C2 domain. This problem was originally motivated by recent X-ray reflectivity measurements on this system (31). First, we simulate an equilibrated lipid bilayer membrane, as described in this Chapter, then introduce the protein to simulate protein - membrane interactions, as described in later Chapters.

We study a mixed lipid bilayer consisting of 1-stearoyl-2-oleoyl-sn-glycero-3-phospho choline (SOPC) lipids and 1-stearoyl-2-oleoyl-sn-glycero-3-phosphoserine (SOPS) lipids in a 7:3 SOPC:SOPS molar ratio, which is a typical physiological concentration in the plasma membranes of living cells (52). To construct the bilayer, we need to decide upon a few vital physical characteristics of the mixed membrane like the area per lipid, the thickness (average distance between phosphorous atoms from both the monolayers) and the arrangement of the SOPS lipids within SOPC lipids. In order to simulate the bilayer in its liquid phase, the gel-to-liquid phase temperature needs to be estimated for the mixed bilayer. Unfortunately, there are no experimental values available for any of these characteristics for such a mixed lipid bilayer though there are experimental values available for single-component SOPC and SOPS lipid bilayer membranes.

For a pure SOPC lipid bilayer membrane, the area per lipid is shown to be 58 ± 2 Å^2 by Ly and co-authors (53) through elasticity measurements based upon surface pressure-area isotherms of SOPC membrane in water, 61.4 ± 0.2 Å^2 by Koenig and co-authors (54) through deuterium NMR measurements, and 51 ± 2 Å^2 by Israelachvili and co-authors (55). Moreover, Rawicz and co-authors (56) used x-ray diffraction to demonstrate a 40 Å width (peak to peak) for the thickness of SOPC membrane in aqueous solution with a deformable hydrocarbon core of 30 Å. Also,

Vilcheze and co-authors (57) showed that the gel-to-liquid temperature for SOPC lipid bilayer is 279 K.

For a pure SOPS lipid bilayer, a thickness of ~ 42 Å is obtained by Brzustowicz and co-authors (58) but no direct experimental values for area per lipid or gel-to-liquid transition temperature is available. However, it is known that 1,2-dioleoyl-*sn*-glycero-3-phospho-L-serine (DOPS) lipid which has two unsaturated bonds has a bilayer area per lipid of ~ 64 $Å^2$ (59). Since SOPS lipid contains only one unsaturated bond, the area per lipid is expected to be smaller. Also, it is worth noting that the gel-to-liquid temperature for 1-palmitoyl-2-oleoyl-*sn*-glycero-3-phosphoserine (POPS) is quoted to be 287 K (60).

Based upon these experimental results for the pure SOPC and SOPS lipid membranes, we decided to aim for an area per lipid of ~ 61 $Å^2$ for a mixed SOPC + SOPS membrane. Further, we decided to keep the membrane thickness at 40 Å for SOPC lipids and 42 Å for SOPS lipids while designing the mixed lipid bilayer membrane. Moreover, we (shall) perform the mixed membrane equilibration at the temperature of 300 K - 310 K that would maintain the mixed membrane in the liquid phase and also conforms to that of X-ray reflectivity experiment temperature.

2.2 Methods

First, we obtained the chemical structure of single SOPC and SOPS lipid molecules using SYBYL7.1 *(Tripos Inc., St. Louis, MO).* From individual residues of SOPC and SOPS (Figure 3), we constructed a mixed lipid bilayer.

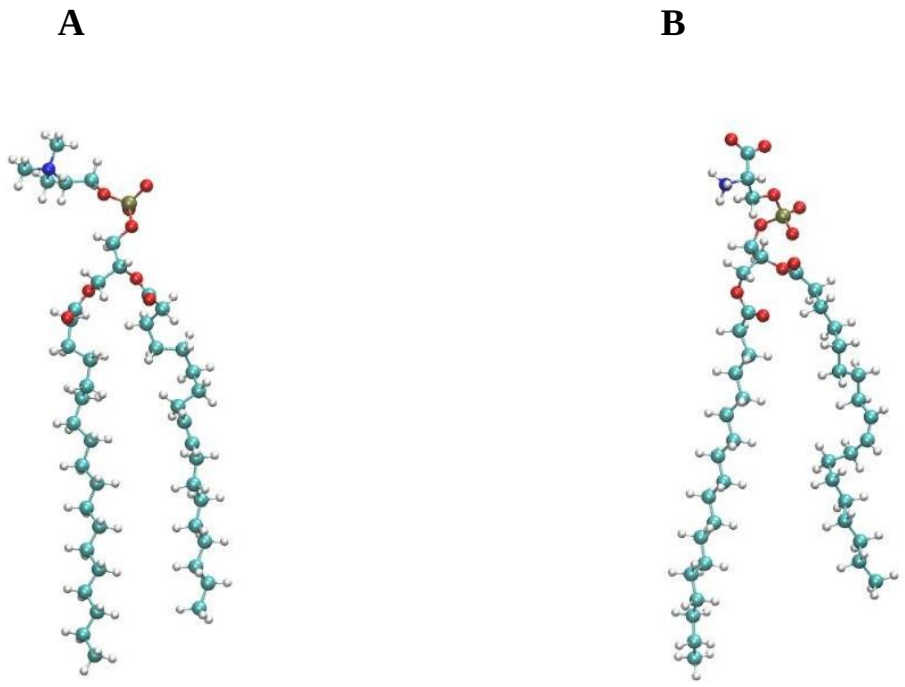

Figure 3: SOPC and SOPS lipids
(A) SOPC and (B) SOPS lipids generated by VMD (50). This is a CPK representation with color coding of the atoms: oxygen (red), nitrogen (blue), phosphorous (brown), carbon (cyan) and hydrogen (white).

Initially, say, in the top leaflet of the bilayer, 100 lipids are arranged in a square grid such that the distance between the phosphorous atoms of adjacent lipids is 8.2 Å. Moreover, SOPS lipids are not placed adjacent to each other to avoid local crowding that might have introduced PS spatial biasing. The bottom leaflet was prepared in a similar manner. Phosphorous atoms of SOPC or SOPS lipid pair(s) in the top and bottom leaflets are arranged such that the distance between them is 40 Å and 42 Å, respectively. With this, we added a water slab above and below the lattice-like arrangement of the mixed bilayer. Overlapping water molecules within 1.5 Å of lipid molecules were removed. Also, Na^+ and Cl^- ions were added using VMD to neutralize and produce a total concentration of 100 mL (50). The starting setup for the complete system is shown in (Figure 4A).

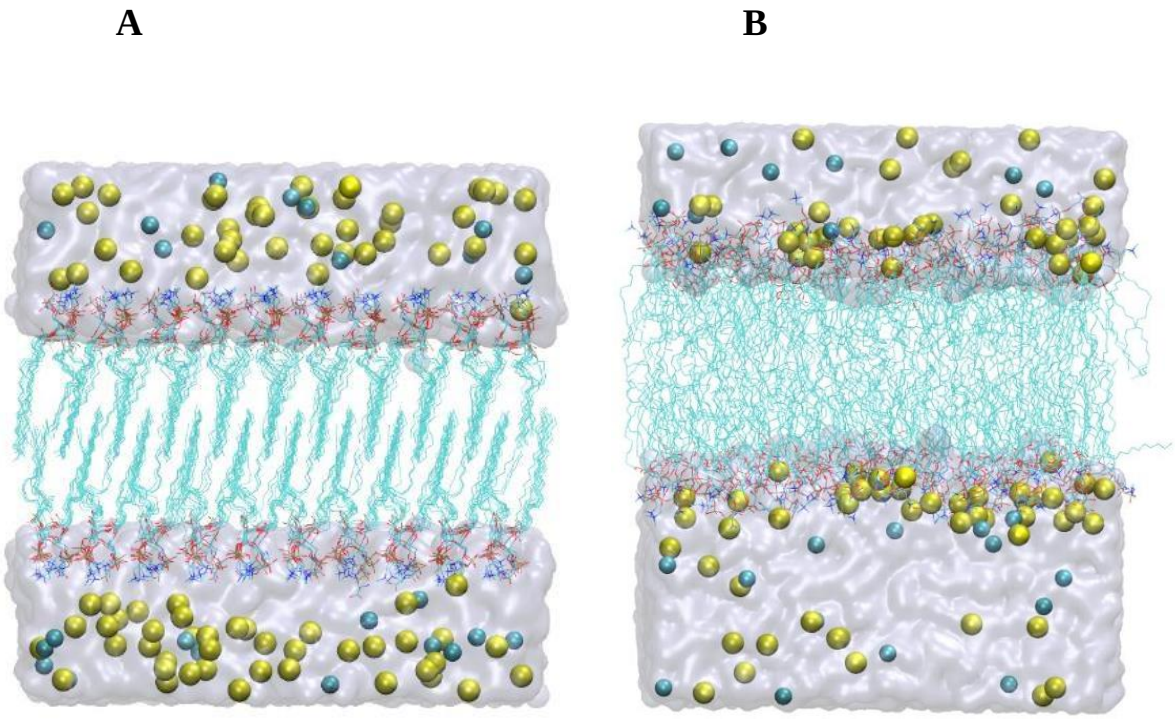

Figure 4: Initial and final mixed bilayer system
(A) Starting configuration and (B) equilibrated system. The lipids are shown as lines, ions are shown in color, Na^+ (cyan) and Cl^- (yellow). Water is shown in surface representation in ice blue color.

The number of carbon atoms and double bonds in the lipid acyl chains is denoted as, for example, SOPC (18:0/18:1). The notation in the bracket means that in the stearoyl sn-1 chain there are 18 carbon atoms and zero double bonds and in the oleate sn-2 chain there are 18 carbon atoms and one double bond. The topology for SOPC (18:0/18:1) and SOPS (18:0/18:1) is derived from 1-palmitoyl-2-oleoyl-sn-glycero-3-phosphocholine (POPC) (16:0/18:1) and POPS (16:0/18:1) respectively in CHARMM 36 (47) by adding two carbon atoms and associated hydrogen atoms to the last acyl chain atom denoted C316 (as represented in the CHARMM topology for POPC/ POPS). As no new atom type was needed, the adapted topology works fine with the standard parameter distribution of CHARMM36 (47).

2.2.1 Simulation Protocol

In general, NAMD (39) software is used to perform the simulations with the CHARMM36 force field parameter set (47) using TIP3P water model as implemented in CHARMM (61). Langevin dynamics with an appropriate damping coefficient, γ, and Langevin piston Nosé-Hoover methods (40, 42) were used to set the temperature as desired and the pressure (= 1 atm) of the system. Long range electrostatic forces were calculated with the Particle Mesh Ewald (PME) method (45) using a grid density of ~ 1 $Å^{-3}$. The van der Waals interaction cutoff was set to 10 Å. Bonded hydrogen atoms were kept rigid, allowing us to use an integration time step of 2 fs for bonded and non-bonded energy calculations.

Since we have simulated many systems under various conditions the simulation protocol for specific systems will be discussed in subsequent sections.

2.2.2 Equilibration of Mixed SOPC + SOPS Bilayer Membrane

The lattice-like bilayer shown in Figure 5A forms a 90 Å x 90 Å x 85 Å box. The objective is to mix SOPS lipids with SOPC lipids as randomly as possible. To achieve this, we treated the system through several steps described below. These include stretching the membrane and subsequently heating it.

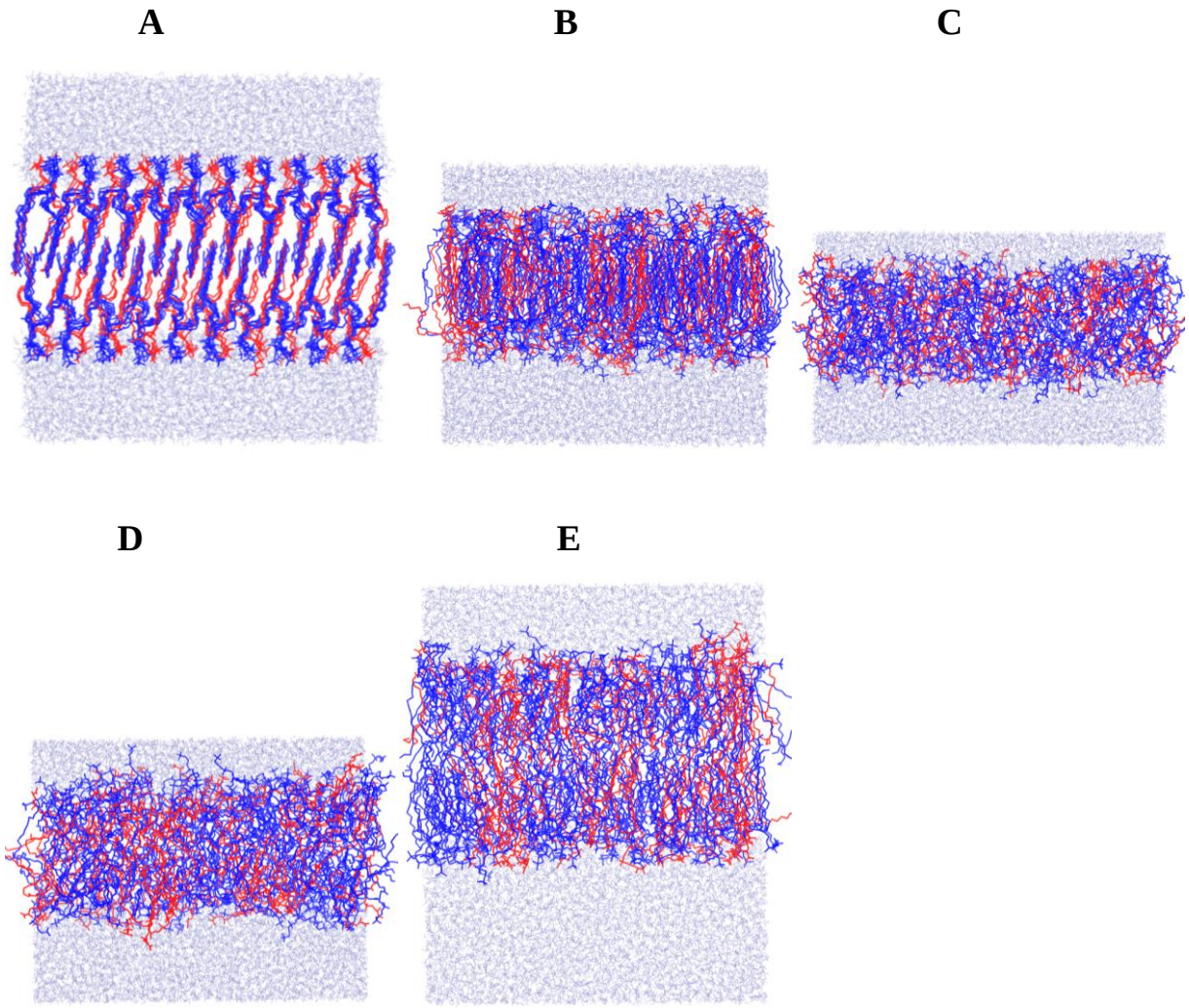

Figure 5: Simulation box size evolution with time
The time evolution of the mixing of SOPC + SOPS membrane is shown at various stages. (A) Initial state, (B) after 30 ns, (C) after 31 ns (i.e., 1 ns after (B), (D) after 35 ns, and (E) final equilibrated state. See text for details.

In **step 1**, we stretched the membrane by applying a surface tension of 50 mN m^{-1} in the *x-y* plane of the membrane. The Langevin damping coefficient, γ, is fixed at 1 ps^{-1}. The system is energy minimized by the conjugate gradient method for 10,000 steps (20 ps), then gradually heated from 10 K to 300 K by an incremental increase of 10 K within 500 steps each. Langevin dynamics is used to assign the temperature. 500 steps (NAMD integrator is implemented) were used to assign

and keep the temperature at (each temperature) rescaling by 10 K. In total 14500 steps (29 ps) were used to raise the temperature to 300 K. Finally, the equilibration continued for 30 ns, which produced a box size of ~ 99 Å x 82 Å x 70 Å (Figure 5B). The stretching changed the box size considerably, but as shown in the Figure 6B the lipids are barely mixed within the membrane.

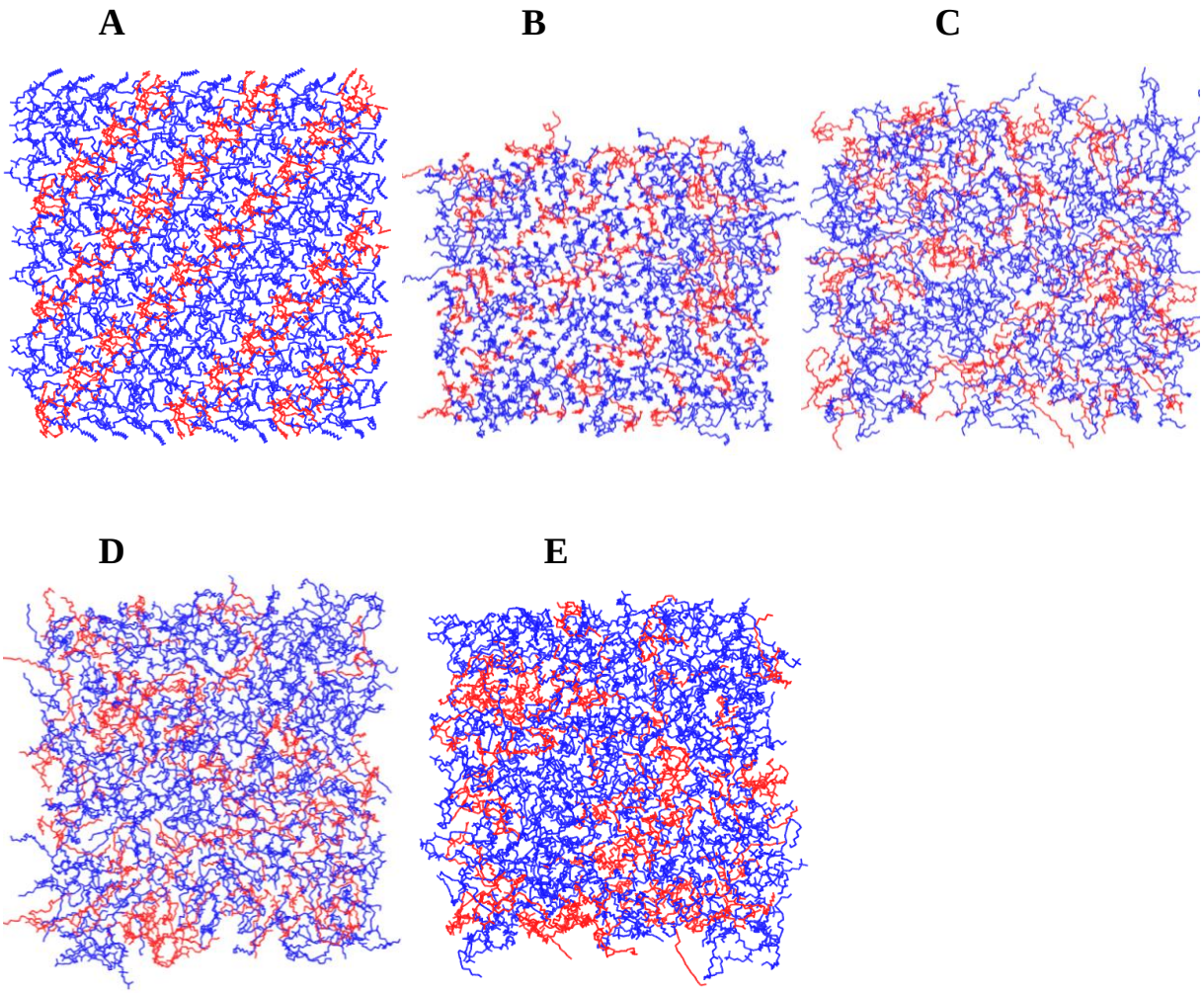

Figure 6: SOPS/SOPC lipid distribution
Top view of the time evolution of mixing of SOPS (red) lipids within SOPC (blue) lipids. (A) The initial arrangement of SOPC and SOPS lipids. (B) The lipid distribution at 30 ns (C) after 31 ns (D) after 35 ns and (E) final distribution.

To further mix the lipids (**step 2**), we applied a surface tension of 50 mN m^{-1} and raised the temperature from 300 K to 450 K directly by setting the Langevin thermostat to 450 K while changing the Langevin coefficient, γ, to 5 ps^{-1}. However, the surface tension force of 50 mN m^{-1} turned out to be too high. The membrane was disrupted. So, we changed the surface tension from 50 mN m^{-1} to 25 mN m^{-1} and kept other simulation conditions unchanged. We further ran the system for an additional 1 ns (i.e., total of 31 ns). The system reached the targeted temperature of 450 K and the membrane was not disrupted, though the box size became ~ 112 Å x 94 Å x 67 Å (Figure 5C). So, in **step 3**, while the temperature was 450 K, we changed γ from 5 ps^{-1} to 1 ps^{-1} and continued to run it for another 4 ns i.e., from 32 ns to 35 ns without any applied surface tension. Figure 5D and Figure 6D reveal that the membrane remains intact and SOPC and SOPS are mixed with a box size of ~ 94 Å x 102 Å x 73 Å. In **step 4**, the system is cooled to 300 K. For this, we changed γ to 5 ps^{-1} and applied a surface tension of 10 mN m^{-1} to control membrane shrinkage. Energy minimization was carried out for 10,000 steps (20 ps), then the temperature was lowered in 5 K steps within 100,000 simulation steps (0.2 ns) each, e.g., the system was taken from 450 K to 445 K in 100,000 steps. So, to reach the targeted temperature 300 K, we needed to run the system for a total of 3,000,000 steps (6 ns i.e., from 36 ns to 41 ns). The system was allowed to equilibrate for an additional 1 ns (i.e., total of 42 ns) at 300 K. The box size after this step was ~ 79 Å x 79 Å x 95 Å. Once the temperature stabilized near 300 K, we removed the surface tension of 10 mN m^{-1} (**step 5**) and continued to equilibrate for another 4 ns (i.e., from 43 ns to 46 ns), thereby achieving a box size of ~ 78 Å x 78 Å x 96 Å (Figure 5E). Figure 4B and Figure 6E illustrate that this final equilibrated mixed membrane system is intact and mixed.

2.3 Results

In order to establish that the obtained mixed membrane system is well behaved, Figure 7A shows the time variation of the total energy, electrostatic energy and van der Waals energy from step 5 (see above). Also, the temperature profile of the bilayer system is shown in Figure 7B.

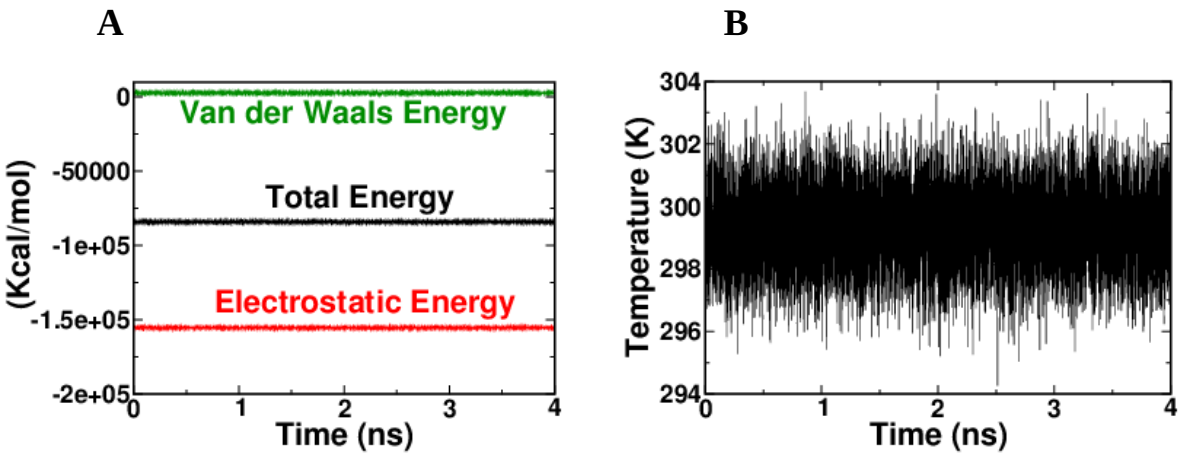

Figure 7: Energies and temperature profile of the bilayer system
Time variation of the (A) energy and (B) temperature for the equilibrated bilayer.

2.4 Area per lipid

Our objective was to obtain a mixed membrane bilayer with an area per lipid of ~ 61 Å^2. A simple way to define the area per lipid is to divide the *x-y* plane surface area of the membrane by the number of the lipids in a monolayer. In our case, the number of lipids in a monolayer is one hundred. Figure 8 shows the area per lipid evolution of our membrane bilayer system. The equilibration of the mixed SOPC + SOPS lipid bilayer membrane was stopped once the area per lipid reached the target value of ~ 61 Å^2.

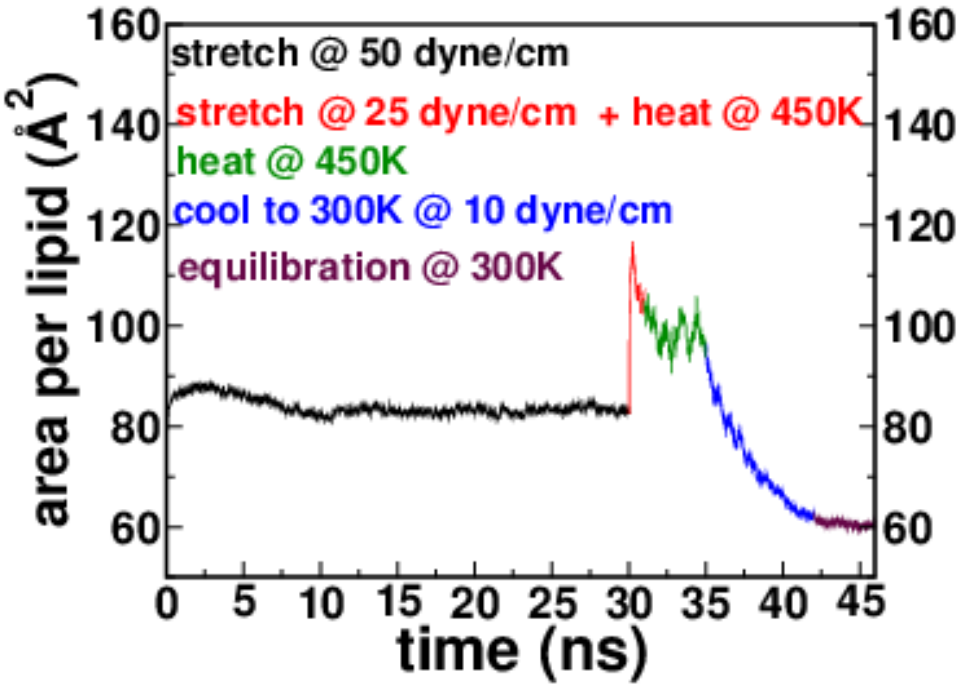

Figure 8: Evolution of area per lipid of bilayer
Complete evolution of the area per lipid during the bilayer membrane preparation steps 1-5 described in Section 2.2.2.

2.4.1 Order Parameter

The acyl chain order parameter is a physical criterion that can show whether membrane is in a liquid, gel, or solid phase i.e., it tells us about the fluidity of the membrane tails (62). The acyl chain order parameter is defined as,

$$S_{CD} = \frac{1}{2} \langle 3\cos^2(\theta_i) - 1 \rangle, \qquad (2.1)$$

Where θ_i is the angle between the vector formed by carbon atoms $C_{(i+1)}$ and $C_{(i-1)}$ from the acyl chain and the membrane normal. In general, when $S_{CD} = 1$, the tails are aligned parallel to the membrane normal (i.e., perpendicular to the membrane), when $S_{CD} = -0.5$, the tails are aligned perpendicular to the membrane normal, and $S_{CD} = 0$ describes random orientation of the acyl

chains. The angular bracket <·····> denotes an ensemble or a time average. Figure 9 shows the order parameter of each sn-1 and sn-2 acyl chains of the individual SOPC and SOPS components of the bilayer membrane. As S_{CD} is below 0.25, one can readily see that the membrane is in a liquid phase with disordered chains.

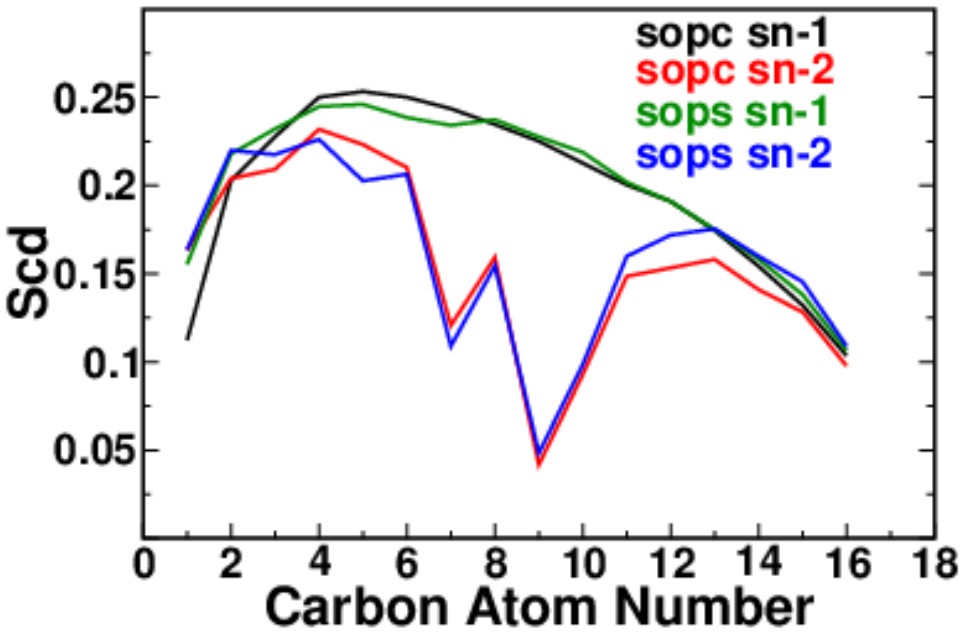

Figure 9: Acyl chain order parameter of mixed bilayer membrane
The order parameter for the two chains of SOPC and SOPS component of the mixed bilayer membrane is shown here.

2.4.2 Density Profile and the Thickness of the mixed membrane

We calculated the mass density as well as the electron density profile of the mixed membrane. Figure 10A shows the mass density and Figure 10B shows the electron density for the mixed bilayer membrane. Further Figure 10C shows the electron density for several components of the mixed membrane.

The membrane thickness is defined as the peak to peak distance for SOPC + SOPS components (green plot in Figure 10B) which in this case is ~ 32.76 Å.

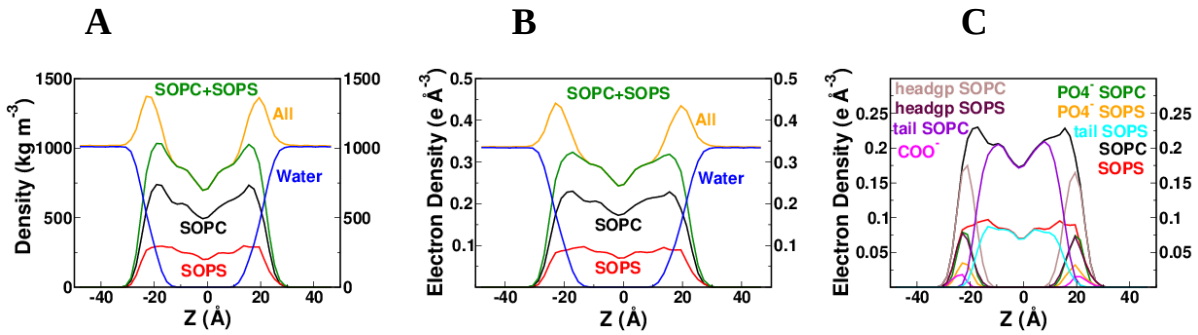

Figure 10: Density profiles of the mixed bilayer membrane
(A) Mass density (B) electron density for 5 components and (C) electron density for 9 components of the mixed membrane.

2.5 Protein Addition to the Mixed Membrane Bilayer System(s)

This mixed lipid bilayer membrane will be subsequently referred to as the Full Membrane (FM) system to distinguish it from the Highly Mobile Membrane Mimetic (HMMM) model described later (63). Our next objective is to add the protein and create a membrane + protein system for computational studies. Our objective is to study the mixed membrane bound configuration of peripheral proteins like PKCα-C2 domain under various conditions. The detailed study of these systems will be presented in the following chapters.

3 MEMBRANE BOUND CONFIGURATION OF PKCα-C2 DOMAIN

3.1 Introduction

Protein kinases are enzymes that transfer a phosphate group from a donor, such as ATP, to a substrate (2, 3, 5, 64, 65). Metabolic and structural changes occur as a result of phosphorylation, which influences numerous functions of the cell, including signal transduction, cell growth, cell division, cell differentiation, cell migration, organelle trafficking, ion channel activity and synaptic activity (2, 5, 66-69). Protein Kinase C (PKC) isozymes, also known as serine/ threonine kinases because they phosphorylate the hydroxyl group of serine/threonine, belong to the AGC (from PKA, PKG, PKC) family of protein kinases, which share certain structural features (5, 70). Among 10 mammalian isozymes of PKC, PKCα is commonly known as a conventional PKC (cPKC) (71, 72). PKCα consists of a highly conserved catalytic domain (C-terminal) and a regulatory domain (N-terminal). In addition to an autoinhibitory pseudosubstrate (73), the regulatory domain has two membrane targeting domains. One is a small 50 residue long globular C1 domain (C1a and C1b) which is sensitive to diacylglycerol (DAG)/ phorbol esters. The other part, which we investigate in this thesis, is called the C2 domain. It is an approximately 140 amino acid tertiary structure containing 8 anti-parallel β-sheets connected by loops (Figure 11).

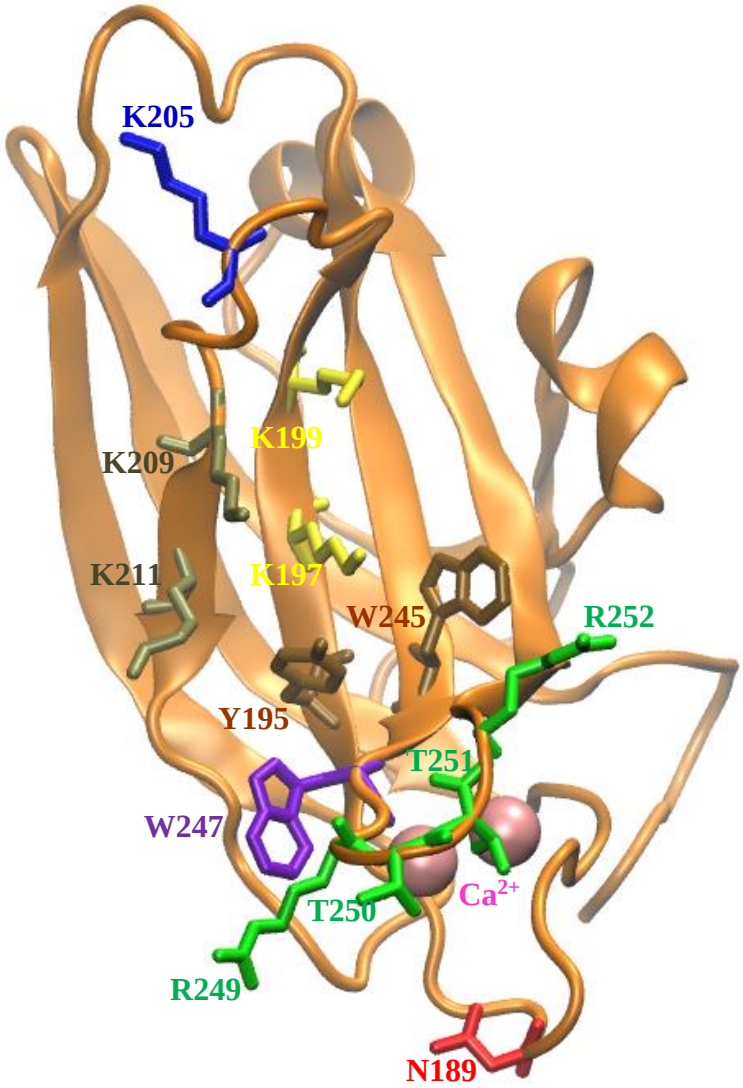

Figure 11: PKCα-C2 domain
Eight critical domain-parts of the PKCα-C2 domain loop1 (N189, red), loop3 (R249, T250, T251, R252, green), strand β3 (K197, K199, yellow), β4 (K209, K211, brown), K205 (blue), Ca^{2+} ions (pink), hpb-2resi (Y195, W245, maroon) and W247 (violet) are shown in licorice representation.

In the conventional scheme of PKCα activation, extracellular signals trigger the hydrolysis of phosphatidylinositol 4,5-biphosphate (PIP2) that produces diacylglycerol (DAG) and inositol 1,4,5-trisphosphate, which in turn, releases Ca^{2+} ions from intracellular stores (74). In the presence

of excess cytosolic Ca^{2+} ions two or three Ca^{2+} ions bind to the three calcium binding loops (CBL1, CBL2 and CBL3) on one end of the C2 domain (23, 27, 75) (Figure 11). Calcium binding drives the PKCα-C2 domain to the membrane (16, 70, 76), where it recognizes phosphatidylserine (PS) (23, 77-81) and PIP2 on the membrane surface (82-86) through interactions with the calcium binding loop regions and the lysine rich cluster (LRC) (74). Once C2 domain binding is achieved, the C1a domain binds to DAG (87, 88), which produces a conformational change in the protein that releases the pseudosubstrate to activate PKCα (16, 70, 76, 87, 89). The initial anchoring and subsequent localization of the C2 domain at the membrane surface is a vital step in the process of PKCα activation (87, 89).

Determination of the membrane bound configuration of PKCα-C2 domain has engaged numerous authors (23, 27-32, 75, 77-86, 90-98). Verdaguer and co-authors suggested that the ternary complex crystal structure of PKCα-C2 in the presence of Ca^{2+} ions and short chain 1,2-dicaproyl-sn-phosphatidyl-L-serine (DCPS) (PKCα-C2 - Ca^{2+} - DCPS) shows that C2 domain-membrane binding is a result of direct bridging of a Ca^{2+} ion to a PS membrane lipid (23). Subsequently, Guerrero-Valero and co-authors, suggested that a quaternary complex crystal structure of PKCα-C2 in the presence of Ca^{2+}, 1,2-dihexanoyl-sn-glycero-3-[phosphor-L-serine], and 1,2-diayl-sn-glycero-3-[phosphor inositol-4,5-biphosphate] (PKCα-C2 - Ca^{2+} - PS – PIP2) shows that PIP2 binds to the LRC region and PS to the CBL region (27). They showed that mutating the hydrophobic residues Y195 and W245, as well as two lysines K209 and K211, eliminated the neuronal differentiation capabilities of the PKCα-C2 domain, even in the presence of excess Ca^{2+} ions and DAG, implying that PIP2 binding to the second site is biologically important even if Ca^{2+} binding to PS is available (27, 71, 89).

Medkova and Cho (95) used mutational studies to demonstrate the importance of hydrophobic interactions in C2 domain binding. Scott and co-authors (99) argued that although hydrophobic interactions play a dominant role in C2 domain binding, electrostatic interactions are dominant in the retention of C2 domains on the membrane. Both of these studies suggested that hydrophobic residues, like W245 and W247, which are situated on CBL3 could penetrate into the membrane. This view of hydrophobic interactions is complementary to domain binding that relies upon electrostatic interactions between Ca^{2+} ions (bound to CBLs) and the negatively charged PS, as well as interactions between LRC strands β3 (K197, K199), β4 (K209, K211) and PS/PIP2 lipids. Other studies have explored the electrostatically driven membrane recruitment of C2 domains (100-102). A recent enzymatic activity study by Egea-Jimenez and co-authors (103) showed that in the presence of 5 mol% of PIP2, the full-length PKCα reaches its full activation strength even in the absence of DAG and low concentration of cytoplasmic Ca^{2+} ions. In the case of isolated PKCα-C2 domain, it has been shown that the presence of PIP2 reduces the concentration of Ca^{2+} ions required for membrane binding (84, 104). These results indicate that the binding of C2 domain to PS and PIP2 plays a defining role in PKCα activation. Simulations of the bound configuration of PKCα-C2 domain to the PC + PS mixed membrane with and without PIP2 can enhance our understanding of the membrane binding of PKCα-C2 and its role in the activation of PKCα.

Biophysical studies have not provided a definitive view of the bound configuration of PKCα-C2. In a 3:1 molar ratio PC:PS lipid vesicles, Electron Paramagnetic Resonance (EPR) experiments showed that the longest strand β2 makes an angle of 68° ± 7° (28, 91) with the membrane normal. More recent EPR measurements show that this angle is 90° for a 2:1 PC:PS ratio (29). X-ray reflectivity demonstrated that the same angle is 35° ± 10° while in a 7:3 molar

ratio PC:PS lipid monolayer (31). In 3:1 PC:PS liposomes, Attenuated Total Reflection Infrared (ATR-IR) experiments showed that it is 51° ± 4° (32). In 2:1 PC:PS lipid vesicles, an EPR study reported that R249 from CBL3 penetrates deepest into the membrane while two bound Ca^{2+} ions remained at -3 ± 3 Å and -5 ± 3 Å from the average position of phosphorus in the lipid head group (29). X-ray reflectivity experiments reported that N189 from CBL1 penetrates deepest into the membrane with a penetration depth of 7.5 ± 2 Å for the C2 domain (31). It is not yet clear whether these different results are due to different preparation conditions or some other aspect of the experiments.

Additional inconsistencies exist within the range of experiments reporting the effect of PIP2 on the orientation of membrane bound C2 domain. EPR experiments reported that PIP2 (2 %) binding to the LRC of the PKCα-C2 domain alters the orientation of the C2 domain from 90° from the membrane normal to 50° ± 10° (29). However, ATR-IR experiments (32) suggest that 5% PIP2 brings the domain closer to the membrane surface, from ~ 51° without PIP2 to ~ 60° with PIP2. Furthermore, EPR measurements, combined with molecular dynamics simulations (30) showed that the C2 domain β-sheet structure lies parallel to a 1:1 molar ratio PC:PS membrane without PIP2. Binding of the C2 domain to a single PIP2 leads to a tilt of ~ 60° from the membrane normal. Binding of a second PIP2 to the same domain reduces the tilt further, to ~ 53°.

Previous MD studies (30, 93) were restricted in their scope. Although MD simulations can test if the protein domain can attain an equilibrium bound configuration starting from an arbitrary unbound configuration, the two simulations in the literature were restricted to testing the stability of a given bound configuration. For example, the binding stability of the crystal structure model (23) was tested by 10 ns MD simulations (93) and the binding stability of the EPR model (29) was

tested in a 30 ns MD simulation (30). Spontaneous binding of the PKCα-C2 domain to the membrane and subsequent equilibrium were not observed in these simulations.

In this thesis, MD simulations are used to probe the binding of PKCα-C2 domain to a mixed PC:PS lipid membrane, with and without PIP2, as well as its subsequent equilibration to a dynamically stable bound configuration. This chapter discusses simulations of the PC + PS membrane system that include long-duration (500 ns) conventional full membrane (FM) model simulations as well as simulations using a recently proposed Highly Mobile Membrane Mimetic (HMMM) model (63). Different starting orientations of the protein were chosen, but the final bound configuration of the protein was similar for both long-duration (500 ns) FM and shorter duration (80 ns) HMMM models. Moreover, the role of bound Ca^{2+} ions was probed by simulations of the PKCα-C2 domain in bulk water, with and without bound Ca^{2+} ions and an HMMM model simulation where we removed the bound Ca^{2+} ions. Furthermore, the effect of different lipid densities on C2 domain binding is investigated within the HMMM model in Chapter 4. The role of PIP2 in the membrane binding of the C2 domain is explored through three long-duration (one 700 ns and two 200 ns each) FM model PC + PS + PIP2 membrane systems in Chapter 5. **TABLE 1** summarizes all of the FM/ HMMM systems (with the nomenclature for the systems used) reported in this study.

TABLE 1 Simulated Systems
HMMM and FM model systems along with respective area per lipid (A_L), damping coefficient (γ), temperature and run time. For FM model systems, temperature was increased to 310 °C and γ was changed to 0.5 ps^{-1} after 300 ns run time. LA denotes Large Area, per denotes perpendicular, tilt denotes tilted, noCAL denotes without calcium. NA denotes not applicable.

Model System	**A_L(Å^2)**	**γ (ps^{-1})**	**Temperature (°)**	**Run Time (ns)**	**# of runs**
HMMM Model Systems - Name					
per1, per2, tilt	81	0.5	310	80	5
LA_per1	125	0.5	310	80	4
LA_per2, LA_tilt (Chapter 4)	125	0.5	310	40	4
Full Membrane Model System					
per1_FM	61	1	300	500	1
per2_FM	61	1	300	500	1
tilt_FM	61	1	300	500	1
PKCα-C2 in Water					
w/ and w/o Ca^{2+} ions	NA	0.5	300	50	1
noCAL per1	81	0.5	310	80	1
pip2_systems					
Sim1	61	0.5	310	700	1
Sim2 and Sim3 (Chapter 5)	61	0.5	310	200	1

3.2 Methods

The atomic coordinates of PKCα-C2 domain were taken as provided by Chen et al. (31), who described the domain sequence of the purified protein as composed of $M^{152}DHH^{155}$ (additional residues from purification protocol), T^{156} to N^{287} (from crystal structure (23) Protein Data Bank ID: 1DSY) and $L^{288}EHHHHHH^{295}$ (additional residues from purification protocol).

The FM and the HMMM model systems are described below in Sections 3.2.1 and 3.2.2. Initial orientations of the C2 domain in the MD simulations of the PC + PS membrane system were taken from experiments, but the protein domain was positioned in the bulk water with protein-bound Ca^{2+} ions at least 6 Å and 14 Å away from the membrane's negative moieties (PO_4^-/ COO^- moieties), respectively, for the FM model and the HMMM model (Figure 12 and Figure 18). This initial configuration separates the protein-bound Ca^{2+} ions from their location in the membrane previously determined by experiments, thus allowing the simulations to follow the binding of the protein to the membrane. Two orientations taken from X-ray reflectivity measurements (31) are referred to as perpendicular 1 (abbreviated as per1) ($\theta = 35^\circ$, $\varphi = 210^\circ$)**,** perpendicular 2 (abbreviated as per2) ($\theta = 35^\circ$, $\varphi = 0^\circ$) and one orientation from EPR measurements (28) is referred to as tilted (abbreviated as tilt) ($\theta = 68^\circ$, $\varphi = 300^\circ$), where (θ, φ) were described in (31). The initial orientations are nearly the same as those shown in Figure 12 and Figure 18.

3.2.1 FM Model Simulations

The protein - membrane system is fabricated by taking only the equilibrated membrane patch from the last frame of the SOPC + SOPS lipids simulation (step 5 described in Section 2.2.2) and adding the protein domain, water and a new set of counterions. The protein domain is positioned above the equilibrated membrane in one of three orientations (per1, per2, or tilt) with

the bound Ca^{2+} ions at least 6 Å from the PO_4^-/ COO^- headgroup moieties of the membrane lipids creating three FM model systems, viz., per1_FM, per2_FM and tilt_FM (Figure 12).

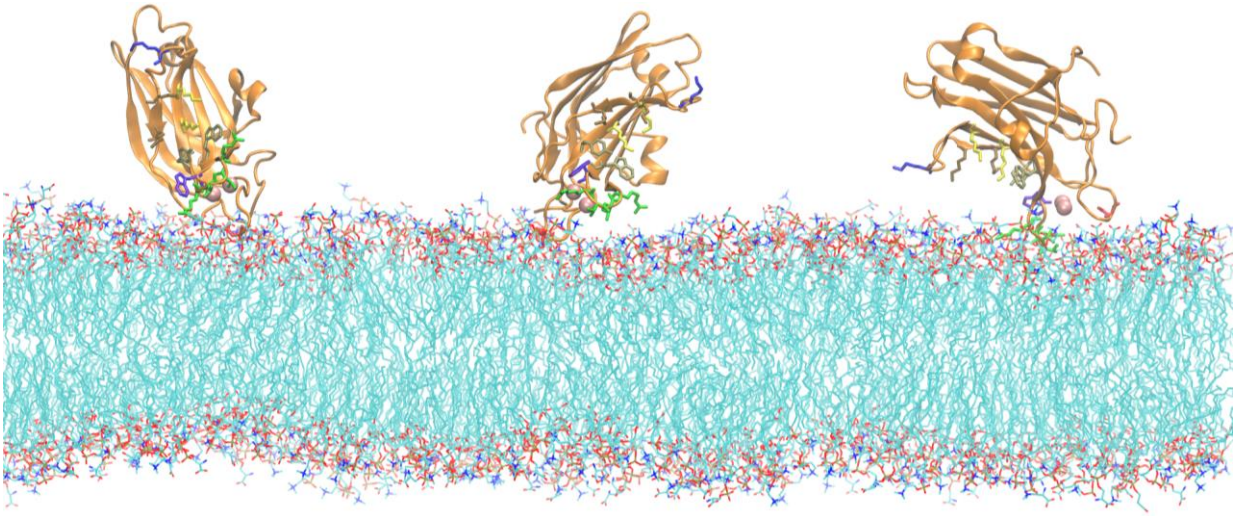

Figure 12: FM model initial state at 50 ps
From left to right: per1_FM, per_FM and tilt_FM. Color code for the protein and its residues is same as that in Figure 11. Water and ions are not shown for clarity.

VMD is used to add water and K^+ Cl^- ions to neutralize as well as achieve a 100 mM electrolyte concentration (50). Water molecules located within 1.4 Å of the C2 domain, which overlap the domain, were removed. Layers of water, ~ 20 Å thick, are located at the top and bottom of the simulation cell to avoid image interactions from neighboring cells that could arise due to our use of periodic boundary conditions. The simulation cell consisted of ~ 82000 atoms with a dimension of ~ 73 x 76 x 120 $Å^3$. Harmonic constraints with a force constant, k = 2 kcal·mol^{-1}·$Å^{-2}$, were applied to the Cα atoms of the C2 domain and to the bound Ca^{2+} ions while the whole system was energy minimized for 60,000 steps (120 ps) at a target pressure of 1 atm. The temperature was

gradually increased to 300 K under constant area ratio for 4 ns. During this equilibration the area per lipid, calculated as *x* times *y* dimensions of the simulation cell divided by the number of lipids in a leaflet (100), attained a value of ~ 61 Å^2 (Figure 13).

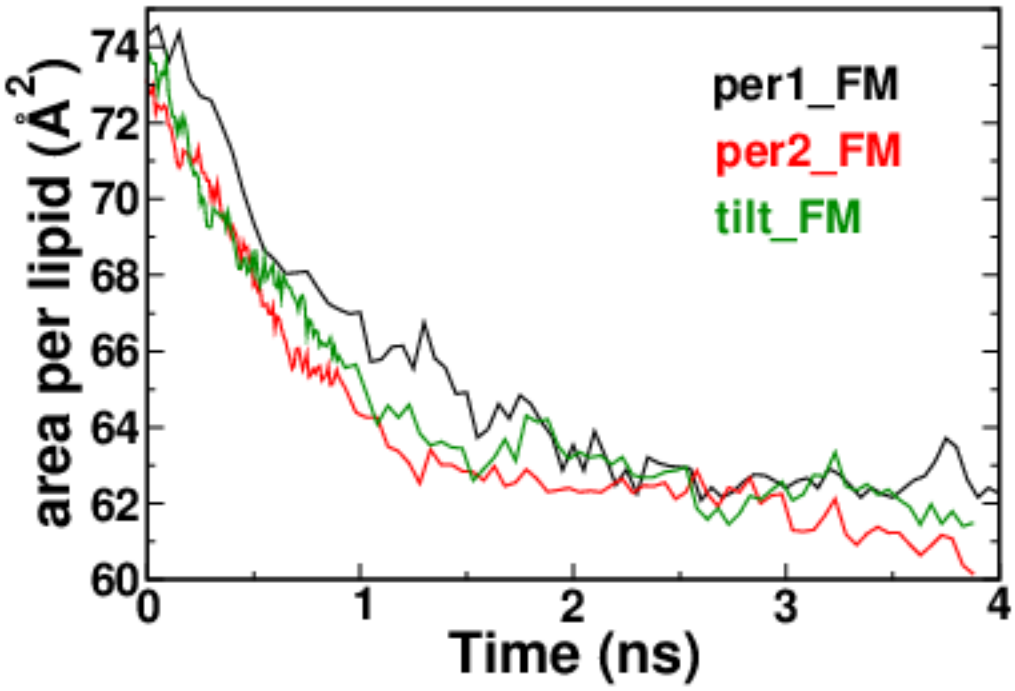

Figure 13: Area per lipid for FM model systems
Each of the FM model system has attained the area per lipid of ~ 61 Å^2.

Subsequently, the cell area was fixed and all three FM model systems were further equilibrated for 10 ns. Figure 14 shows the energy components; Figure 15 shows the temperature stabilization; Figure 16 shows the chain order parameter; and Figure 17 shows the mass density and the electron density profiles of the FM model systems. These figures show that all three systems are equilibrated equivalent systems. Finally, the harmonic constraints on the PKCα-C2 domain were removed and simulations proceeded for 500 ns for per1_FM, per2_FM and tilt_FM systems.

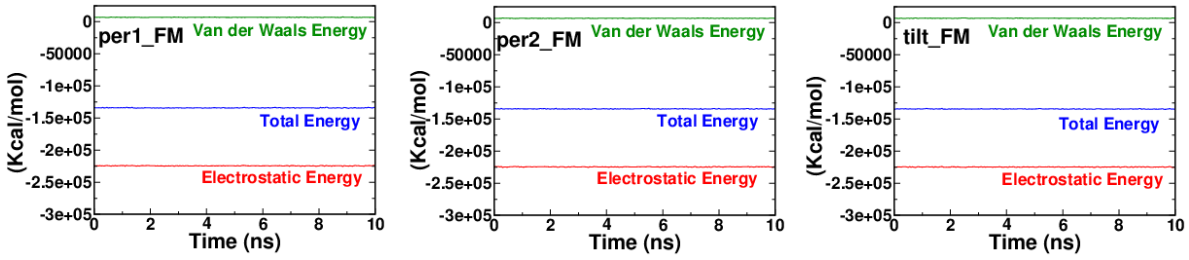

Figure 14: Energy components for FM model systems
Left to right: per1_FM, per_FM, and tilt_FM. The equilibrated systems show conserved energy components for the system.

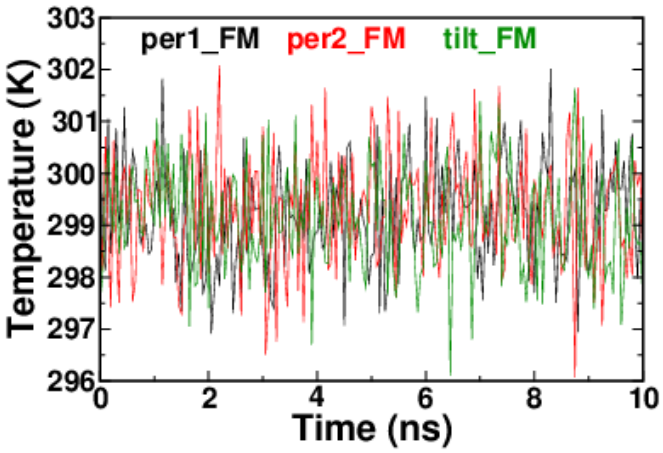

Figure 15: Temperature for FM model systems
All FM model systems attained s steady temperature.

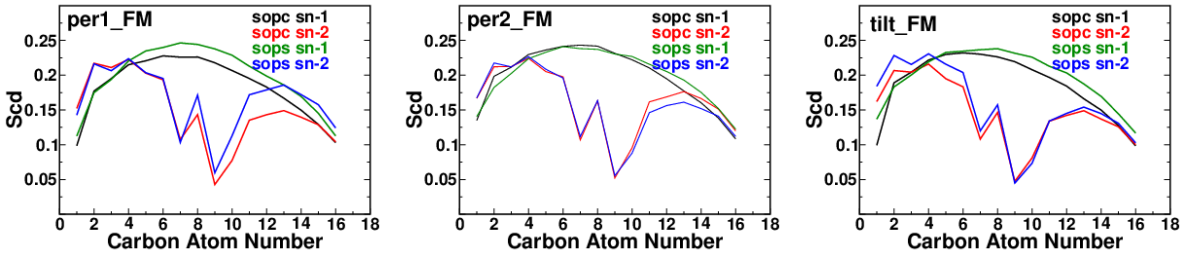

Figure 16: Acyl chain order parameter for FM model systems
All FM model systems are effectively equivalent.

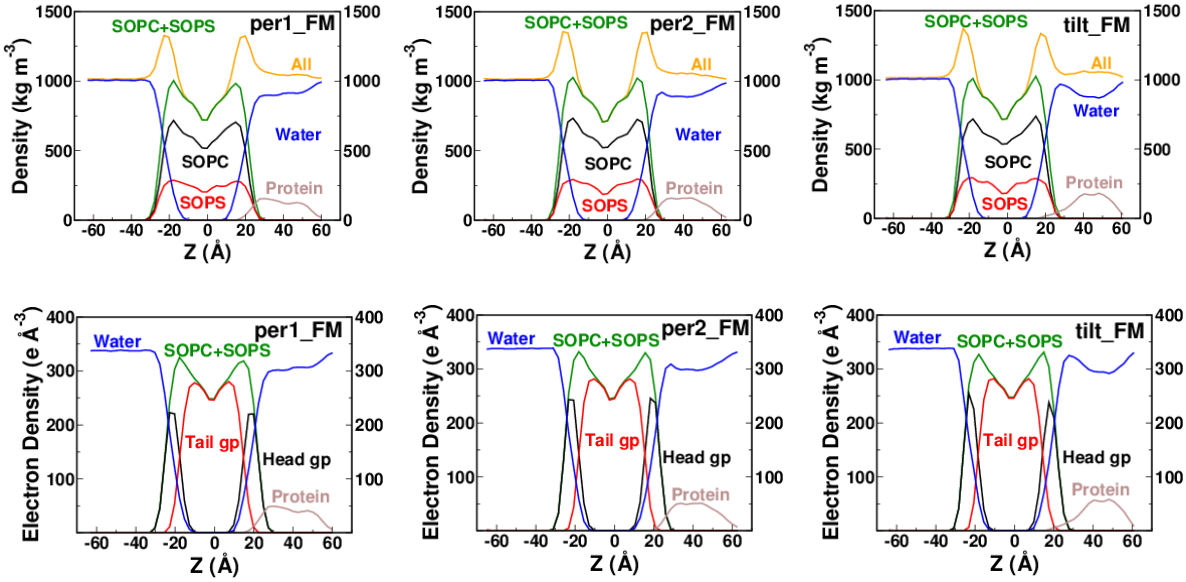

Figure 17: Mass and electron density profiles for FM model systems
Mass density (top row) and electron density (bottom row) profiles for FM model systems calculated just before the start of the production run.

3.2.2 HMMM Model Simulations

The HMMM model uses a combination of two monolayers of short-chain lipids that sandwich a layer of a small molecule solvent (1,1-dichloroethane) to mimic a bilayer consisting of two layers of long-chain lipids (63). HMMM equilibrates much faster than the FM model. Comparison of results from the two models may provide insight into equilibration of the FM model, as well as the applicability of the HMMM model. A mixed lipid HMMM model was constructed by randomly mixing 30 divalerylphosphatidylserine (DVPS) lipids (containing two –$(CH_2)_4CH_3$ chains) and 70 divalerylphosphatidylcholine (DVPC) lipids within a leaflet to achieve the same PC:PS ratio used in the FM model. Since there is no experimental data available for the area per lipid for such a mixed lipids membrane, in HMMM model systems a larger area per lipid was chosen to be ~ 81 $Å^2$ to further accelerate the domain - membrane equilibration process (63, 105) and to investigate non-systematically the effect of lipid packing on protein binding. This is done in a more controlled way later when the HMMM system is also used for studies of a second lower lipid density. Three systems were prepared with the initial orientations discussed previously (per1, per2 and tilt, see Figure 18). The PKCα-C2 domain was positioned with its bound Ca^{2+} ions at least 14 Å from PO_4^-/ COO^- headgroup moieties of the membrane lipids. VMD (50) was used to solvate the HMMM model systems in water and to add K^+ and Cl^- ions to neutralize the system and achieve a 100 mM electrolyte concentration. Water molecules located within 1.2 Å of the domain were removed. The HMMM simulation cell consisted of ~ 98,000 atoms. Each HMMM modeled system was energy minimized for 10,000 steps (20 ps) with a target pressure of 1 atm and a gradual increase in the temperature to 310 K during which the membrane area in the *x-y* plane was kept constant while Cα atoms of the PKCα-C2 domain and bound Ca^{2+} ions were harmonically constrained with a force constant of k = 2 kcal·mol^{-1}·$Å^{-2}$. A further constrained

simulation of 100,000 steps (0.2 ns) occurred after this. Subsequently, all constraints on the PKCα-C2 domain were removed and five simulations for each of the per1, per2 and tilt systems were performed for 80 ns apiece.

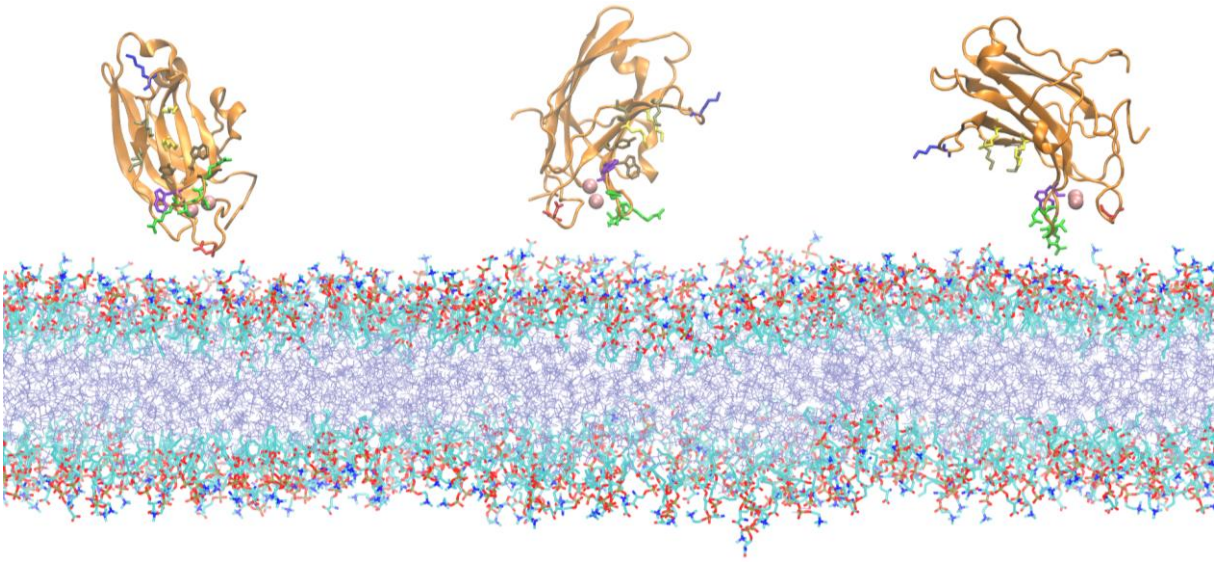

Figure 18: FM model initial state at 50 ps
From left to right: per1, per2 and tilt. Inner core of the HMMM model system as represented by 1,1-dichloroethane (DCE) is shown in ice blue color. Color code for the protein and its residues is same as that in Figure 11. Water and ions are not shown for clarity.

3.2.3 PKCα-C2 in Bulk Water with and without Bound Ca^{2+} Ions

Two simulations of an isolated PKCα-C2 domain in bulk water were carried out for 50 ns apiece. In one case the bound Ca^{2+} ions were kept intact within the CBLs of the C2 domain. In the other simulation the bound Ca^{2+} ions were removed. Using VMD (50) the C2 domains were solvated in a water box with a free water layer of at least ~ 20 Å all around. Ions (K^+ and Cl^-) were added to neutralize the system and to produce 100 mM overall salt concentration. The simulation cell contained ~ 49,000 atoms. Initially, Cα atoms and bound Ca^{2+} ions (where applicable) were

constrained with a force constant of k = 2 kcal·mol^{-1}·Å^{-2} and the systems were energy minimized for 10,000 steps with a target pressure of 1 atm and a gradual increase in the temperature up to 300 K. The constrained systems were further simulated for 1 ns. Subsequently, the constraints were removed to simulate the systems for 50 ns each.

3.2.4 HMMM Model + PKCα-C2 Domain without Bound Ca^{2+} Ions

Another system was prepared and simulated in order to further explore the role of the bound Ca^{2+} ions to the PKCα-C2 domain. We took a per1 system (based upon the HMMM model) and then just removed the bound Ca^{2+} ions (abbreviated as noCAL_per1). Further, the noCAL_per1 system was energy minimized for 10,000 steps, the temperature was set to 310 K, the pressure was set to 1 atm, and Cα atom constrained simulation was done for 100,000 steps. Eventually, an unconstrained production run of 80 ns was performed.

3.2.5 Simulation Protocol

NAMD2 (39) was used for all simulations on a home-built GPU workstation and on a Beowulf cluster. CHARMM36 force field parameters (47) were used for the lipids along with compatible CHARMM CGenFF for DCE (49) and CHARMM22/ CMAP corrected force field parameters for the protein (106). The systems are solvated with rigid TIP3P water implemented in NAMD2 (40). All FM/ HMMM model simulations were performed in the NP_nAT ensemble (P_n is constant membrane normal pressure and A is fixed membrane area). Langevin dynamics with a damping coefficient γ of 0.5 ps^{-1} and Langevin piston Nosé-Hoover methods (41, 42) were used to set the temperature to 310 K and pressure to 1 atm for most of the simulations. Long simulations for the FM model systems up to 300 ns duration and for the aqueous solution simulations were carried out at 300 K with a damping coefficient, γ, set to 1 ps^{-1}. Long range electrostatic interactions were computed by the Particle Mesh Ewald (PME) method (45) using a grid density

of ~ 1 $Å^{-3}$. Short range van der Waals interactions were smoothly truncated between 10 Å and 12 Å. Bonded hydrogen atoms were kept rigid through the use of the SETTLE/ SHAKE algorithm (43, 44), allowing us to use an integration time step of 2 fs.

3.3 RESULTS

First, we present results from the analysis of MD simulation trajectories from 5 runs each of the HMMM model per1, per2 and tilt systems up to 80 ns and henceforth collectively denoted as N = 15 HMMM model systems ("N=15") and one 500 ns run each of the FM model per1_FM, per2_FM and tilt_FM. Second, the analysis results for two aqueous solution runs of 50 ns each are described. Finally, we present results from an 80 ns simulation of noCAL_per1 system.

3.3.1 Critical Membrane Binding Residues

The domain - membrane interface is a complex region with numerous possibilities for binding. Eight parts of the PKCα-C2 domain have been implicated in membrane docking in many experiments. For example, X-ray reflectivity measurements (31) implicate loop 1 (N189), K205; EPR measurements (28) implicate loop 3 (R249, T250, T251, R252), LRC strands β3 (K197, K199), β4 (K209, K211); crystallographic measurements (23, 27, 75) implicate Ca^{2+} ions, LRC strands β3 (K197, K199), β4 (K209, K211), hpb-2resi (Y195, W245), W247 and biochemical experiments (82, 84, 93, 95) implicate Ca^{2+} ions, LRC strands β3 (K197, K199) and β4 (K209, K211). Any mention of these eight parts of the domain in this study would imply the associated critical residues as shown in parentheses (Figure 11), unless otherwise stated. The role of these domain parts and residues will be noted in the following discussion of the simulations.

These simulations determine a molecular level model of the membrane bound configuration of PKCα-C2 domain. The results described below show that loop 3, strand β4 and W247 penetrate stably into the membrane. Parallel strands β3 - β4 lie in a nearly vertical plane

with the joint residue K205 localized on the membrane surface. This geometry exposes the -OH of Y195 and the LRC to membrane lipids, with W247 penetrating further into the membrane. Loop 1 fluctuates randomly above the membrane surface but Ca^{2+} ions are in stable contact with the membrane surface, once they are dislodged from contact with loop 1. Loop 1, Ca^{2+} ions and the -OH of Y195 position themselves in an approximate horizontal plane.

Four quantities were used to characterize the membrane bound configuration of PKCα-C2 domain, namely angle (θ), relative heights $h_r(z)$, minimum distance (d_{min}) and number of direct contacts (N_c). These terms are defined below.

3.3.2 Angle (θ)

Two vectors were chosen to define the angles through which one can characterize the angular variation of the PKCα-C2 domain. For vector 1, we have chosen two residues situated at the ends of the largest beta sheet #2 within the PKCα-C2 domain. Vector 1 is defined as a vector from the center of mass (COM) of the Cα-N moiety of the residue L173 to the COM of the Cα-N moiety of the residue A180 of PKCα-C2 domain. Angle θ_1 is defined as an angle between vector 1 and the z-axis. Vector 2 is defined as a vector that connects the COM of the two bound Ca^{2+} ions and the Cα-N moiety of the K205 residue of the PKCα-C2 domain. Angle θ_2 is defined as an angle between the vector 2 and the z-axis. These two angles, (θ_1, θ_2), (Figure 19) are used to measure the angular variations of the PKCα-C2 domain from a direction perpendicular to the membrane. Although the information from these two angles is somewhat redundant, both angles were computed to facilitate comparison to values in the literature.

Figure 20 shows the angular variation for the HMMM model per1, per2 and tilt systems and the FM model systems.

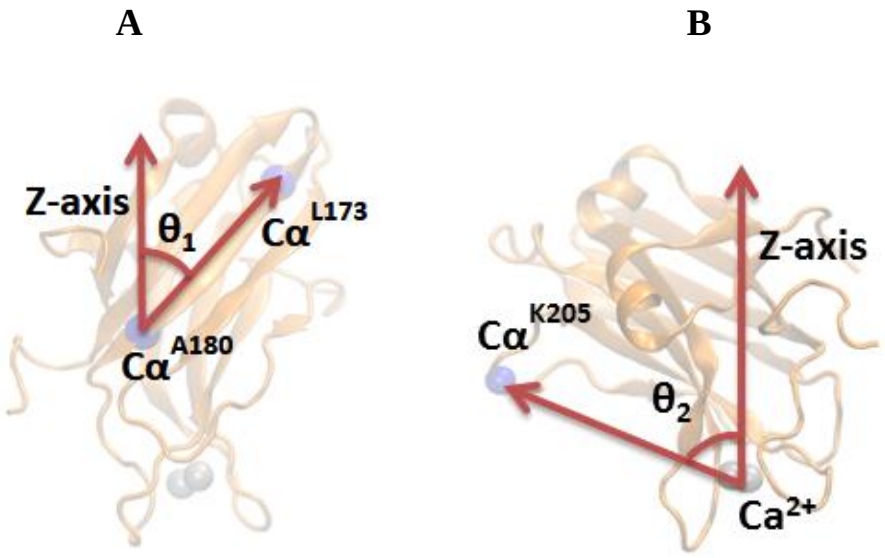

Figure 19: The definition of angle (θ_1, θ_2) for the orientation
(A) The angle θ_1 is defined as the angle between a vector that connects the center of mass (COM) of the Cα atom of the residue A180 and the COM of the Cα atom of the residue L173 and the Z-axis. (B) The angle θ_2 is defined as the angle between a vector that connects the center of mass (COM) of the two Ca^{2+} ions and the COM of the Cα atom of the residue K205 and the Z-axis.

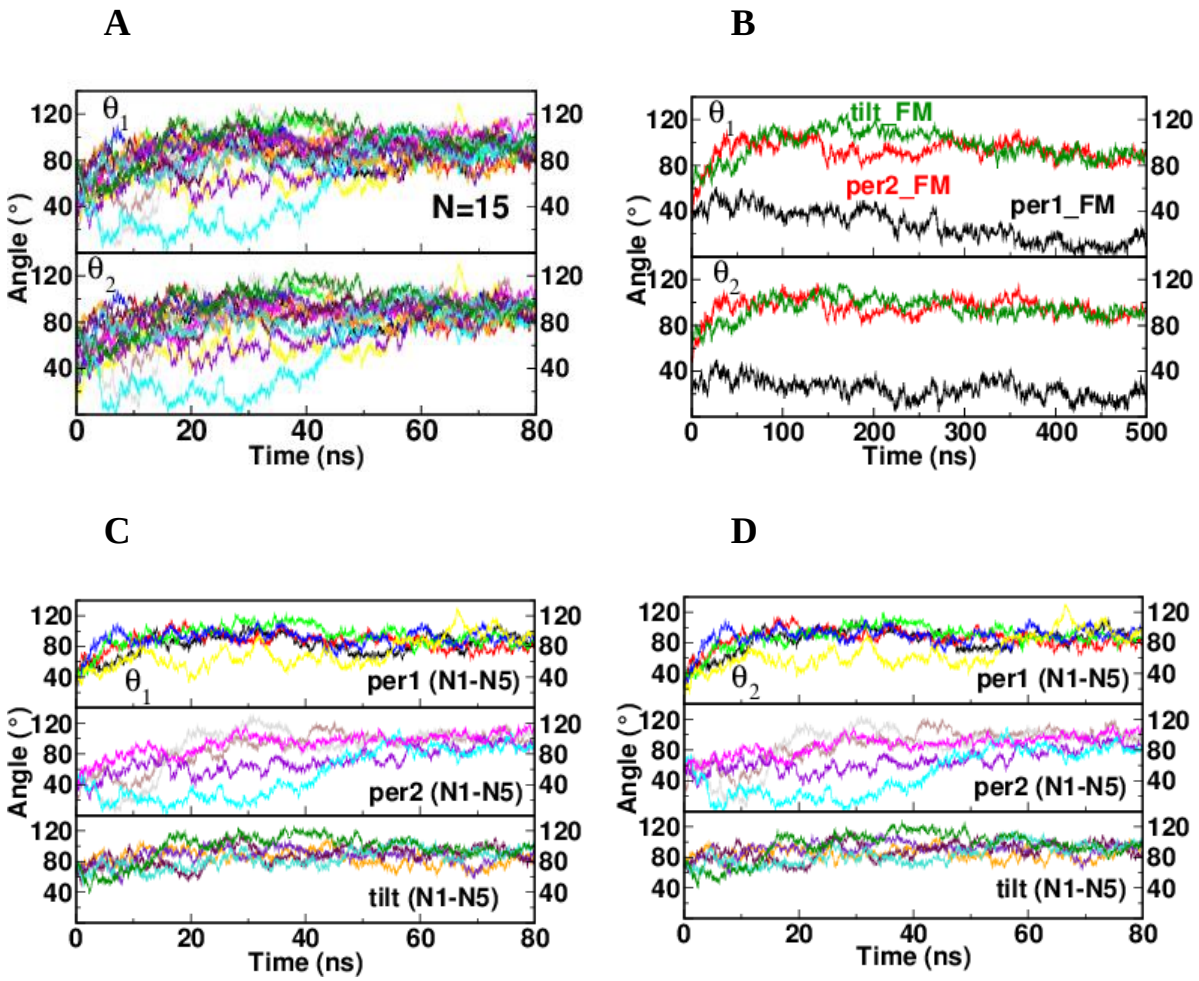

Figure 20: Orientation angle for FM/ HMMM model systems
Angle θ_1 and θ_2 for (A) N = 15 HMMM model systems (B) FM model systems. (C) And (D) shows θ_1 and θ_2 for the individual per1, per2 and tilt HMMM Model systems.

TABLE 2 shows the mean values of the angles for N = 15 HMMM model systems. Any calculations of the mean values with standard deviation in this study is performed for the last 30 ns of HMMM model trajectories, unless otherwise stated.

TABLE 2 Mean angle for N = 15 HMMM model systems
Mean (with standard deviation in parenthesis) of the PKCα-C2 domain orientation angles (θ) for N = 15 HMMM model systems calculated for the last 30 ns of the trajectories, where data is saved every 50 ps.

Angle (°)	per1	per2	tilt	N = 15
θ_1	87.0 (3.8)	95.3 (3.5)	89.4 (3.5)	90.6 (1.9)
θ_2	87.2 (4.0)	90.6 (3.2)	91.9 (3.2)	89.9 (2.1)

3.3.3 Relative Heights $h_r(z)$

The relative height, $h_r(z)$, is defined as the distance perpendicular to the plane of the membrane of domain-bound Ca^{2+} ions and critical domain residues, such as R249 (in loop 3), K209 (in strand β4), and W247 from two different planes parallel to the membrane surface: the average plane, <P>, defined by phosphorous atoms of the lipid PO_4^- groups and the average plane, <C>, defined by carbon atoms of the lipid COO^- groups. This parameter determines the extent of domain penetration into the membrane.

Figure 21 shows the relative heights for N = 15 HMMM model systems taken together and Figure 22 - 24 show the relative heights for each individual HMMM model systems for the per1, per2 and tilt systems.

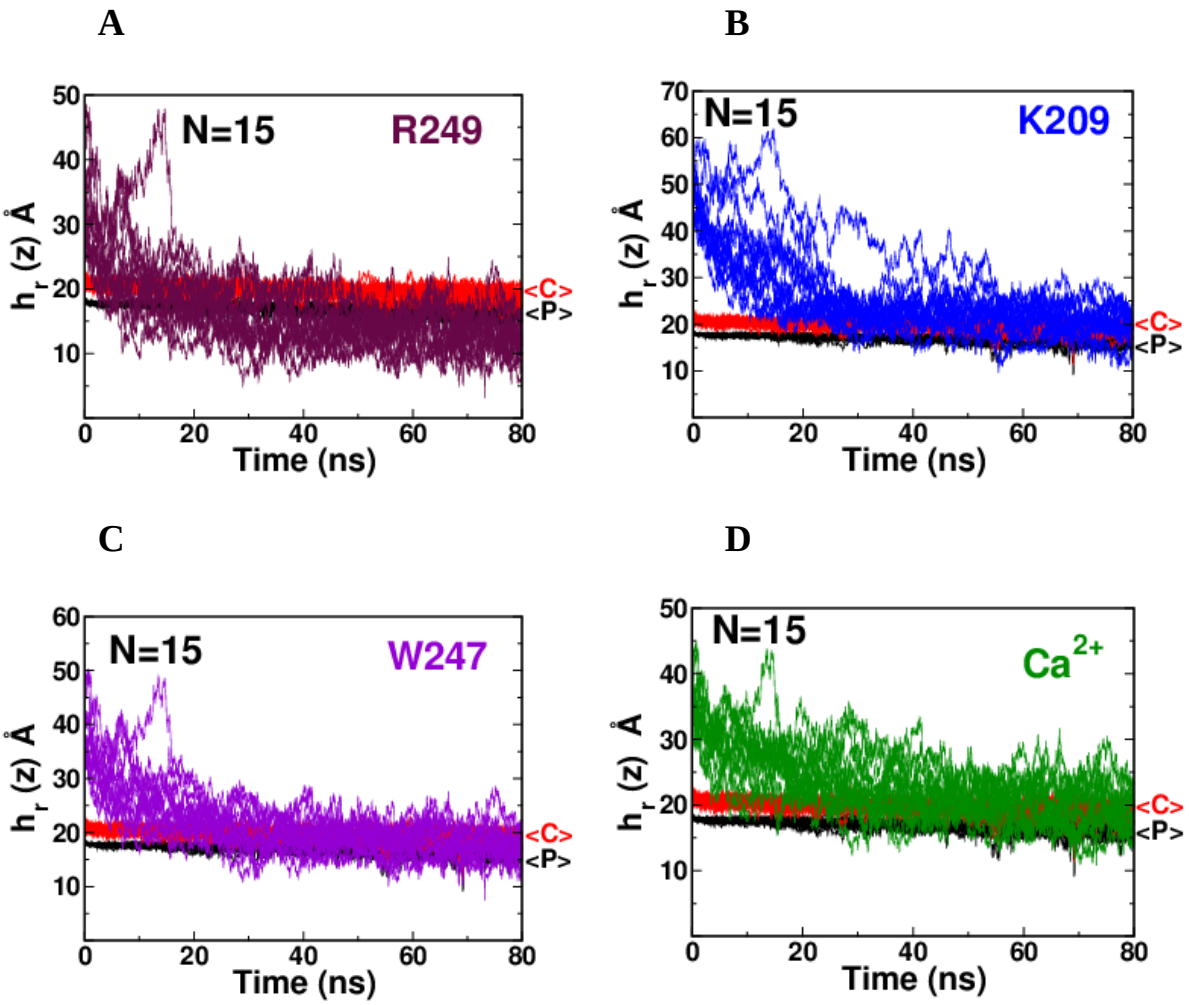

Figure 21: The relative heights, $h_r(z)$, for four critical residues $h_r(z)$ for HMMM model systems (A) R249 (B) K209 (C) W247 and (D) Ca^{2+} ions. The C-atoms of the COO^- moiety <C> plane and the P-atoms of the PO_4^- moiety <P> plane are shown in red and black color respectively.

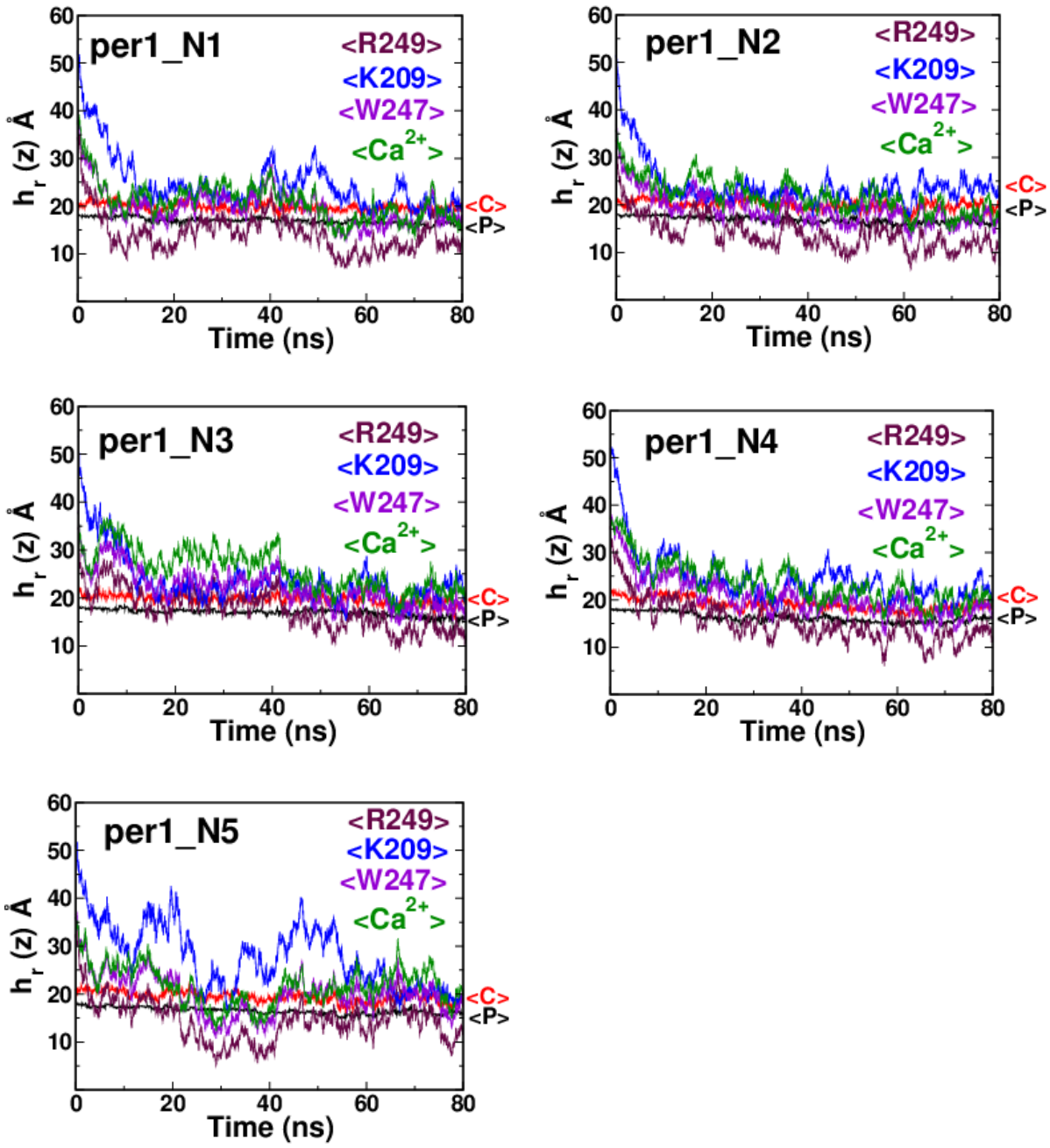

Figure 22: The relative heights, $h_r(z)$, for per1 HMMM model system $h_r(z)$ for five runs of per1 HMMM model system. The C-atoms of the COO^- moiety <C> plane and the P-atoms of the PO_4^- moiety <P> plane are shown in red and black color respectively.

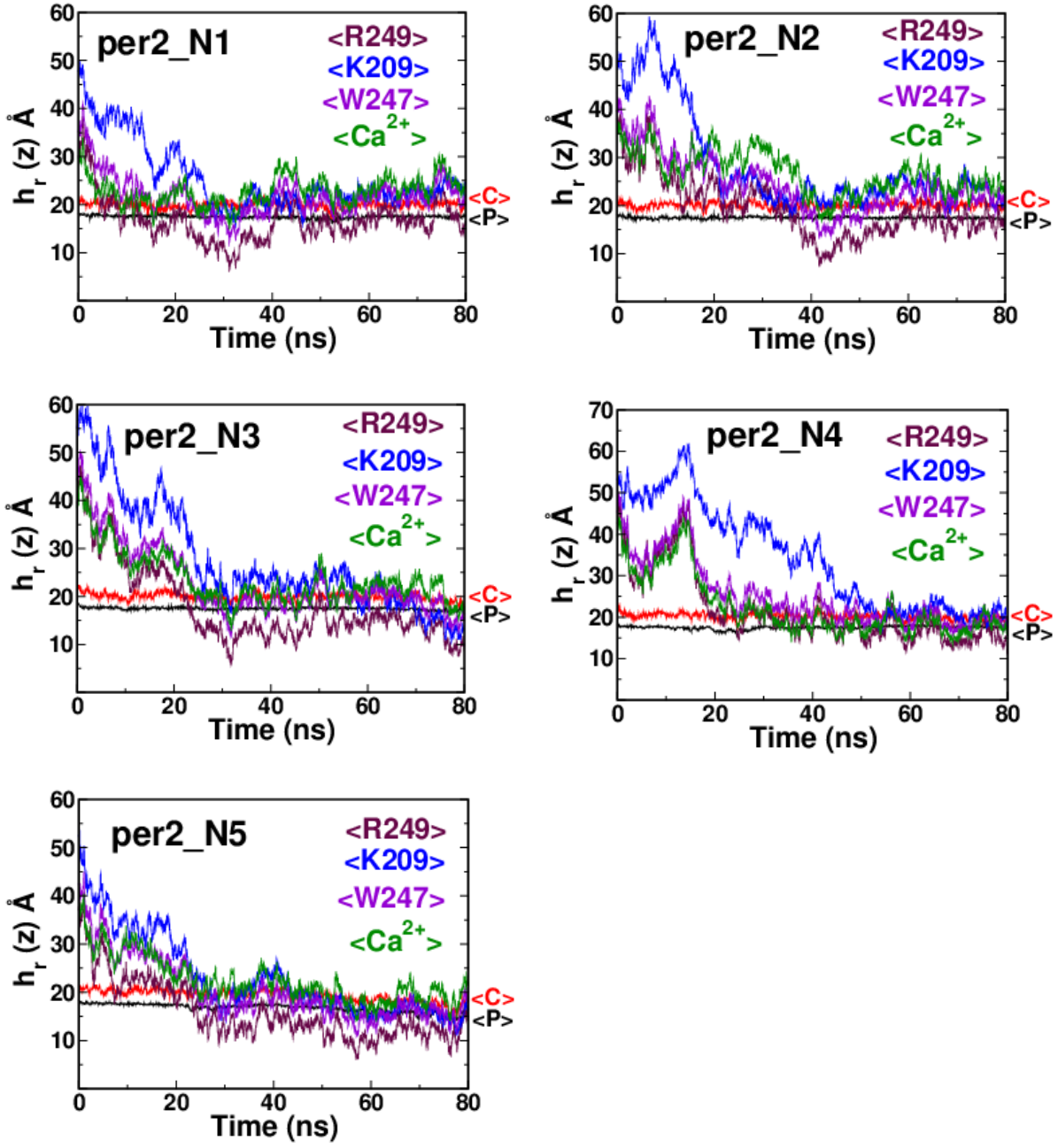

Figure 23: The relative heights, $h_r(z)$, for per2 HMMM model system
$h_r(z)$ for five runs of per2 HMMM model system. The C-atoms of the COO^- moiety <C> plane and the P-atoms of the PO_4^- moiety <P> plane are shown in red and black color respectively.

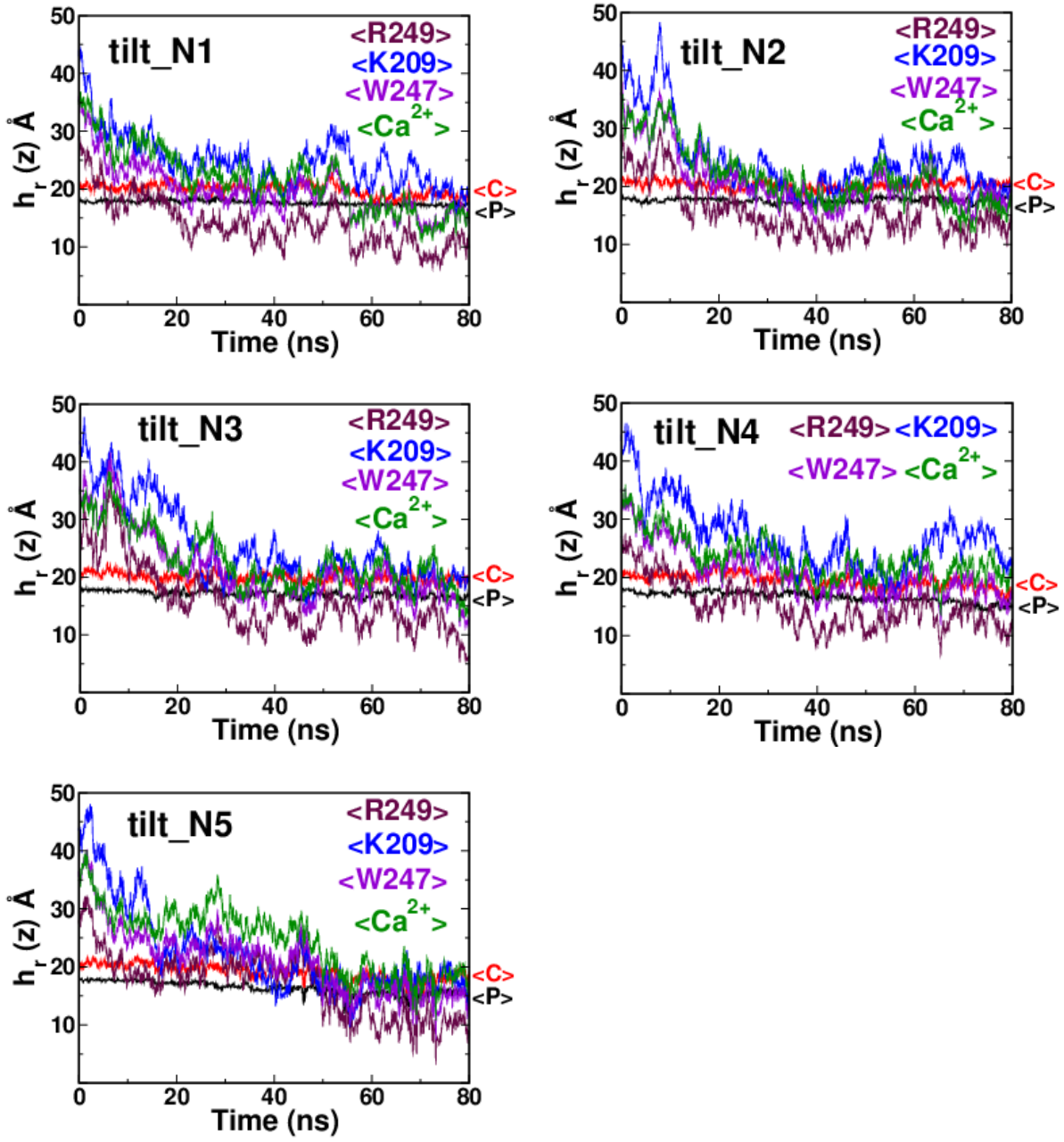

Figure 24: The relative heights, $h_r(z)$, for tilt HMMM model system $h_r(z)$ for five runs of tilt HMMM model system. The C-atoms of the COO^- moiety <C> plane and the P-atoms of the PO_4^- moiety <P> plane are shown in red and black color respectively.

3.3.4 Minimum Distance d_{min}

The minimum distance, d_{min}, is defined as the minimum distance between any atom in the PO_4^- or COO^- moieties of the lipid headgroups in the top leaflet of the bilayer and eight critical domain-parts (residues) of the PKCα-C2 domain, viz. loop1, loop3, Ca^{2+} ions, K205, strand β3, strand β4, hpb-2resi and W247. **TABLE 3** shows the mean value of the d_{min} (with standard deviation) for combined N = 15 HMMM model systems. Figure 25 shows the time series of the d_{min} for the same systems. Moreover, Figure 26 - 28 show d_{min} for per1, per2 and tilt N = 15 individual HMMM model systems and Figure 29 for the individual FM model systems respectively.

TABLE 3 Mean minimum distance for N = 15 HMMM model systems
Mean (with standard deviation in parenthesis) of the PKCα-C2 domain parts minimum distance (d_{min}) for N = 15 HMMM model systems calculated for the last 30 ns of the trajectories, where data is saved every 50 ps.

Domain Parts	per1	per2	tilt	N=15
loop1 (N189)	4.7 (0.6)	4.6 (0.6)	4.6 (0.5)	4.6 (0.3)
loop3 (R249, T250,T251, R252)	1.7 (0.03)	1.7 (0.04)	1.7 (0.04)	1.7 (0.02)
R249	1.9 (0.2)	1.8 (0.1)	1.8 (0.1)	1.8 (0.09)
T250	3.7 (0.4)	3.5 (0.3)	3.6 (0.5)	3.6 (0.2)
β3 (K197, K199)	3.7 (0.9)	2.8 (0.5)	1.9 (0.2)	2.8 (0.3)
β4 (K209, K211)	2.1 (0.5)	1.8 (0.2)	1.8 (0.2)	1.9 (0.2)
K209	2.5 (0.7)	2.0 (0.3)	2.1 (0.3)	2.2 (0.3)
K211	2.9 (0.7)	2.7 (0.6)	2.5 (0.5)	2.7 (0.3)
Ca^{2+} ions	4.9 (0.3)	3.2 (0.2)	3.5 (0.1)	3.9 (0.1)
K205	2.9 (1.2)	3.2 (0.5)	2.9 (0.6)	3.0 (0.5)
hpb_2resi (Y195, W245)	4.3 (0.5)	3.6 (0.5)	2.8 (0.4)	3.6 (0.2)
OH-moiety (of Y195)	4.7 (0.7)	4.1 (0.6)	3.4 (0.5)	4.1 (0.3)
W247	2.6 (0.3)	2.6 (0.3)	2.9 (0.3)	2.7 (0.1)
NH moiety (of W247)	3.2 (0.5)	3.1 (0.5)	3.5 (0.5)	3.3 (0.2)

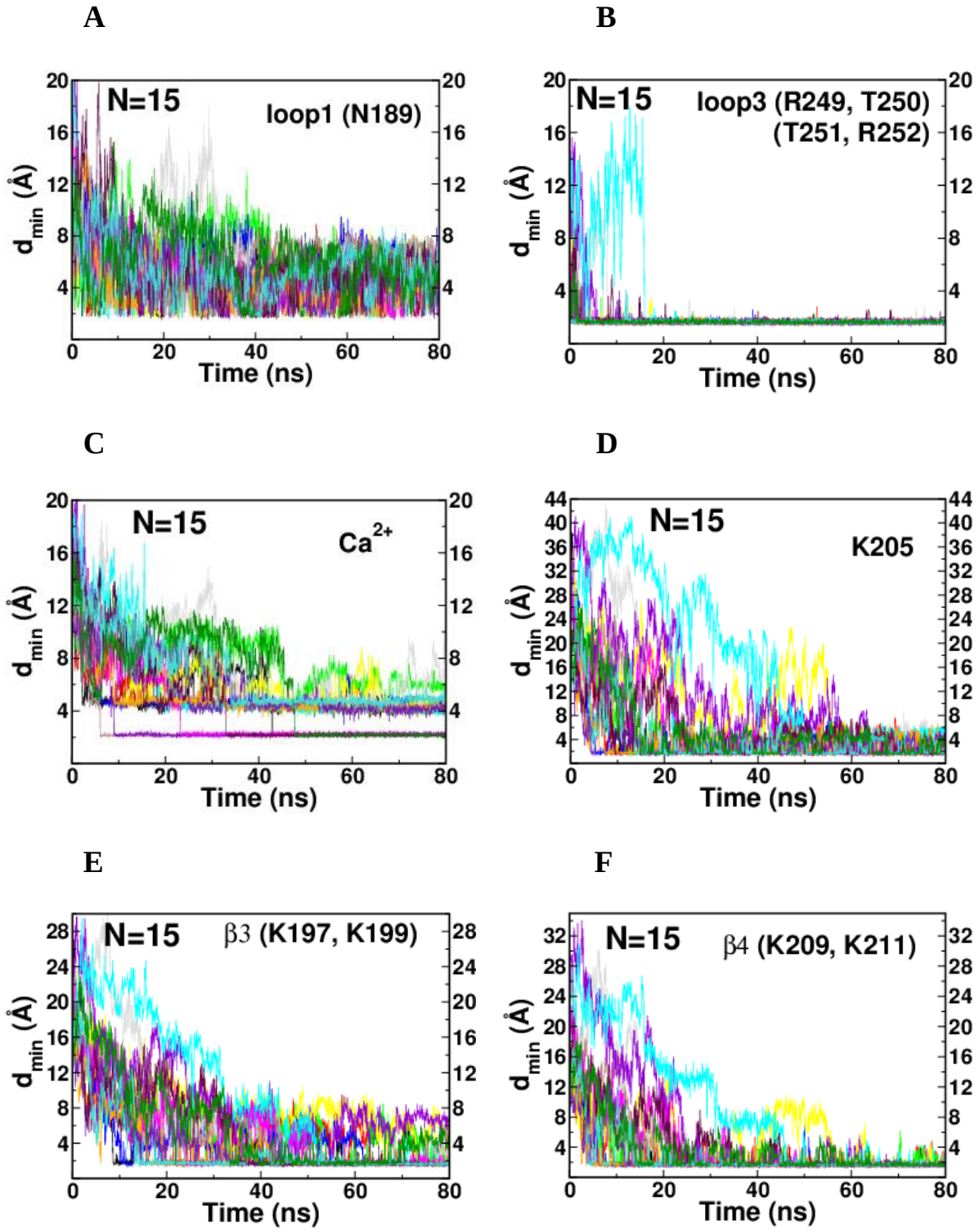
A
N=15
loop1 (N189)
B
N=15
loop3 (R249, T250)
(T251, R252)
C
N=15
Ca2+
D
N=15
K205
E
N=15
β3 (K197, K199)
F
N=15
β4 (K209, K211)
dmin (Å)
Time (ns)

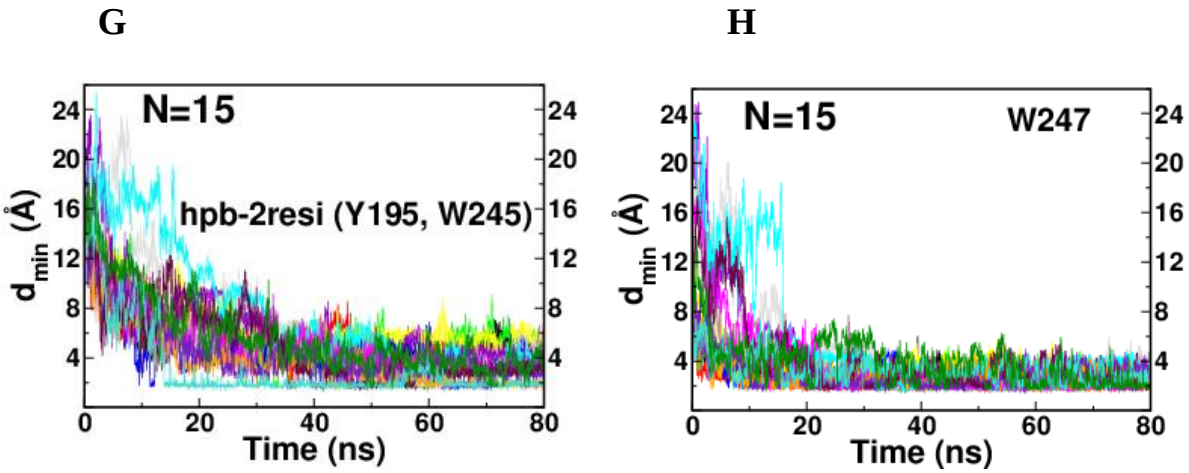

Figure 25: The minimum distance, d_{min}, for N = 15 HMMM model systems d_{min} for (A) loop1 (N189) (B) loop3 (R249, T250, T251, R252) (C) Calcium ions (D) K205 (E) β3 (K197, K199) (F) β4 (K209, K211) (G) hpb-2resi (Y195, W245) and (H) W247.

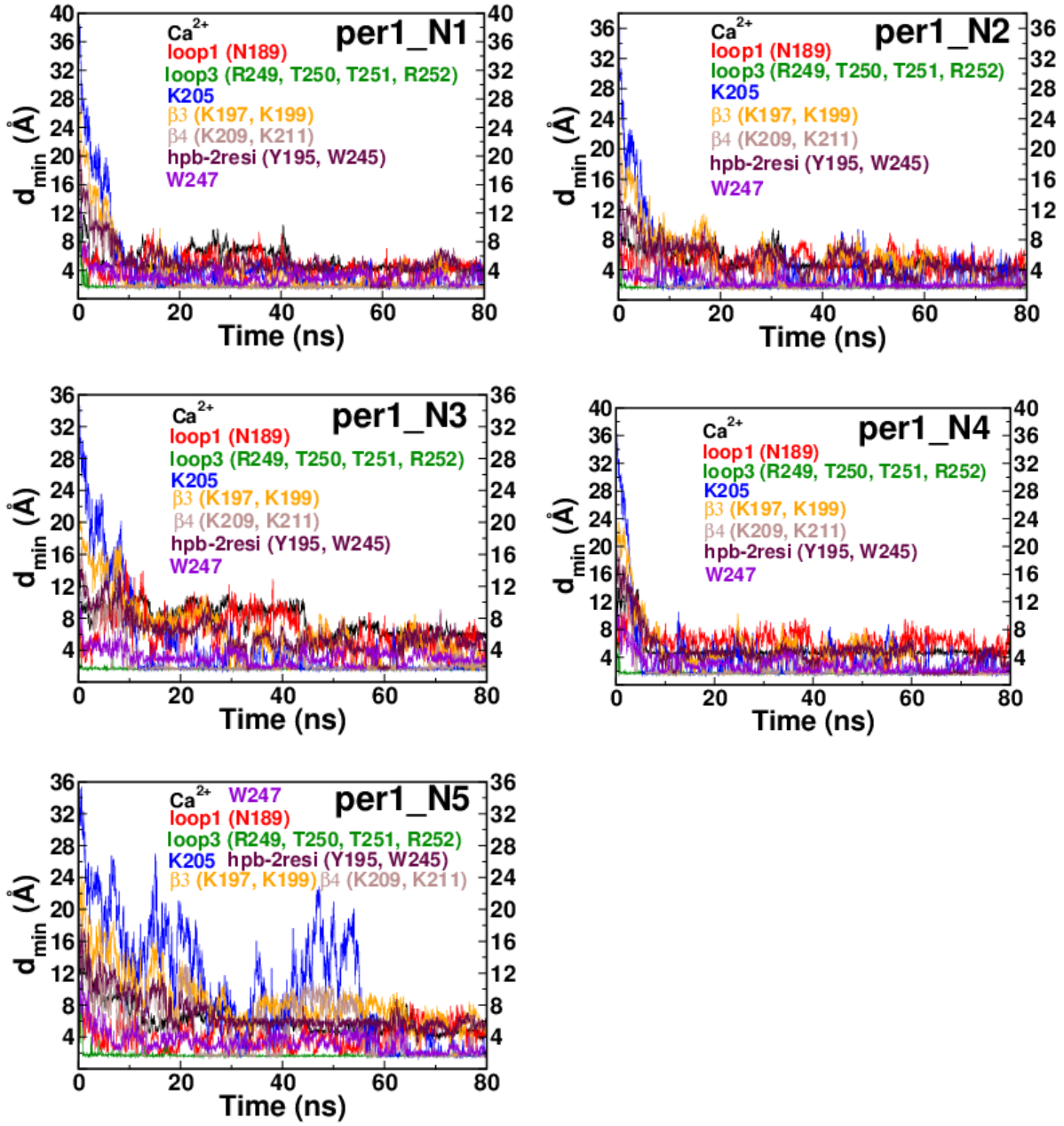

Figure 26: The minimum distance, d_{min}, for per1 HMMM model systems d_{min} for eight critical parts of the domain is shown for five runs of per1 case.

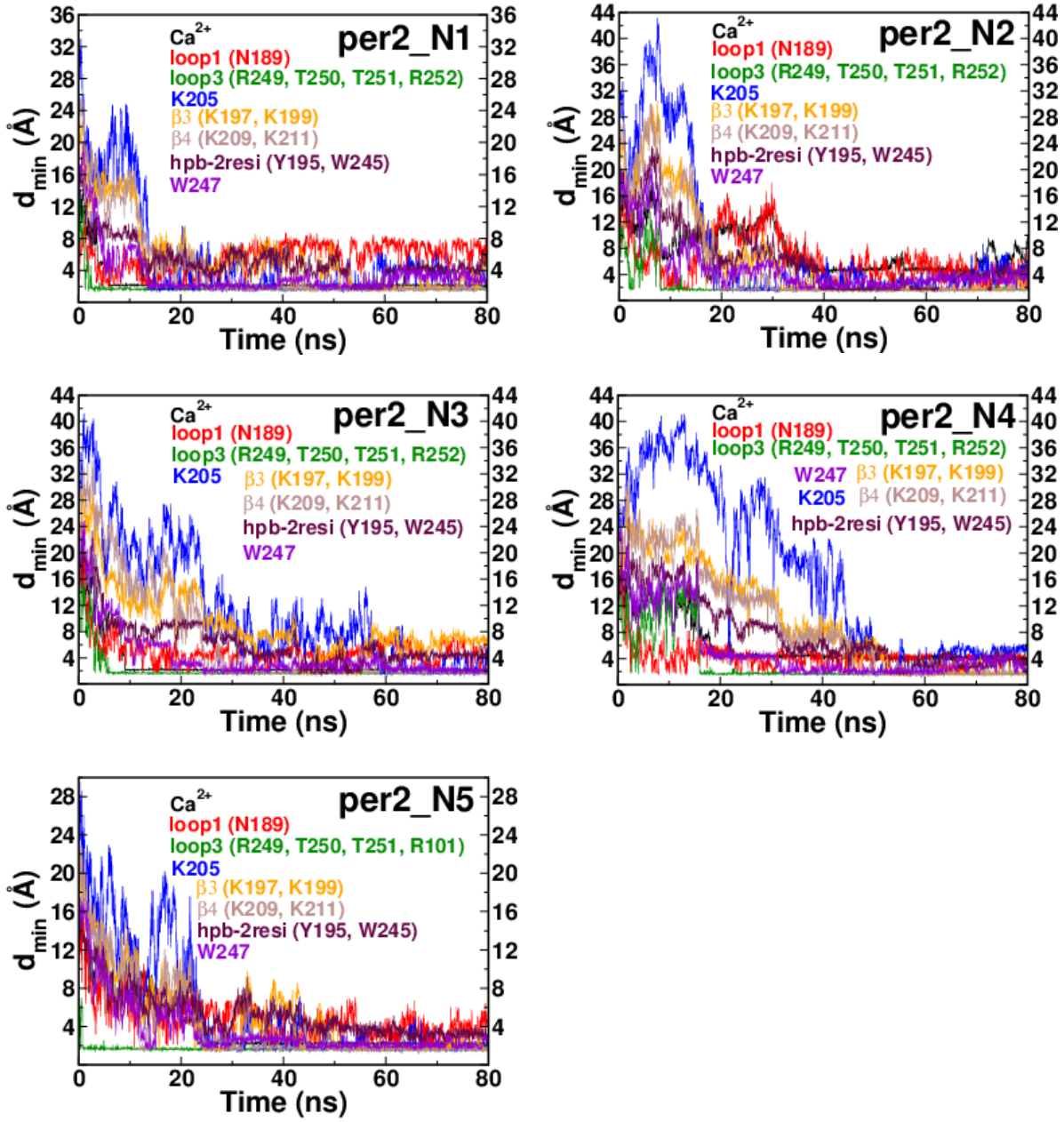

Figure 27: The minimum distance, d_{min}, for per2 HMMM model systems
d_{min} for eight critical parts of the domain is shown for five runs of per2 case.

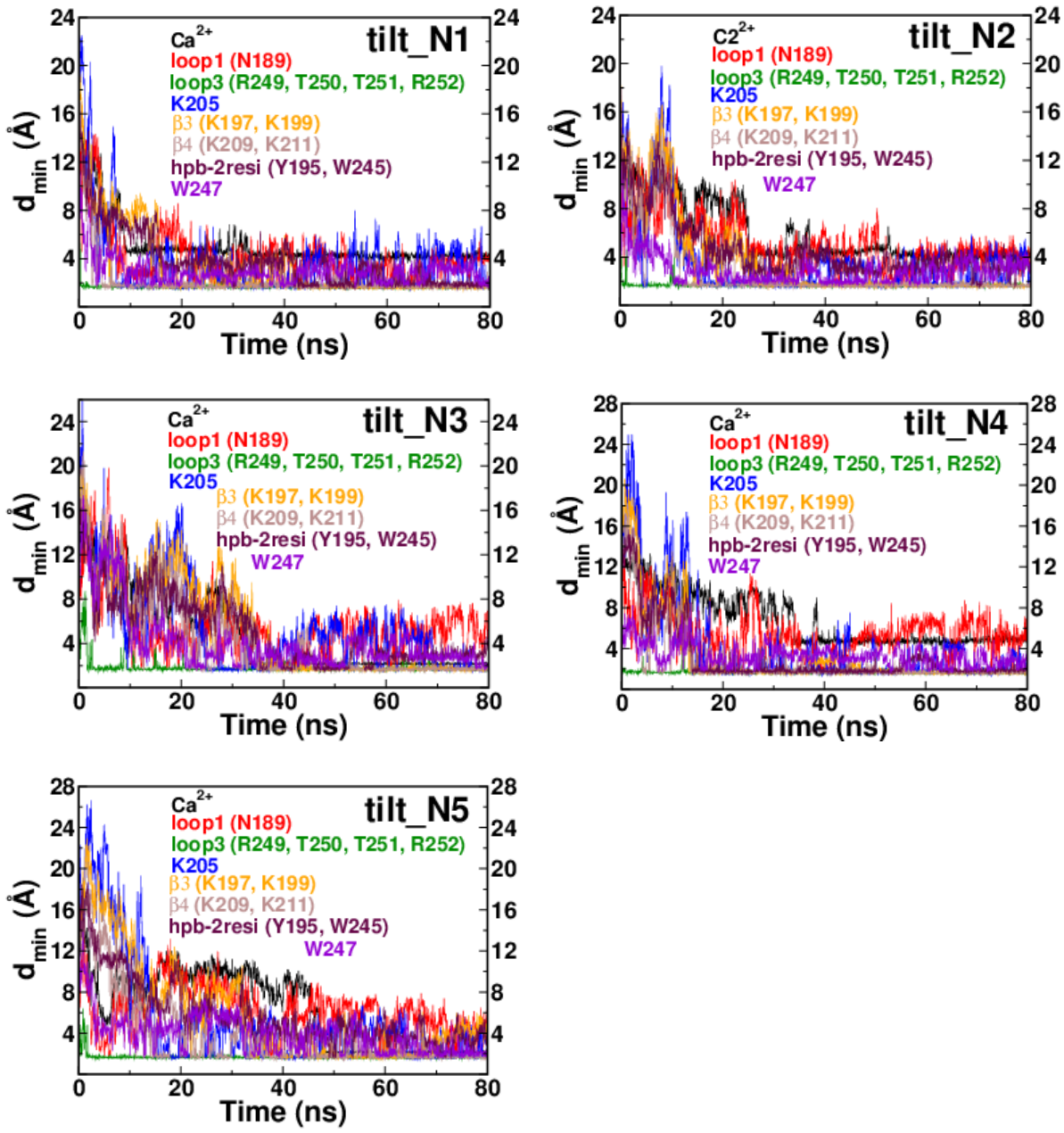

Figure 28: The minimum distance, d_{min}, for tilt HMMM model systems
d_{min} for eight critical parts of the domain is shown for five runs of tilt case.

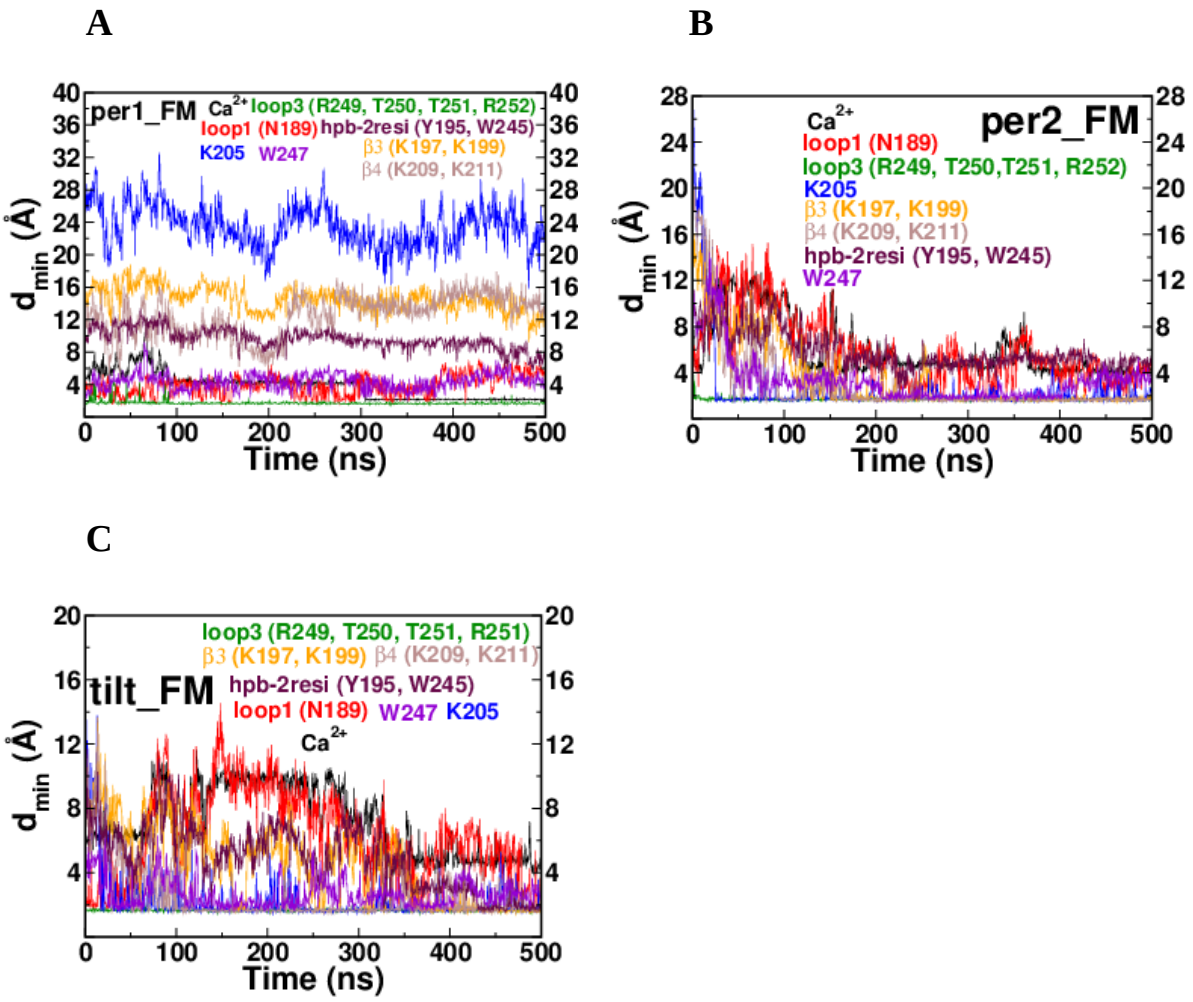

Figure 29: The minimum distance, d_{min}, for FM model systems
d_{min} for eight critical parts of the domain for (A) per1_FM (B) per2_FM and (C) tilt_FM cases.

3.3.5 Number of Direct Contacts (N_c)

A direct contact between two groups is defined whenever any atom from say, group 1 comes within 6 Å of any atom in another group say, group 2. We defined an interaction between the domain (forming group 1) and the membrane (forming group 2) through N_c and its strength is measured through the number of direct contacts. We calculated the mean value of N_c (with standard deviation) for the same components as we calculated $d_{\min}$. **TABLE 4** lists N_c between say, set 1 groups i.e., the eight critical domain parts as group 1 and the PO_4^- or COO^- moieties of the lipid headgroups in the top leaflet of the bilayer as group 2 for HMMM model systems.

TABLE 4 Mean number of direct contacts for N = 15 HMMM model systems
Mean (with standard deviation in parenthesis) of the PKCα-C2 domain parts' number of direct contacts (N_c) for N = 15 HMMM model systems calculated for the last 30 ns of the trajectories, where data saved every 50 ps. Ca^{2+} ions are shown for two distances.

Domain parts	per1	per2	tilt	N=15
loop1 (N189)	3.7 (1.2)	4.3 (1.2)	4.9 (1.2)	4.3 (0.7)
loop3(R249, T250, T251, R252)	34.2 (2.0)	38.5 (2.0)	35.7 (2.4)	36.1 (1.2)
R249	16.4 (1.5)	17.3 (1.7)	17.1 (1.2)	16.9 (0.8)
β3 (K197, K199)	5.7 (1.8)	8.8 (1.5)	12.6 (1.4)	9.0 (0.9)
β4 (K209, K211)	15.8 (1.7)	18.4 (2.3)	18.0 (1.9)	17.4 (1.3)
K209	10.5 (1.5)	13.1 (2.0)	10.6 (1.2)	11.4 (1.0)
K211	8.2 (1.6)	9.0 (1.9)	9.8 (1.8)	9.0 (1.0)
Ca^{2+} ions (6Å)	2.8 (0.7)	4.9 (0.5)	4.1 (0.4)	3.9 (0.3)
Ca^{2+} ions (7Å)	4.7 (0.9)	8.2 (0.7)	6.0 (0.6)	6.3 (0.5)
K205	10.8 (1.9)	9.4 (1.8)	8.2 (1.7)	9.5 (0.9)
hpb_2resi (Y195, W245)	4.9 (1.1)	7.9 (1.3)	12.0 (1.4)	8.3 (0.8)
OH-moiety (of Y195)	3.2 (1.3)	4.5 (0.9)	5.4 (1.0)	4.4 (0.6)
W247	12.9 (1.5)	13.9 (1.4)	12.8 (1.4)	13.2 (0.8)
NH moiety (of W247)	5.4 (1.0)	8.3 (1.3)	5.5 (0.9)	6.4 (0.7)

3.4 DISCUSSION

Snapshots of N = 15 HMMM model systems at 80 ns (Figure 30) show that all systems have converged to a similar bound configuration. Moreover, the FM model system snapshots at 500 ns (Figure 30 bottommost row) also look very similar to the configuration of HMMM model systems, except for the per1_FM case, which may be stuck in a non-equilibrium state. We describe the membrane bound configuration of PKCα-C2 domain based upon the simulation results.

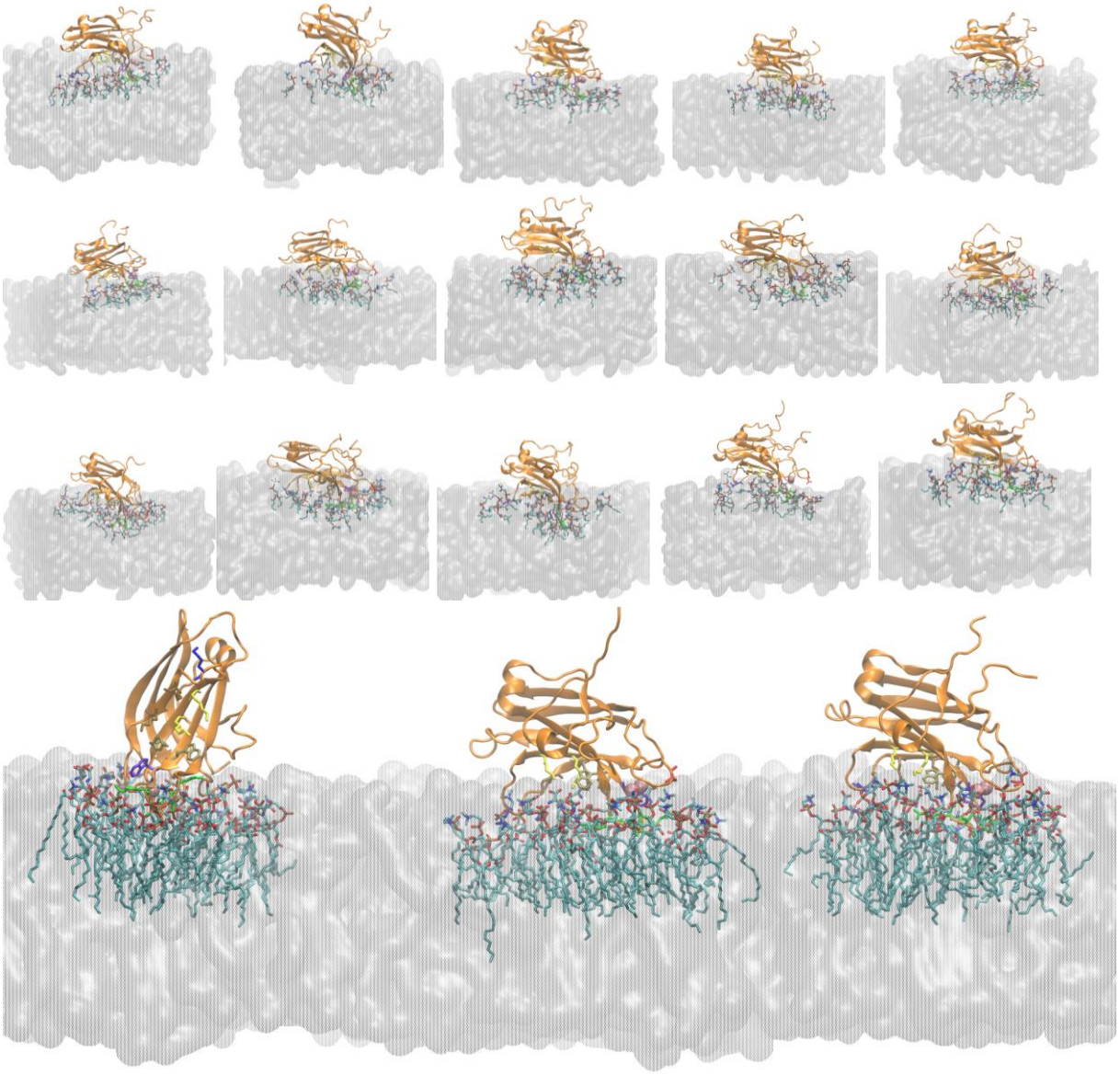

Figure 30: The configuration of HMMM and FM model systems
Top three rows show the membrane bound configuration for per1, per2 and tilt N = 15 HMMM model systems at the end of 80 ns run time, respectively. The membrane is shown in quicksurf representation in gray and the lipids within 6 Å of the protein are shown in CPK representation. (bottom most row) The final configuration of FM model systems after 500 ns are shown from left to right: per1, per2 and tilt. The lipids within 6 Å of the protein are also shown in CPK representation.

3.4.1 Membrane Bound Orientation

The orientation of the PKCα-C2 domain is partially characterized by the angle (θ_1, θ_2). Figure 20A shows angle calculations from the HMMM model systems and **TABLE 2** shows their mean values with standard deviations. The HMMM model systems converged to a very similar final orientation with a mean value of ~ 90°. Angles (θ_1, θ_2) are fairly consistent not only within each case of per1, per2 and tilt but also across all three cases (Figure 20C,D; TABLE 2). Moreover Figure 20B shows the angles (θ_1, θ_2) calculated for FM model systems. The per2_FM and the tilt_FM systems converged to match the mean value of ~ 90° for the HMMM model systems. The per1_FM simulation (black curve in Figure 20B) did not vary much over 500 ns from its original θ of ~ 40°. A similar observation was made for one of the per2 HMMM simulation for the first 40 ns, but this simulation eventually equilibrated to ~ 90° (Figure 20C). It is possible that the per1_FM simulation is stuck in a local minimum in spite of the 500 ns duration of the simulation. The HMMM model systems sustain their orientation angle for at least 30 ns and the FM model systems for at least 200 ns.

3.4.2 Spatial - Temporal Localization of Critical Residues

The binding configuration of a partially flexible protein cannot be characterized entirely in terms of rigid body rotations. Further characterization of the bound configuration is established by identifying the spatial-temporal localization of critical residues with respect to the membrane.

Figure 21 - 24 show the penetration of the domain into the membrane according to the relative heights, $h_r(z)$, of the domain-bound Ca^{2+} ions and critical domain residues, such as R249 (in loop 3), K209 (in strand β4), and W247 from <P> and <C> planes. The distances $h_r(z)$ for all three systems (per1, per2 or tilt) indicate that R249 penetrates deepest into the membrane, the lysine chain of K209 is parallel to the membrane surface and localized near <C>, W247 penetrates

past <P> close to the hydrophobic core and Ca^{2+} ions are bound and fairly localized on the membrane surface.

In addition to the relative heights $h_r(z)$ along the membrane normal, the minimum distances, d_{min}, were determined between any atom in the PO_4^- or COO^- moieties of the lipid headgroups (in the top leaflet of the bilayer) and representative locations in the domain (loop1, loop3, Ca^{2+} ions, K205, strand β3, strand β4, hpb-2resi and W247). The variation of the values of d_{min} with simulation time presents a three dimensional spatial-temporal characterization of the domain-membrane interface. Figure 25 - 28 show the d_{min} time series for N = 15 HMMM model systems and **TABLE 3** lists the mean values of d_{min} for the last 30 ns of the simulations. Figure 29 shows the d_{min} time series for the FM model systems individually. For all HMMM and FM model systems, it is seen that interesting membrane binding and configuration defining interactions occur within ~ 2 to 6 Å of the lipid PO_4^-/ COO^- moieties.

TABLE 4 lists the mean number of direct contacts N_c between parts of the domain and the membrane for HMMM simulations. A contact between two groups (i.e., a set of residues or atoms) is counted as direct when any atom from group 1 is within 6 Å of any atom in the PO_4^- or COO^- moieties. Values of N_c are fairly consistent across the per1, per2 and tilt systems. **TABLE 3** shows that loop3 and strand β4 are within ~ 2 Å of the PO_4^-/ COO^- moieties and W247 is within ~ 2.5 Å. **TABLE 4** shows that the same parts have the highest N_c values. As a result of their proximity and number of contacts, these domain parts are likely important for membrane docking. In these domain parts, the residues R249 of loop3 and K209/ K211 of strand β4 provide the closest proximity (Figure 31) and largest number of contacts to PO_4^-/ COO^- moieties (**TABLE 5**). Thus, R249, K209, and W247 were chosen to represent membrane penetrating residues as depicted in Figure 21.

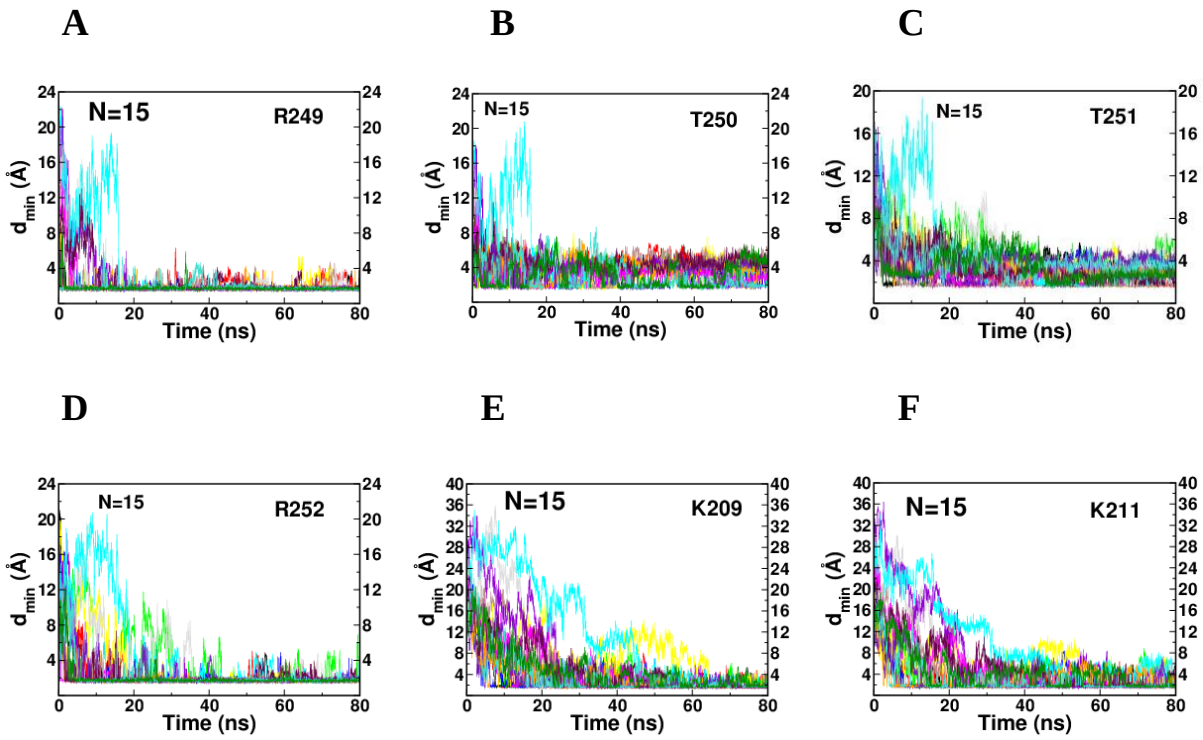

Figure 31: The minimum distance, d_{min}, for loop3 and β4 residues
To show the steadiest residue within loop3 and β4. d_{min} for (A) R249 (B) T250 (C) T251 (D) R252 (E) K209 and (F) K211.

TABLE 5 Mean number of direct contacts for loop3 and β4
Mean (with standard deviation in parenthesis) number of direct contacts (N_c) for critical residues of the PKCα-C2 domain's loop3 and β4 sheet for N = 15 HMMM model systems as calculated for the last 30 ns of the trajectories where data is saved every 50 ps.

Domain Parts	per1	per2	tilt	N = 15
loop3 (R249, T250,T251, R252)	34.2 (2.0)	38.5 (2.0)	35.7 (2.4)	36.1 (1.2)
R249	16.4 (1.5)	17.3 (1.7)	17.1 (1.2)	16.9 (0.8)
T250	6.9 (1.1)	8.0 (1.3)	5.7 (0.8)	6.9 (0.6)
T 251	9.1 (1.3)	11.6 (0.9)	8.9 (1.2)	9.9 (0.8)
R252	15.1 (1.9)	17.3 (1.4)	16.6 (1.5)	16.3 (1.1)
β4 (209, K211)	15.8 (1.7)	18.4 (2.3)	18.0 (1.9)	17.4 (1.3)
K209	10.5 (1.5)	13.1 (2.0)	10.6 (1.2)	11.4 (1.0)
K211	8.2 (1.6)	9.0 (1.9)	9.8 (1.8)	9.0 (1.0)

3.4.3 Role of Lysine Rich Cluster (LRC) and K205

Within the LRC, strand β4 is within ~ 2 Å of the PO_4^-/ COO^- moieties for the last ~ 40 ns of the simulation time (Figure 25F) but strand β3 fluctuates within ~4 Å of PO_4^-/ COO^- (Figure 25E). The mean value of d_{min} for strand β4 is always lower than that of β3 except for the HMMM_tilt simulation where they have similar values (**TABLE 3**). However, the N_c values are always considerably larger for strand β4 than β3 (**TABLE 4**).

To better understand the spatial location of the LRC (strands β3 versus β4), and to reaffirm the extent of contacts, we tightened the convergence criteria by calculating direct contacts between strands β3, β4 and Ca^{2+} ions and only the oxygen atoms of PO_4^- or COO^- (Figure 32 – 34). This calculation also shows that strand β4 has many more contacts than β3.

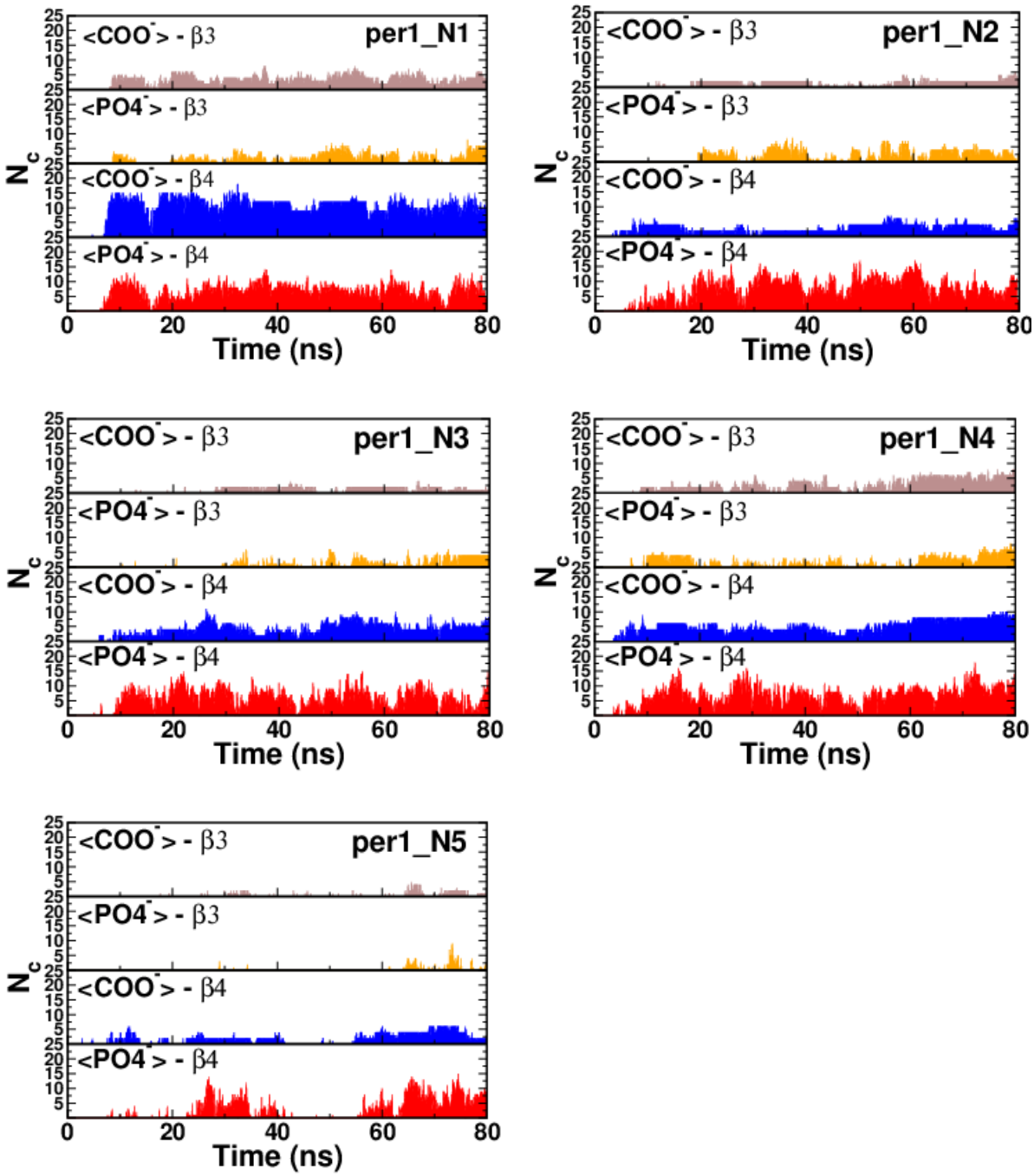

Figure 32: The number of contacts, N_c, for per1 HMMM model systems
N_c for β3, β4 with oxygen atoms of PO_4^- or COO^- are shown for five runs of per1 case.

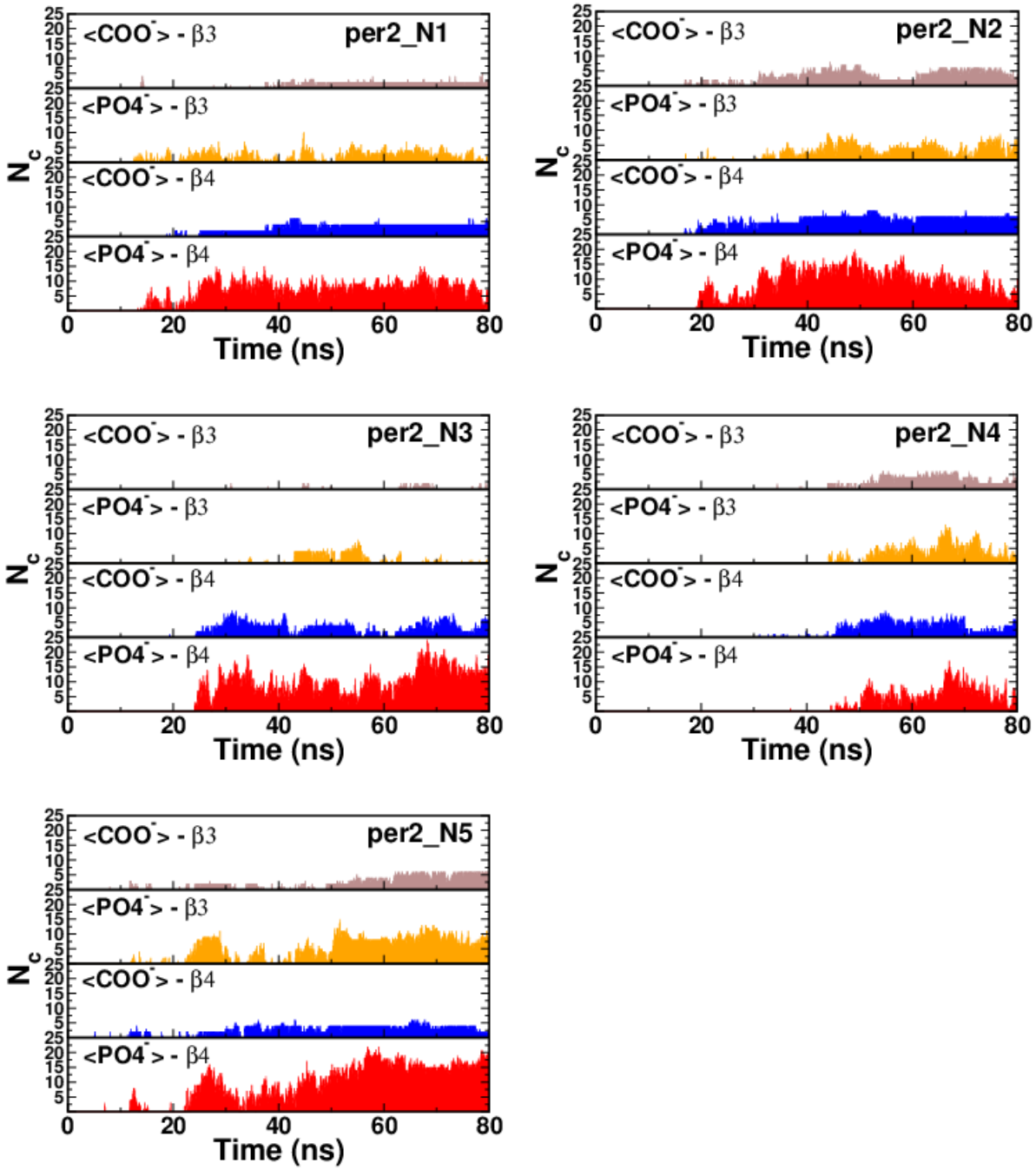

Figure 33: The number of contacts, N_c, for per2 HMMM model systems N_c for β3, β4 with oxygen atoms of PO_4^- or COO^- are shown for five runs of per2 case.

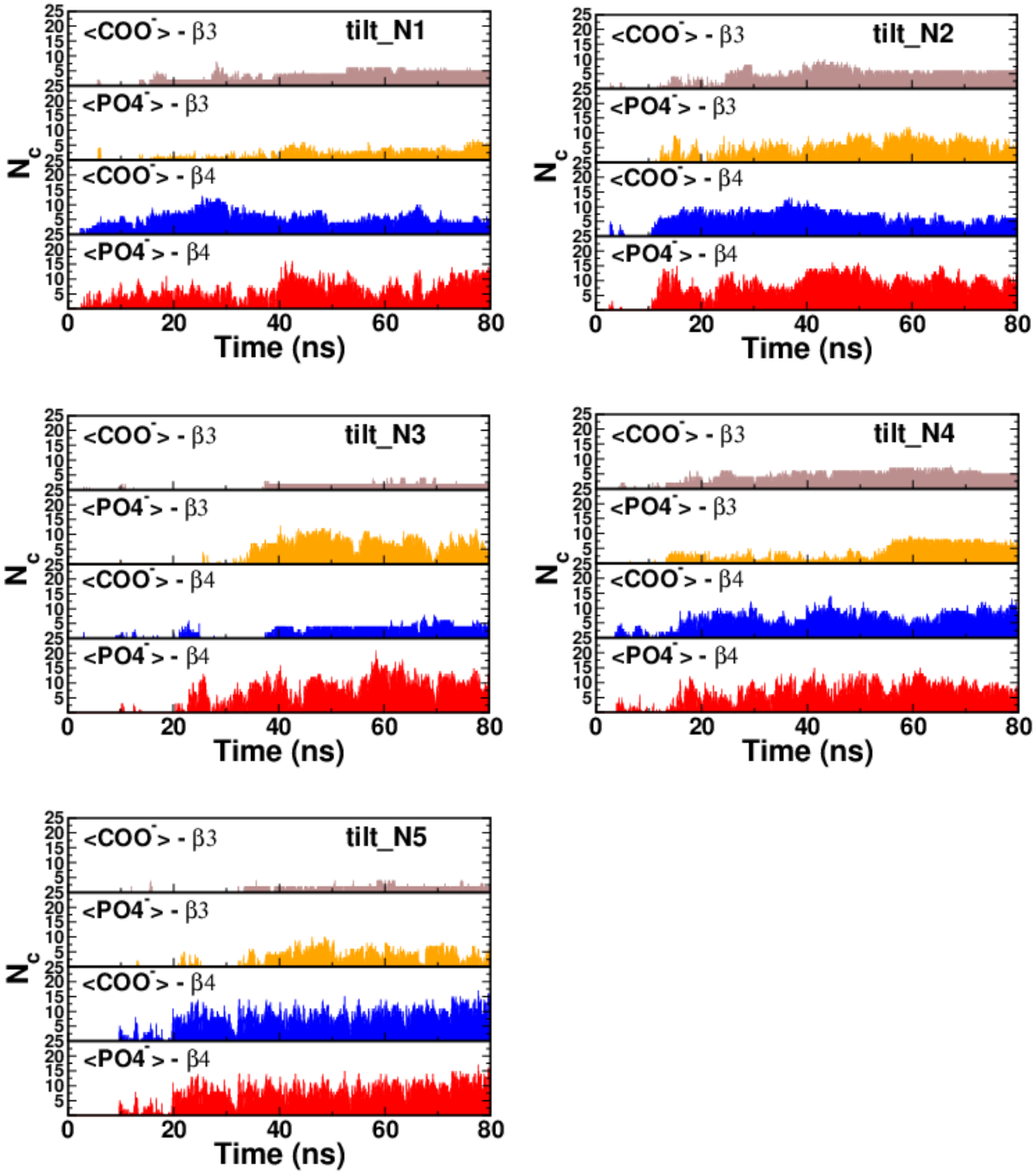

Figure 34: The number of contacts, N_c, for tilt HMMM model systems
N_c for β3, β4 with oxygen atoms of PO_4^- or COO^- are shown for five runs of tilt case.

In general, strand β4 is closer to the membrane (smaller d_{min}) and has more direct contacts (larger N_c) with the membrane than strand β3. This indicates that strands β4 and β3 are not in the same horizontal plane. Instead, they are in an almost vertical plane with strand β3 positioned above β4, as illustrated in snapshots Figure 35 - 40 of N = 15 HMMM model systems. Figure 35, Figure 37 and Figure 39 show a more detailed time evolution of the N = 15 HMMM model systems. Figure 36, Figure 38 and Figure 40 show time stamped snapshots for bound configurations of N = 15 HMMM model systems.

Residue K205 occupies a unique position as a link between strands β3 and β4. It is located within 3 Å of the PO_4^-/ COO^- part of the lipids (**TABLE 3**) with 9 to 10 contacts (**TABLE 4**). This consistent position for all simulations (Figure 25D) suggests that K205 ought to play a critical role in defining the binding configuration of the PKCα-C2 domain.

per1_N1

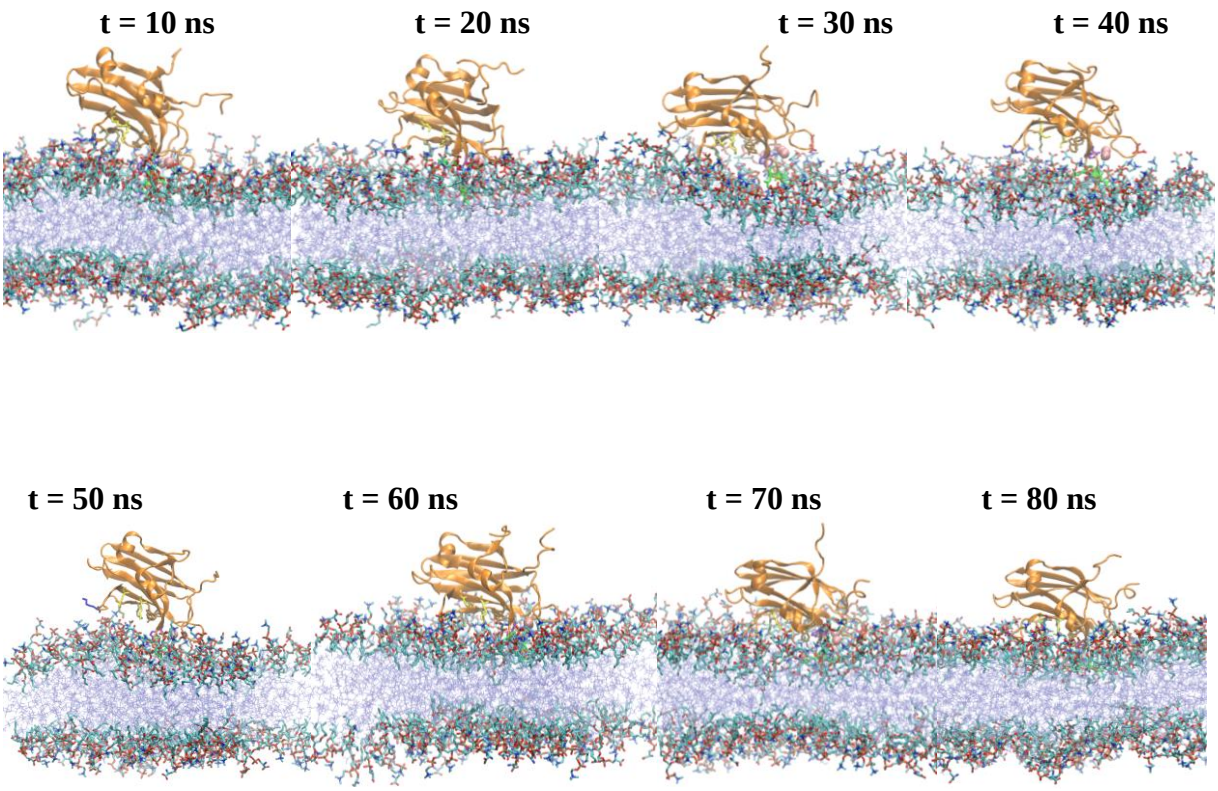

per1_N2

t = 10 ns t = 20 ns t = 30 ns t = 40 ns

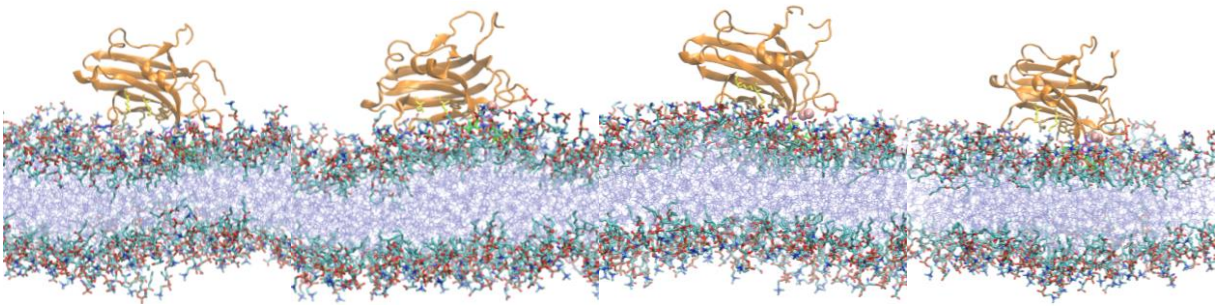

t = 50 ns t = 60 ns t = 70 ns t = 80 ns

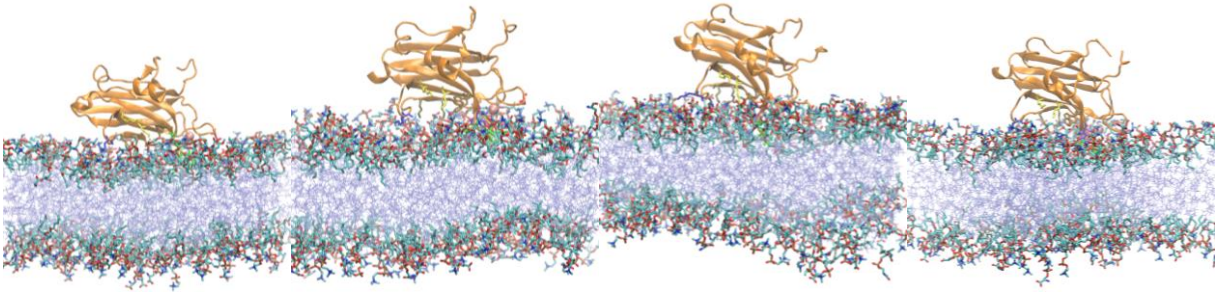

per1_N3

t = 10 ns t = 20 ns t = 30 ns t = 40 ns

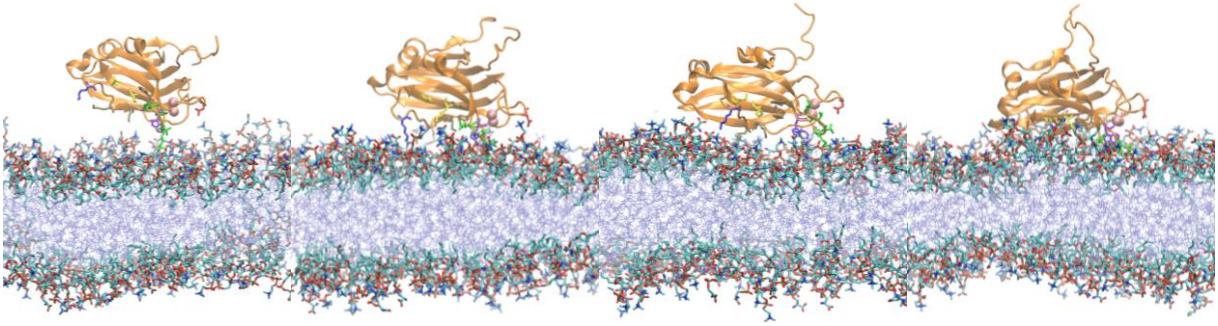

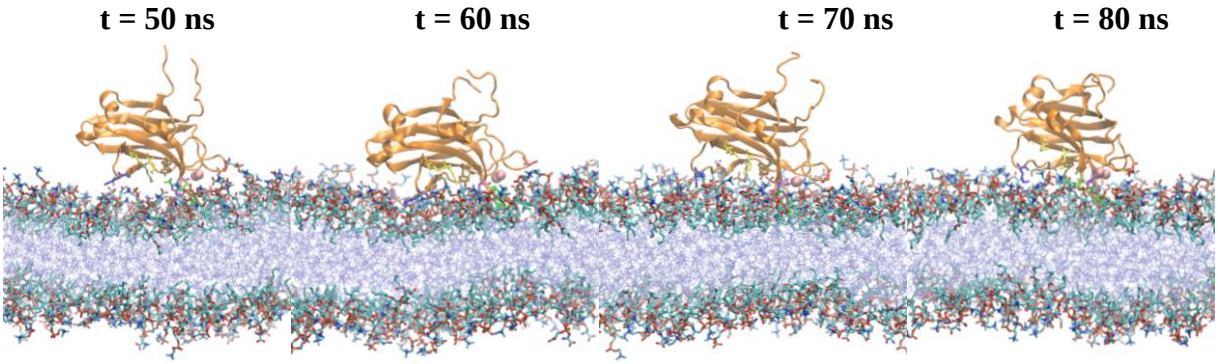
t = 50 ns
t = 60 ns
t = 70 ns
t = 80 ns

per1_N4

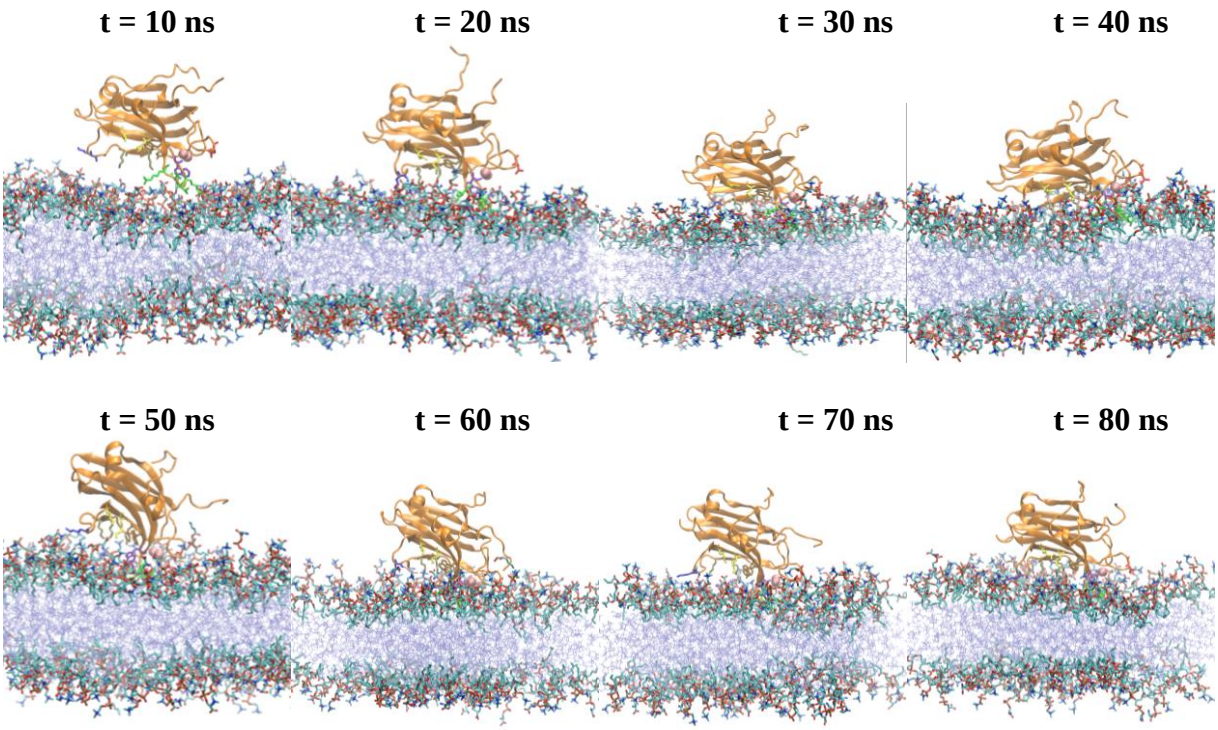
t = 10 ns
t = 20 ns
t = 30 ns
t = 40 ns
t = 50 ns
t = 60 ns
t = 70 ns
t = 80 ns

per1_N5

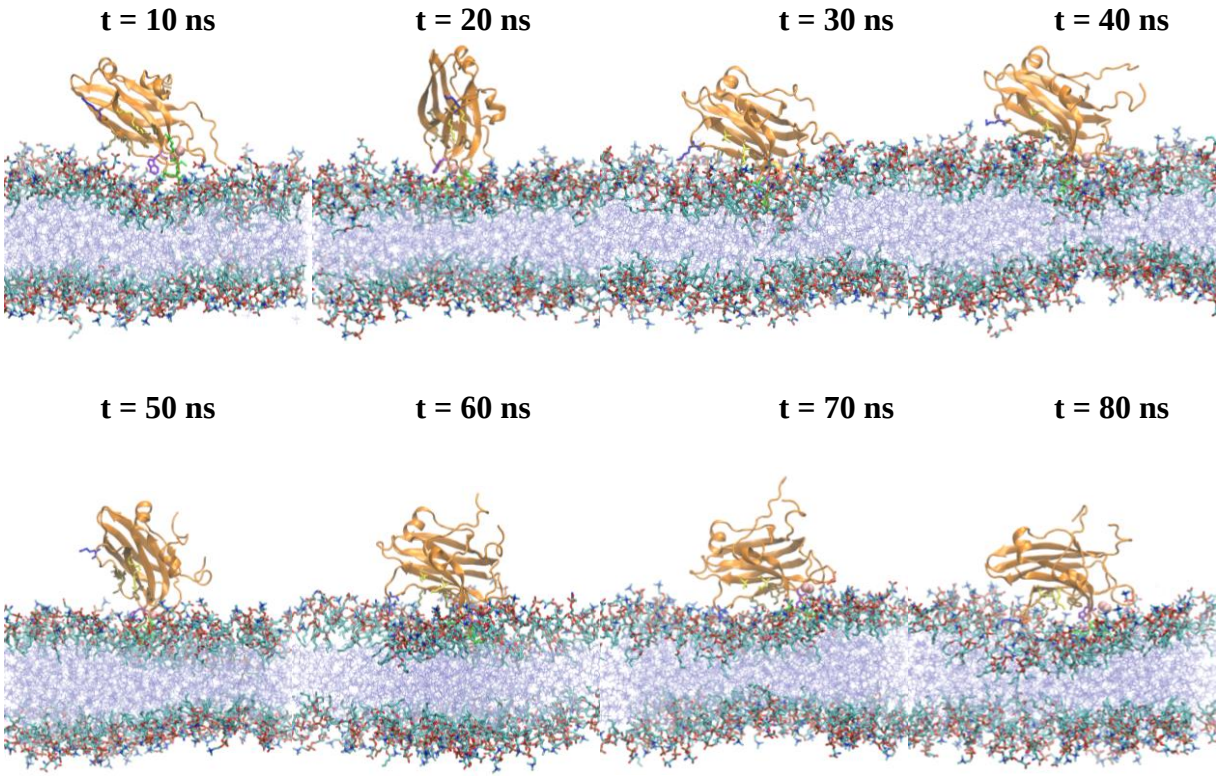

Figure 35: Time series snapshots for HMMM model per1 case
Starting at top left, snapshots from 10 ns to 80 ns with the interval of 10 ns are shown for all five runs for per1 case. The short-tail lipids are in licorice representation. Inner core of the HMMM model system as represented by Dichloroethane (DCE) is shown in iceblue color. Color code for the protein and its residues is same as that in Figure 11. Water and ions are not shown for clarity.

per1 (N1 – N5)

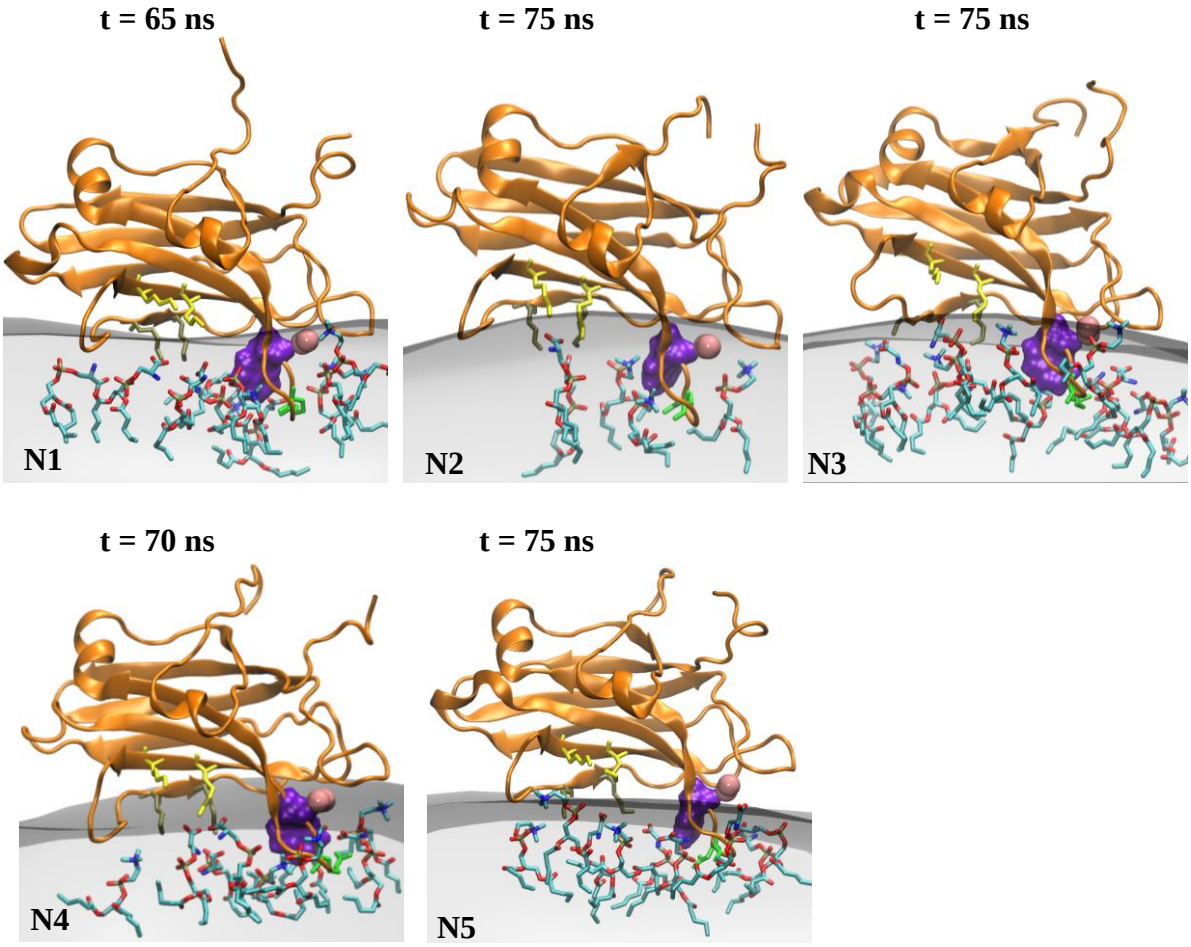

Figure 36: Open faced configuration for HMMM model per1
Close-up snapshots of membrane bound configuration of per1 HMMM model systems. The system representation (draw method, color): Membrane (quicksurf, grey); PKCα-C2 domain (secondary structure, gold); R249 (licorice, green); β3 (licorice, yellow); β4 (licorice, brown) and W247 (surf, violet); Ca^{2+} ions (VDW, pink). PC/ PS short-tail lipids in CPK representation are also shown as within 6 Å of R249, β3 (K197, K199), β4 (K209, K211), W247 and Ca^{2+} ions.

per2_N1

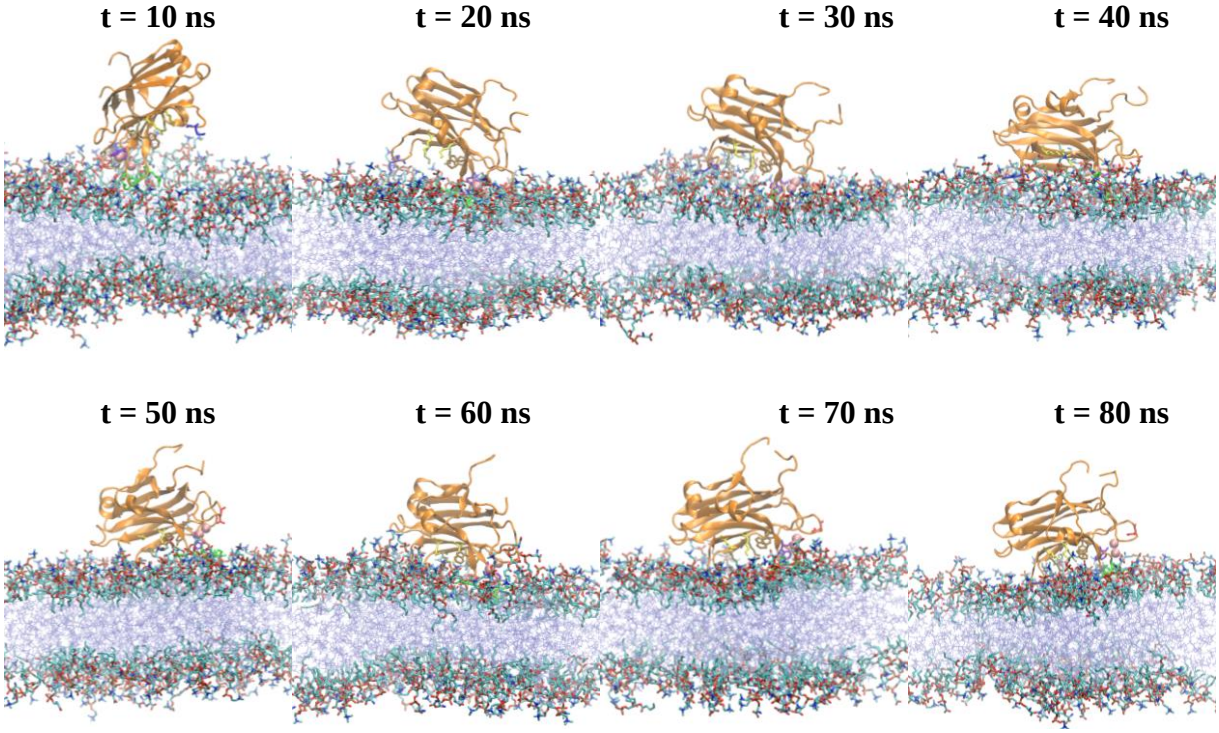

per2_N2

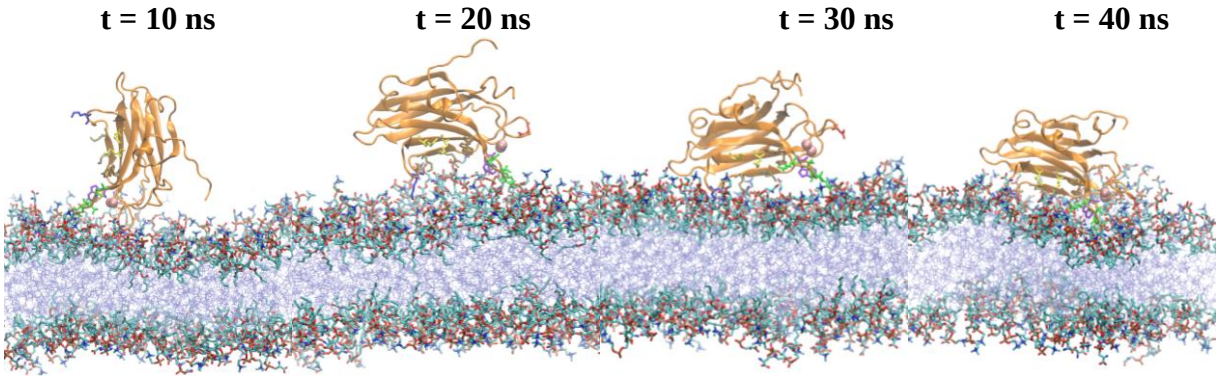

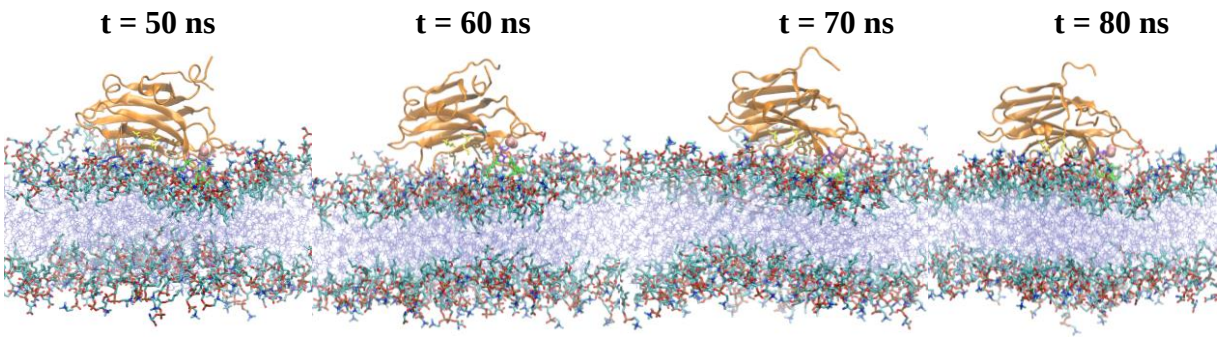
t = 50 ns
t = 60 ns
t = 70 ns
t = 80 ns

per2_N3

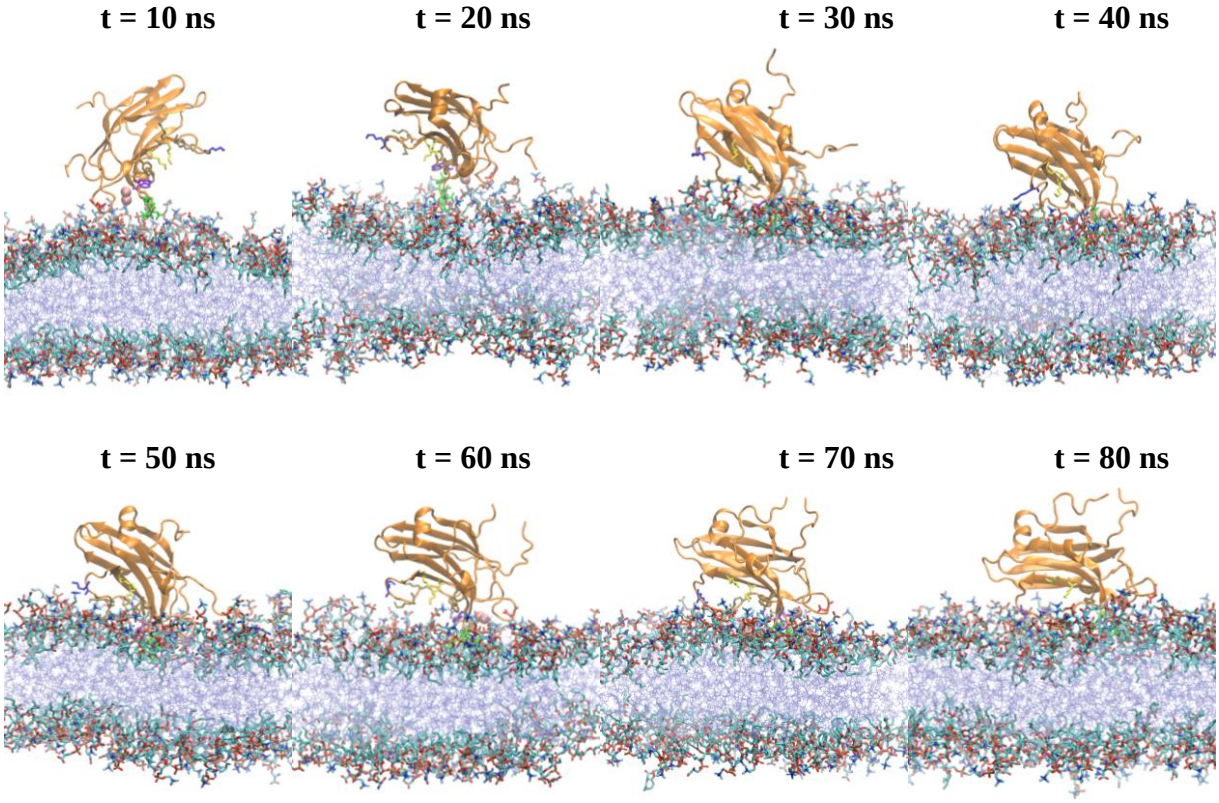
t = 10 ns
t = 20 ns
t = 30 ns
t = 40 ns
t = 50 ns
t = 60 ns
t = 70 ns
t = 80 ns

per2_N4

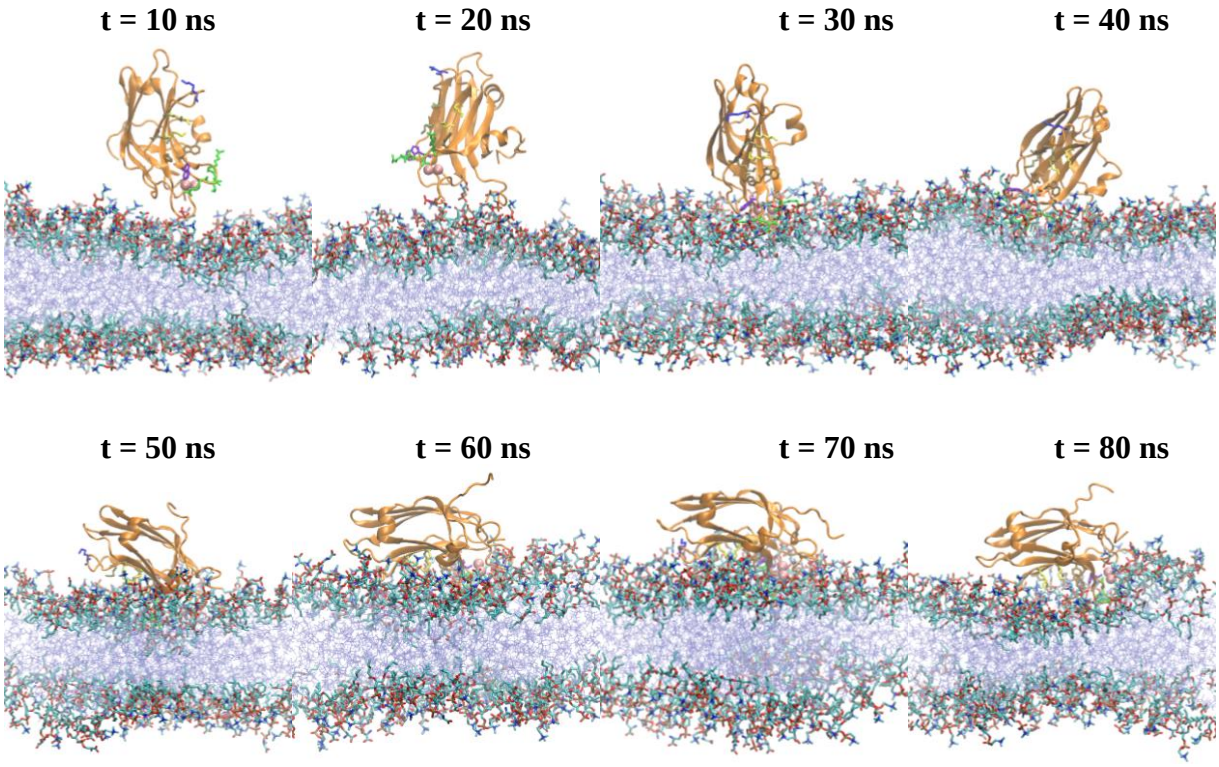

per2_N5

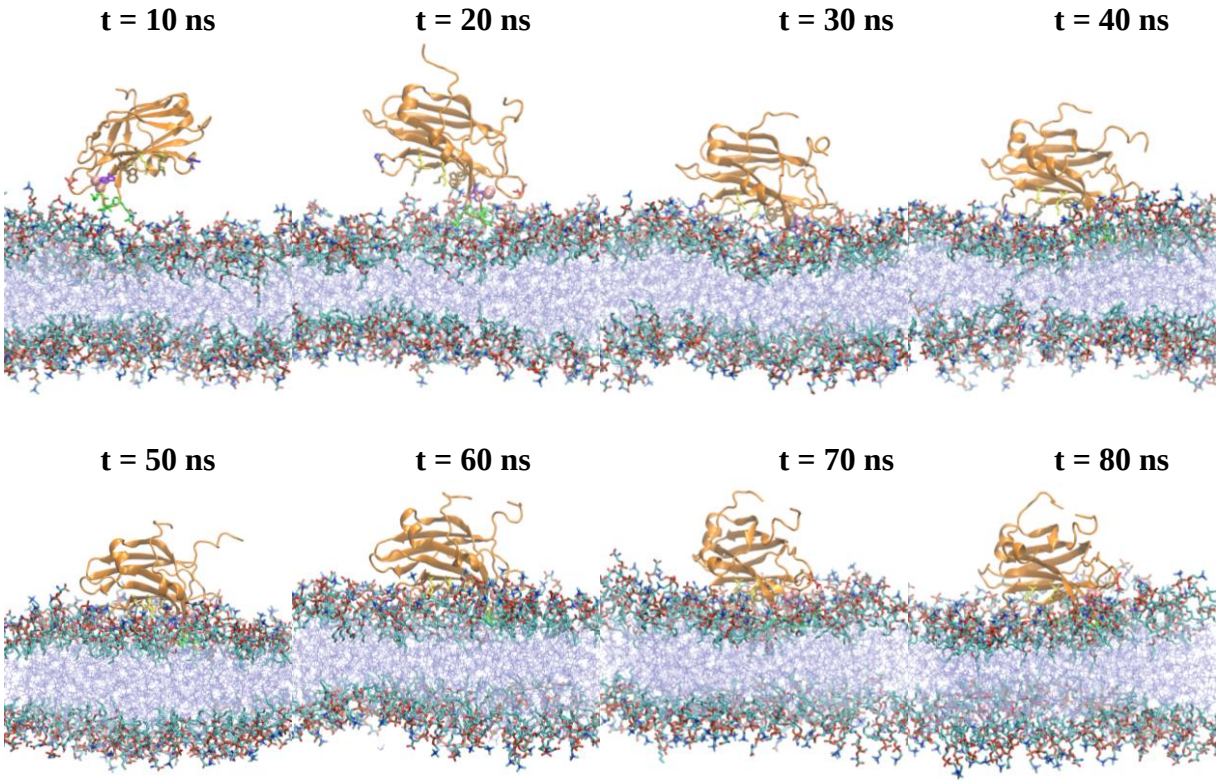

Figure 37: Time series snapshots for HMMM model per2 case
Starting at top left, snapshots from 10 ns to 80 ns with the interval of 10 ns are shown for all five runs for per2 case. The short-tail lipids are in licorice representation. Inner core of the HMMM model system as represented by Dichloroethane (DCE) is shown in iceblue color. Color code for the protein and its residues is same as that in Figure 11. Water and ions are not shown for clarity.

per2 (N1 – N5)

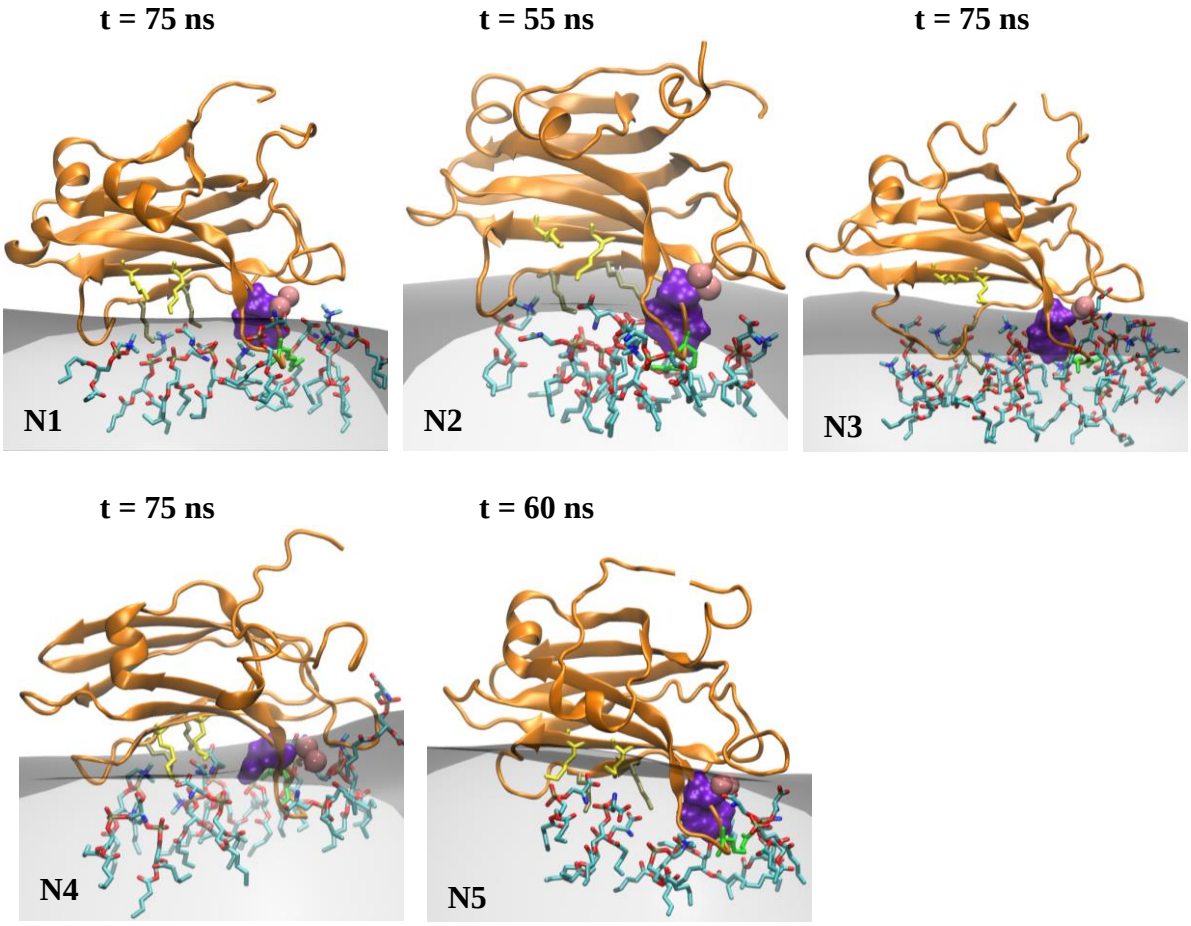

Figure 38: Open faced configuration for HMMM model per2
Close-up snapshots of membrane bound configuration of per2 HMMM model systems. The system representation (draw method, color): Membrane (quicksurf, grey); PKCα-C2 domain (secondary structure, gold); R249 (licorice, green); β3 (licorice, yellow); β4 (licorice, brown) and W247 (surf, violet); Ca^{2+} ions (VDW, pink). PC/ PS short-tail lipids in CPK representation are also shown as within 6 Å of R249, β3 (K197, K199), β4 (K209, K211), W247 and Ca^{2+} ions.

tilt_N1

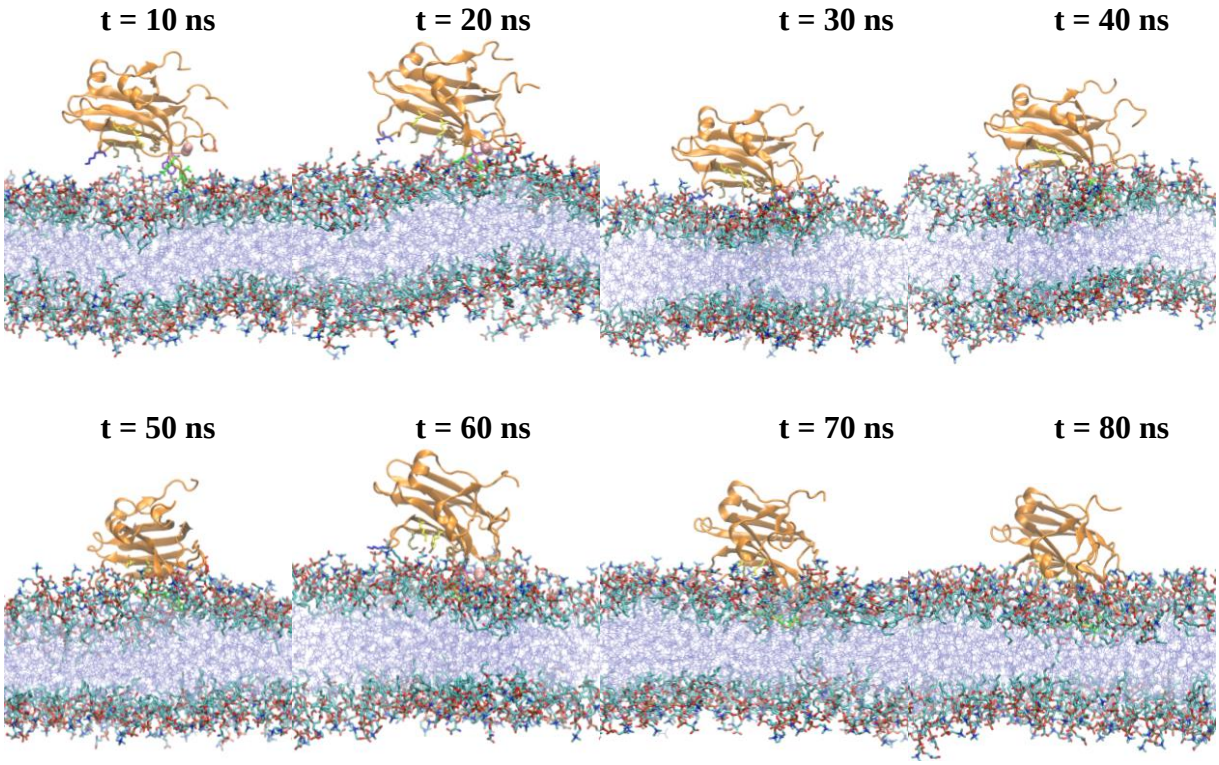

tilt_N2

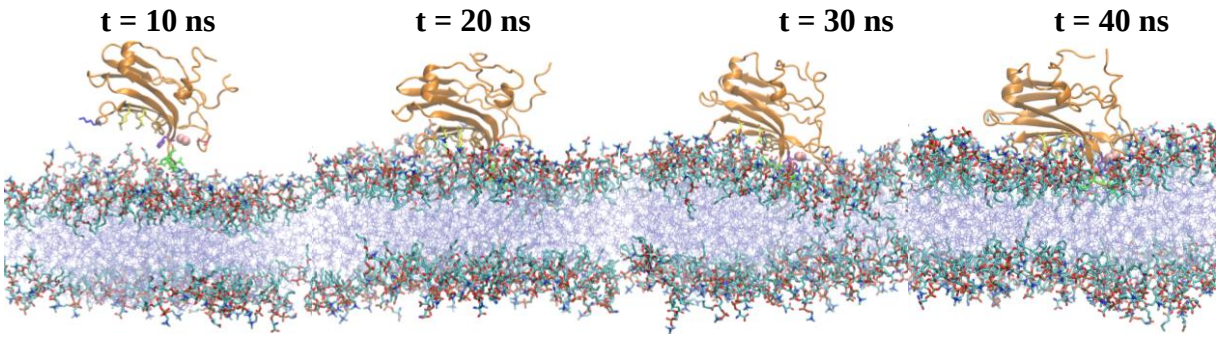

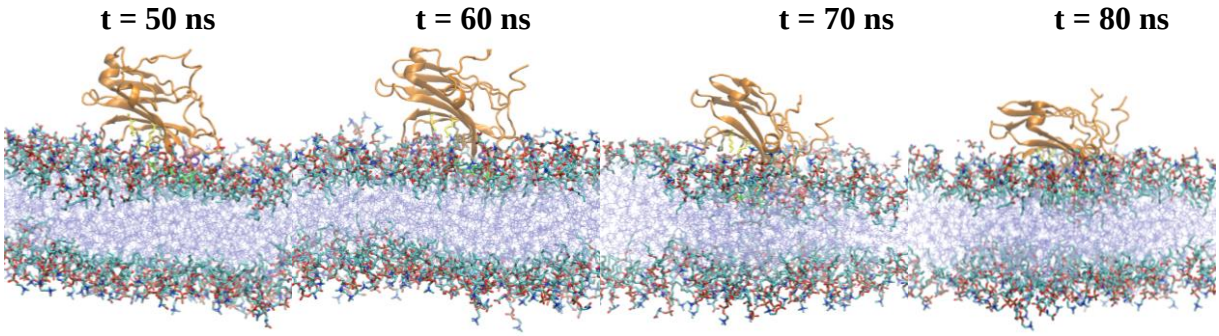
t = 50 ns
t = 60 ns
t = 70 ns
t = 80 ns

tilt_N3

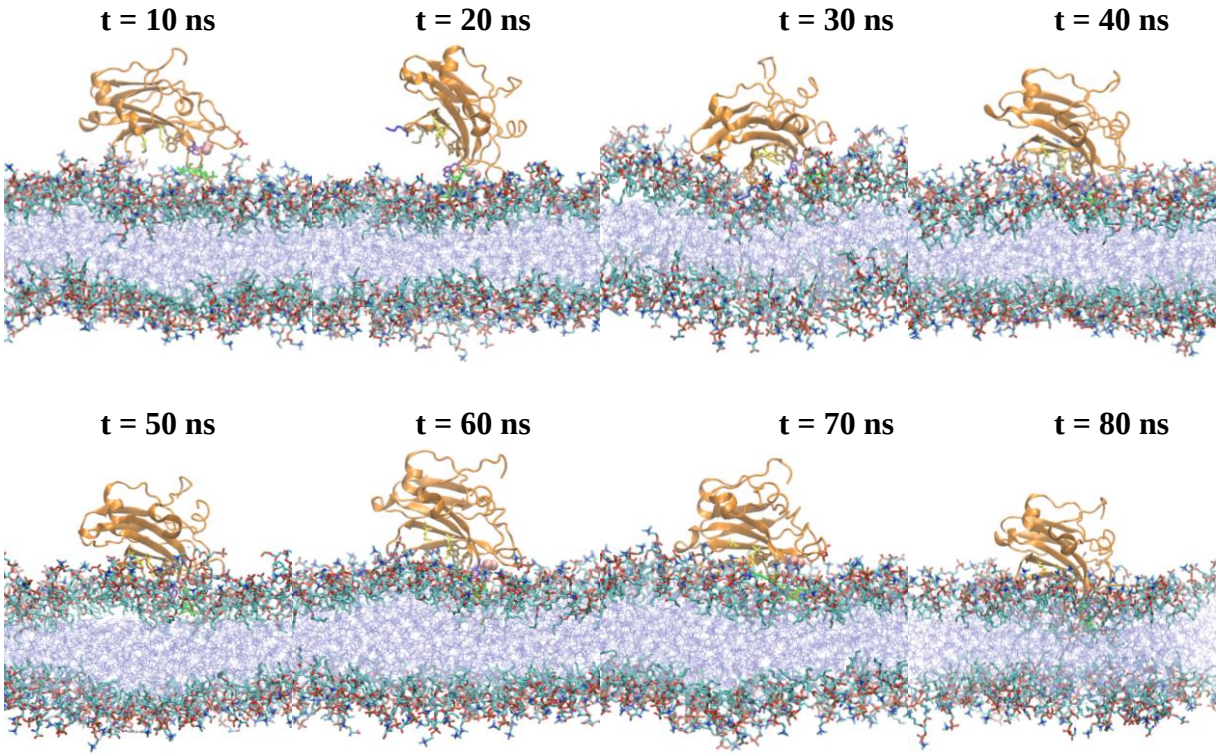
t = 10 ns
t = 20 ns
t = 30 ns
t = 40 ns
t = 50 ns
t = 60 ns
t = 70 ns
t = 80 ns

tilt_N4

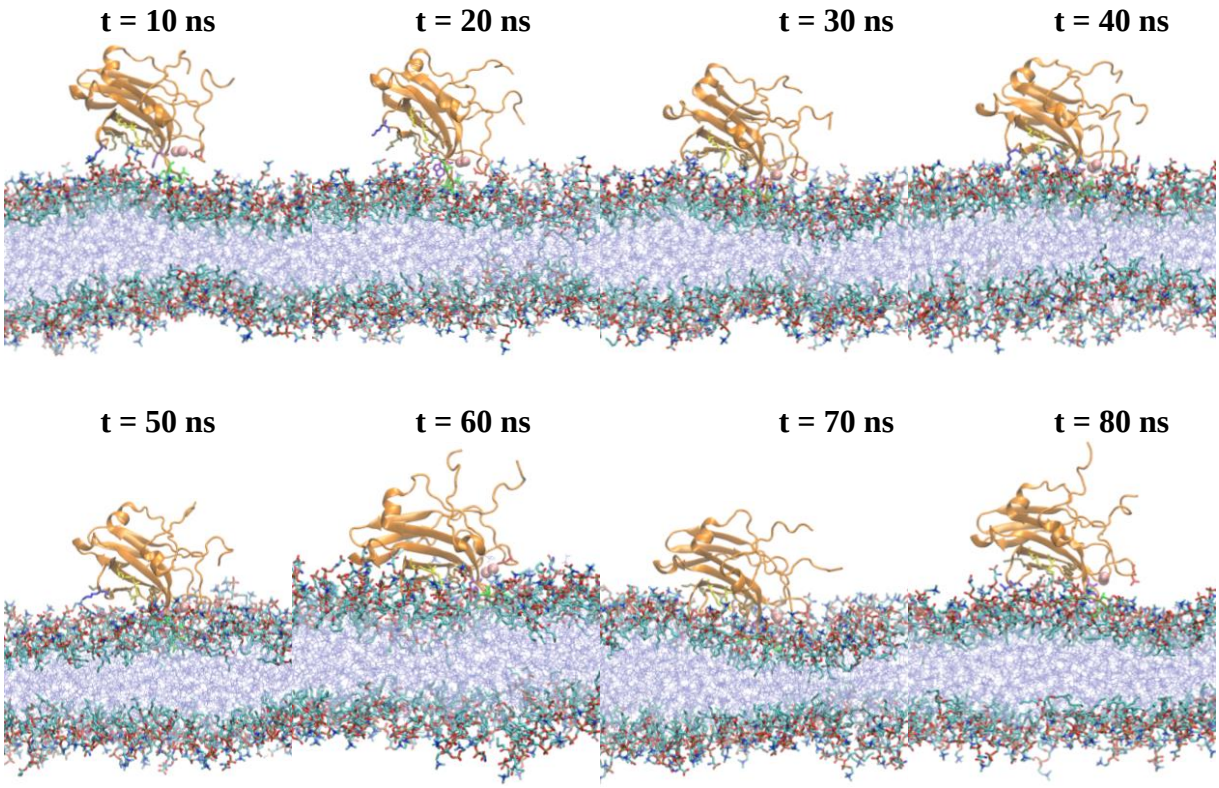

tilt_N5

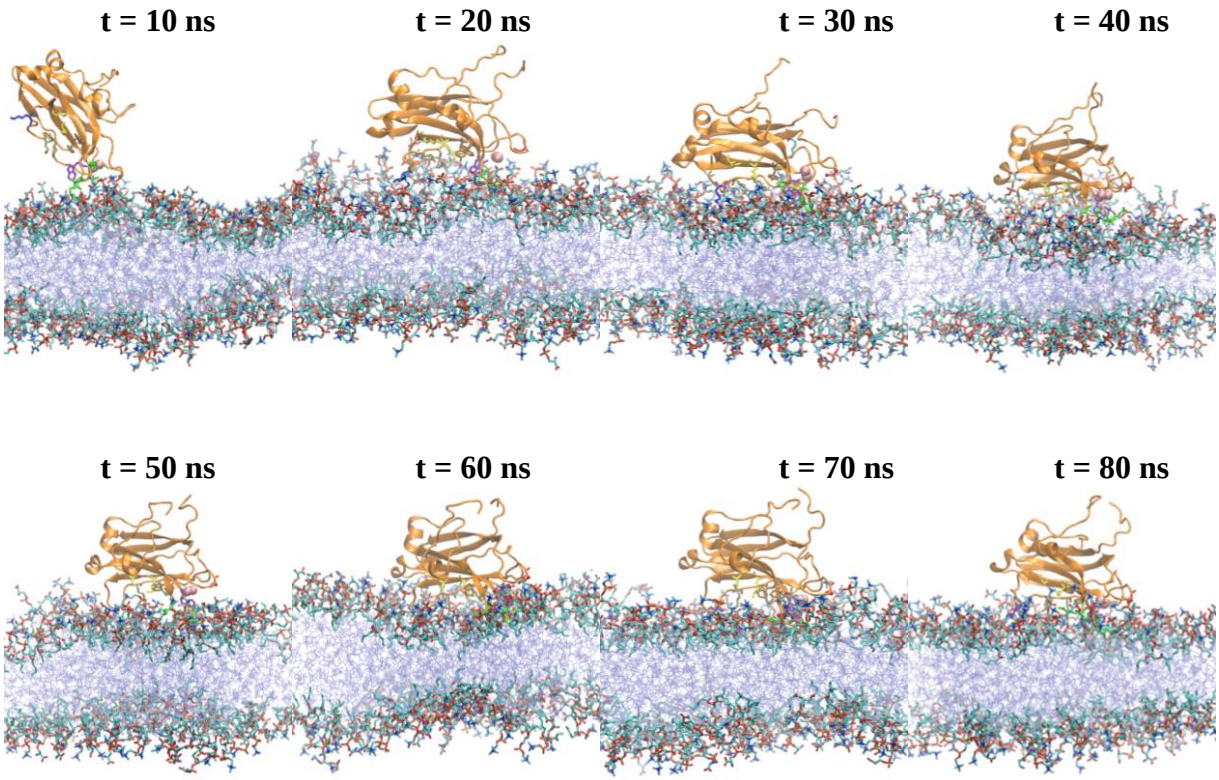

Figure 39: Time series snapshots for HMMM model tilt case
Starting at top left, snapshots from 10 ns to 80 ns with the interval of 10 ns are shown for all five runs for tilt case. The short-tail lipids are in licorice representation. Inner core of the HMMM model system as represented by Dichloroethane (DCE) is shown in iceblue color. Color code for the protein and its residues is same as that in Figure 11. Water and ions are not shown for clarity.

tilt (N1 – N5)

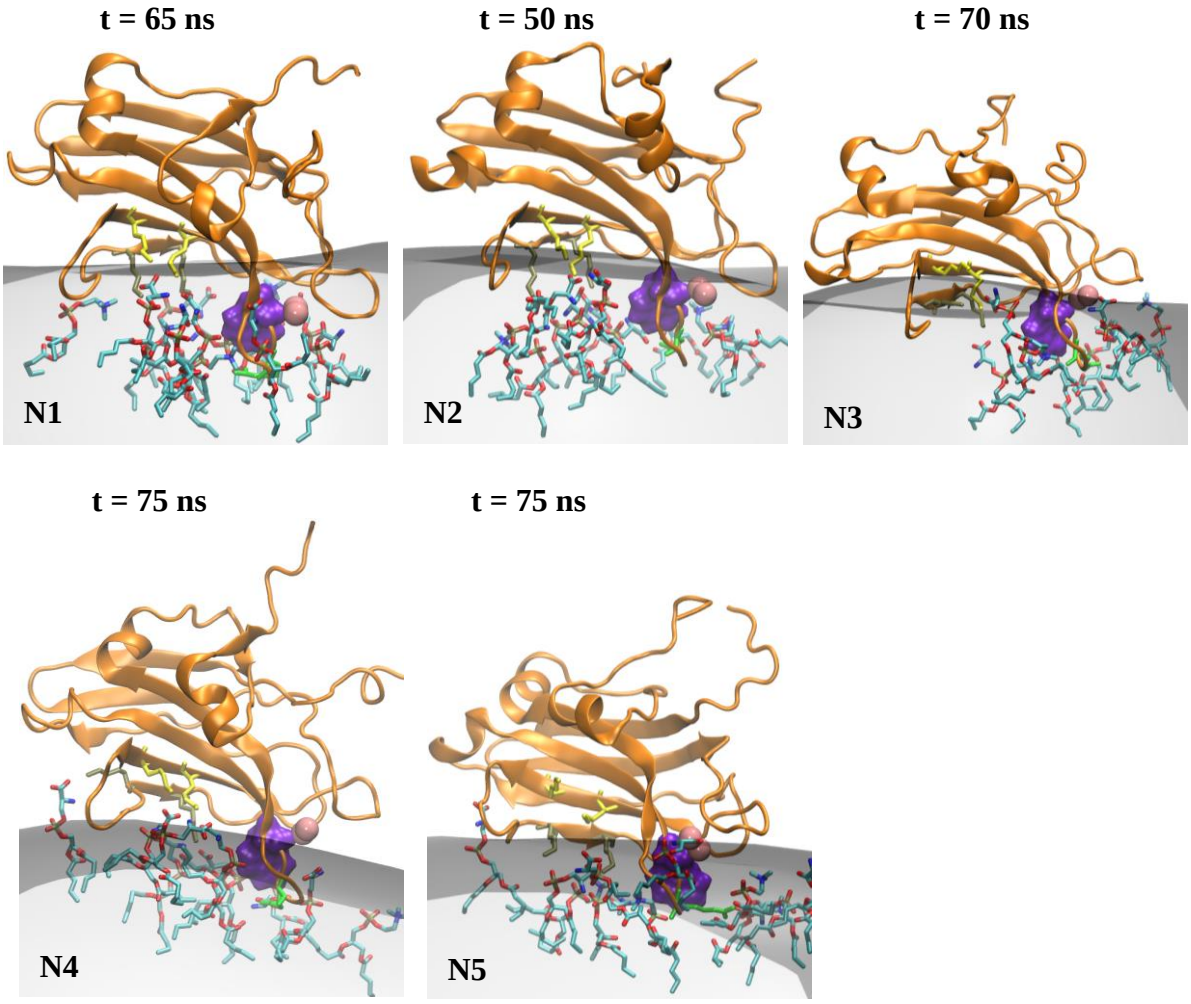

Figure 40: Open faced configuration for HMMM model tilt
Close-up snapshots of membrane bound configuration of tilt HMMM model systems. The system representation (draw method, color): Membrane (quicksurf, grey); PKCα-C2 domain (secondary structure, gold); R249 (licorice, green); β3 (licorice, yellow); β4 (licorice, brown) and W247 (surf, violet); Ca^{2+} ions (VDW, pink). PC/ PS short-tail lipids in CPK representation are also shown as within 6 Å of R249, β3 (K197, K199), β4 (K209, K211), W247 and Ca^{2+} ions.

3.4.4 Role of Ca^{2+} Ion

Ca^{2+} ions have a mean value d_{min} of ~ 5 Å, ~ 3 Å and ~ 3.5 Å for per1, per2 and tilt systems, respectively (**TABLE 3**). Generally, the ions fluctuate within 3 to 6 Å, though occasionally Ca^{2+} ions are within ~ 2 Å of COO^- (see the brown, violet, magenta, indigo and turquoise data curves in (Figure 25C). The location of Ca^{2+} ions and negative moieties interactions can be disturbed even after remaining at a well defined distance for more than 10 ns (see grey and blue curves in Figure 25C). In the per2_FM and tilt_FM simulations, this disturbance can occur even after more than 100 ns of steady state positioning (black curves in Figure 29). In the anisotropic environment, the number of direct contacts, N_c, for Ca^{2+} ions increases by more than 50% when there is an increase in the interaction defining length by 1 Å (i.e., from 6 Å to 7 Å) (**TABLE 4**). The range of interaction of Ca^{2+} ions seems to be substantial. Ca^{2+} ions are coordinated by five aspartic acid residues: D187, D193 from loop 1 and D246, D248, D254 from loop 3. Loop 3 binds stably early in the simulation (Figure 25B), but loop 1 has random fluctuations (Figure 25A and red curve in Figure 29) throughout the simulation. In general, Ca^{2+} ions appear to follow the fluctuations of loop 1 (Figure 26 – 29) for long periods of time, attaining a steady state position only after disengaging from loop 1.

Moreover, the number of direct contacts, N_c, for HMMM model systems, shows that Ca^{2+} ions interact similarly with oxygen-atoms of PO_4^- and COO^- moieties (Figure 41 – 43).

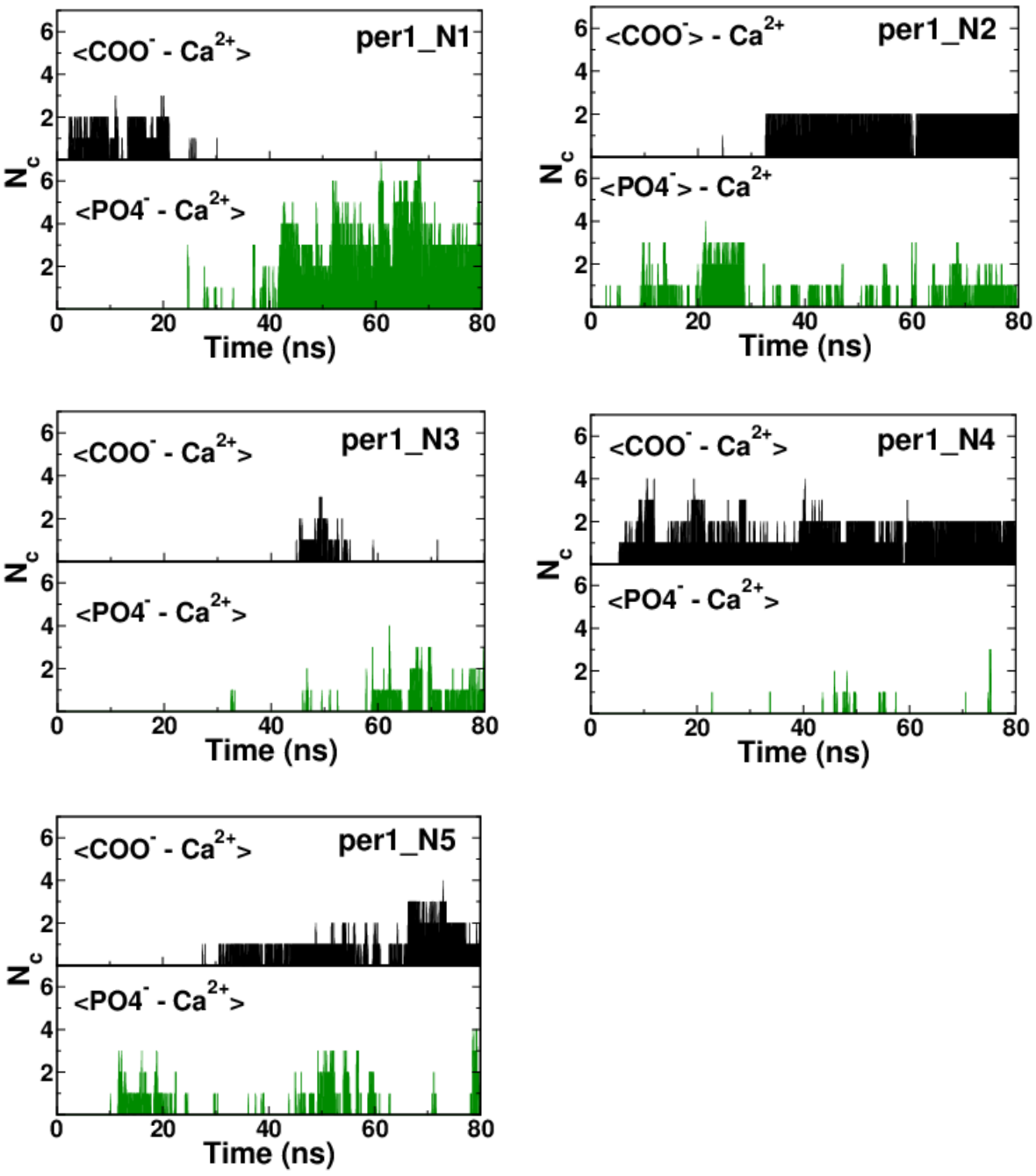

Figure 41: Number of contacts, N_c, of set 2 groups for HMMM model per1 N_c between Ca^{2+} ions and oxygen-atoms of PO_4^- or COO^- moieties. <COO^-> and <$PO4^-$> represents oxygen-atoms for respective systems.

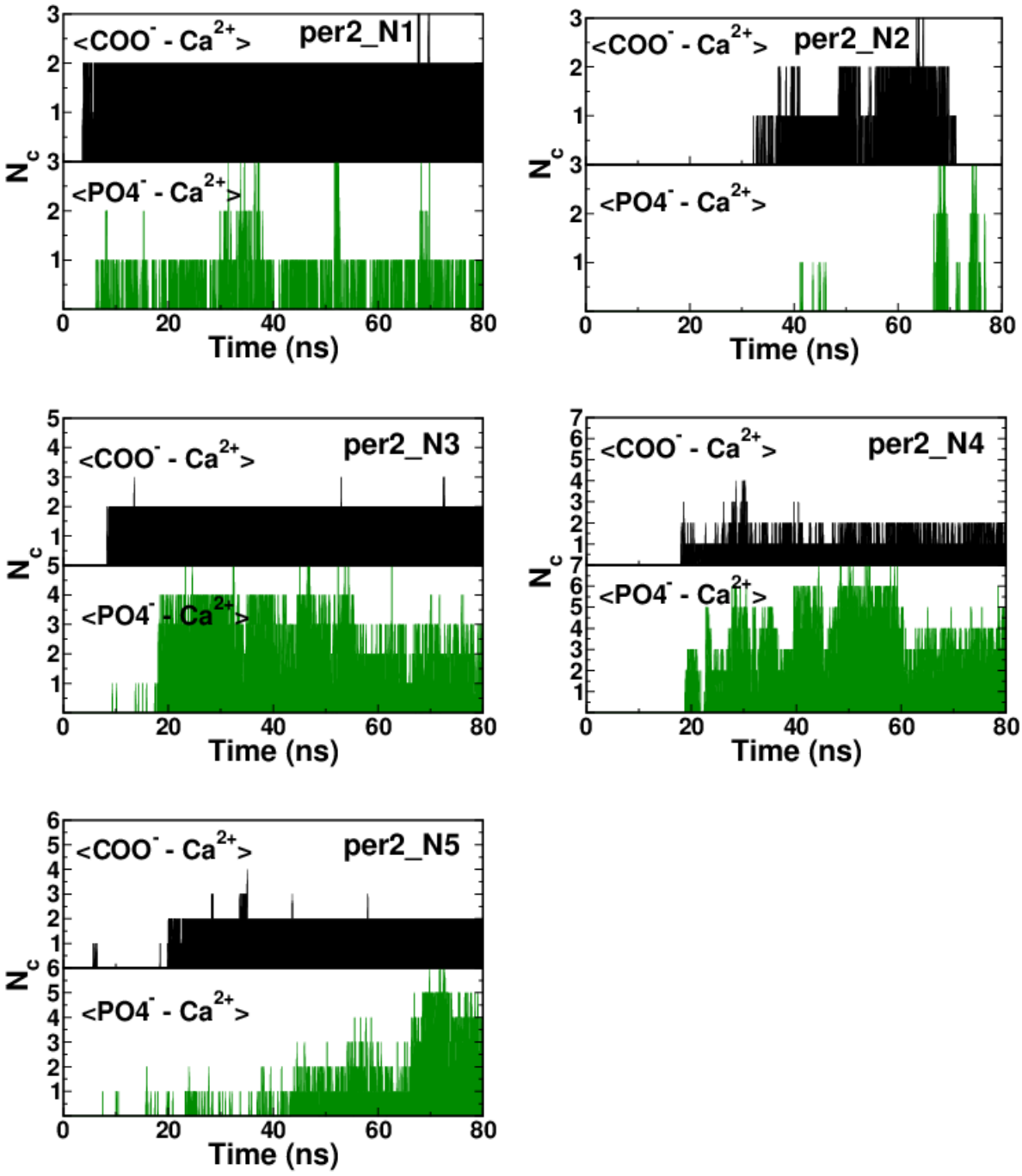

Figure 42: Number of contacts, N_c, of set 2 groups for HMMM model per2 N_c between Ca^{2+} ions and oxygen-atoms of PO_4^- or COO^- moieties. <COO^-> and <$PO4^-$> represents oxygen-atoms for respective systems.

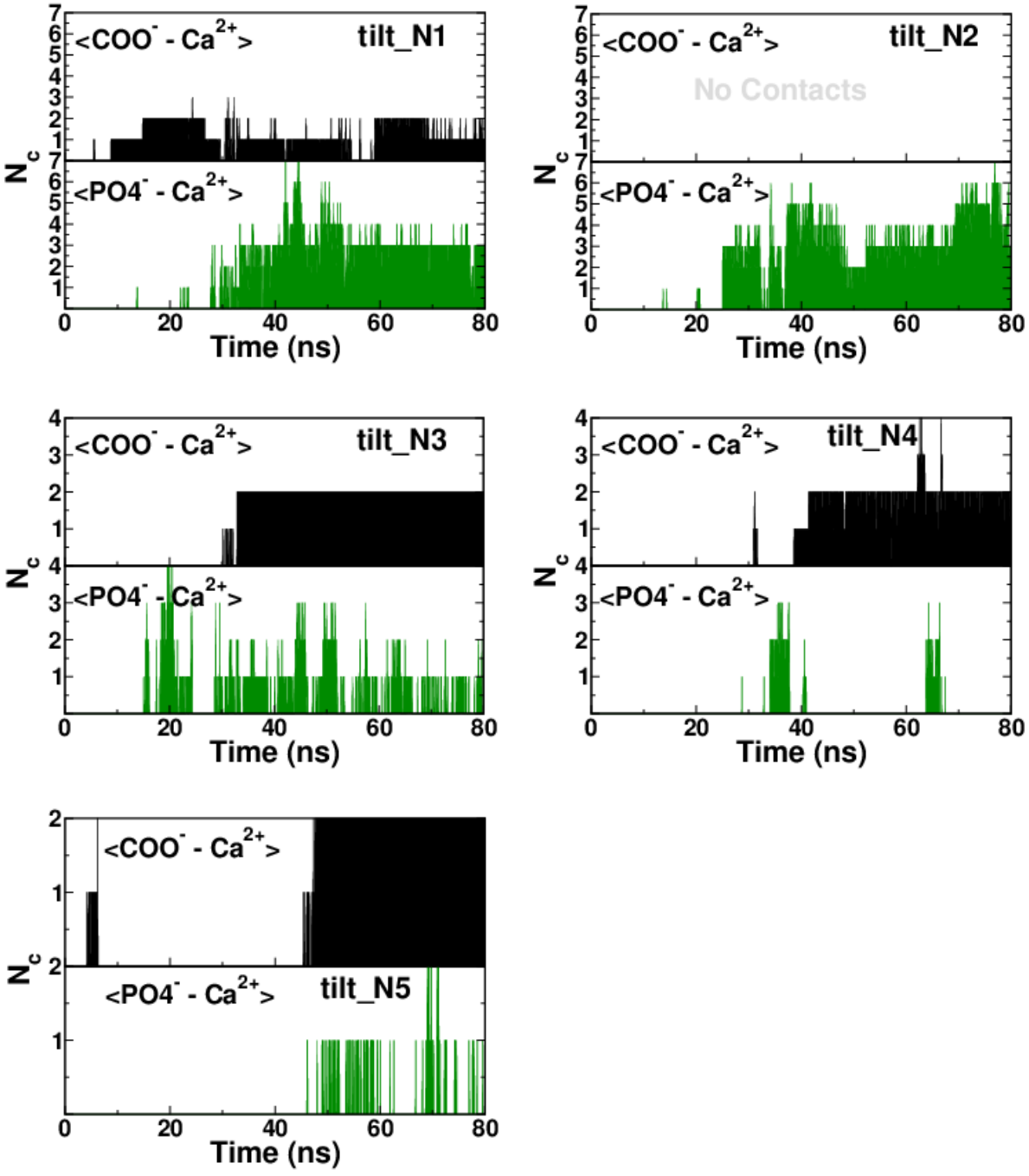

Figure 43: Number of contacts, N_c, of set 2 groups for HMMM model tilt
N_c between Ca^{2+} ions and oxygen-atoms of PO_4^- or COO^- moieties. <COO^->
and <$PO4^-$> represents oxygen-atoms for respective systems.

Ca^{2+} ions interact with the oxygen atoms, which are negatively charged, not with C or P, which have partial positive charge. Calculations of direct contacts (within 6 Å) show that Ca^{2+} ions are closer to C-atoms of COO^- than to P-atoms of PO_4^- (Figure 44 – 46). This shows that Ca^{2+} ions are bound to the membrane, but do not penetrate far inside the membrane. This is further evident from the $h_r(z)$ (Figure 21D) where Ca^{2+} ions mostly remain at the membrane surface near the C-atom plane of COO^-.

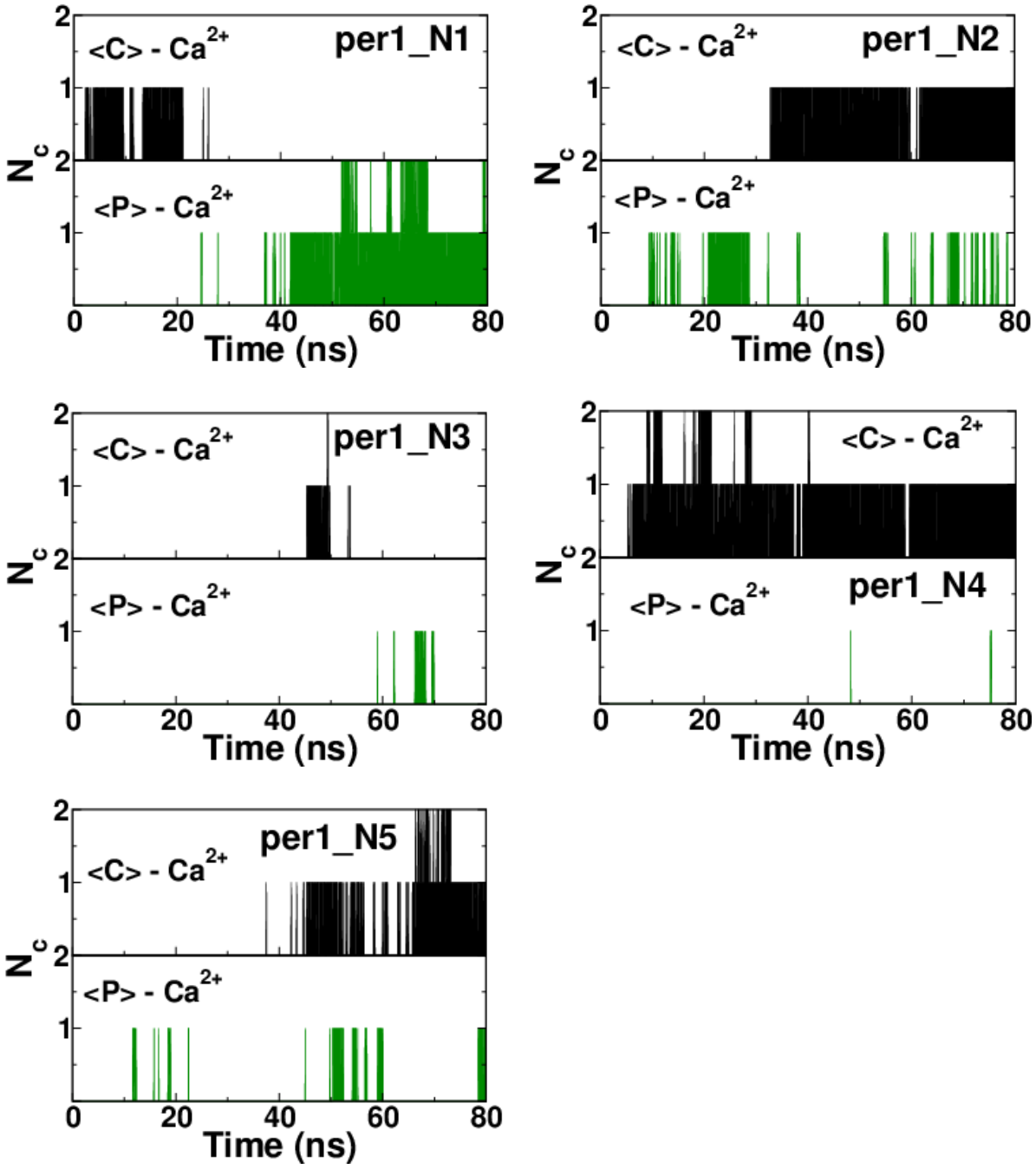

Figure 44: Number of contacts, N_c, of set 3 groups for HMMM model per1
N_c between Ca^{2+} ions and P-atoms of PO_4^- moieties (represented as <P>) and C-atoms of COO^- moieties (represented as <C>).

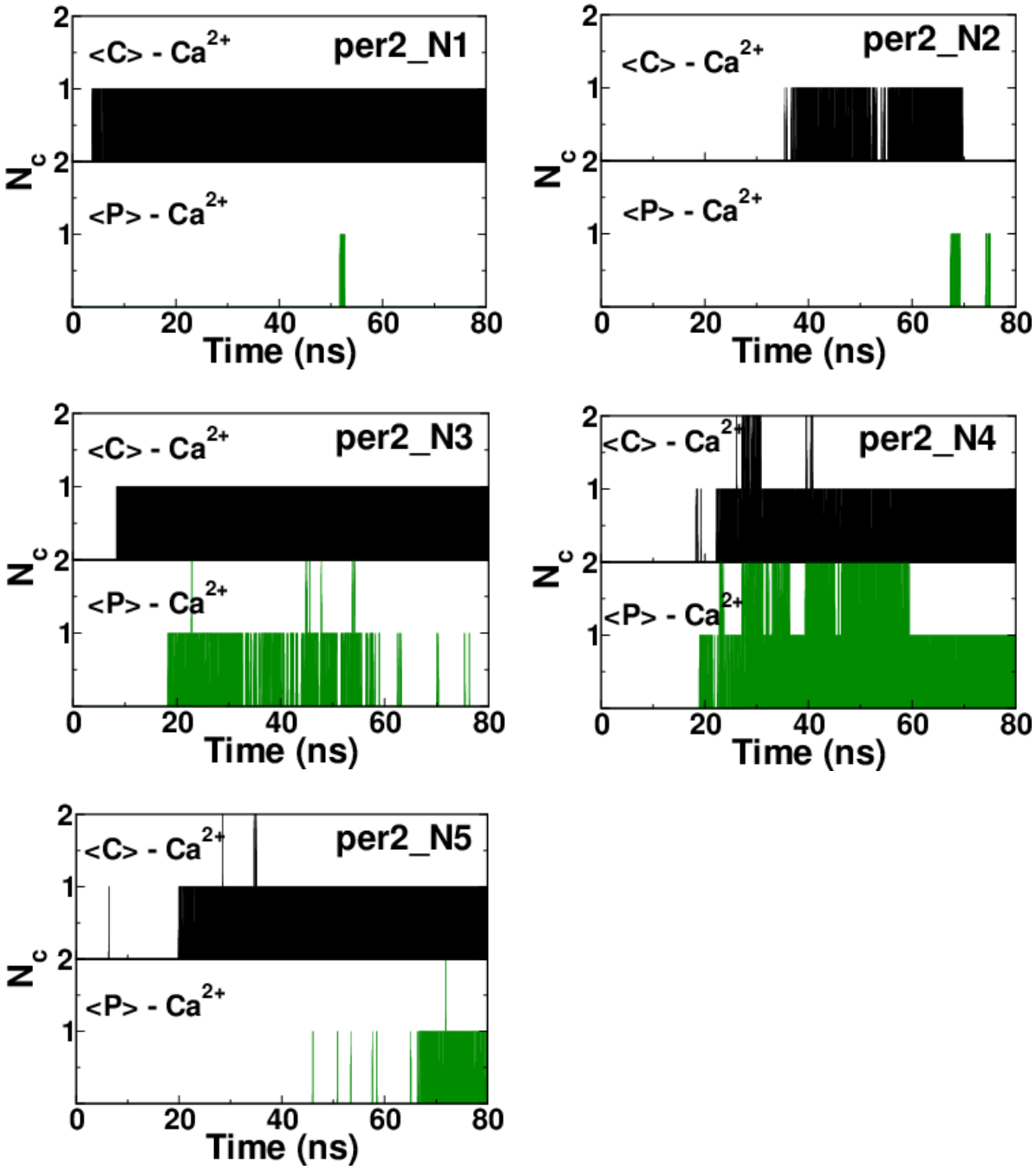

Figure 45: Number of contacts, N_c, of set 3 groups for HMMM model per2 N_c between Ca^{2+} ions and P-atoms of PO_4^- moieties (represented as <P>) and C-atoms of COO^- moieties (represented as <C>).

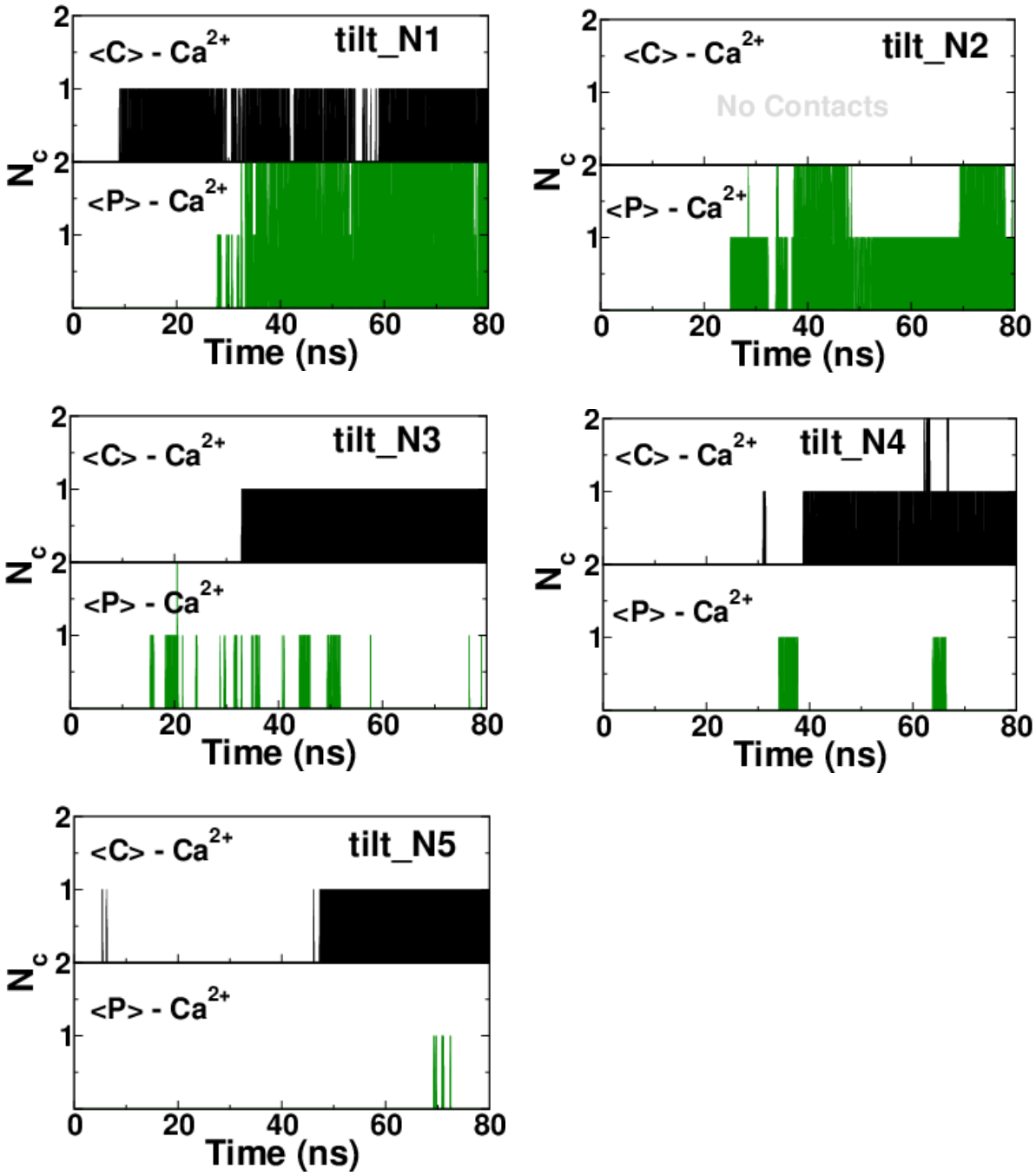

Figure 46: Number of contacts, N_c, of set 3 groups for HMMM model tilt
N_c between Ca^{2+} ions and P-atoms of PO_4^- moieties (represented as <P>) and C-atoms of COO^- moieties (represented as <C>).

To further determine the role of Ca^{2+} ions, the root mean square deviation (RMSD) from the crystal structure (PDB ID: 1DSY) of the PKCα-C2 domain with and without Ca^{2+} ions in bulk water is calculated (Figure 47 and **TABLE 6**).

.

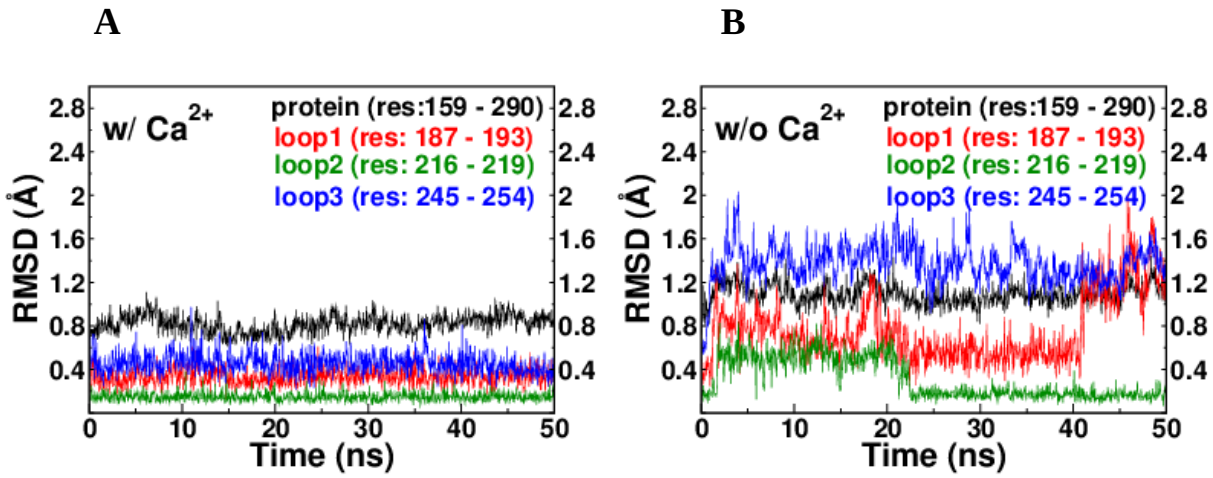

Figure 47: RMSD for in solution PKCα-C2 with and without Ca^{2+} ions
Root mean square deviation (RMSD) of the in solution protein (black) and its loop1 (red), loop2 (green4) and loop3 (blue) with Ca^{2+} ions (A) and without Ca^{2+} ions (B). The reference structure for the RMSD is taken as the minimized structure of the PKCα-C2 domain.

TABLE 6 Mean RMSD for protein in solution
Mean (with standard deviation in parenthesis) root mean square deviation (RMSD) for in solution PKCα-C2 domain with and without Ca^{2+} ions.

PKCα-C2 (Residues)	**RMSD (Å)**	
	w/ Ca^{2+} ions	w/o C^{2+} ions
Protein (159 - 290)	0.82 (0.09)	1.09 (0.10)
loop1 (187 - 193)	0.33 (0.08)	0.76 (0.30)
loop2 (216 - 219)	0.15 (0.04)	0.31 (0.19)
loop3 (245 - 254)	0.46 (0.10)	1.37 (0.18)

The RMSD values increase by ~ 50% when Ca^{2+} ions are absent, which shows that Ca^{2+} ions stabilize the conformation of the CBLs. Ca^{2+} ions are embedded deep inside the CBLs groove and not directly accessible to lipid headgroups except through long range electrostatic interactions.

Furthermore, in another HMMM model, noCAL_per1 system (Section 3.2.4), where we have removed the bound Ca^{2+} ions from the beginning, the RMSD for the protein and its three loops are shown in Figure 48.

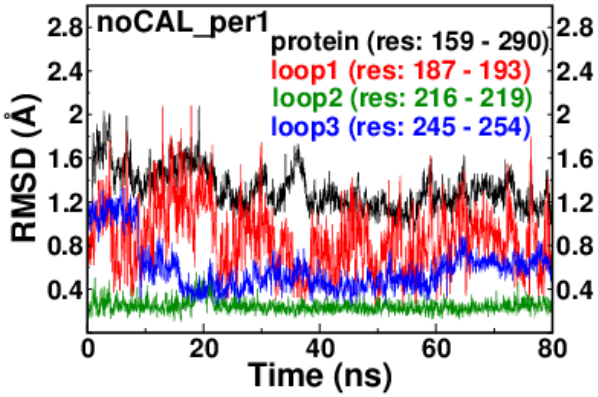

Figure 48: RMSD of HMMM model noCAL_per1 system
Root mean square deviation (RMSD) of the protein (black) and its loop1 (red), loop2 (green4) and loop3 (blue) without Ca^{2+} ions for a HMMM model system. The reference structure for the RMSD is taken as the minimized structure of the PKCα-C2 domain.

In noCAL_per1 system, the absence of the Ca^{2+} ions makes loop 1 fluctuate wildly. Moreover, the RMSD values of the protein (~ 1.1 Å) and loop 2 (~ 0.2 Å) match the simulation of PKCα-C2 domain in bulk water without Ca^{2+} ions (Figure 47B). Also, the pattern is very similar for loop 3 for the two systems without Ca^{2+} ions though the value of the RMSD for loop 3 is higher in bulk water (~ 1.4 Å) than in the noCAL_per1 HMMM model system (~ 0.6 Å). The smaller

value of the loop 3 RMSD can be attributed to its interaction with the membrane in noCAL_per1. These results show that Ca^{2+} ions stabilize the loops.

Furthermore, for noCAL_per1 HMMM model system, the angle θ_1, $h_r(z)$, d_{min} and N_c (Figure 49A-D) and the time series of the snapshots (Figure 50) show that the dynamical behavior and configuration of the domain match very well with N = 15 HMMM model systems that include Ca^{2+} ions (Figure 20C, Figure 22, Figure 26, Figure 32 and Figure 35).

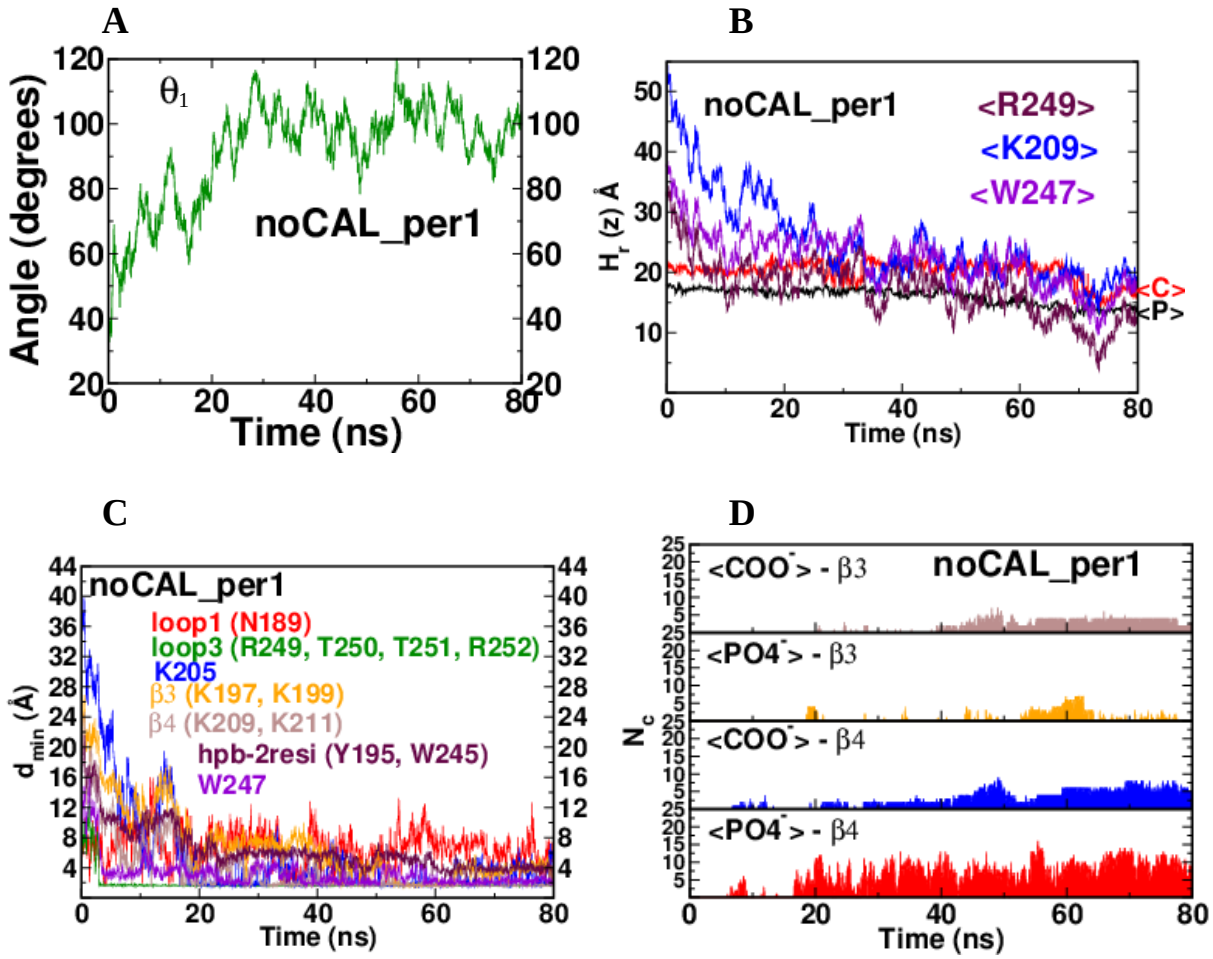

Figure 49: Bound configuration defining quantities for noCAL_per1 system (A) The angle θ_1, (B) the relative heights $h_r(z)$, (C) the minimum distance d_{min} and (D) the number of direct contacts N_c for noCAL_per1 system. All these values match very well with HMMM model per1, per2 and tilt case results.

noCAL_per1

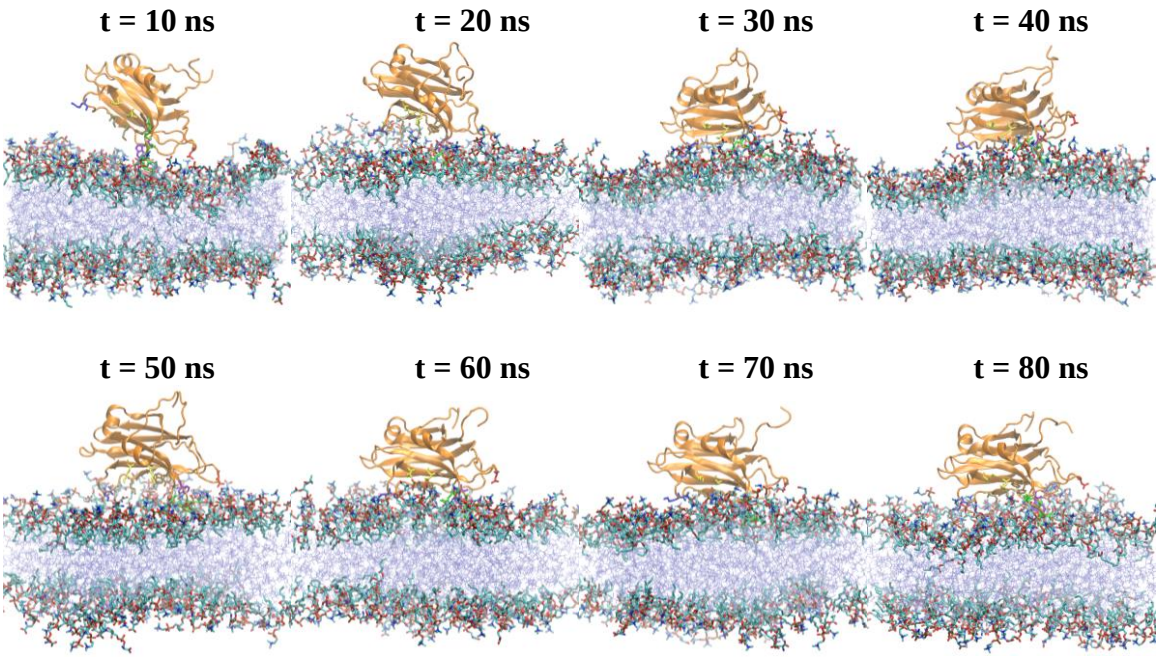

Figure 50: Time series snapshots for noCAL_per1 HMMM model system
Starting at top left, snapshots from 10 ns to 80 ns with the interval of 10 ns are shown for all five runs for noCAL_per1 system. The short-tail lipids are in licorice representation. Inner core of the HMMM model system as represented by DCE is shown in iceblue color. Color code for the protein and its residues is same as that in Figure 11. Water and ions are not shown for clarity.

This similarity between systems with and without Ca^{2+} ions suggests that Ca^{2+} ions are not critical to determining the membrane-bound configuration of PKCα-C2 domain.

3.4.5 Role of Y195 and W247

A hydrogen bond analysis (Figure 51) shows that -NH of W247 consistently forms H-bonds with PO_4^- and COO^- of the lipid membrane but the -OH of Y195 does not.

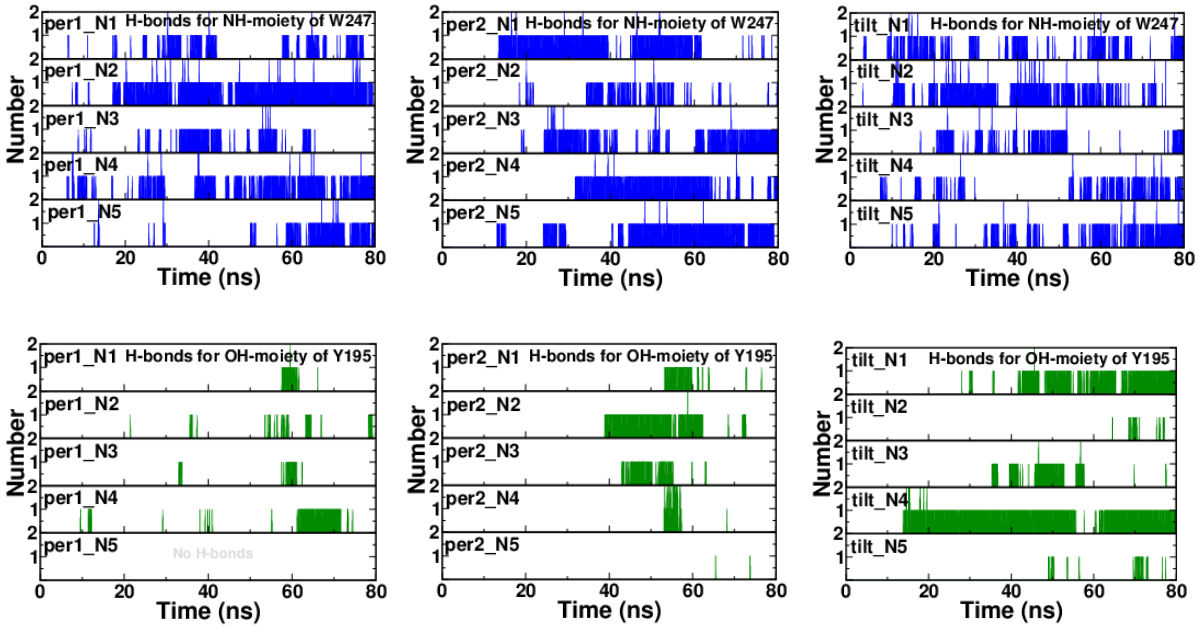

Figure 51: H-bonds for NH- W247 and OH- Y145
Hydrogen bonds for (top row): NH-moiety of W247 and (bottom row): OH-moiety of Y195 for all HMMM model systems. Left to right are per1, per2 and tilt cases.

Interestingly, Ca^{2+} ions and OH-moiety of Y195 [or hpb-2resi (Y195, W245)] have essentially the same mean values (within a standard deviation) for $d_{\min}$ (**TABLE 3**) and N_c (**TABLE 4**). This positions them on an approximate horizontal plane while bound to the membrane. The direct contacts between residue W247 and short-tail acyl chain plus DCE (Figure 52A-C, for HMMM model) and acyl chain (Figure 52D for FM model) shows the hydrophobic nature of the membrane binding. **TABLE 7** shows the mean values of the direct contacts for the

same in the HMMM and the FM models. The number of direct contacts are fairly consistent across per1, per2 and tilt cases in HMMM model. The per1_FM hardly has any direct contacts. The relatively higher number of direct contacts in HMMM model with respect to FM model (per2_FM, tilt_FM) could be attributed to the faster equilibration of HMMM model that facilities insertion of the proteins.

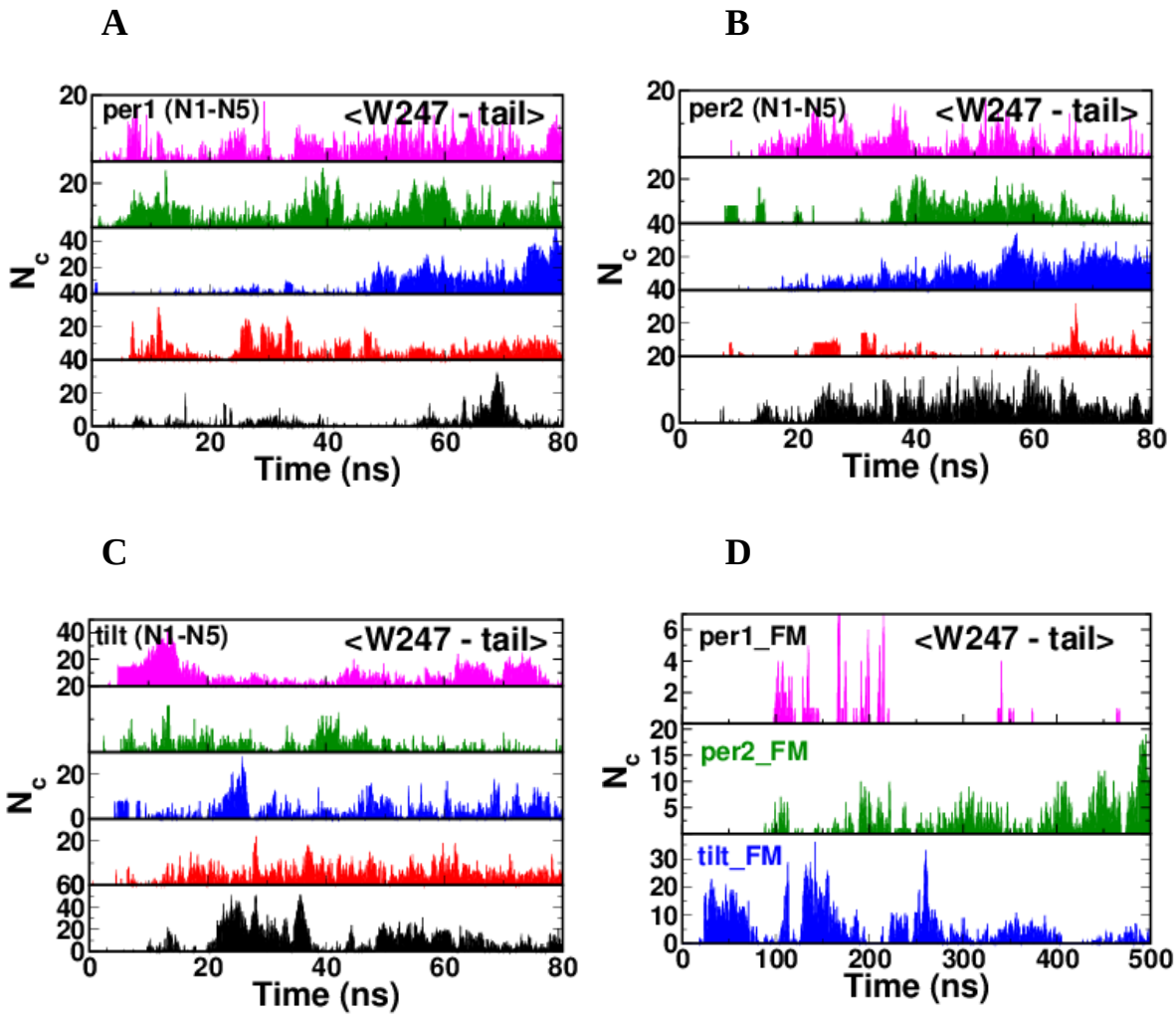

Figure 52: Number of direct contacts, N_c, between W247 and hydrophobic core Number of contacts between W247 and short-tail acyl chain + DCE for HMMM model (A, B and C) and between W247 and acyl chain for FM model (D).

TABLE 7 Mean number of direct contacts for W247 vs. acyl chain
Mean value of the number of direct contacts N_c for W247 and acyl short-tail plus DCE for HMMM model N=15 systems calculated for the last 30 ns of the trajectories where data is saved every 50 ps and for W247 and acyl tail for FM model systems for the last 200 ns of the trajectories where data is saved every 500 ps.

	per1	**per2**	**tilt**	**N = 15**
N_c	6.8 (2.5)	5.4 (1.8)	4.5 (1.7)	5.6 (1.1)

	per1_FM	**per2_FM**	**tilt_FM**
N_c	0.03 (0.2)	3.4 (3.7)	1.9 (2.2)

3.4.6 Modes of Approach to the Bound State

The simulations show that the approach of PKCα-C2 domain from bulk water to the membrane occurred in one of three distinct modes, which will be denoted as duel mode, sharp fall mode and perpendicular-to-parallel mode. The primary differences between these modes lie in the initial approach of the domain to the membrane.

Duel Mode: Loop 3 contacts the membrane first in the duel mode. Soon after, the Ca^{2+} ions and loop 1 engage the membrane. Vigorous rearrangement of these three domain segments leads to contact of K205 with the membrane, along with the two LRC strands β4, β3. Thus, the simulations illustrate a duel between two regions – loop 3, loop 1, Ca^{2+} ions on the one hand and K205, LRC strands β4, β3 on the other (Figure 39, tilt_N4 10 ns vs. 20 ns). During this time, K205 contact with the membrane fluctuates. Although loop 3 binds first, within 10 ns (Figure 25B), fluctuations of K205 bring strands β4 and β3 towards the membrane to eventually bind β4 to the

membrane. By ~ 40 ns, hpb-2resi (Y195, W245) (Figure 25G) and W247 (Figure 25H) are stably bound to the membrane. Further mild fluctuations of K205 and strand β3 fine-tune the orientation and bound configuration. Loop 1 remains fluctuating randomly above the membrane (Figure 25A). Ca^{2+} ions eventually disengage from loop 1 and diffuse on the surface of the membrane to make stable contact ~ 5 Å from the PO_4^-/ COO^-.

Sharp Fall Mode: After preliminary engagement of loop 3 with the membrane, the C2 domain moves abruptly to position strand β4 to lie flat on the membrane surface (Figure 35, per1_N3 10 ns - 20 ns). This leaves loop 1 and the Ca^{2+} ions on the water side of the interface. Over the next 20 ns to 30 ns, the domain binds to the membrane by fluctuating in a manner similar to that described for the duel mode. Ca^{2+} ions eventually diffuse from ~ 10 Å to within ~ 5 Å of the PO_4^-/ COO^- groups (green, grey, turquoise data curves in Figure 25C and black curve in Figure 29: per2_FM case) or randomly to within ~ 2 Å (brown, green4 data curves in Figure 25F).

Perpendicular-to-Parallel Mode: The PKCα-C2 domain orients itself with the β strands nearly perpendicular to the membrane. Loop 1 penetrates deeper into the membrane than loop 3 and Ca^{2+} ions penetrate into the headgroup region of the lipid membrane (Figure 37, per2_N4 10 ns - 40 ns). The residue K205 remains 15 to 20 Å into the bulk water (yellow, cyan, violet, maroon data curves in Figure 25D). By ~ 20 ns, loop 3 penetrates as deeply as loop 1, bringing strands β4 and β3 into contact with the membrane. Fluctuations of β4, β3, K205 and loop 1 lead to penetration of loop 3 deeper than loop 1, as well as penetration of β4 deeper than β3 and K205 settles on the membrane surface (cyan, violet, maroon data curves in Figure 25D). Subsequently, from 50 ns to 80 ns, the system stabilizes as in the other two modes.

3.4.7 Stubborn per1 Case

An exception to the perpendicular-to-parallel mode occurred in at least 3 simulations for per1 and per2 initial orientations, for which it is observed that loop 1 penetrates deeper than loop 3 and K205 remained far from the membrane for simulation times as long as 80 ns. This final orientation as well as the final orientation as maintained by per1_FM even after 500 ns of run time is similar to that measured by X-ray reflectivity (31). It is possible that this mode is stabilized in experiments by the presence of many proteins on the surface, or by differences in the area per lipid molecule. We shall explore the role of larger area per lipid on the PKCα-C2 domain orientation in chapter 4.

It is worthwhile to mention that, within the FM model, where per1_FM case was marked as stuck in a local minimum notwithstanding a run time of 500 ns (Figure 30), we attempted another trial for ~ 250 ns using per1_FM orientation where we repositioned the C2 domain in bulk water at least 14 Å away from the membrane surface. The domain sharply falls on the membrane onto its strand β4 within 10 ns and effectively attained a configuration similar to what we have for tilt_FM from ~ 150 ns to ~ 300 ns (Figure 53). We stopped this trial simulation and anticipate that the trial case would have also followed a similar pathway as followed by other HMMM/ FM systems undergoing the sharp fall mechanism.

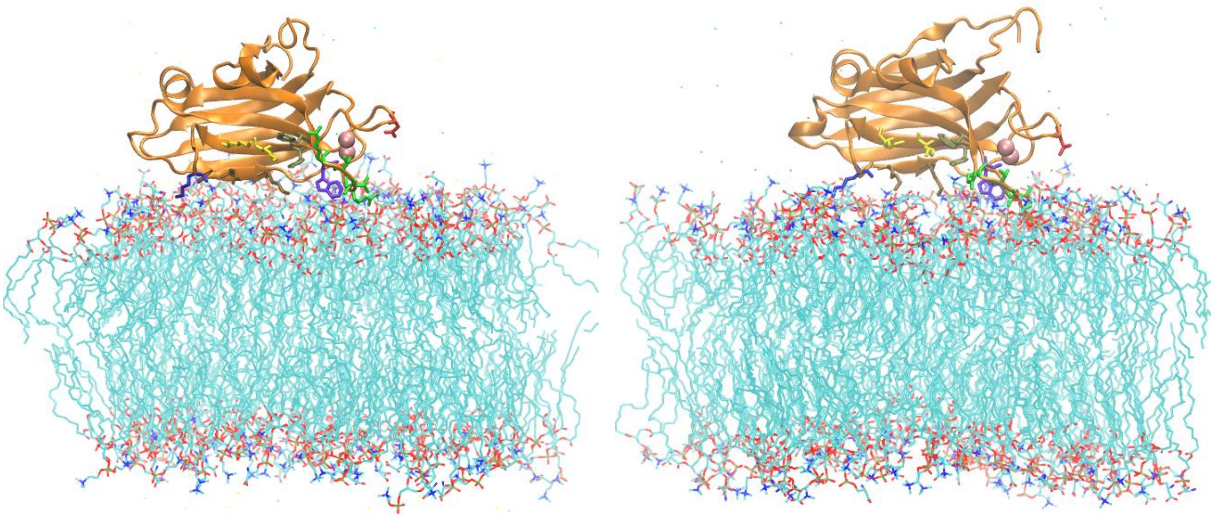

Figure 53: snapshot for two separate FM model systems
(Left): Trial per1 FM model system snap at 246 ns and (right): tilt_FM model system snap at 300 ns.

3.5 SUMMARY

MD simulations using a full molecular membrane model (FM) and a highly mobile membrane mimetic model (HMMM), which equilibrates faster, were used to determine the configuration of PKCα-C2 domain bound to a mixed PC/ PS membrane. The final configuration was independent of the three different initial orientations chosen to start the simulation. The PKCα-C2 domain was not bound to the membrane at the start of the simulation, instead it was placed in bulk water, far from the membrane surface. Spontaneous binding was followed during the simulation. HMMM model systems were run for up to 80 ns and converged to an equilibrium state prior to the last ~ 30 ns of each simulation. Much longer simulations were required for the FM model, on the order of 500 ns in order to exhibit 200 ns of the equilibrated state. Although the

HMMM and FM models are molecularly different, they reproduced almost identical PKCα-C2 membrane bound configurations.

The dynamical fluctuations of loop 1, K205 and strand β3 dictate whether PKCα-C2 domain will have a close-faced docking orientation or an open-faced docking orientation.

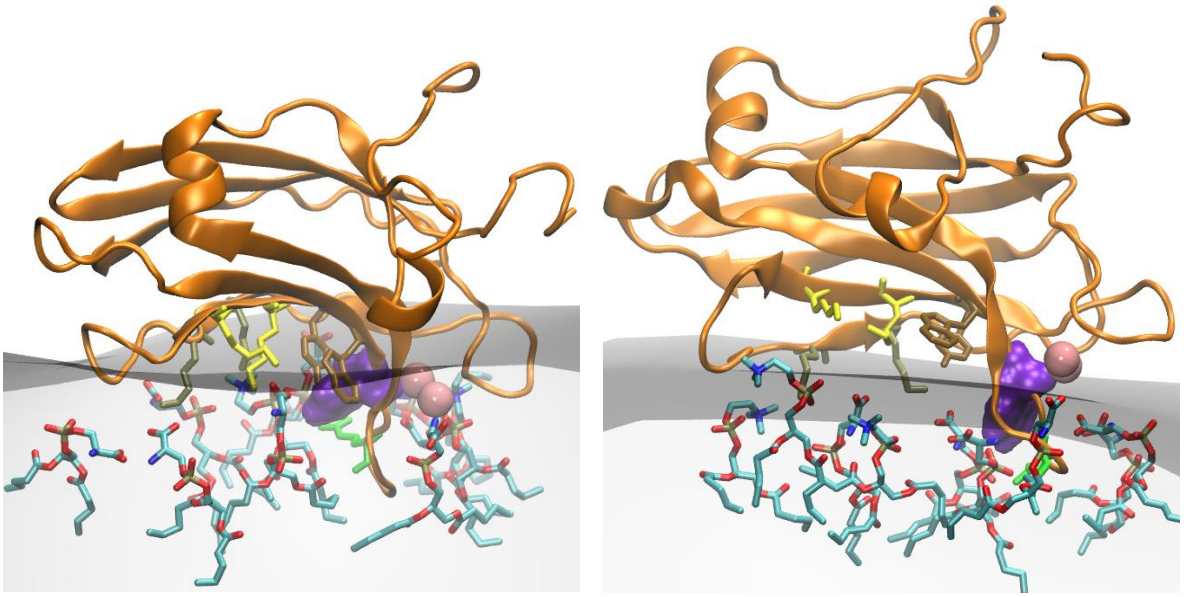

Figure 54: Close-faced and open-faced configurations
A typical depiction of membrane bound configuration of PKCα-C2 domain in a close-faced state (left) and an open-faced state (right).

A close-faced docking orientation is characterized by parallel strands β3 and β4 located in a horizontal plane and K205 just touching the membrane. It has been suggested that this orientation could be an intermediate between the starting configuration and the open-faced configuration (29, 30, 93). In this state, big headgroup lipids like PIP2 are constrained from binding to the LRC docking region. However, if strand β4 penetrates deeper into the membrane, thus aligning β3 and β4 along an almost vertical plane, and K205 is localized on the membrane surface, this open-faced

docking configuration has an exposed OH-moiety of Y195 and LRC region. This provides access to membrane lipids that diffuse laterally across the membrane surface (Figure 36, Figure 38 and Figure 40).

The open faced docking configuration is the equilibrated state of most of the simulations. This docking configuration provides an unconstrained path along the membrane for laterally diffusing lipids, like PIP2, to bind to either the exposed OH-moiety of Y195 or to the lysine rich cluster without severely altering the overall orientation of the domain.

4 Role of Lipid Densities in PKCα-C2 Domain Bound Configuration

4.1 Introduction

In this chapter we investigate the role of a different area per lipid on the configuration of PKCα-C2 domain bound to PC:PS (7:3 molar ratio) mixed membranes. Chapter 3 demonstrated that the FM and the HMMM models produced nearly identical open-faced membrane bound configurations of PKCα-C2 domain. Although these models consistently produced similar bound configurations, the configuration differed greatly from X-ray reflectivity measurements (31). Since these simulations were performed for different areas per lipid (~ 61 $Å^2$ and ~ 81 $Å^2$ for the FM and the HMMM models, respectively) than the X-ray reflectivity measurements at an area per lipid of ~122 $Å^2$, more simulations were done to calculate the bound configuration at an area per lipid comparable to the measured value in the X-ray reflectivity measurements. Here, we use the faster equilibrating HMMM model to simulate systems at a larger area per lipid.

X-ray reflectivity measurements were carried out on monolayers supported on water in a Langmuir trough. The surface pressure of the lipid layer prior to adding protein to the system was ~25 mN/m, comparable to other experiments done to mimic biomembranes (31, 107, 108). X-ray reflectivity measures the variation in electron density perpendicular to the interface. Reflectivity data from the lipids with protein were analyzed by fitting the data to a model that assigns a separate slab of uniform electron density to model the tail groups and the head groups, as well as a model for the protein based upon the Protein Data Bank atomic coordinates for crystallized PKCα-C2 domain (31). The area per lipid can be determined by dividing the number of electrons in the two tail groups (288) by the product of the fitted electron density in the tail group region (0.21 $e^-/Å^3$) and the thickness of the tail group (10.7 Å), which is 128 $Å^2$ (31). In the X-ray reflectivity studies, two slightly different bound configurations were equally likely to describe the data. The other

configuration led to slightly different parameters for the lipid layer, resulting in an area per lipid of 116 $Å^2$. These values of area per lipid are similar to previously measured monolayers at similar surface pressures of SOPC monolayers (107) and mixed SOPC/ SOPS/ DPPtdIns(3)P monolayers (108) without adsorbed proteins. Simulations were performed at 125 $Å^2$.

4.2 Methods

A set of HMMM model systems with area per lipid 125 $Å^2$ was prepared as described in Chapter 3 (Section 3.2.2). Three systems were prepared with the initial orientations discussed previously (per1, per2 and tilt). The systems are abbreviated as LA_per1, LA_per2 and LA_tilt (where prefix LA – signifies Larger Area). The PKCα-C2 domain was positioned with its bound Ca^{2+} ions at least 14 Å from PO_4^-/ COO^- headgroup moieties of the membrane lipids. VMD (50) plugins were used to add water, counterions and 100 mM KCl electrolyte concentration. The HMMM simulation cell consisted of ~ 93000 atoms. Each HMMM system was energy minimized for 10,000 steps (20 ps) with a target pressure of 1 atm and a gradual increase in the temperature to 310 K during which the membrane area in the *x*-*y* plane was kept constant while Cα atoms of the PKCα-C2 domain and bound Ca^{2+} ions were harmonically constrained with a force constant of k = 2 kcal·mol^{-1}·$Å^{-2}$. A further constrained simulation of 500,000 steps (1 ns) occurred after this. Subsequently, all constraints on the PKCα-C2 domain were removed and four simulations each of the LA_per1 for 80 ns, LA_per2 for 40 ns and LA_tilt for 40 ns were performed.

4.2.1 Simulation Protocol

Simulation protocol is essentially the same as that of other HMMM model systems used in this thesis (Section 3.2.5).

4.3 Results and Discussions

The quantities of angle (θ_1, θ_2) (Figure 55), $h_r(z)$ (Figure 56 – 58), d_{min} (Figure 59 – 61) and N_c (Figure 62 – 64) as well as a time series of snapshots for LA_per1 (Figure 65, Figure 68), LA_per2 (Figure 66, Figure 69) and LA_tilt (Figure 67, Figure 70) are shown below.

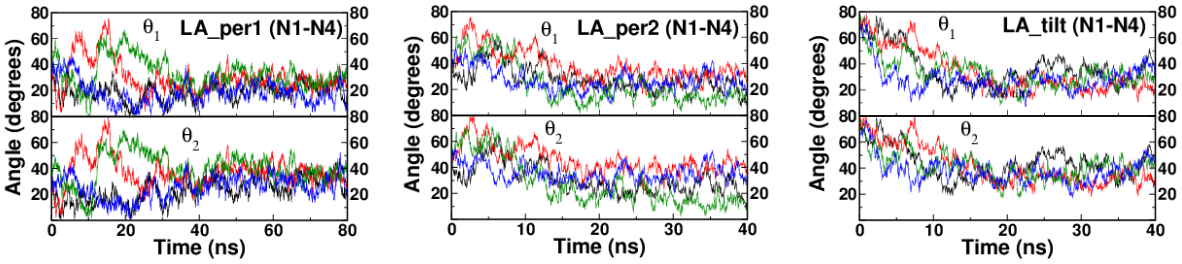

Figure 55: Orientation angles for larger area per lipid systems
Left to Right: Angle θ_1 and θ_2 for 4 runs of HMMM model LA_per1, LA_per2 and LA_tilt system. Angle (θ_1, θ_2) are taken as defined in Figure 19.

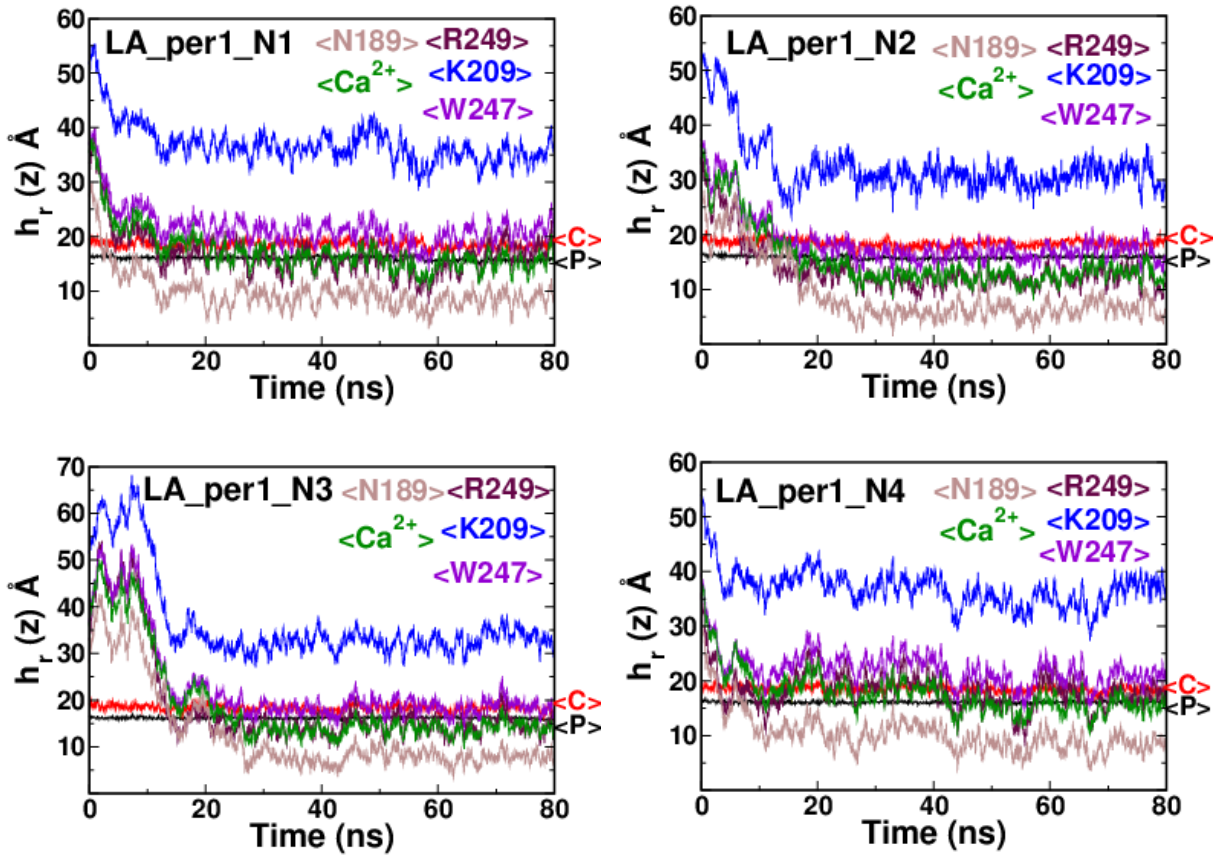

Figure 56: Relative heights for LA_per1 systems
Heights $h_r(z)$ for four runs (N1 - N4) of LA_per1 HMMM model systems. The C-atoms of the COO^- moiety plane, <C>, and the P-atoms of the PO_4^- moiety plane, <P>, are shown in red and black color respectively.

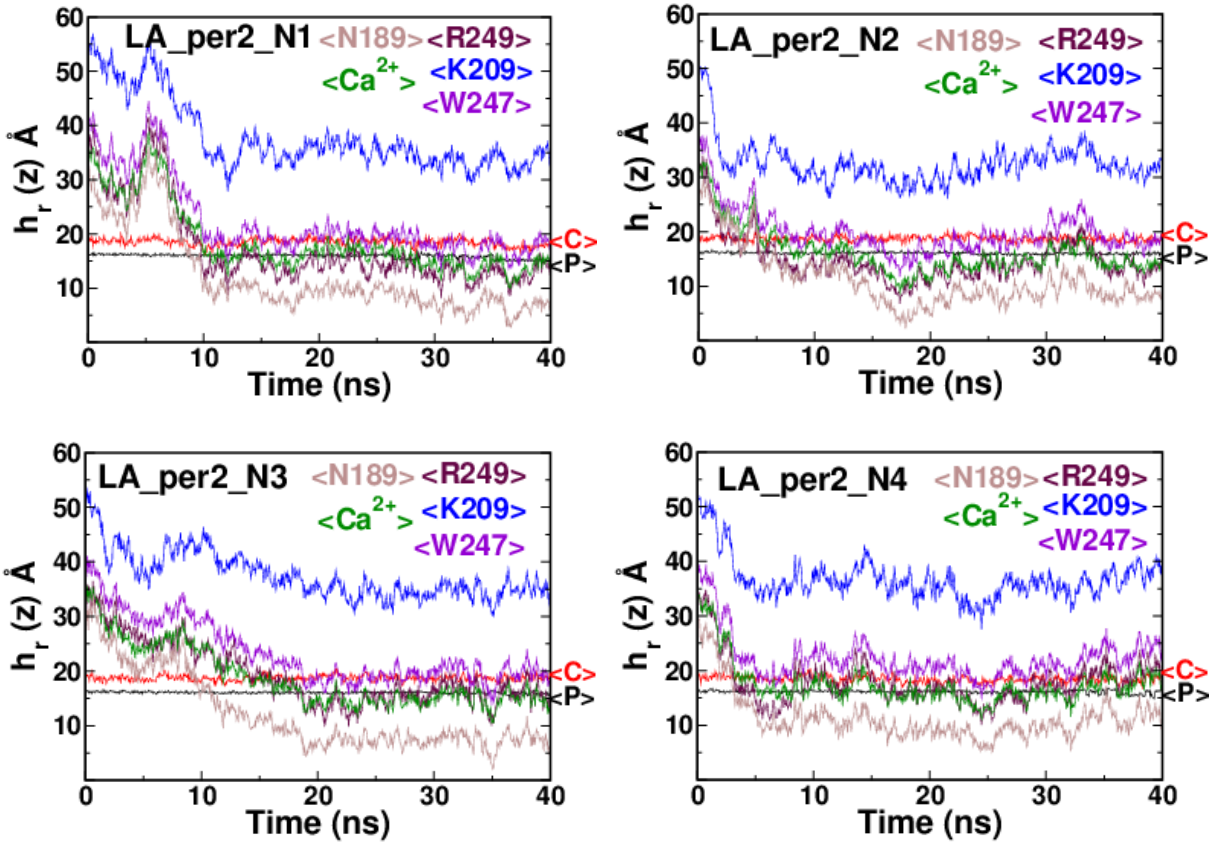

Figure 57: Relative heights for LA_per2 systems
Heights $h_r(z)$ for four runs (N1 - N4) of LA_per2 HMMM model systems. The C-atoms of the COO^- moiety plane, <C>, and the P-atoms of the PO_4^- moiety plane, <P>, are shown in red and black color respectively.

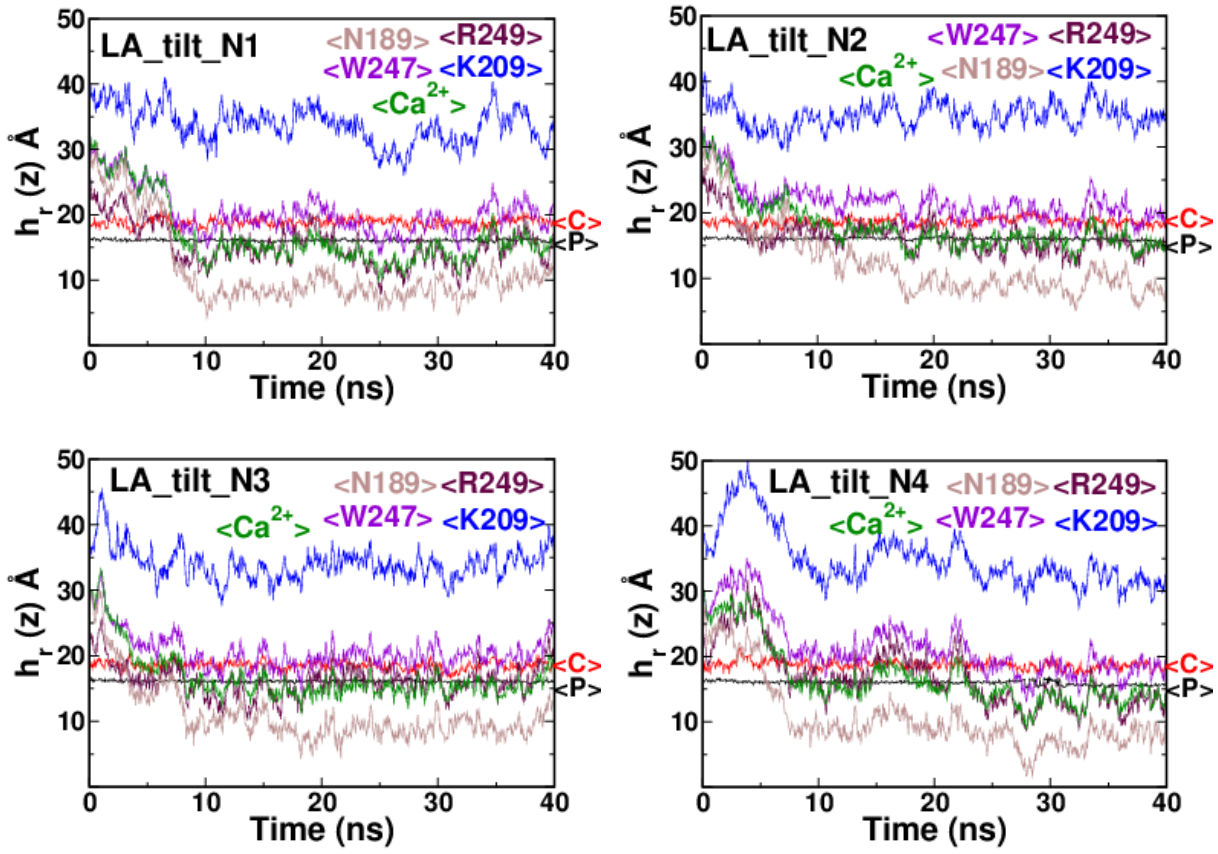

Figure 58: Relative heights for LA_tilt systems
Heights $h_r(z)$ for four runs (N1 - N4) of LA_tilt HMMM model systems. The C-atoms of the COO^- moiety plane, <C>, and the P-atoms of the PO_4^- moiety plane, <P>, are shown in red and black color respectively.

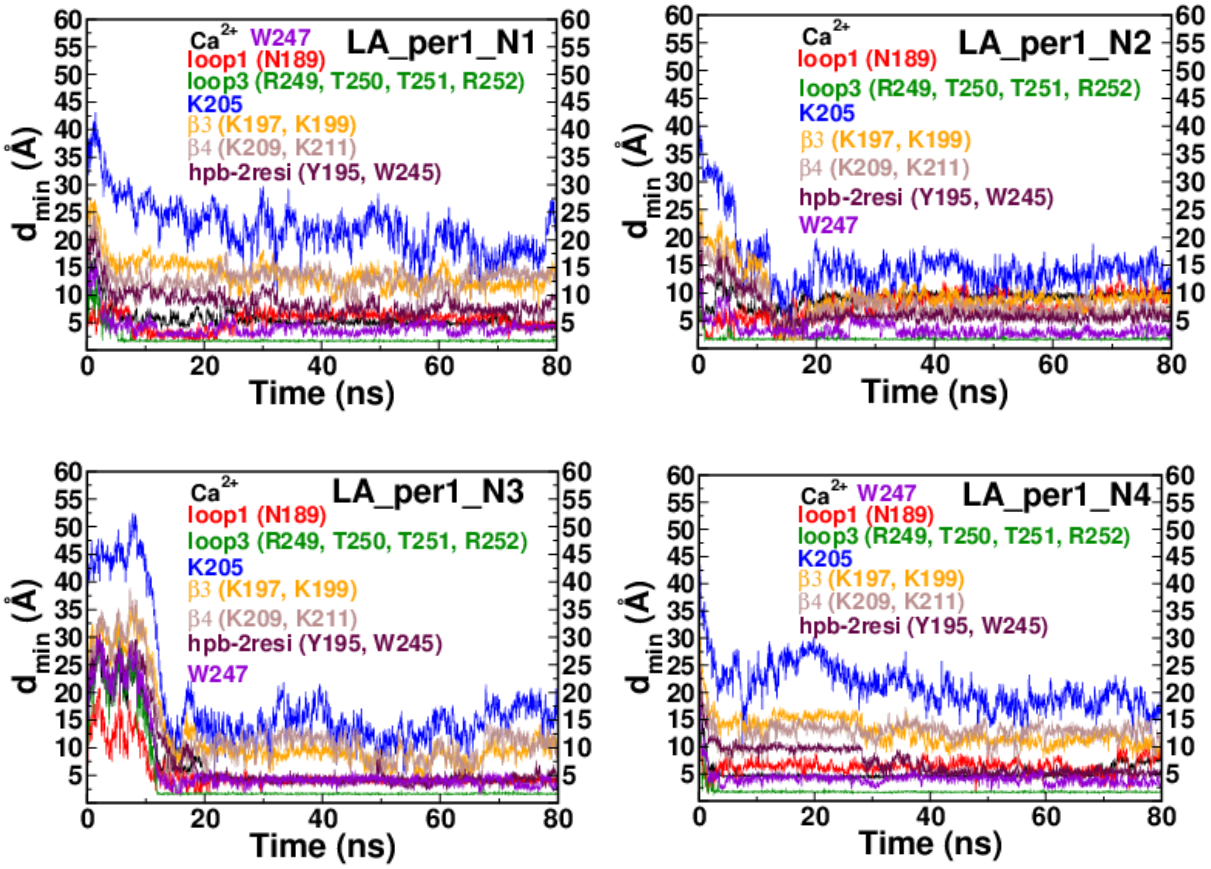

Figure 59: The minimum distance for LA_per1 systems
d_{min} for four runs (N1 - N4) of LA_per1 HMMM model systems.

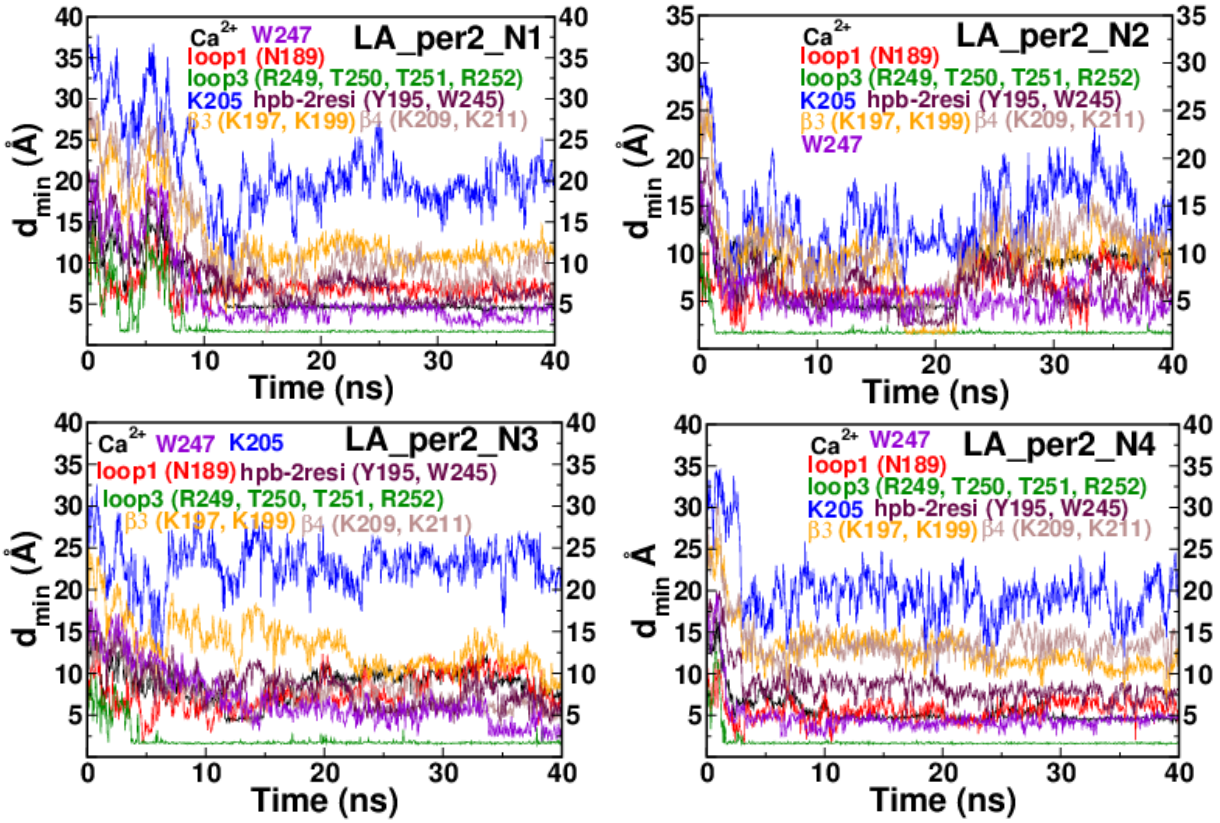

Figure 60: The minimum distance for LA_per2 systems
d_{min} for four runs (N1 - N4) of LA_per2 HMMM model systems.

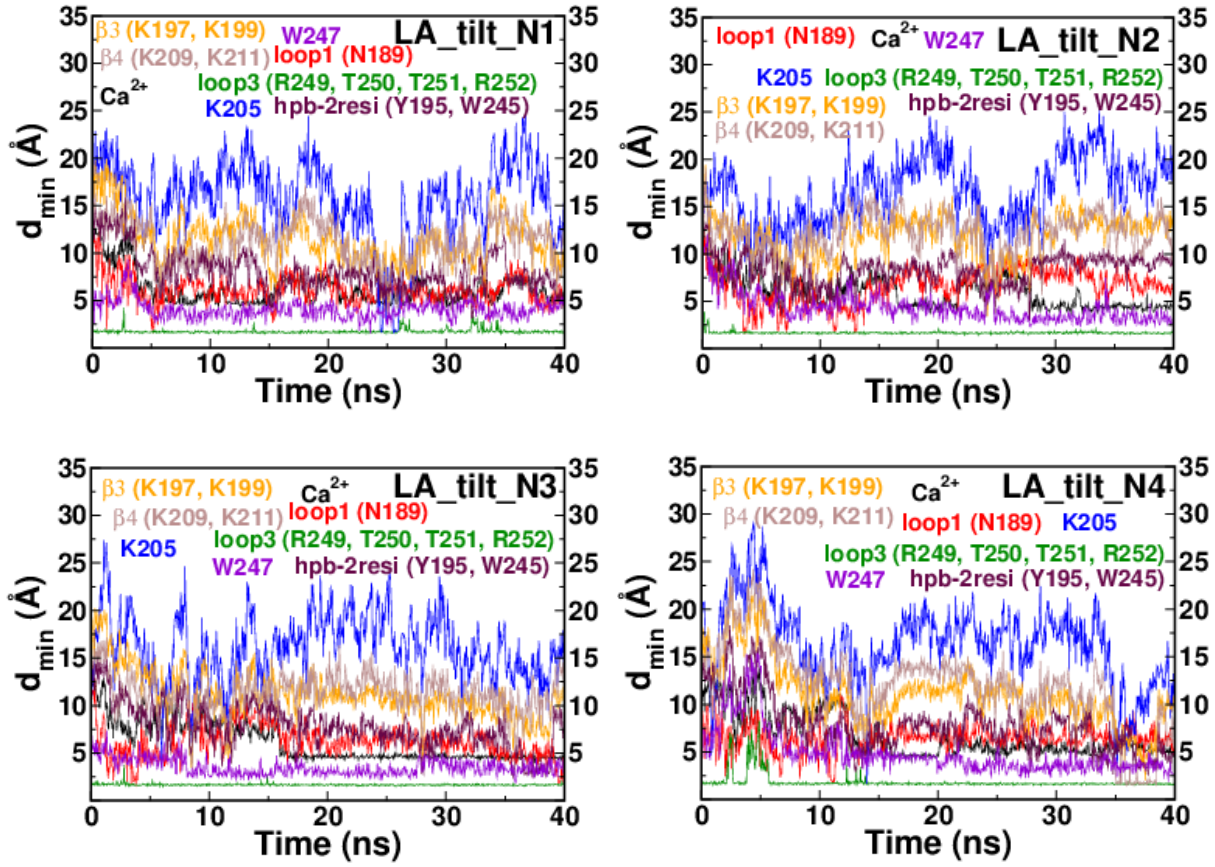

Figure 61: The minimum distance for LA_tilt systems
d_{min} for four runs (N1 - N4) of LA_tilt HMMM model systems.

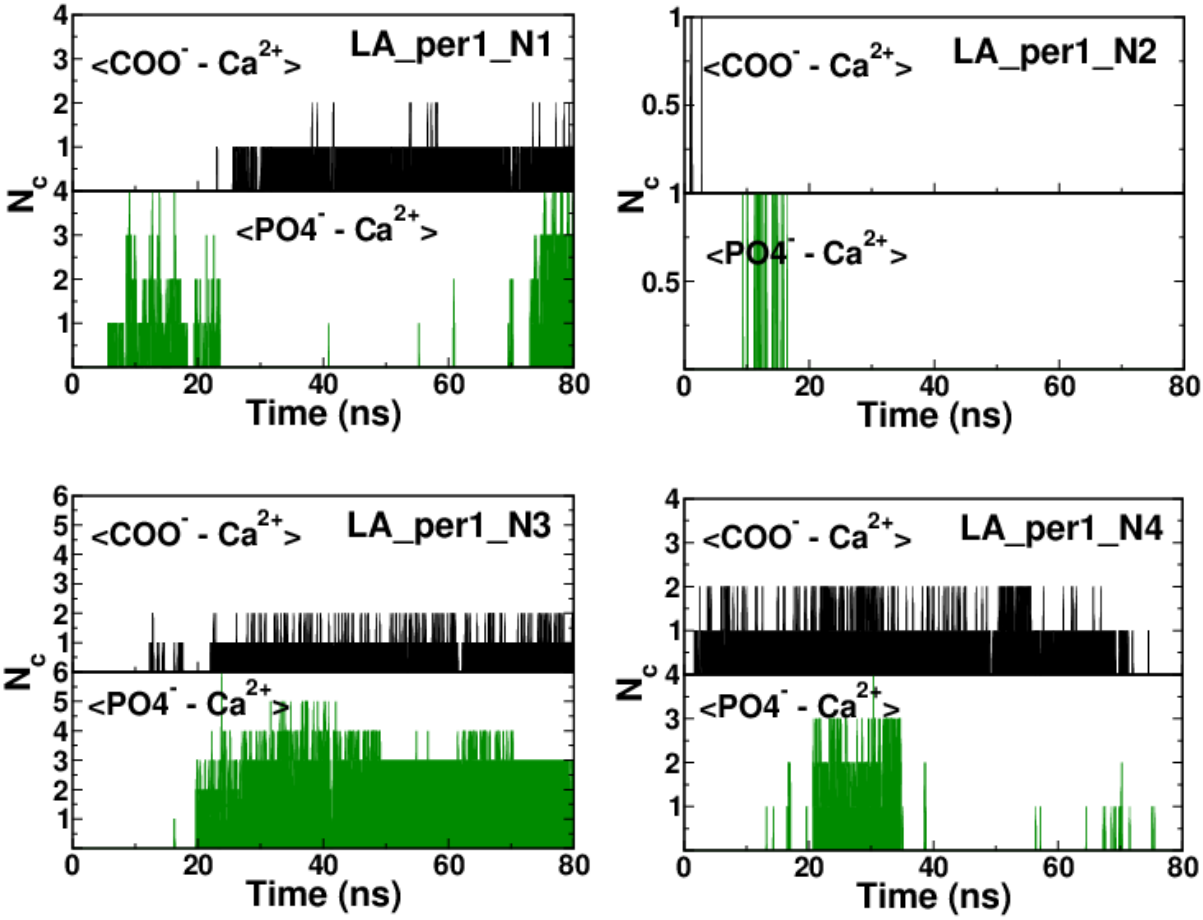

Figure 62: Number of contacts for LA_per1 systems
Number of direct contacts, N_c, between Ca^{2+} ions and oxygen-atoms of PO_4^- or COO^- moieties. <COO^-> and <PO4$^-$> represent oxygen-atoms for respective systems.

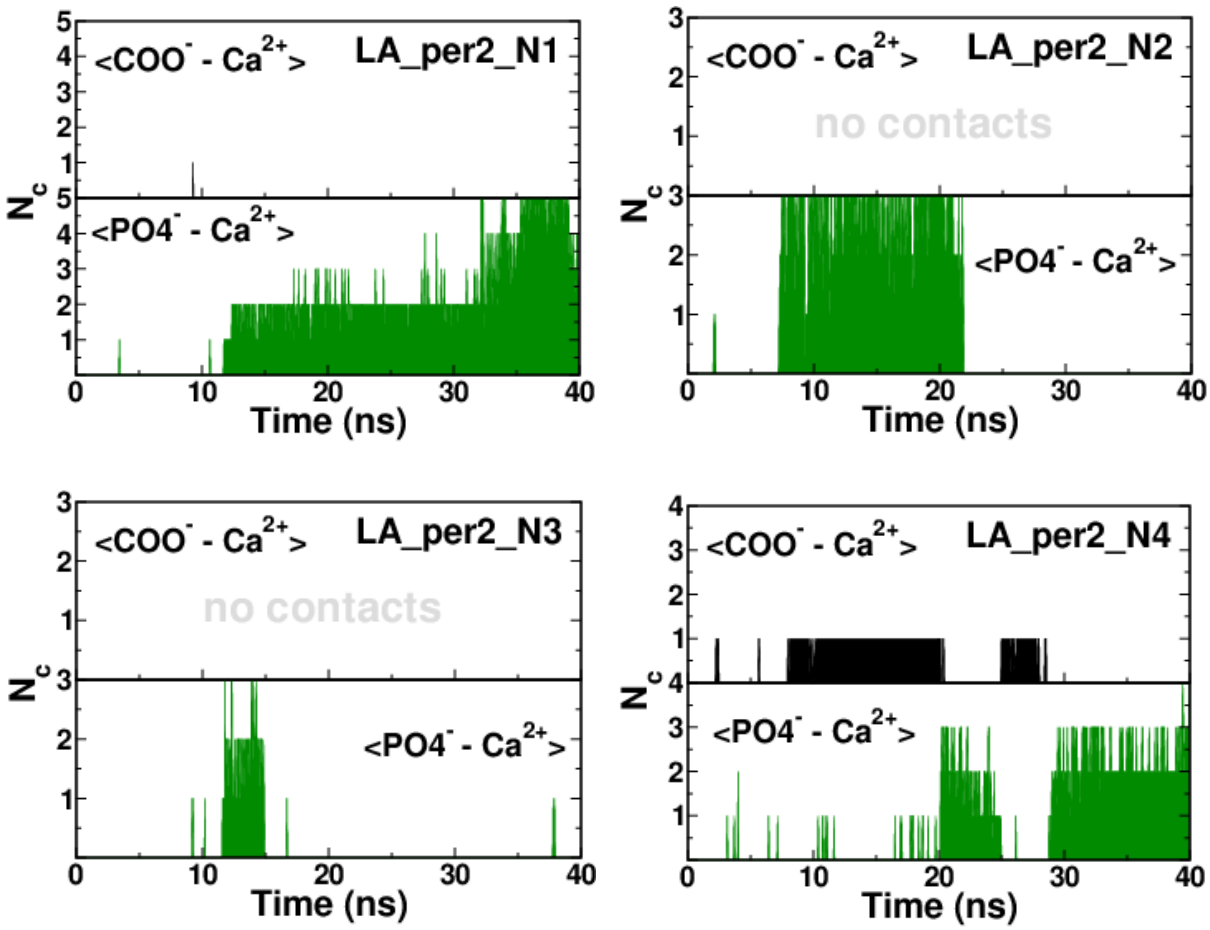

Figure 63: Number of contacts for LA_per2 systems
Number of direct contacts, N_c, between Ca^{2+} ions and oxygen-atoms of PO_4^- or COO^- moieties. <COO⁻> and <PO4⁻> represent oxygen-atoms for respective systems.

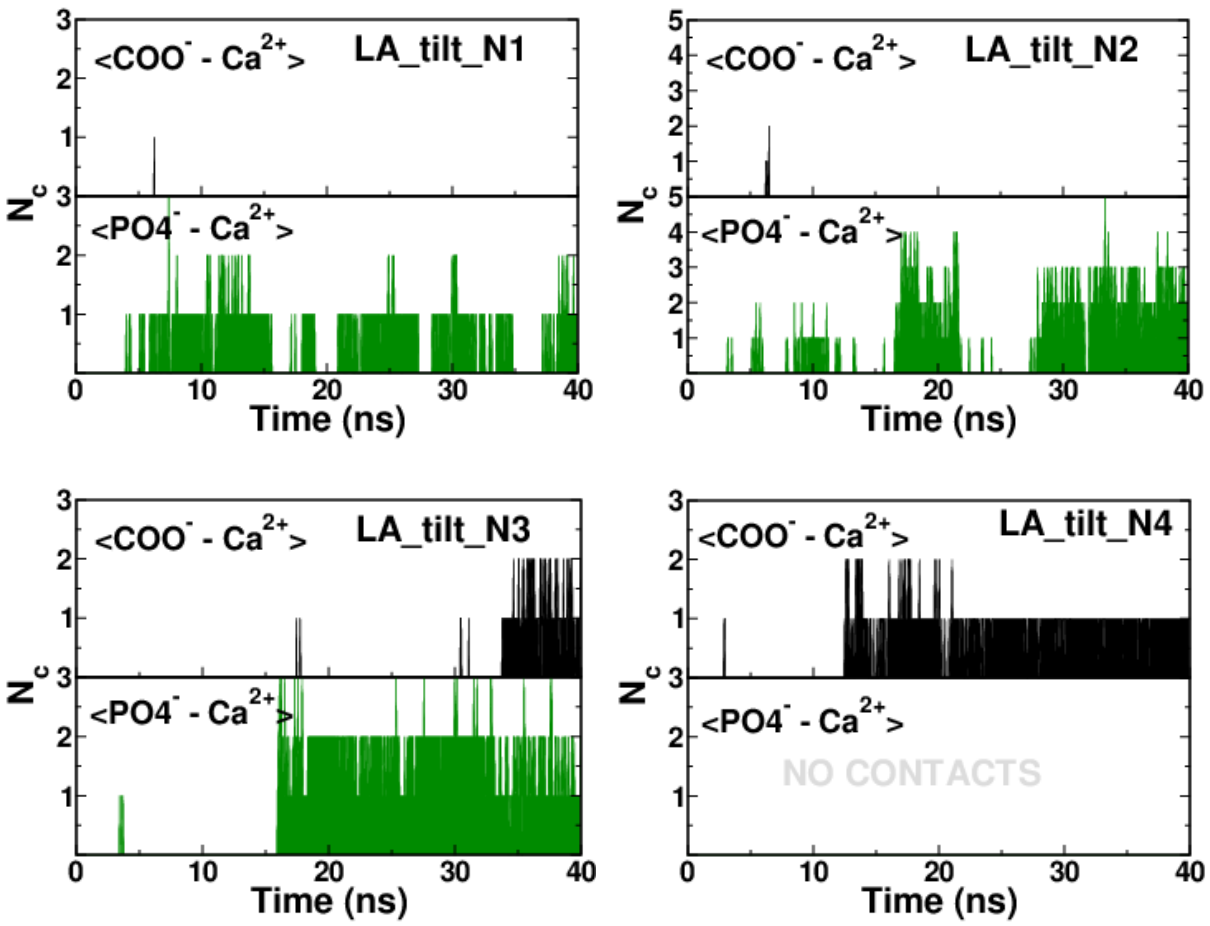

Figure 64: Number of contacts for LA_tilt systems
Number of direct contacts, N_c, between Ca^{2+} ions and oxygen-atoms of PO_4^- or COO^- moieties. <COO^-> and <$PO4^-$> represent oxygen-atoms for respective systems.

LA_per1_N1

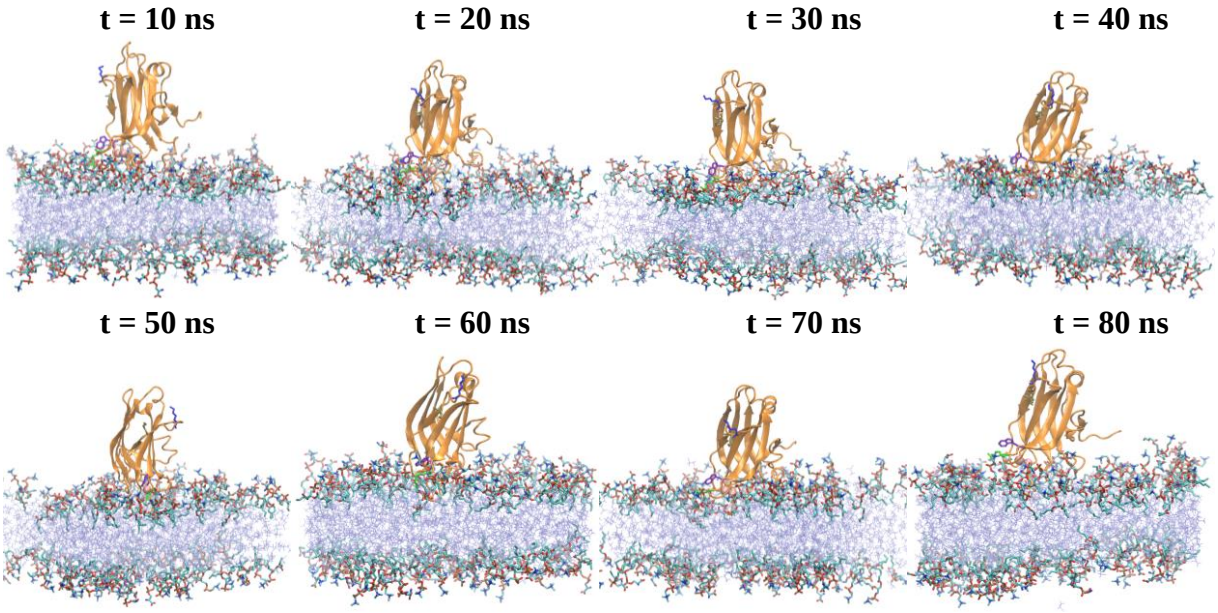

LA_per1_N2

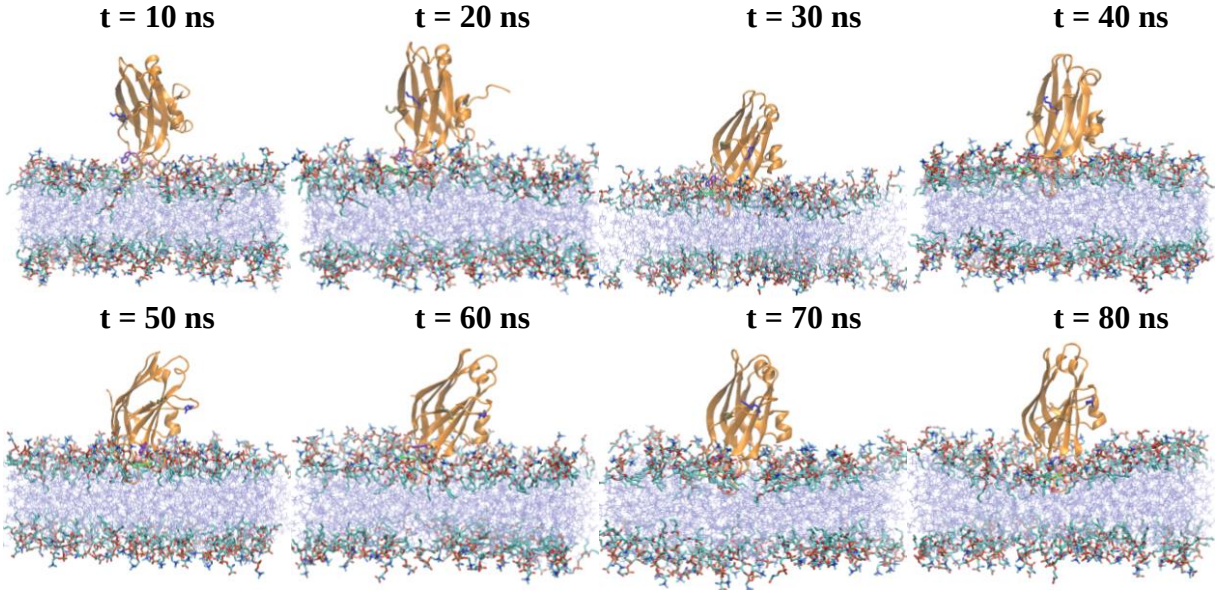

LA_per1_N3

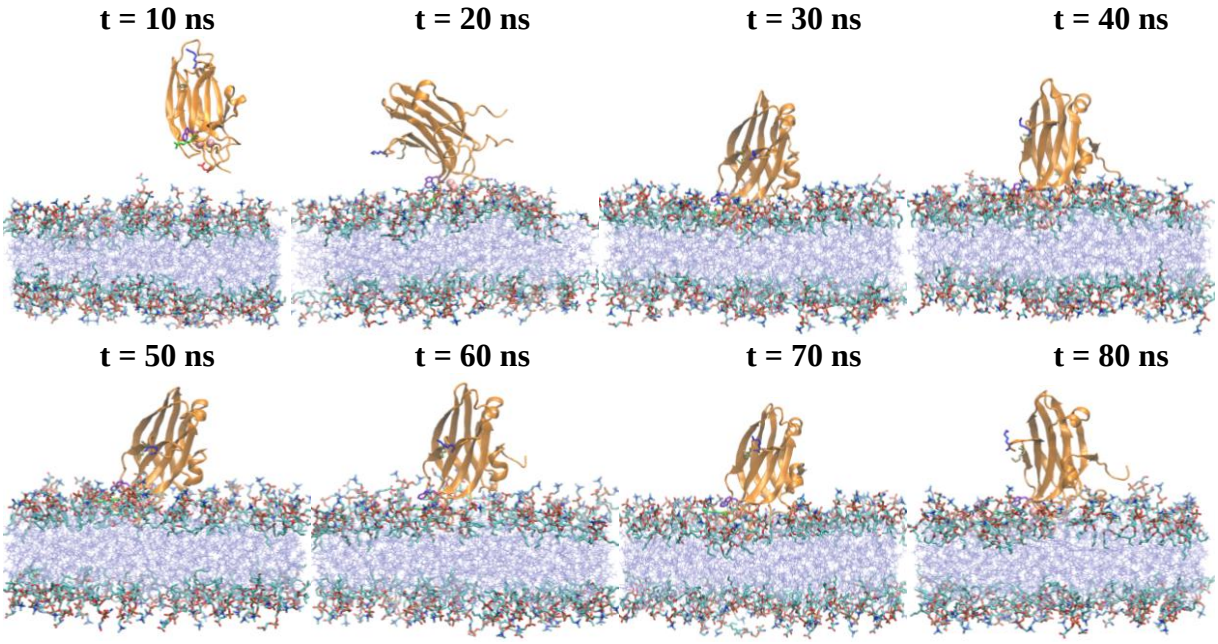

LA_per1_N4

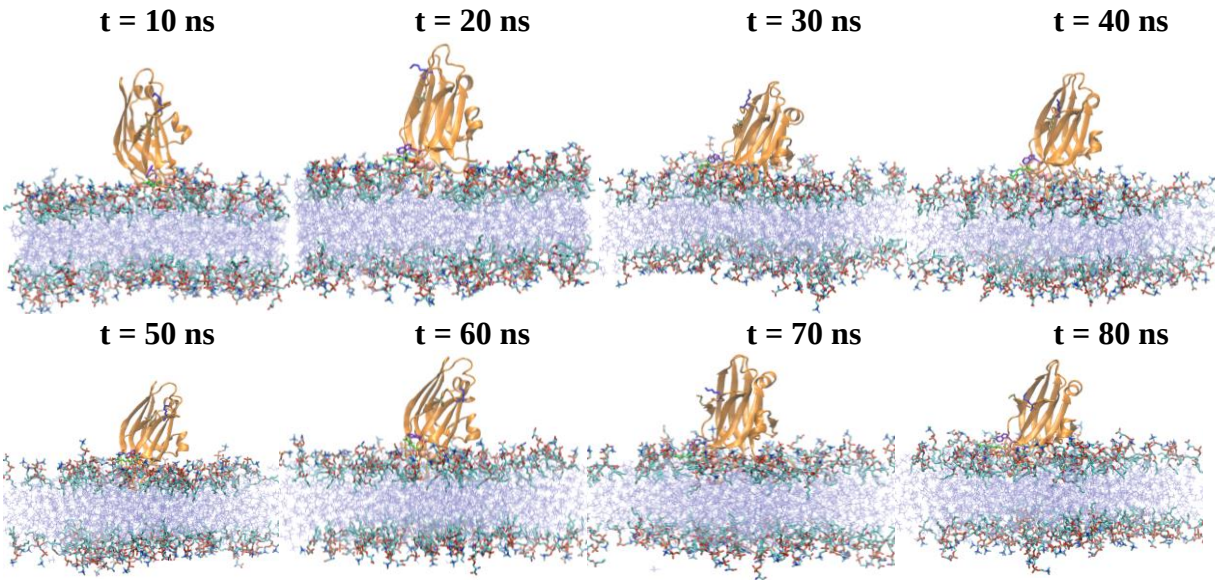

Figure 65: Time series snapshots for LA_per1 systems
Snapshots at the interval of 10 ns (starting from 10 ns and up to 80 ns) are shown for four runs of LA_per1 HMMM model systems. Water is not shown for clarity.

LA_per2_N1

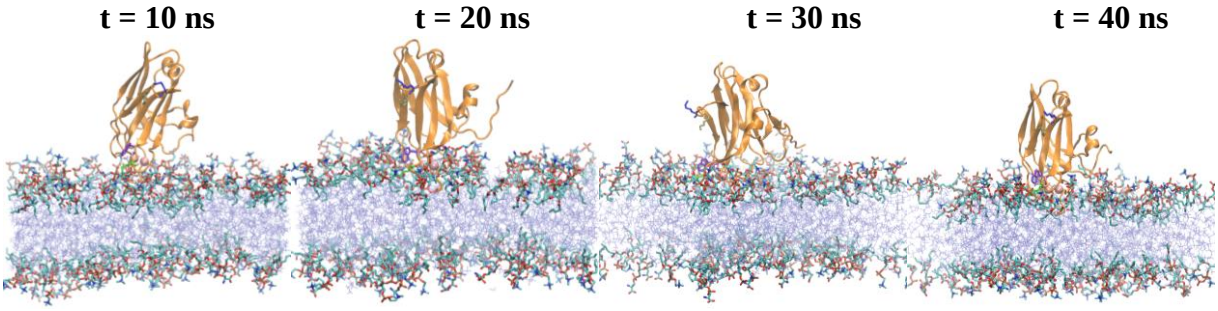

LA_per2_N2

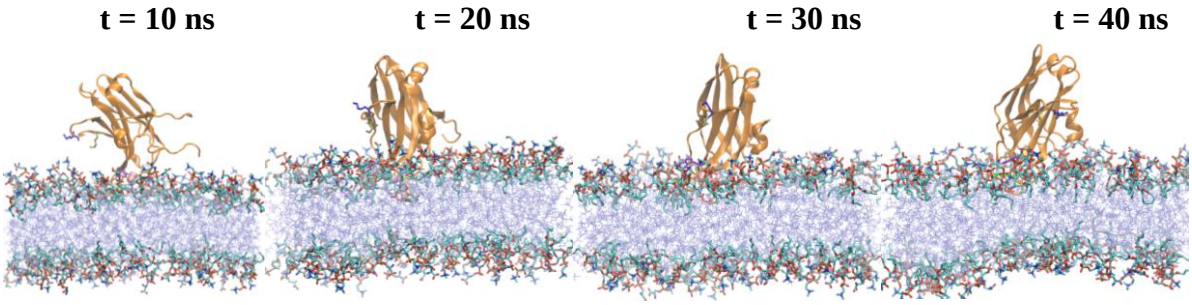

LA_per2_N3

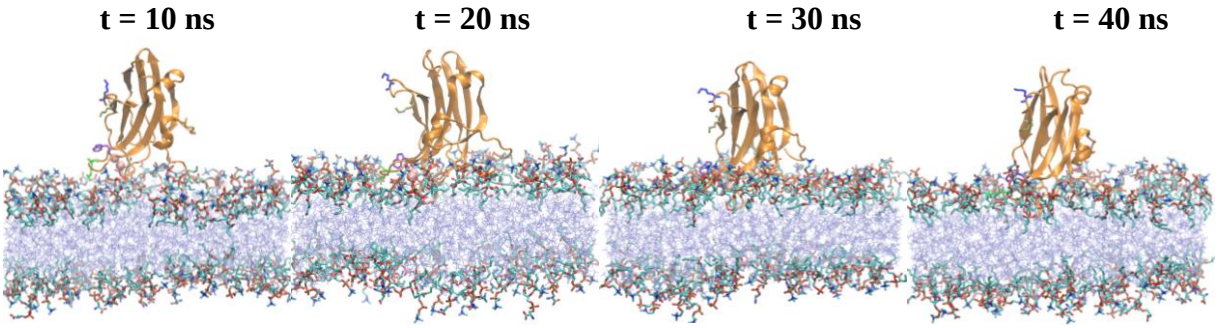

LA_per2_N4

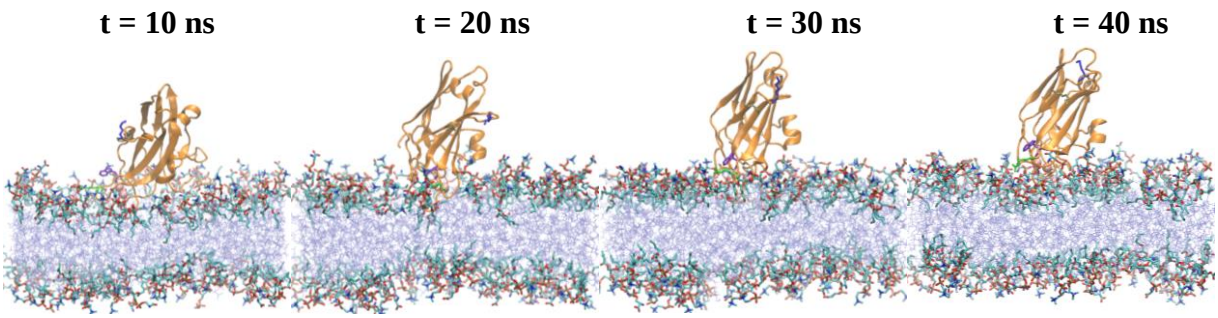

Figure 66: Time series snapshots for LA_per2 systems
Snapshots at the interval of 10 ns (starting from 10 ns and up to 40 ns) are shown for four runs of LA_per2 HMMM model systems. Water is not shown for clarity.

LA_tilt_N1

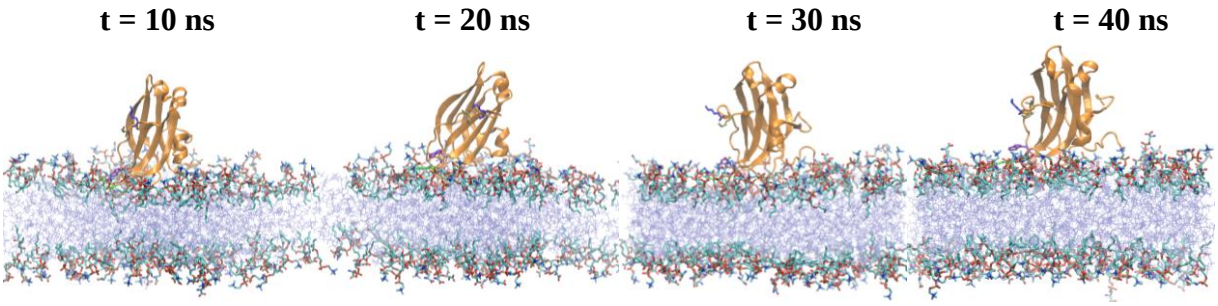

LA_tilt_N2

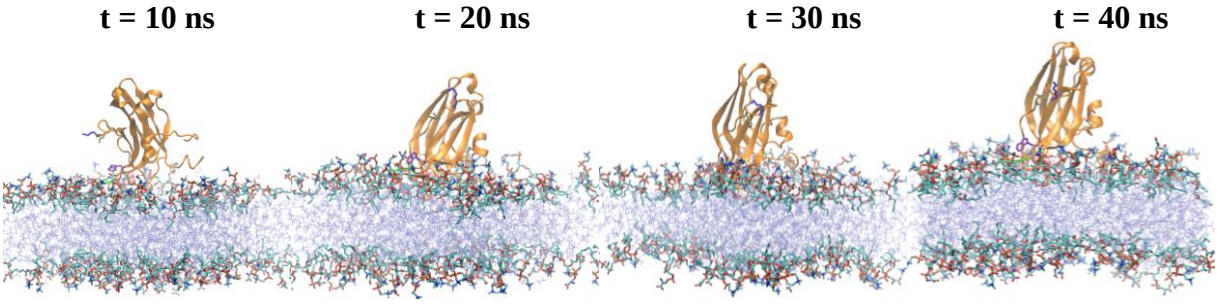

LA_tilt_N3

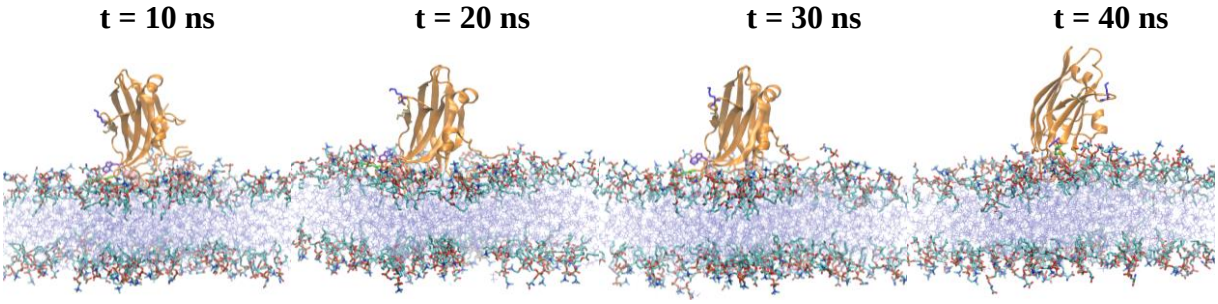

LA_tilt_N4

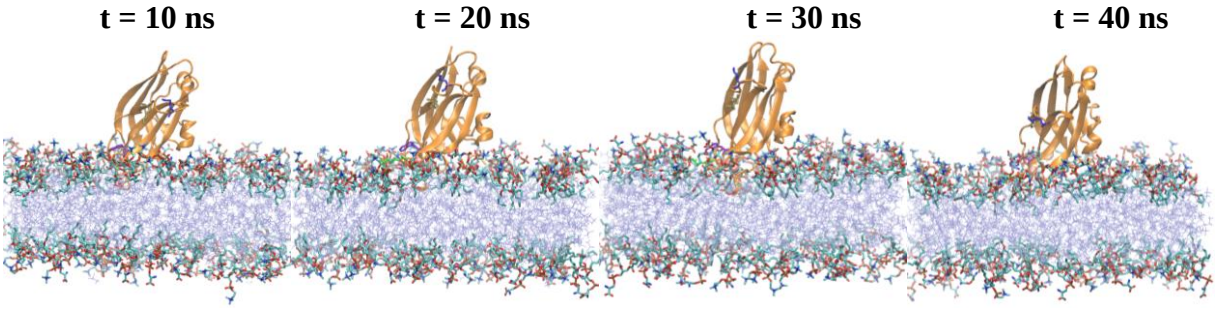

Figure 67: Time series snapshots for LA_tilt systems
Snapshots at the interval of 10 ns (starting from 10 ns and up to 40 ns) are shown for four runs of LA_tilt HMMM model systems. Water is not shown for clarity.

LA_per1_N1

t = 10 ns **t = 20 ns** **t = 30 ns** **t = 40 ns**

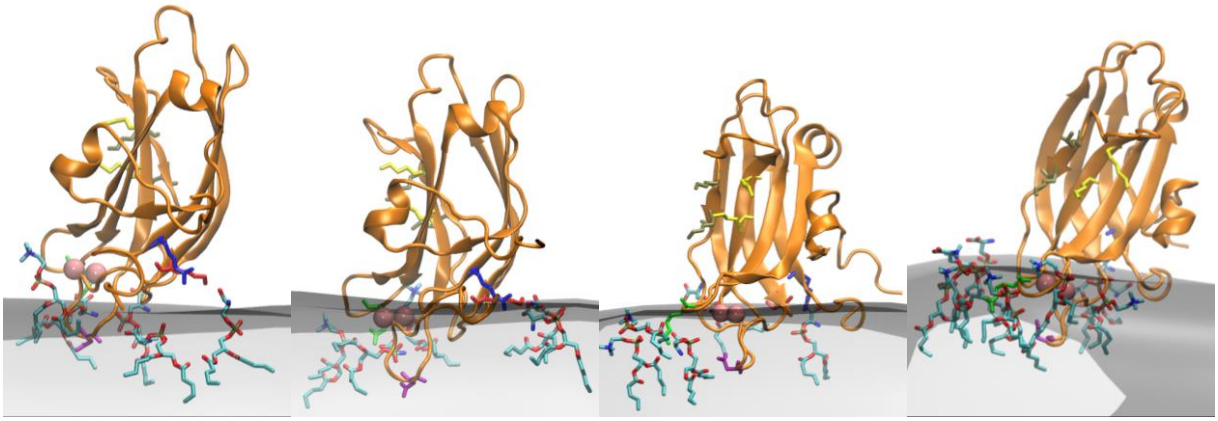

t = 50 ns **t = 60 ns** **t = 70 ns** **t = 80 ns**

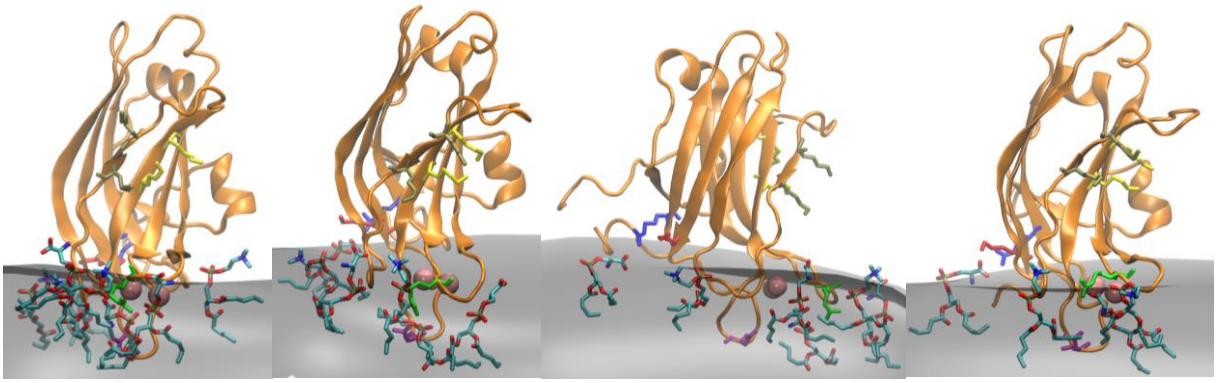

LA_per1_N2

t = 10 ns **t = 20 ns** **t = 30 ns** **t = 40 ns**

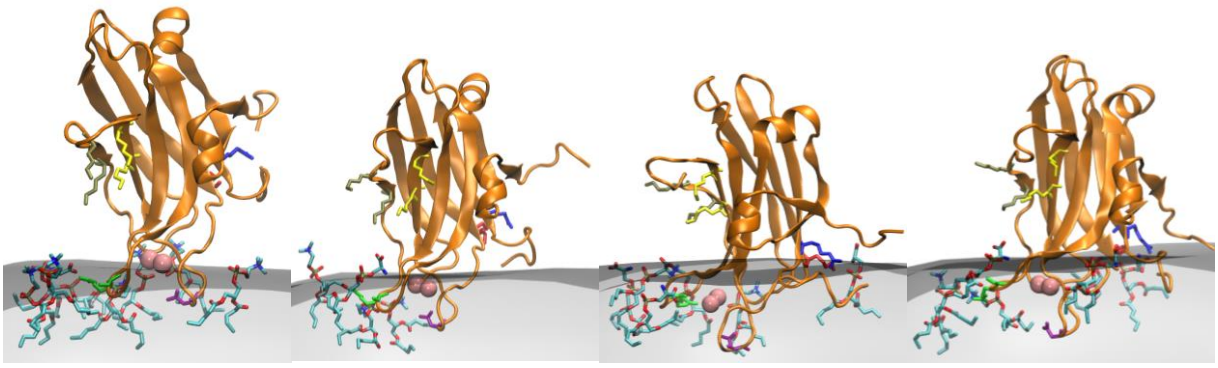

t = 50 ns **t = 60 ns** **t = 70 ns** **t = 80 ns**

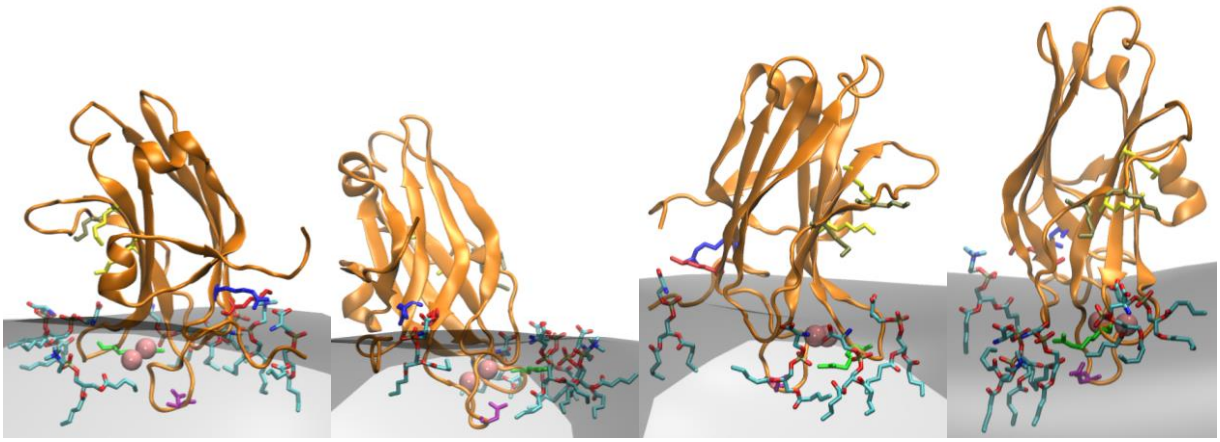

LA_per1_N3

t = 10 ns **t = 20 ns** **t = 30 ns** **t = 40 ns**

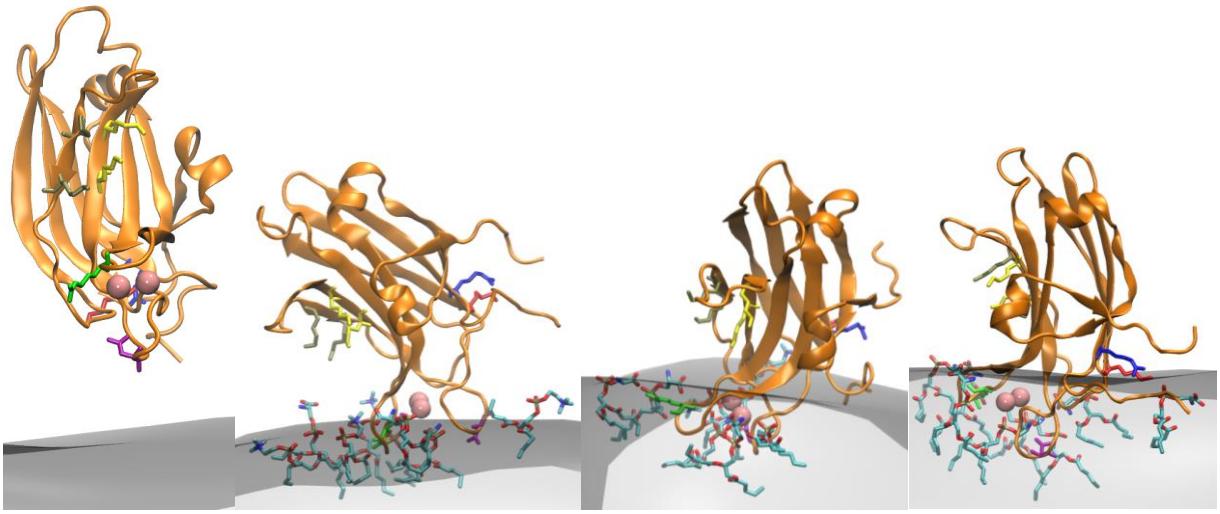

t = 50 ns **t = 60 ns** **t = 70 ns** **t = 80 ns**

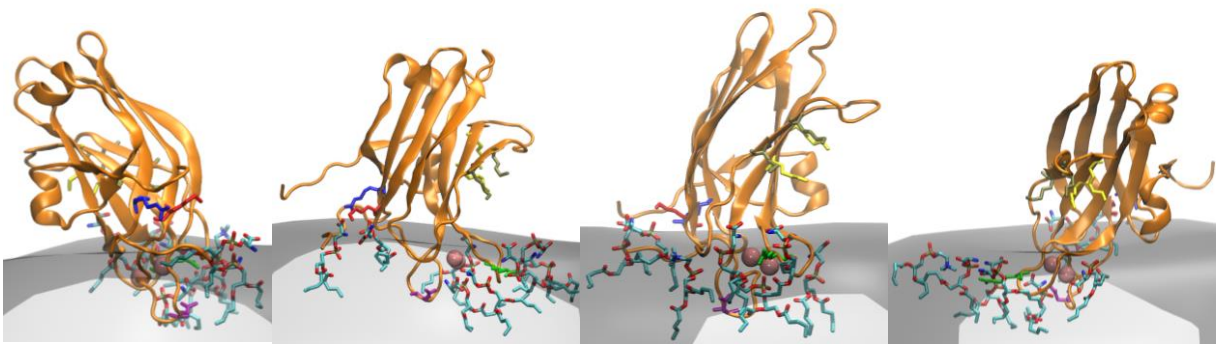

LA_per1_N4

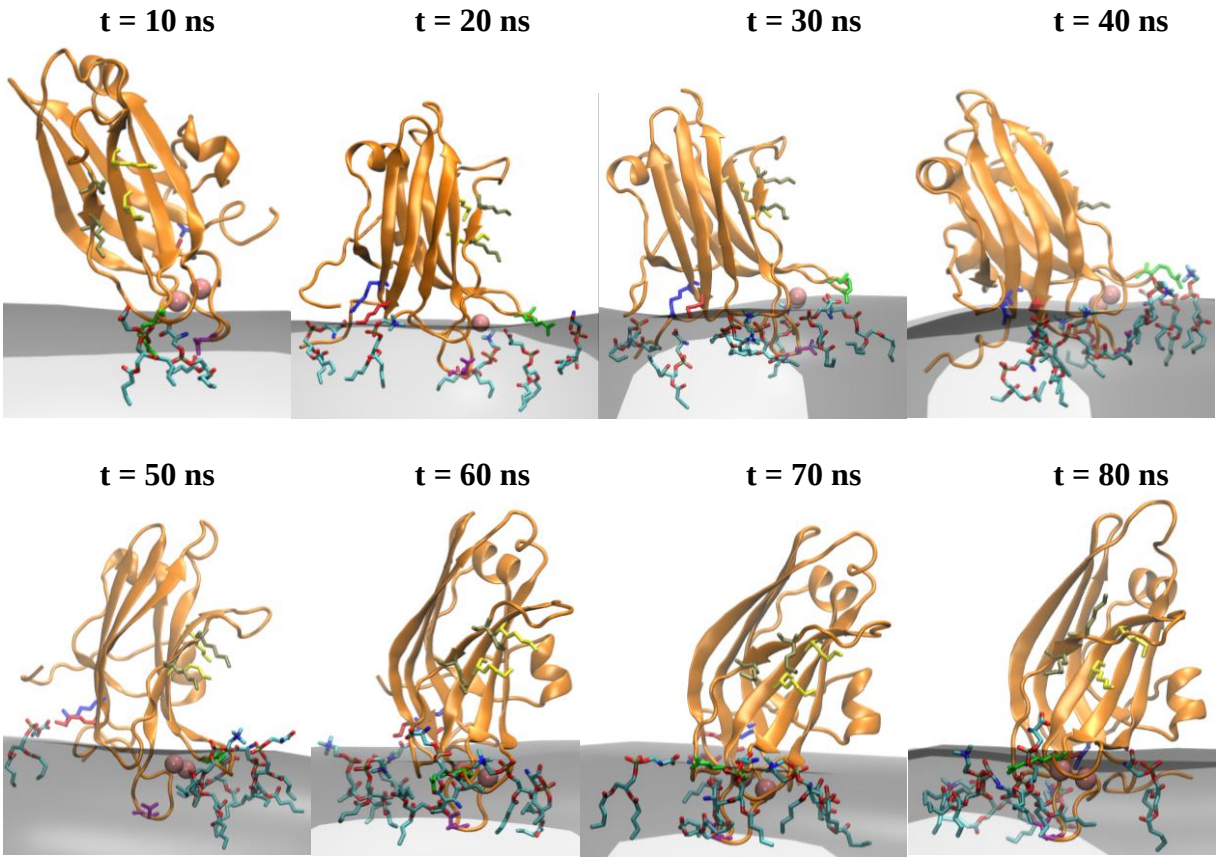

Figure 68: Close up snapshots for LA_per1 systems
Snapshots at the interval of 10 ns for four runs of LA_per1 HMMM model systems. Protein's residues R249 from loop3 (green), N189 from loop1 (purple), R161 from strand β1 (blue), K181 from strand β2 (red), strand β3 (yellow), strand β4 (tan) and Ca^{2+} ions (pink) are also shown. Membrane is represented as quicksurf in grey. PC/ PS short-tail lipids are also shown as within 6 Å of R249, N189, R161, K181 and Ca^{2+} ions. Water and ions are not shown for clarity.

LA_per2_N1

t = 10 ns **t = 20 ns** **t = 30 ns** **t = 40 ns**

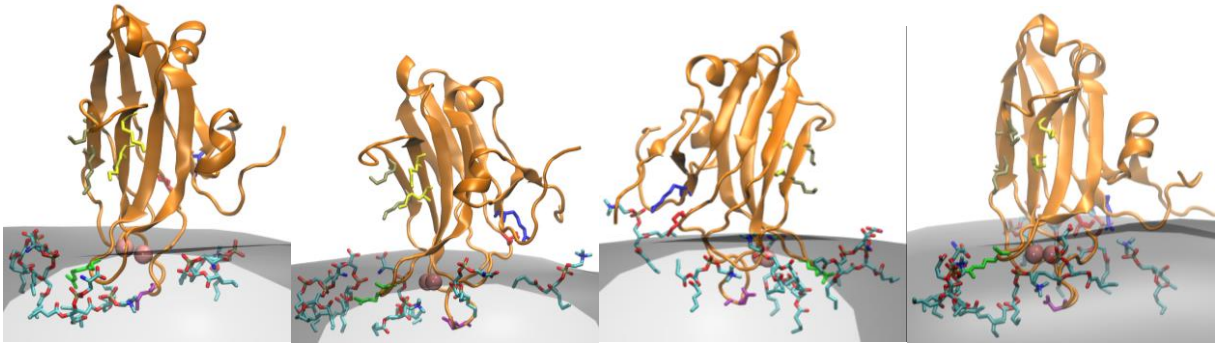

LA_per2_N2

t = 10 ns **t = 20 ns** **t = 30 ns** **t = 40 ns**

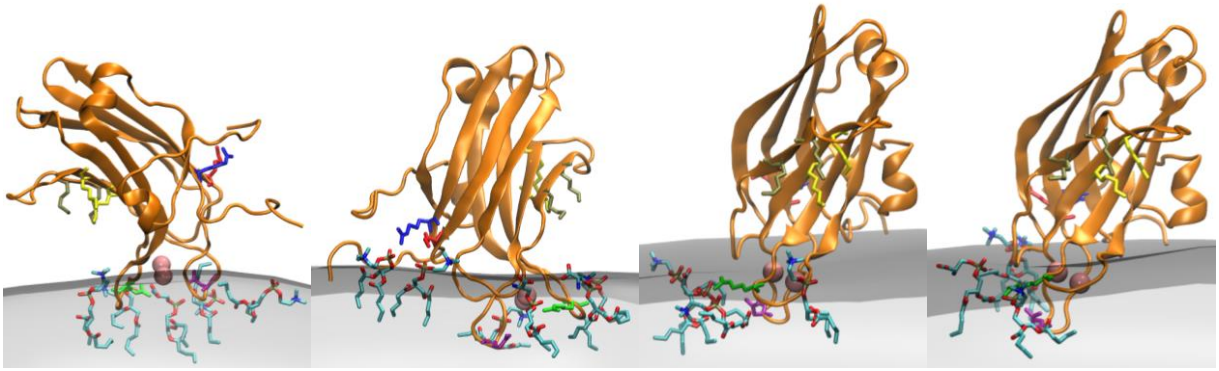

LA_per2_N3

t = 10 ns **t = 20 ns** **t = 30 ns** **t = 40 ns**

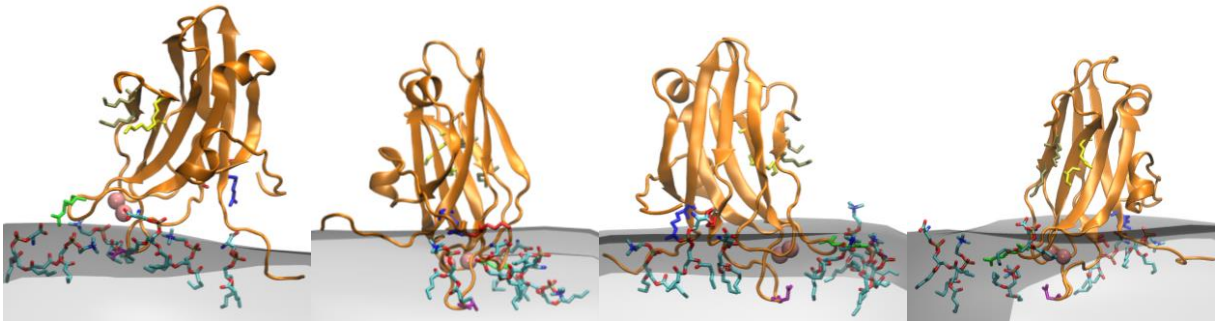

LA_per2_N4

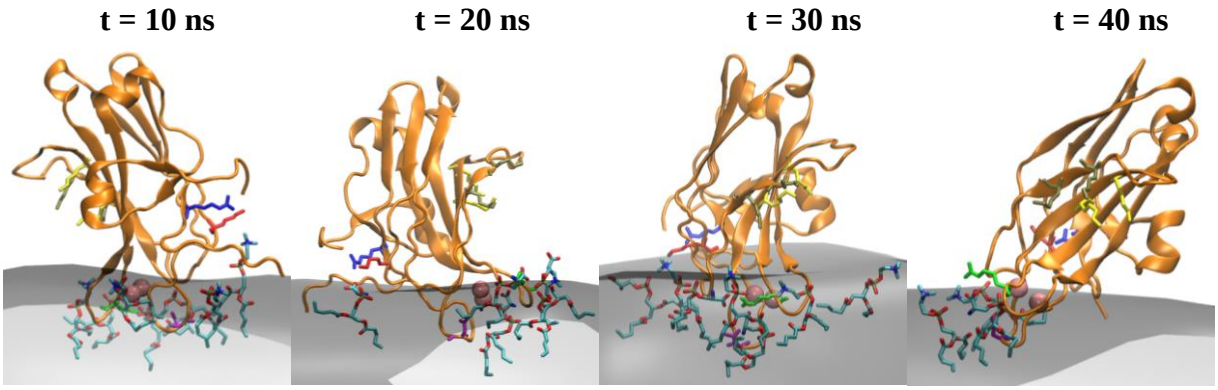

Figure 69: Close up snapshots for LA_per2 systems
Snapshots at the interval of 10 ns for four runs of LA_per2 HMMM model systems. Protein's residues R249 from loop3 (green), N189 from loop1 (purple), R161 from strand β1 (blue), K181 from strand β2 (red), strand β3 (yellow), strand β4 (tan) and Ca^{2+} ions (pink) are also shown. Membrane is represented as quicksurf in grey. PC/ PS short-tail lipids are also shown as within 6 Å of R249, N189, R161, K181 and Ca^{2+} ions. Water and ions are not shown for clarity.

LA_tilt_N1

t = 10 ns **t = 20 ns** **t = 30 ns** **t = 40 ns**

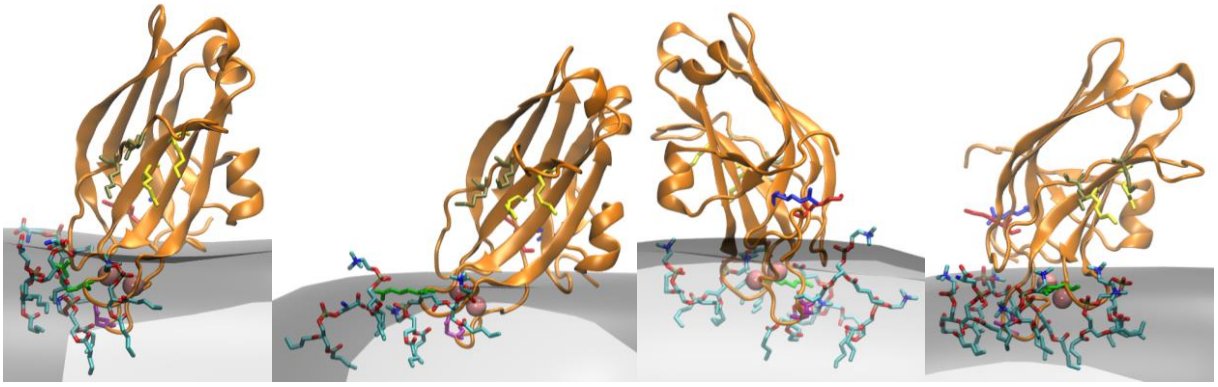

LA_tilt_N2

t = 10 ns **t = 20 ns** **t = 30 ns** **t = 40 ns**

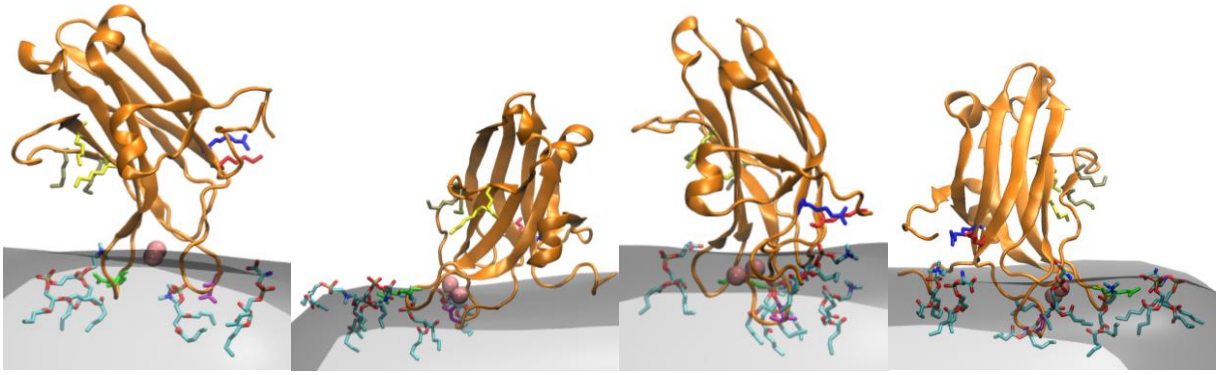

LA_tilt_N3

t = 10 ns **t = 20 ns** **t = 30 ns** **t = 40 ns**

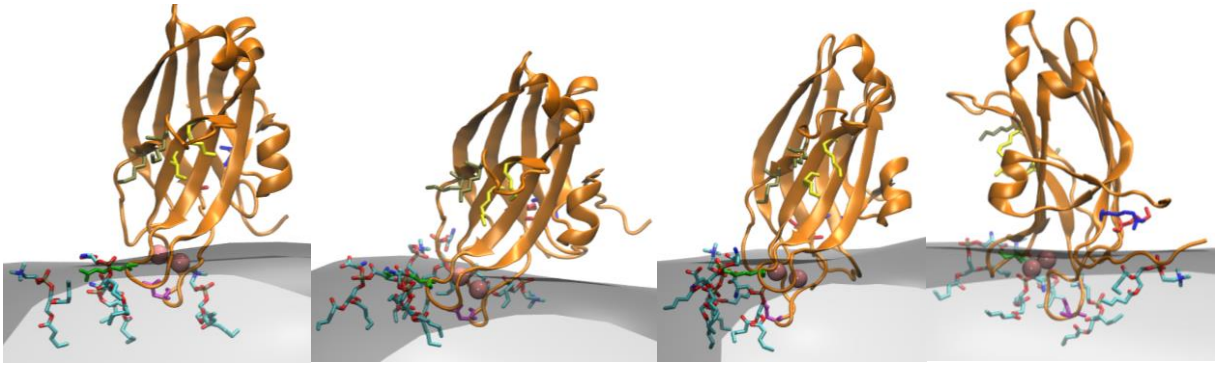

LA_tilt_N4

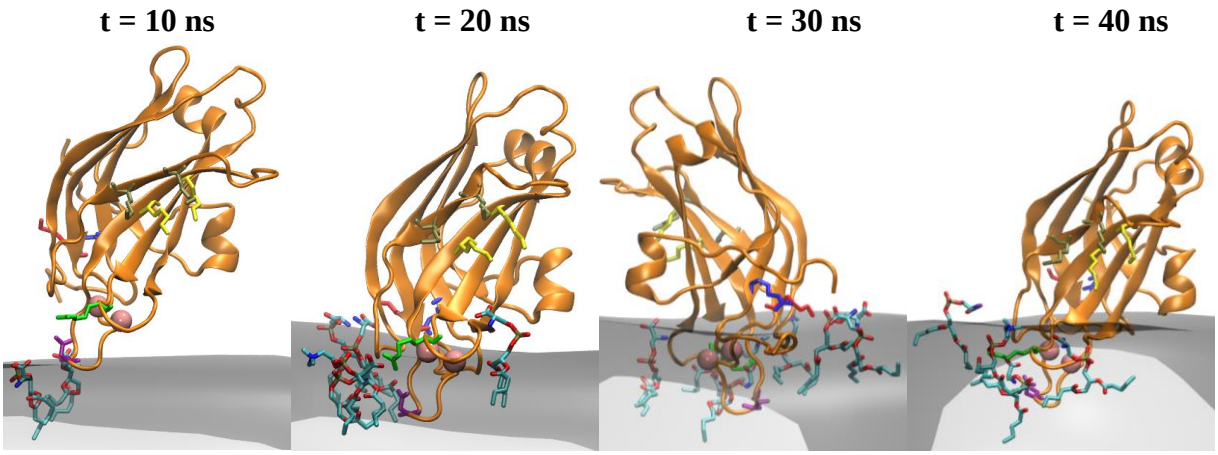

Figure 70: Close up snapshots for LA_tilt systems
Snapshots at the interval of 10 ns for four runs of LA_tilt HMMM model systems. Protein's residues R249 from loop3 (green), N189 from loop1 (purple), R161 from strand β1 (blue), K181 from strand β2 (red), strand β3 (yellow), strand β4 (tan) and Ca^{2+} ions (pink) are also shown. Membrane is represented as quicksurf in grey. PC/ PS short-tail lipids are also shown as within 6 Å of R249, N189, R161, K181 and Ca^{2+} ions. Water and ions are not shown for clarity.

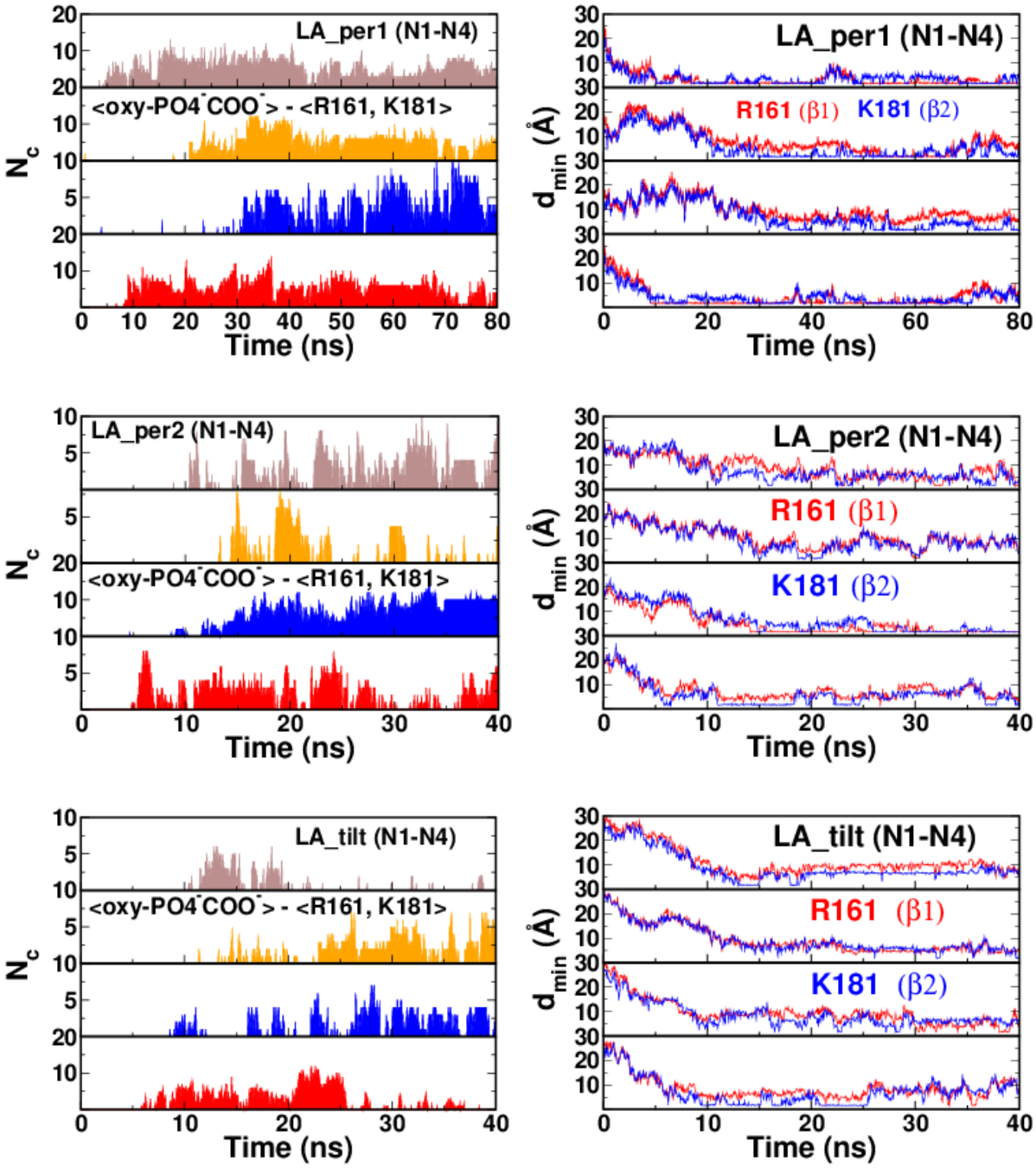

Figure 71: Direct contacts and minimum distance for strands β1 and β2
The direct contacts, N_c, between (R161, K181) and oxygen atoms of PO_4- or COO^- moieties from membrane top leaflet for LA_per1, LA_per2 and LA_tilt systems (left column) and minimum distance, d_{min}, between R161 (β1, red), K181 (β2, blue) and PO_4-/ COO^- moieties from membrane top leaflet for the same systems (right column).

In systems with area per lipid of 125 $Å^2$, we observe that loop 1 is deepest and K205 is far from the membrane (Figure 56 – 58) and the orientation angle remains ~ 30 ° (Figure 55). These three observations match the X-ray reflectivity measurements (31). However recall that Chen and co-authors (31) had proposed two experimentally indistinguishable final states per1 ($\theta = 35^\circ$, $\varphi = 210^\circ$) and per2 ($\theta = 35^\circ$, $\varphi = 0^\circ$). We can characterize the distinction between these two configurations, by CBLs insertion within the membrane. In the per1 state (mentioned as preferred in Chen's paper) loop 1 is deepest inserted within the headgroup region, the loop 2 was mentioned as on the membrane surface and the loop 3 was said to be above the membrane surface. This distinction among the sequence of CBLs positioning with respect to the membrane was very clear. Nevertheless, in per2 state, loop 1 was mentioned to be deepest within the headgroup region, afterwards the loop 3 was positioned and then the loop 2 was located i.e., the sequence of the positioning of the CBLs with respect to the membrane was respectively as loop 1, loop 3 and loop 2. However, the positional distinction between loop2 and loop3 was not sharp, especially the position of loop 3 was not clear. In simulations, through close observation of the trajectories and snapshots, the final configurations from all runs is in more accordance with Chen's per2 state.

The Ca^{2+} ions are appropriately interacting with the negative moieties (PO_4^-/ COO^-) of the membrane (Figure 62 - 64) though a key difference from N = 15 HMMM model systems (area per lipid 81 $Å^2$) and FM model systems (area per lipid ~ 61 $Å^2$) is that loop 1 does not continue to fluctuate randomly, but attains a steady state (red data curve in Figure 59 – 61). Moreover, visual inspection of the snapshots (Figure 65 – 70) show that the PKCα-C2 domain eventually attains a so-called perpendicular orientation (31) as the dynamically stable membrane bound configuration. So, in conclusion, when we simulate the experimentally available orientations such as X-ray reflectivity per1, per2 (31) or EPR tilt (28) as the starting orientation, eventually these orientations

attain a bound configuration that is very close to that measured by X-ray reflectivity when the area per lipid of the membrane is comparable to the experimental value.

We have observed a clear distinction in the orientation of the C2 domain based upon the lipid densities irrespective of the initial starting orientation. In Chapter 3, when we used area per lipid as 81 $Å^2$, the final steady state orientation attained by the C2 domain is so-called parallel but as in this chapter when we used a larger area per lipid, 125 $Å^2$, the final equilibrated steady state orientation is perpendicular. Area per lipid makes such a large difference in the final outcome of the bound configuration in the PKCa-C2 domain.

A recent study by Honigmann and co-authors (109) showed that Synaptotagmin-1 C2B domain can simultaneously bind to two different membranes namely PIP2-contaning plasma membrane through polybasic patch and PS containing vesicle membrane through Ca^{2+} ions. Such a binding puts C2B domain in perpendicular orientation. However, the same C2B domain binds in parallel orientation to a plasma membrane containing both PIP2 and PS through polybasic patch and Ca^{2+} ions respectively. In another study by Ohkubo and co-authors (63) of a human coagulation factor VII GLA domain using FM model with area per lipid as ~ 65 $Å^2$ and HMMM model with area per lipid as ~ 127 $Å^2$, the authors did not observe any significant change in the GLA domain binding with the membrane.

It seems in the case of PKCα-C2 domain, the local factors, especially the initial approach of the domain towards membrane plays key role in deciding the final orientation. For example, in case of larger area per lipid (i.e., lesser lipid densities), once loop 1 (N189, neutral though polar) residue get inserted into the membrane it get fully stabilized within ~ 10 ns to 20 ns (brown data cure Figure 56 - 58, red data curve Figure 59 – 61). With quicker and deep insertion of loop 1 into the membrane, residue R161 at strand β1 and K181 at strand β2 get engaged with membrane

negative moieties (Figure 68 – 70). Moreover, R161 and K181 have consistent direct contacts with oxygen atoms of PO_4^- or COO^- moieties (Figure 71, left column) and by and large, they are steady and remain within ~ 6 Å of PO_4^- and/ or COO^- negative moieties as evident from minimum distance, d_{min} (Figure 71, right column). Strand β1 and β2 are on the opposite side of the LRC strands β3 and β4. The engagement of these residues from β1 and β2 help anchor the domain from another side instead and renders LRC deprived of its chance of an early engagement with the membrane. At least, it seems that the continual interactions of R161 (β1) and K181 (β2) keep the domain in upright position and not let it inclined towards the membrane. Importantly, K205 remains far away in the bulk water and there were no wild fluctuations observed for it. Moreover, Loop 3 though it has least minimum distance (Figure 59 – 61) with the membrane negative moieties, it follows the penetration depth and pattern as that of Ca^{2+} ions (Figure 56). This is a role reversal between loop 3 and loop 1 from the dense lipid systems of area per lipid ~ 81 $Å^2$. Since there were no wild fluctuations in the system (like that of loop 1 or K205 in dense lipid ~ 81 $Å^2$ systems), under this scenario, the LRC and K205 which interacts electrostatically with the PS/ PIP2 was not able to come under the influence of them. This keeps C2 domain in perpendicular orientation in lesser lipid densities systems.

The real life biological systems are too complex. There are myriad of factors that could affect the bound configuration, lipid densities is just one of them. One of the advantages of MD is that one can play around and try out any model system not necessarily a physical one! This leave us with lots of excitement and almost infinite possibilities to change or tweak the lipid densities in a more systematic way along with trying out FM models in future given to the real world constraint of the availability of computer time!

5 Role of PIP2 in PKCα-C2 domain Bound Configuration

5.1 Introduction

In this chapter, we explore the hypothesis proposed at the end of Chapter 3 that the addition of phosphatidylinositol-4,5-biphosphate (PIP2) into the PC + PS mixed membrane system does not affect the overall configuration of the membrane bound PKCα-C2 domain in an open-faced configuration. These studies utilize the smaller area per lipid, 61 $Å^2$ for the FM model that were studied in Chapter 3.

Several studies have explored the role of PIP2 in defining the membrane bound configuration of the PKCα-C2 domain and its effect on subsequent activation of the enzyme (27, 29, 30, 32, 93, 103, 110).

We first review the traditional scheme of PKCα activation discussed in Chapter 3 (Section 3.1). Extracellular signals trigger the hydrolysis of PIP2 which produces diacylglycerol (DAG) and inositol 1,4,5-trisphosphate that, in turn, releases Ca^{2+} ions from intracellular stores. In the presence of excess cytosolic Ca^{2+} ions, two or three Ca^{2+} ions bind to the C2 domain, which drives it to the plasma membrane where it bridges the C2 domain to anionic phospholipids, in particular, to phosphatidylserine (PS) in the plasma membrane. In addition, DAG in the membrane binds to the C1 domain (74). The PKCα-C2 domain recognizes both PS (23, 77-81) and PIP2 (27, 82-86, 111) at the membrane surface. Studies of the configuration of PKCα-C2 bound to a PC + PS mixed membrane that includes PIP2 are required to understand the role of the interaction between PIP2 and PKCα-C2 in the activation of the full-length PKCα enzyme.

It is established that two different protein motifs of the PKCα-C2 domain bind to two different phospholipids in the plasma membrane (74). The lysine rich cluster (LRC) of PKCα-C2

domain is thought to bind to PIP2 (27, 29, 30, 82, 84-86, 94, 104) and the Ca^{2+} ions complexed with calcium binding loops (CBLs) bind to PS lipids (23, 27, 77-81).

However, the issue of PIP2 binding to the C2 domain becomes very interesting within the scheme of PKCα activation as a few studies challenge the aforementioned traditional activation scheme. Using their results on the ternary complex crystal structure of PKCα-C2 in the presence of Ca^{2+} ions and short chain 1,2-dicaproyl-sn-phosphatidyl-L-serine (DCPS) (PKCα-C2 - Ca^{2+} - DCPS), Verdaguer and co-authors suggested that the C2 domain - membrane binding is a result of direct bridging of a Ca^{2+} ion to PS membrane lipid (23). Subsequently, Guerrero-Valero and co-authors suggested that PIP2 binds to the LRC region and PS to the CBL region (27). They showed that the phosphate moieties of PIP2, apart from making direct contacts with the lysine residues (K197, K209 and K211), also make direct contacts with aromatic residues (Y145, W245) present within the LRC region of the domain. Interestingly, they showed that the hydrophobic residues Y195 and W245 were crucial for plasma membrane binding. Mutating these hydrophobic residues critically impaired the ability of the full-length PKCα enzyme to translocate to the plasma membrane even in the presence of excess Ca^{2+} ions and DAG (27, 74, 112, 113). Moreover, through mutational studies Medkova and Cho (95) described the hydrophobic nature of C2 domain binding. Recently, Scott and co-authors used stopped-flow spectroscopy to argue that although hydrophobic interactions play a dominant role in binding the C2 domain to the membrane, the electrostatic interactions are responsible for retention of the C2 domain at the membrane (99). Both of these studies suggested that hydrophobic residues, like W245 and W247, which are situated on CBL3, could penetrate the membrane. However, the conventional view of PKCα-C2 membrane binding is that electrostatic interactions between the positively charged Ca^{2+} ions (bound to CBLs), the LRC strands β3 (K197, K199), β4 (K209, K211), and the negatively charged PS and/ or PIP2

in the membrane drives the binding and eventually dictates the overall configuration of the C2 domain at the membrane surface. This view is in line with other studies of the electrostatically driven membrane recruitment of the C2 domains (100, 101, 114). Furthermore, a recent enzymatic activity study by Egea-Jimenez and co-authors (103) showed that in the presence of 5 mol% PIP2, the full-length PKCα reaches its full activation strength even in the absence of DAG and a low concentration of cytoplasmic Ca^{2+} ions. Moreover, in the case of isolated PKCα-C2 domain, it is shown that the presence of PIP2 clearly reduces the concentration of Ca^{2+} ions required for membrane binding (84, 104). These results show that the binding of C2 domain to PS and PIP2 play a defining role in the enzyme's activation.

The effects of the PIP2 in defining the membrane bound configuration is further demonstrated by a few biophysical studies. EPR and the ATR-IR experiments have studied PKCα-C2 on mixed PC/ PS/ PIP2 membranes. However, the contradictory results were reported for the effect of PIP2 on the overall orientation of the C2 domain. For example, EPR site-directed and relaxation experiments (29) showed that the PKCα-C2 domain assumed an orientation parallel to the PC + PS membrane but the presence of PIP2 re-oriented the long axis of the domain to make an angle θ_1 of 50° ± 10° with respect to the membrane normal i.e., the domain is pushed away from the membrane. Similarly, an EPR guided MD simulation study (30) showed that the C2 domain lies parallel to the membrane in PC + PS membrane but PIP2 binding to the LRC region pushes the C2 domain away from the membrane so that the tilt angle, θ_2, becomes 53° ± 2°. If two PIP2 bind to the LRC region then the domain is pulled closer to the membrane to attain a tilt angle $\theta_2 = 60° \pm 1°$. However, ATR-IR spectroscopy experiments (32) showed that the orientation of the C2 domain bound to a PC + PS membrane is closer to a perpendicular orientation with $\theta_1 \sim 51°$ but in the presence of PIP2, $\theta_1 \sim 60°$, i.e., the C2 domain is oriented closer to the membrane surface.

It is not yet clear whether these different results are due to different preparation conditions or some other aspect of the experiments.

Here, through three distinct MD simulations we probe the recognition of PIP2 by the PKCα-C2 domain and its effect on the membrane bound configuration of the PKCα-C2 domain, as well as identify the molecular level interactions between domain residues and lipid moieties.

5.2 Methods

The Full Membrane (FM) model is used in this chapter. An SOPC lipid from the previously equilibrated SOPC + SOPS mixed membrane will be replaced by a PIP2 lipid. The PKCα-C2 domain is positioned initially so that LRC is close to PIP2 under the expectation that it will bind there. In principle, the negatively charged phosphate moieties of the PIP2 could bind and interact with positive residues of the LRC region in an innumerable ways. Keeping this in mind, we have simulated three PC + PS + PIP2 systems differing in the initial orientation and placement of the inositol ring with respect to the LRC region of the PKCα-C2 domain. One system with 1DSY crystal structure (as provided by Chen et al (31)) (abbreviated as Sim1) is simulated for 700 ns and other two systems with 3GPE crystal structure (abbreviated as Sim2 and Sim3) were simulated for 200 ns each (see details below). Collectively, all three systems that involved PIP2 are referred as "pip2_systems". Sim1 is modeled such that to establish spontaneous binding of the PIP2 to the PKCα-C2 domain. Sim2 is performed to test the stability of the crystallographic structure of the docked PIP2 to the PKCα-C2 domain (27) and to test the orientation of the domain with respect to the membrane as mentioned in the literature (29, 30, 32). Sim3 is modeled based upon the insights obtained through Sim1 and Sim2 to establish the stable membrane bound configuration of the PIP2 docked PKCα-C2 domain.

5.2.1 Sim1 Model System

From our FM model system described in Chapter 3, we took a snapshot of the tilt_FM model system at 300 ns (Figure 72A), then replaced an SOPC lipid located close to the LRC region with a PIP2 lipid such that the phosphorous atom, P1, of the PIP2 occupied almost the same position as that of the phosphorous atom of the SOPC (Figure 72B). Moreover, PIP2 is arbitrarily oriented with its inositol ring somewhat perpendicular to the membrane plane (Figure 72D). The starting orientation of the PKCα-C2 domain is shown in Figure 72C, where, we see that the strand β4 is lying flat above the membrane, strands β3 and β4 are parallel in a vertical plane such that β3 is located above β4, and two bound Ca^{2+} ions are lying away from the membrane in the bulk water (also see close up Figure 72D). This configuration is similar to an intermediate state orientation adopted by several FM/ HMMM model systems that followed the sharp fall mode described in Chapter 3, Section 3.4.6.

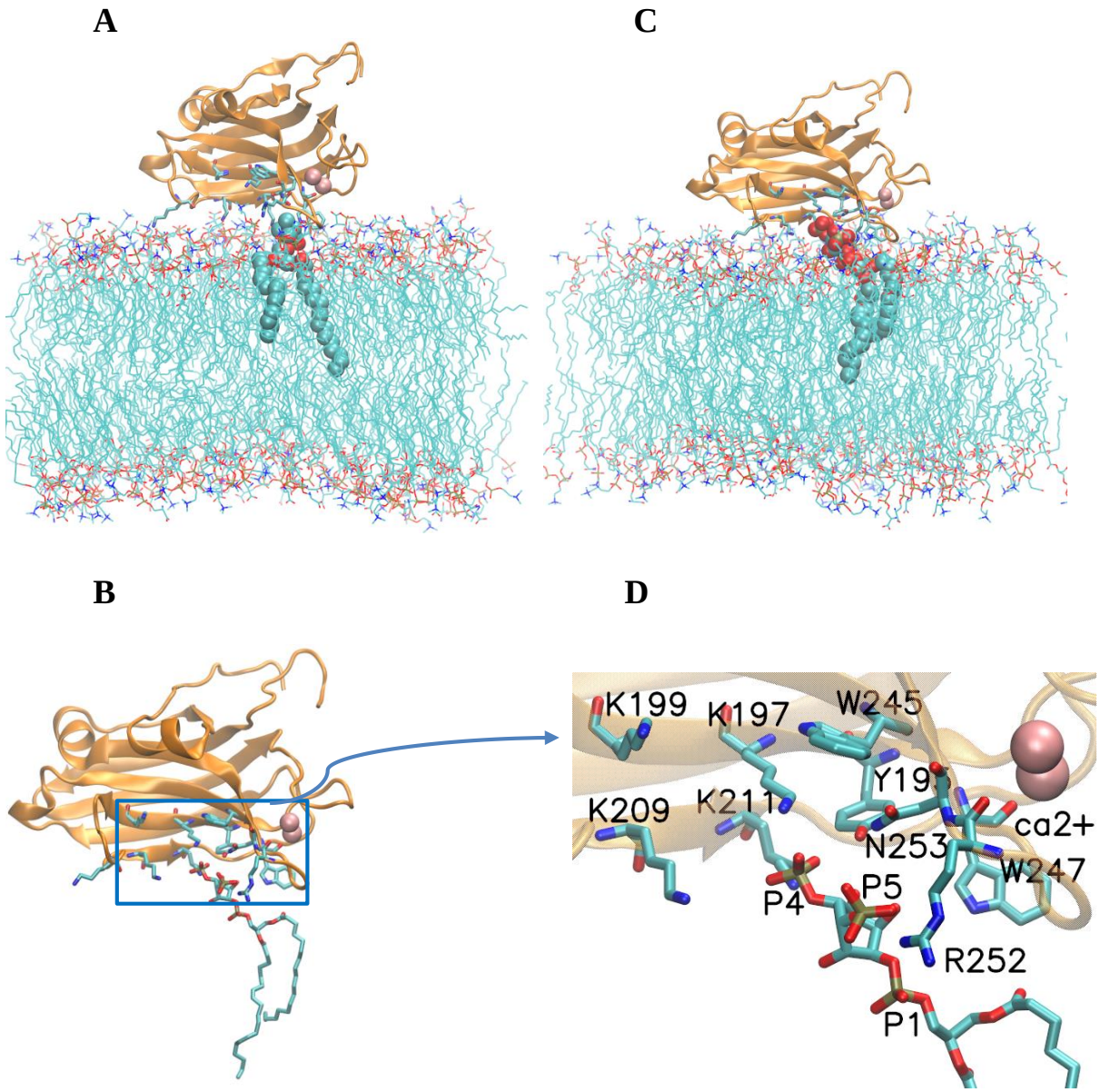

Figure 72: Preparation of Sim1 model system
(A) tilt_FM at 300 ns with SOPC shown in VDW representation (B) SOPC is replaced by PIP2 (C) Initial configuration for Sim1 system. PIP2 is shown in VDW representation. (D) Close-up of the inositol ring as positioned in LRC region. Strands β3 (K197, K199) and β4 (K209, K211) are in a vertical plane. Initial orientation of inositol ring is somewhat perpendicular to the membrane plane. LRC region residues and PIP2 are shown in licorice representation. Ca^{2+} ions are also shown in VDW representation in pink color.

Na^+ Cl^- ions were added to neutralize the system and attain a 100 mM concentration. The system was energy minimized for 5000 steps (10 ps) and then the temperature was gradually raised to 310 K. Thereafter, it was run for 300,000 steps (0.6 ns) during which time the phosphorous atom, P1, of the PIP2 lipid, the Cα atoms of the C2 domain, and Ca^{2+} ions were harmonically constrained with a force constant, k = 2 kcal·mol^{-1}·Å^{-2}. The system is further run for 100,000 steps (0.2 ns) with relaxed constraints on the PIP2 phosphorous atoms, P1, but the Cα atoms of the C2 domain and Ca^{2+} ions were still harmonically constrained with a force constant, k = 2 kcal·mol^{-1}·Å^{-2}. Eventually, all constraints were removed and the system was freely equilibrated for 50,000 steps (0.05 ns). The restart files generated through the last step of free equilibration are then used, along with the usual initial coordinate pdb file, topology psf file, and parameters file to run the system on Anton supercomputer (D E Shaw Research, New York) for 700 ns.

5.2.2 Sim2 Model System

The initial set up for Sim2 system is shown in Figure 73. Here we took the system as prepared above i.e., Sim1 system and replaced the PKCα-C2 domain, the bound Ca^{2+} ions plus the inositol ring by the crystal structure of the ternary complex comprising PKCα-C2 domain + Ca^{2+} ions + soluble PIP2 inositol ring (27) (PDB ID: 3GPE). We have to move around and/ or tweak the headgroups/ tails of a few membrane lipids in order to avoid any steric clashes/ overlaps with the domain. Due to the flexibility of the PIP2 tail, based upon 3GPE crystal structure, one can conceive several initial orientation(s) for the PIP2 bound PKCα-C2 domain. However, the choice of initial state is guided by two considerations – the overall configuration and the orientation angle of the PKCα-C2 domain. The overall configuration is kept as close-faced that resembles the final state as predicted in literature (29, 30). The predicted orientation angle has a range of ~ 40° to ~ 60° with respect to the membrane normal in literature (29, 30, 32) (see introduction, Section 5.1).

We set the initial orientation angle θ_1 (or θ_2) as ~ 70° in anticipation that if PIP2 binding indeed affect the domain orientation as predicted either by pushing it away from the membrane (29, 30) or by pulling towards the membrane (32) it might converge within the predicted range of ~ 40° to ~ 60° with respect to the membrane.

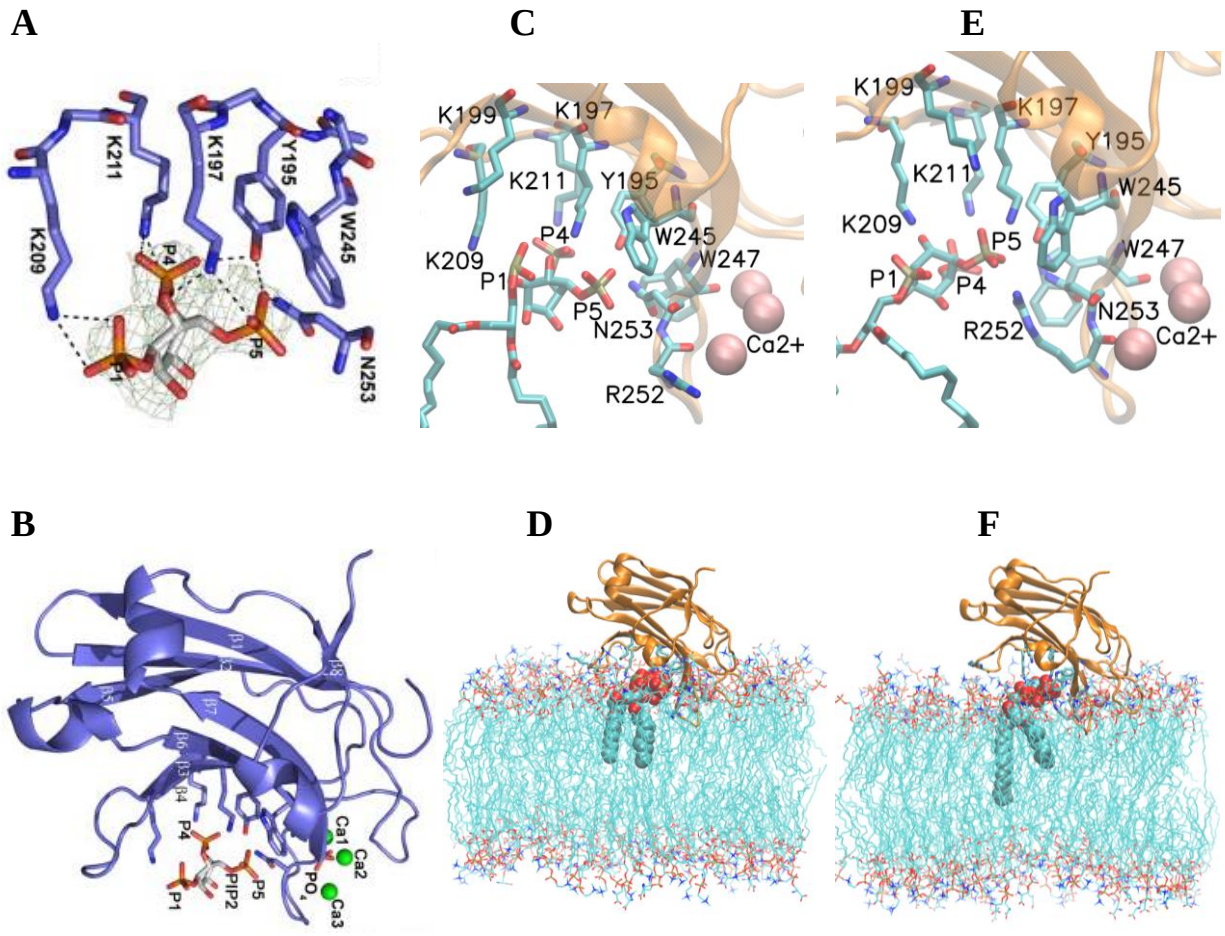

Figure 73: Preparation of Sim2 model system
(A) And (B) show the crystallographic model representing docked inositol ring to the LRC region (Figure 1 from Guerrero-Valero et al. (27)). Residues and phosphate moieties are marked. (C) Shows MD style close-up representation of docked PIP2 to the domain residues based upon crystallographic model (27). (D) Shows one of the membrane embedded representation of the (C) state. (E) Shows the close-up representation of the docked PIP2 and the domain residues at the conclusion of the constrained equilibration step i.e., the initial structure from where production run is initiated. (F) Shows the membrane embedded representation of (E) state.

5.2.3 Sim3 Model System

The initial configuration of the PKCα-C2 domain and the orientation of the inositol ring of the Sim3 system (Figure 74) is guided by the results obtained from Sim1 and Sim2. The Sim3 system is identical to Sim2 except that the initial placement of the P1 atom of the inositol ring was closer to that of the final docked state of the same in Sim1 and Sim2 system. However, the overall configuration is kept as open-faced such that θ_1 (or θ_2) is ~ 90° (Figure 19).

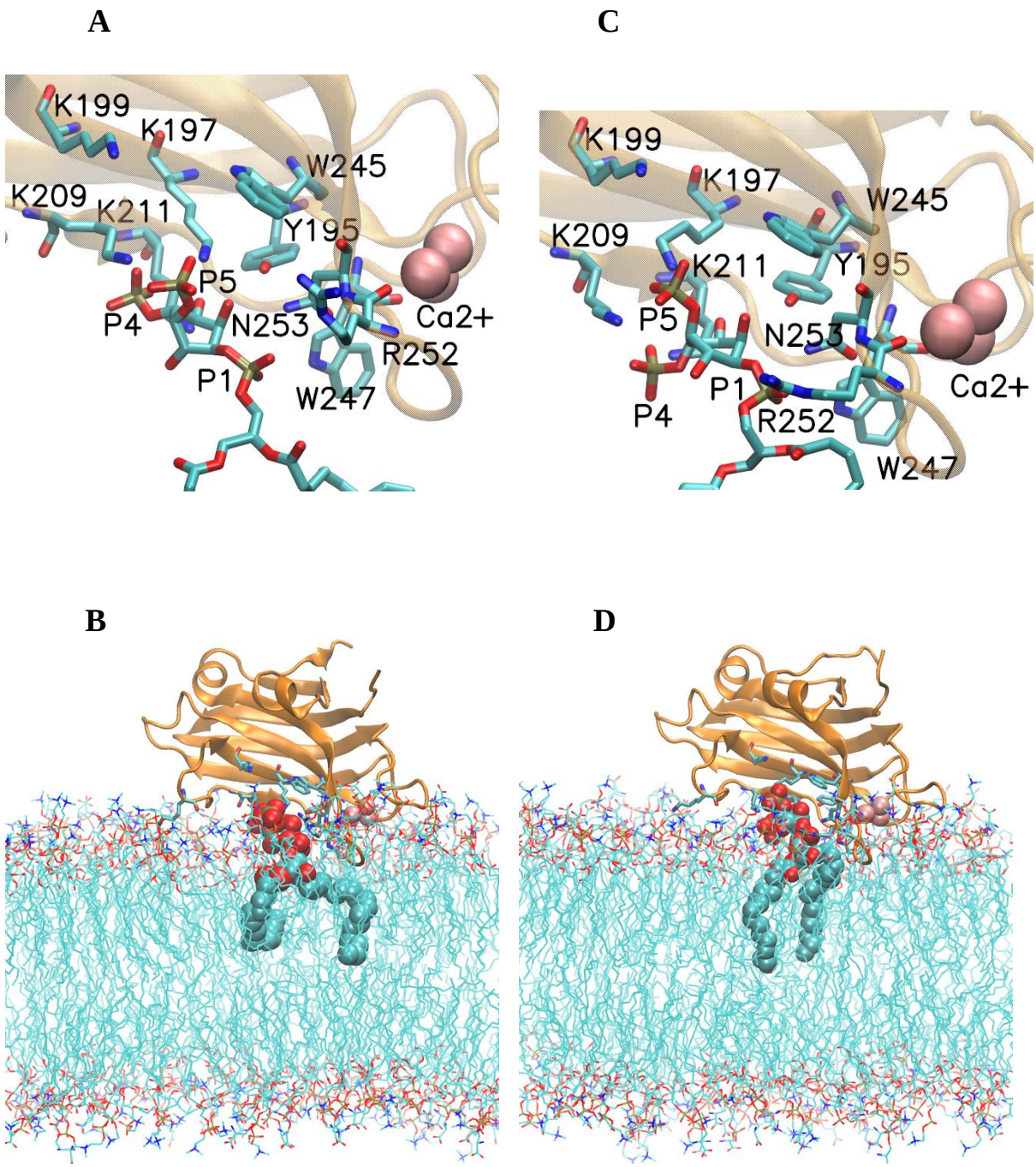

Figure 74: Preparation of Sim3 model system
(A) Shows a close-up positioning of inositol ring in the LRC region as per Sim3 model preparation protocol (see details in methods). (B) Shows the membrane embedded (A) state. (C) Shows close-up representation of inositol ring as docked to domain after constrained equilibration (see text for details). (D) Shows the membrane embedded representation of (C) state. This is the initial configuration in Sim3 case.

For both Sim2 and Sim3 systems, VMD plugin molefaction (50) was used to tweak the lipids. Moreover, K^+ Cl^- ions were added to neutralize the system and attain a 100 mM concentration. The system was energy minimized for 10,000 steps (20 ps) and then temperature was gradually raised to 310 K in increment of 10 K through 500 steps (1 ps) starting from 10 K. For constrained equilibration, all phosphorous atoms of the membrane, P1, P4 and P5 atom of the PIP2 lipid, the Cα atoms along with three bound Ca^{2+} ions were harmonically restrained with a force constant, k = 2 kcal·mol^{-1}·Å^{-2}, and then the system was simulated for 5 ns. Further, the phosphorous atoms of the membrane lipids were relaxed i.e., the restraints were removed from them and the system, still with constrained P1, P4, P5 atom of the PIP2 lipid, the Cα atoms and bound Ca^{2+} ions, was further simulated for 5 ns. Furthermore, two additional steps in constrained equilibration were performed for Sim3 system only and not for Sim2 system. We specifically treated the PKCα-C2 domain, the bound Ca^{2+} ions and the docked inositol ring in Sim2 as a single entity as per the crystallographic structure so we constrained or relaxed these three entities together in Sim2 system. However, in Sim3 system, we treated them separately. So, for Sim3 system only, the constrained on P1, P4 and P5 atoms of the PIP2 lipid were removed but the constrained on Cα atoms along with three bound Ca^{2+} ions were still harmonically restrained with a force constant, k = 2 kcal·mol^{-1}·Å^{-2}, and the system was run for 5 ns. As the last constrained equilibration step in Sim3 system, the restrains on all atoms were removed except that on the bound Ca^{2+} ions and the system was further run for 5 ns. Finally, all constraints were removed and the Sim1 and Sim2 systems were freely equilibrated for 200 ns each.

5.2.4 Simulation Protocol

The simulation protocol is essentially the same as that of other FM model systems used in this thesis (Chapter 3, Section 3.2.5). The only new addition is the parameters for PIP2 provided by Lupyan and co-authors (115).

5.3 Results and Discussions

We present results from the analysis of the MD trajectories from 700 ns long Sim1 and 200 ns long Sim2 and Sim3 systems. The purpose of three simulations are distinct. The Sim1 system shows the spontaneous binding of the PIP2 to the PKCα-C2 domain (pdb ID: 1DSY (23)) such that the domain attained an open-faced docking configuration similar to what it was in PC + PS only membrane. Sim2 shows that the crystallographic structure of inositol ring docked to PKCα-C2 domain (pdb ID: 3GPE (27)) is not stable. Sim3 further establishes the stability and robustness of open-faced PIP2 docked configuration of PKCα-C2 domain (pdb ID: 3GPE (27)) during 200 ns of simulation time. Nevertheless, all three simulations show that the binding of PIP2 does not change the orientation of the PKCα-C2 domain.

The convergence of the angles (θ_1, θ_2), the relative heights $h_r(z)$ and the minimum distance d_{min} are shown in Figure 75A,B,C for the Sim1 system that includes PIP2. The values exhibit striking similarities with the corresponding FM/ HMMM model systems without PIP2 (Chapter 3).

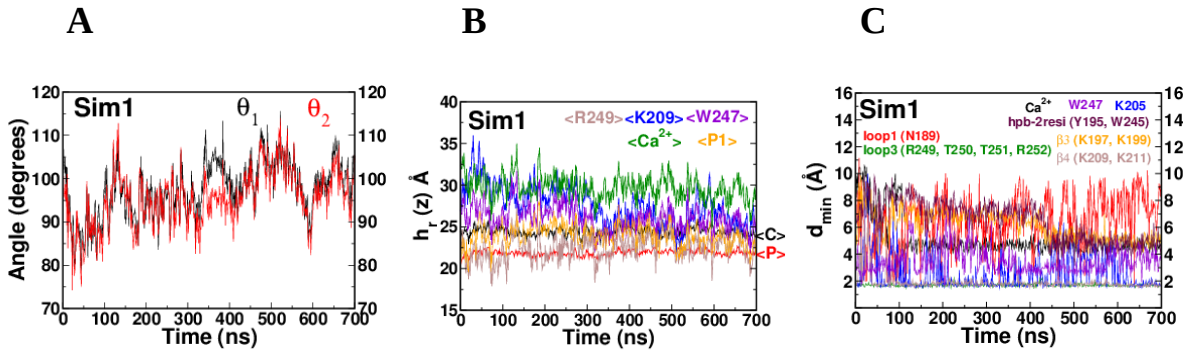

Figure 75: Convergence criteria for Sim1 system
(A) The angles (θ_1, θ_2), (B) relative heights $h_r(z)$, and (C) minimum distance d_{min}.

The angles (θ_1, θ_2) (Figure 75A) were ~ 90° for the initial 100 ns, rising to ~ 100° from 300 ns to 700 ns. This is fairly consistent with the PC + PS system where θ is ~ 90°. This shows that the addition of PIP2 into the membrane system and its binding to the LRC region of the C2 domain does not significantly alter the angular orientation of the PKCα-C2 domain.

On the other hand, the β4 strand penetrates further into the membrane, suggesting a strengthened binding. Furthermore, the relative heights $h_r(z)$ (Figure 75B) reveal that the C2 domain is localized to the membrane in a similar manner as in systems without PIP2 (Chapter 3, Figure 21). For instance, residue R249 penetrates deepest within the membrane, K209 is consistently localized around the <C> plane, W247 penetrates below the <P> plane closer to the hydrophobic core, and Ca^{2+} ions are bound and localized on the membrane surface. Furthermore, Figure 75C (black data curve) shows that the Ca^{2+} ions diffuse towards the membrane from ~ 10 Å initially to ~ 5 Å to come in the contact with the PO_4^- and COO^- moieties within 100 ns. The number of direct contacts N_c between Ca^{2+} ions and oxygen atoms of PO_4^- and COO^- moieties

(Figure 76A) shows that Ca^{2+} ions eventually maintain a sustained contact with the membrane. Furthermore, to reinforce the hydrophobic part of the membrane binding, Figure 76B shows a number of contacts N_c between W247 and the acyl tail of the membrane.

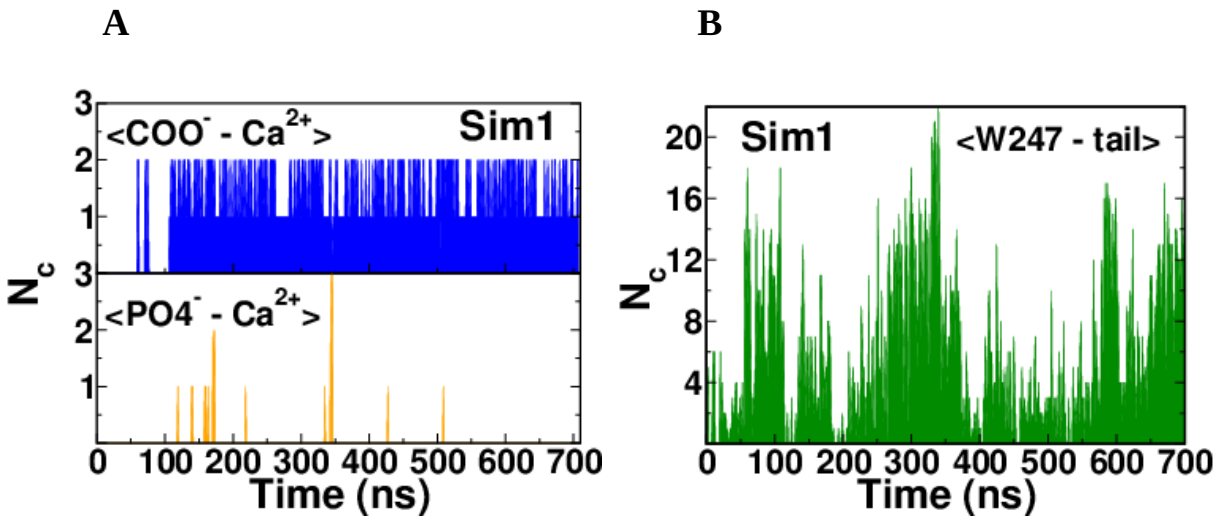

Figure 76: number of direct contacts, N_c, for Sim1 system
Number of direct contacts for (A) Ca^{2+} ions with oxygen atoms of COO^- (top) and PO_4^- (bottom) and (B) W247 with acyl tail.

Figure 77A shows that the number of direct contacts between LRC (strands β3, β4) and oxygen atoms of PO_4^- or COO^- moieties are comparable to the number of contacts for systems without PIP2, viz., per2_FM and tilt_FM models (Figure 77C,D). Oxygen atoms of the phosphate moieties of the inositol ring also have sustained contacts with strands β3 and β4 (Figure 77B). Further, the interaction between phosphate moieties and the LRC seems to be strong as the minimum distance between them is maintained at less than 2 Å (Figure 77E). So, the presence of PIP2 not only enhances the number of direct contacts with the membrane but also increases the strength of the binding.

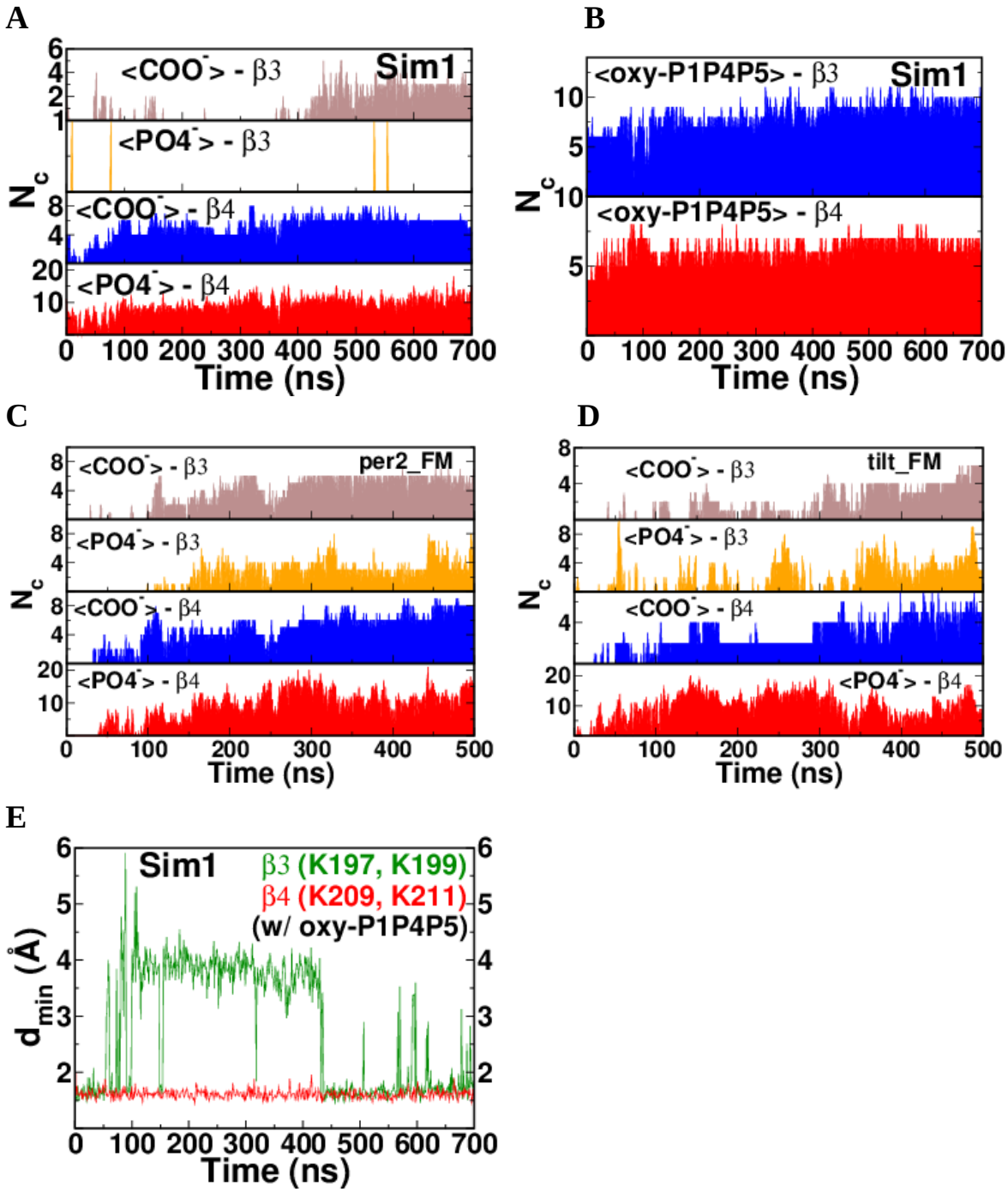

Figure 77: Role of LRC in Sim1 system
Number of direct contacts, N_c, between strands β3, β4 and (A) oxygen atoms of PO_4- or COO^- moieties from top leaflet of membrane (B) oxygen atoms of all three phosphate moieties of inositol ring. (C) And (D) shows the number of direct contacts between strands β3, β4 and oxygen atoms of PO_4^- or COO^- moieties for per2_FM and tilt_FM respectively. (E) The minimum distance, d_{min}, between strands β3, β4 and oxygen atoms of phosphate moieties.

Finally, critical domain residues are within ~ 2 to 6 Å of the PO_4^-/ COO^- moieties of the top leaflet of the bilayer (Figure 75C). This is similar to the position of the same residues studied by FM/ HMMM model systems without PIP2 (Chapter 3, Figure 29 and Figure 25).

These results show that if the PKCα-C2 domain is bound to the PC + PS mixed membrane in an open-faced configuration, then the introduction of PIP2 into the membrane system does not alter the orientation of the membrane bound PKCα-C2 domain, though it appears to create a stronger binding of the domain with the membrane.

The time evolution of the system is shown in Figure 78.

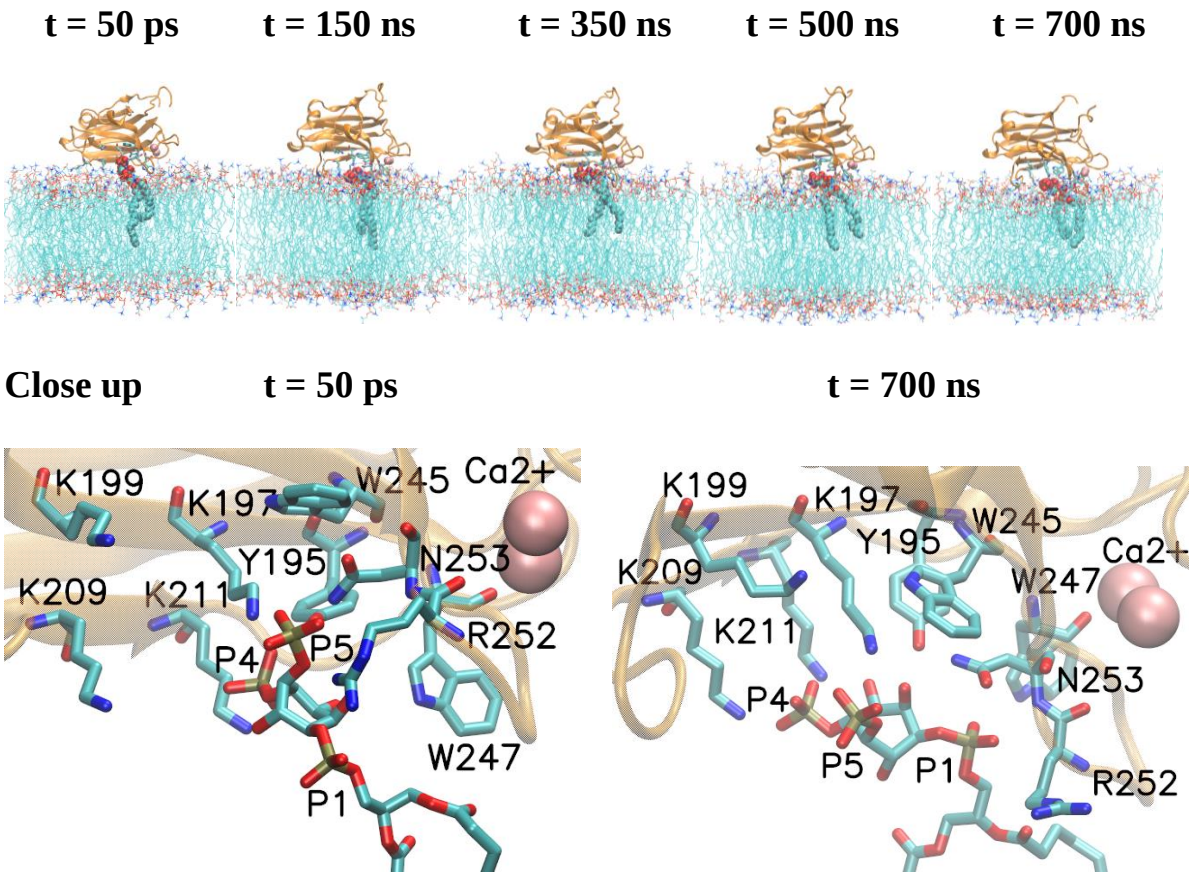

Figure 78: Time series of membrane bound configuration of PKCα-C2 in Sim1 Initial configuration at 50 ps (top far left) and final configuration at 700 ns (top far right). Bottom row shows a close-up of inositol ring interacting with the LRC region residues. Residues, as marked, are drawn in licorice representation. PIP2 is drawn in VDW (top) and licorice (bottom) representation. Coloring is by atom type where red is oxygen, blue is nitrogen, cyan is carbon and brown is phosphorous. Domain is shown as transparent in orange color. Ca^{2+} ions are also shown (pink).

Snapshots of the inositol ring shows that it attained a somewhat flatter orientation (with respect to the membrane surface) so that all three phosphate moieties make direct contact with the C2 domain (Figure 78 bottom row at 700 ns). This ring orientation is in line with the crystal structure (27) where it was shown that all phosphate moieties of the ring make direct contact with the LRC region residues, although the exact interacting pairs of residues and phosphate moieties

are different. Notably, in the crystal structure it was shown that the partially solvent exposed phosphate P1 moiety makes a salt bridge with the strand β4 residue K209. This could be possible only when strand β4 remains close to the membrane. Arguably, this is possible either when strand β4 goes deep within the membrane headgroup region (as shown in our results) or the P1 phosphate moiety moves slightly away from the membrane. Figure 79 shows that the phosphorous atom P1 of PIP2 lies in the same plane as that of the phosphorous atom plane of the SOPC/ SOPS. Other inositol ring phosphorous atoms, P4 and P5, also lie within the headgroup region of the membrane lipids.

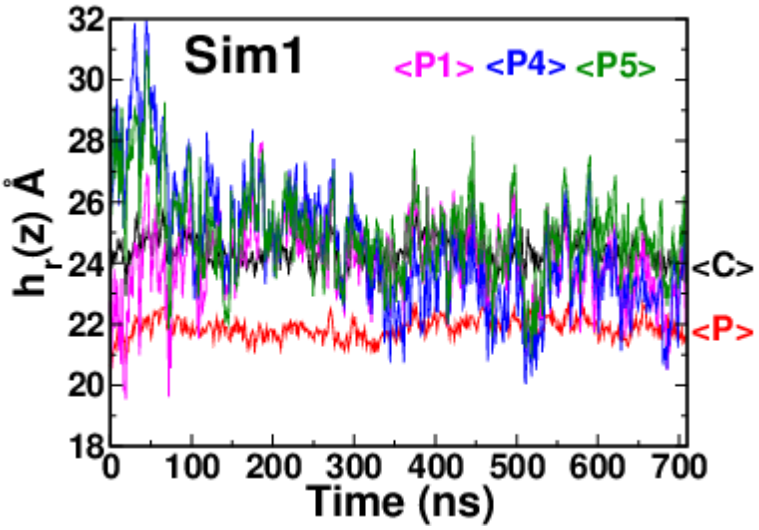

Figure 79: Relative heights for phosphorous atoms of PIP2 in Sim1
The relative heights $h_r(z)$ of phosphorous atom P1 (magenta), P4 (blue) and P5 (green) of inositol ring is shown with respect to the C-atom plane of COO^- moieties (<C> black) and P-atom plane of PO_4^- moieties (<P> red).

The interacting pairs between C2 residues and PIP2 moieties observed in the crystal structure are not observed in the MD simulations. In Sim1 system, the initial position of the PIP2

lipid allowed the P1 phosphate moiety to move towards K209 as suggested in the crystal structure. Instead it moved towards N253, which the crystal structure suggests should have a weak hydrogen bond with the P5 phosphate moiety. So, we have a reversal of interacting pairs (Figure 78 close-up at 700 ns). Although it seems sensible that maximum and stable binding is attained with all phosphate moieties of the ring interacting with the C2 domain, further investigation is needed to test the steric specificity and the exact binding mode among the phosphate moieties and the protein residues.

To test the steric specificity of the PIP2 as docked in crystallographic structure (27), we have modeled and simulated Sim2 system which is essentially a replication of crystallographic structure in an MD appropriate mixed membrane environment (see methods, Section 5.2.2 for details). A simulation of 200 ns revealed two key results. First, one of the distinctive feature of the crystallographic structure, the binding of P1 phosphate moiety ($P1O_4^-$) to K209, is not stable. It is said that P1 phosphate moiety makes a solvent exposed salt bridge with K209 (27). Figure 80 shows the time series snapshots representing the distance between P1 (of $P1O_4^-$ moiety) and the Nitrogen atom (at ζ position of the NH_3^+ moiety in K209) with time. It changes from ~ 4 Å to ~ 8.5 Å within 2 ns. The $P1O_4^-$ moiety moved away from the K209 influence very early on clearly suggesting that the salt bridge did not remain intact. Instead, through careful look at the trajectory, it appears that it goes towards N253/ R252 which are situated on loop 3. By the initial 5 ns, the distance between P1 (of $P1O_4^-$) vs. nitrogen of NH_3^+ moiety in K209 and side chain nitrogen (at η^1 position of H_2N^+ moiety in R252) was ~ 7.5 Å and ~ 5.5 Å respectively and by the 10 ns, the distance became ~ 8.5 Å and ~ 4 Å for the same. Eventually, the distance between P1 (of $P1O_4^-$) and nitrogen atom (of NH_3^+ in K209) and nitrogen atom (of H_2N^+ moiety in R252) stabilizes for ~ 8.5 Å and ~3.5 Å respectively over a period of 200 ns (Figure 80). Thus, there is a complete re-

orientation of the inositol ring in Sim2 system and $P1O_4^-$ moiety goes towards N253/ R252 similar to Sim1 system. Moreover, we tried many other test runs (data not shown) where we have changed the overall orientation of the domain but kept the geometry between inositol ring and the domain as it is in the crystal structure (27) and employed varied MD protocols during constrained equilibration phase. Within the membrane embedded scenario in MD, we have noted that during production runs the P1 moiety of inositol ring did not remain bound to K209.

t = 50 ps **t = 1 ns** **t = 2 ns**

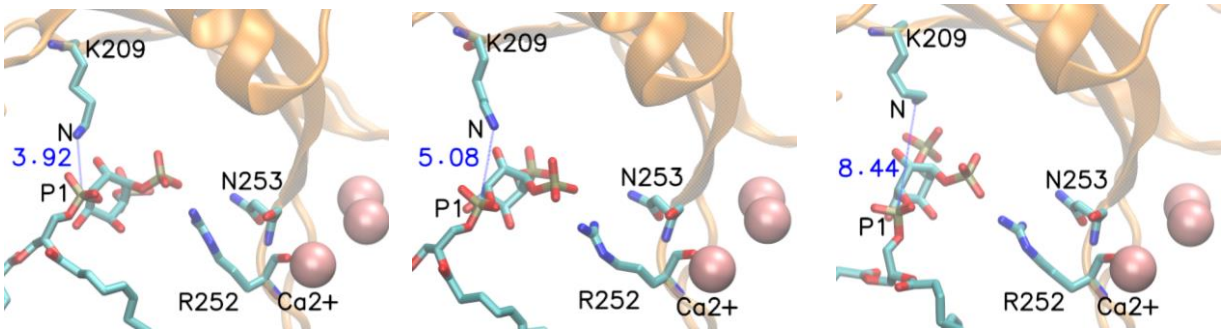

t = 5 ns **t = 10 ns** **t = 50 ns**

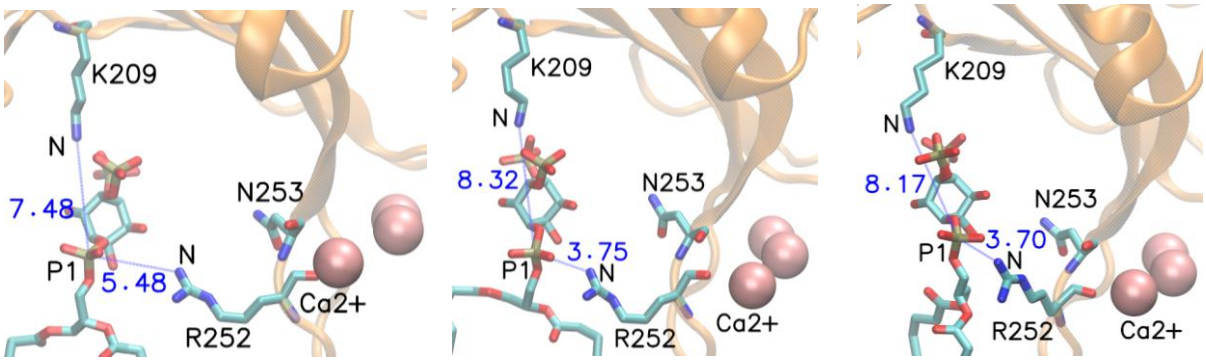

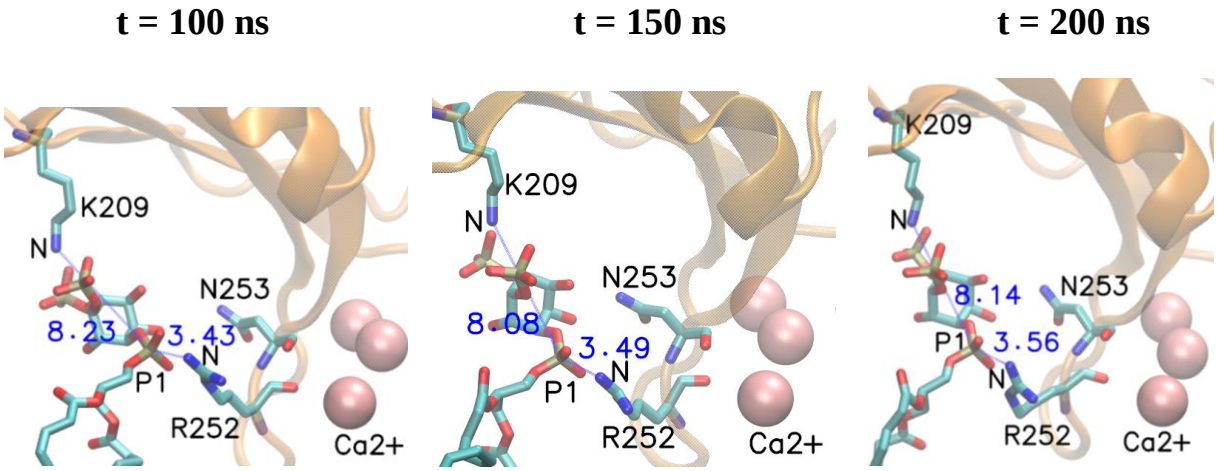

Figure 80: Close up of inositol ring orientation in Sim2 system
P1 moiety of PIP2 get detached from K209 very early on as evident in the time series snapshots (top row). Engagement of P1 with R252 is shown (middle row). Stabilization of the P1 with respect to the R252 is shown (bottom row). Domain is represented as transparent in orange color. PIP2 and residues are as marked in licorice representation. Ca^{2+} ions are shown in VDW representation in pink color. Distances are given in Å.

Second key result is that the angular orientation of the domain, as defined through angles (θ_1, θ_2), show that it remains ~ 70° over 200 ns long run time (Figure 81A). The changing orientations and steric specificities of the inositol ring of the PIP2 do not alter the overall orientation of the domain even in Sim2 system.

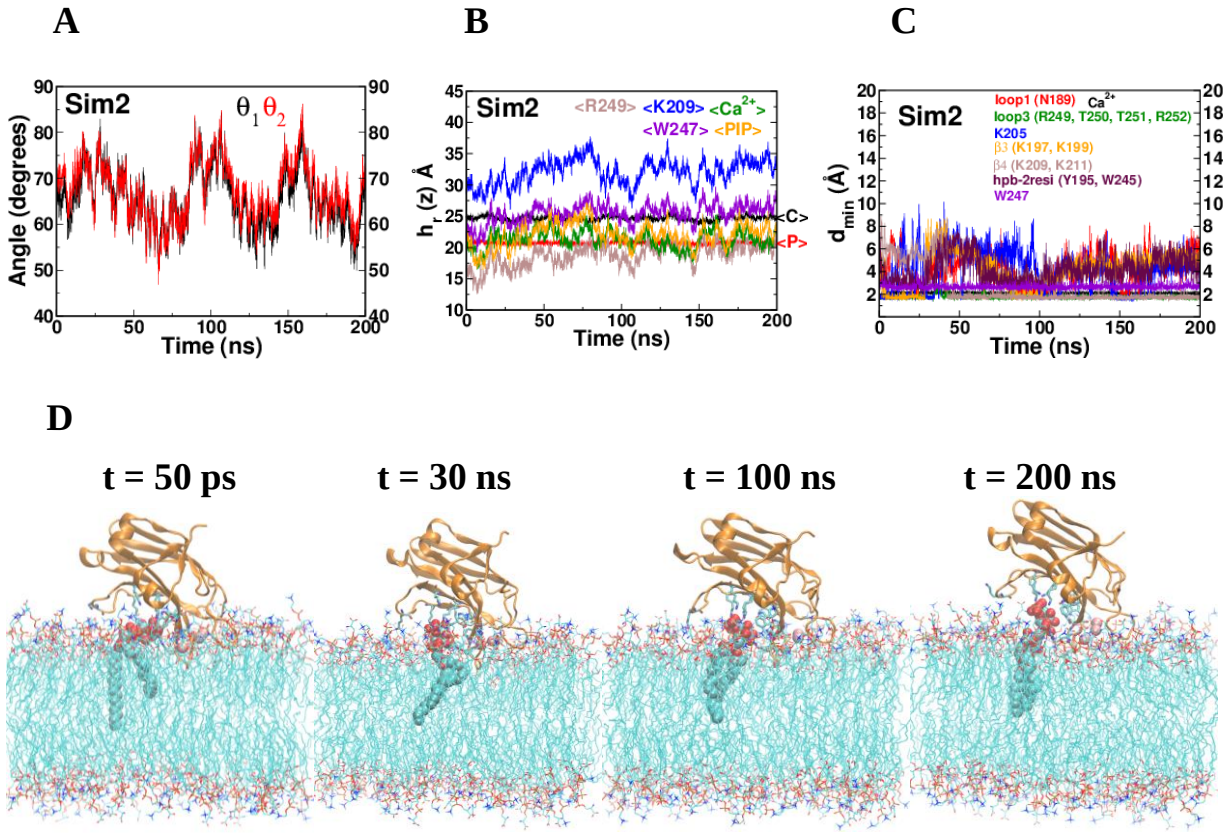

Figure 81: Convergence criteria for Sim2 system
The top row: (A) angles (θ_1, θ_2), (B) relative heights $h_r(z)$, and (C) minimum distance d_{min}. The bottom row: (D) Time series snap shots for Sim2 system.

This is significant as the initial configuration of Sim2 system is modeled with an orientation angle ~ 70° in a close-faced configuration that fairly resembles the final state configuration as predicted by Landgraf and coworkers but with an orientation angle of ~ 50° (29) and by Lai and coworkers but with an angle orientation of ~ 60° (30). Furthermore, Lai and coworkers (30) suggested that binding of one PIP2 lipid would orient the C2 domain more perpendicular to the membrane (~ 53° with respect to the membrane normal) but binding of a second PIP2 would orient the C2 domain in the other direction (~ 60° with respect to the membrane normal), which they

attributed to enhanced electrostatic interactions. In literature, the reported effect of PIP2 on the PKCα-C2 domain is that of introducing a tilt angle of ~ 40° to ~ 60° with respect to membrane normal (29, 30, 32). We had carefully chosen the initial orientation angle of ~ 70° with respect to membrane normal in anticipation that if PIP2 had any effect on the domain orientation, as reported in the literature, then final orientation might fall within the predicted range. However, we observed in Sim2 case that the PKCα-C2 domain remained membrane bound in close-faced configuration with an orientation angle of ~ 70° throughout 200 ns simulation time (Figure 81).

Recall that Landgraf and co-authors (29) used EPR and Lai and co-authors (30) used EPR guided MD simulations to demonstrate that the PKCα-C2 domain is oriented towards the membrane normal in the presence of PIP2. We have already showed (Chapter 3, Section 3.5) that the PC + PS membrane bound C2 domain orientation observed by Landgraf, Lai and co-workers (29, 30) is in the close-faced orientation that is an intermediate state to the open-faced orientation in our longer simulations. Similarly, we conclude that the close-faced Sim2 system could be stuck in an intermediate state even with the PIP2.

We have seen in Sim1 case that the PKCα-C2 domain remains bound in an open-faced configuration without significant re-orientation upon binding with PIP2 upon careful choice of the initial position of PIP2 in the LRC region and a sufficiently long simulation (700 ns). All three phosphate moieties establish and maintain direct contact with the protein in the open-faced configuration, in particular P1 moiety get bound to N253/ R252. In Sim2 case PKCα-C2 domain remained as close-faced configuration over a simulation time of 200 ns. Moreover, it is observed that P1 moiety of PIP2 get moved away from K209 towards N253/ R252 (Figure 80). However, we have also observed in test runs based upon Sim2 model (data not shown) that P1 moiety may not move towards N253/ R252 and may not remain under the influence of PKCα-C2 domain

residues. Our understanding is that the initial state as represented by Sim2 system lead to an intermediate state but still we can derive a clue that P1 moiety might move towards and interact with N253/ R252. Landgraf and co-authors (29) concluded that the P1 phosphate does not interact with the C2 domain, in contrast to our Sim1, Sim2 simulation results and crystallographic results (27).

With the understanding that all phosphate moieties interact with the domain and this is essential for robust and stable binding of the PIP2 with the PKCα-C2 domain, we modeled and simulated Sim3 system. The Sim3 system is essentially same as Sim2 system except that the P1 moiety of PIP2 is initially positioned close to N253/ R252 (Figure 74, see methods Section 5.2.3).

For Sim3 system, the convergence of the angles (θ_1, θ_2), the relative heights $h_r(z)$ and the minimum distance d_{min} are shown in Figure 82. The values exhibit striking similarities with the corresponding Sim1 (Figure 75) and FM/ HMMM model systems without PIP2 (Chapter 3).

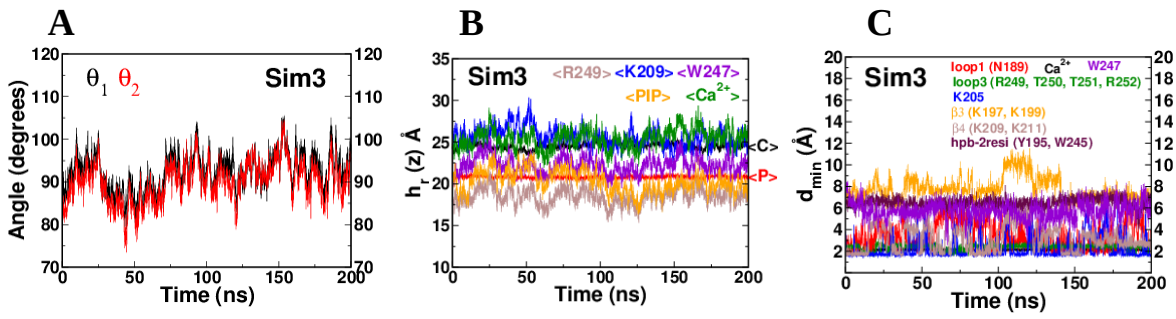

Figure 82: Convergence criteria for Sim3 system
From left to right: (A) Angles (θ_1, θ_2), (B) relative heights $h_r(z)$, and (C) minimum distance d_{min}.

The angles (θ_1, θ_2) (Figure 82A) were remained ~ 90° for the entire duration of 200 ns. This is fairly consistent with the PC + PS system where θ_1 (or θ_2) is ~ 90° (Figure 20). This further

reinforced that the addition of PIP2 into the membrane system and its binding to the LRC region of the C2 domain does not alter the angular orientation of the PKCα-C2 domain.

Moreover, the relative heights $h_r(z)$ (Figure 82B) even further reinforced that the residue R249 penetrates deepest within the membrane, K209 is consistently localized around the <C> plane, W247 penetrates below the <P> plane closer to the hydrophobic core, and Ca^{2+} ions are bound and localized on the membrane surface similar to Sim1 (Figure 75B) and FM/ HMMM model systems (chapter 3). Furthermore, Figure 83A and Figure 83B respectively show consistent number of contacts, N_c, for Ca^{2+} ions vs. oxygen atoms of PO_4^- and COO^- moieties and W247 vs. the acyl tail of the membrane reasserting the stability of the system on electrostatic as well as hydrophobic basis.

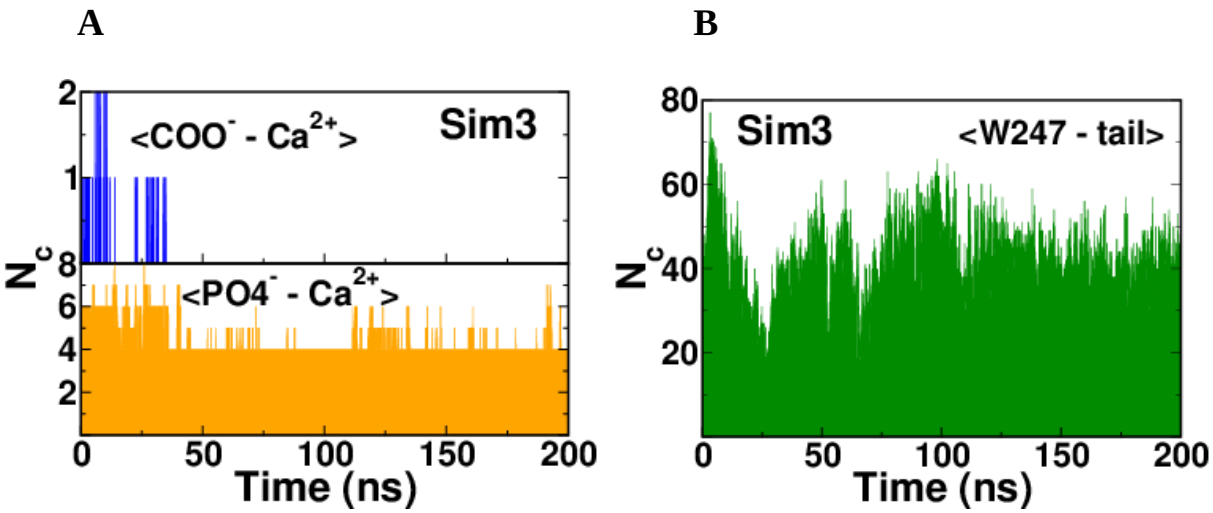

Figure 83: number of direct contacts, N_c, for Sim3 system
Number of direct contacts between Ca^{2+} ions with oxygen atoms of COO^- (A, top) and PO_4^- (A, bottom) and W247 with acyl tail (B).

The dynamical stability of Sim3 system and the binding of the PIP2 to the domain maintaining an open-faced configuration throughout simulation time of 200 ns is further revealed by Figure 84A,B,C.

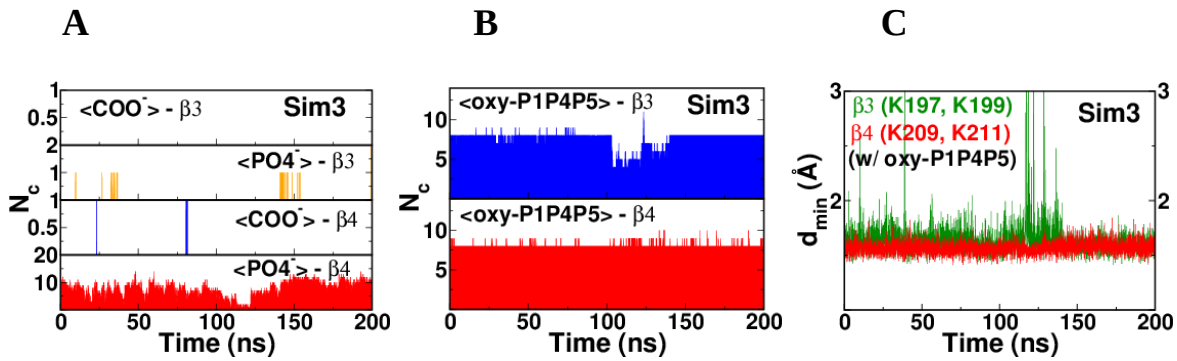

Figure 84: Role of LRC in Sim3 system
Number of direct contacts, N_c, between strands β3, β4 and (A) oxygen atoms of PO_4- or COO^- moieties from top leaflet of membrane (B) oxygen atoms of all three phosphate moieties of inositol ring. (C) The minimum distance, d_{min}, between strands β3, β4 and oxygen atoms of phosphate moieties.

In the presence of PIP2 in Sim3, the strand β4 has sustained and sufficient number of contacts with oxygen atoms of PO_4^- or COO^- moieties but β3 hardly has any contacts with them (Figure 84A) shows that strands β4 and β3 are in a vertical plane where β3 is above β4 as per open-faced configuration description. This is further revealed in the time series snapshots for Sim3 (Figure 85).

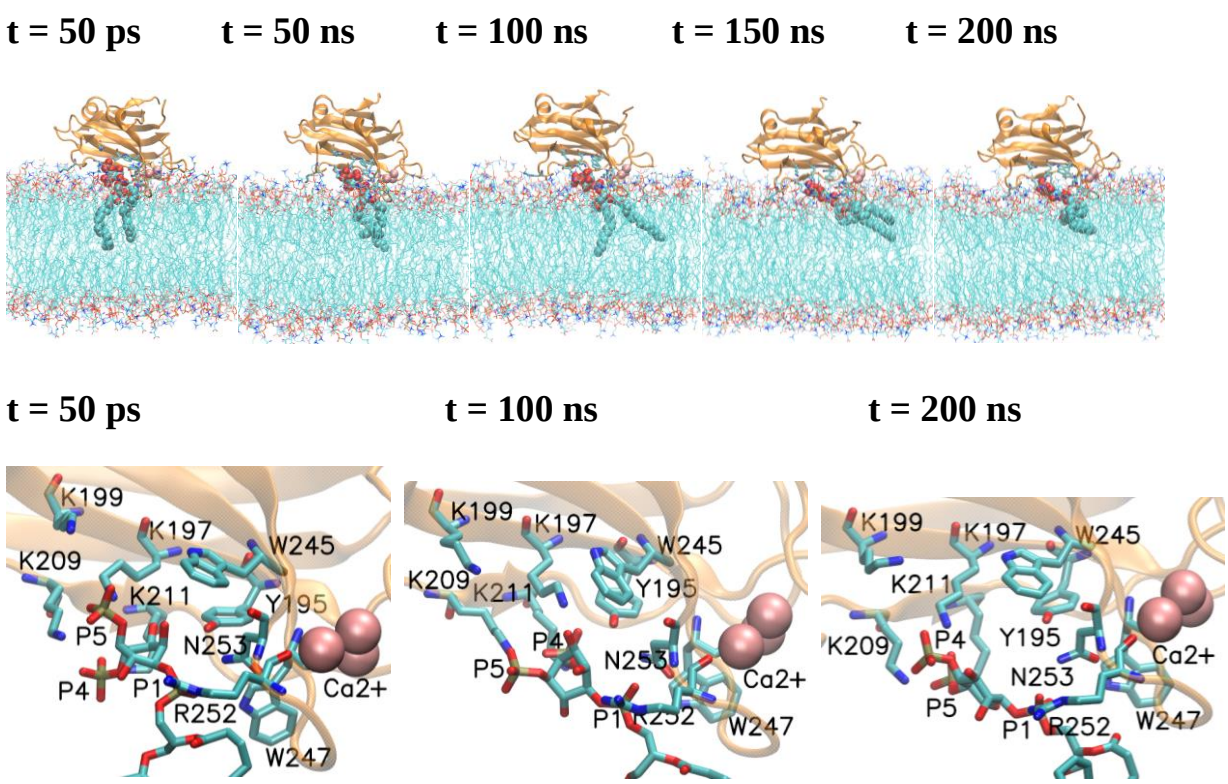

Figure 85: Time series of membrane bound configuration of PKCα-C2 in Sim3 Initial configuration at 50 ps (top far left) and final configuration at 200 ns (top far right). Bottom row shows a close-up of inositol ring interacting with the LRC region residues. Residues, as marked, are drawn in licorice representation. PIP2 is drawn in VDW (top) and licorice (bottom) representation. Coloring is by atom type where red is oxygen, blue is nitrogen, cyan is carbon and brown is phosphorous. Domain is shown as transparent in orange color. Ca^{2+} ions are also shown (pink).

The presence of PIP2 greatly enhanced the direct contacts between the membrane and the domain while maintaining an open-faced configuration is further evident where the oxygen atoms of phosphate moieties of PIP2 consistently maintained similar number of contacts with β3 and β4 (Figure 84B). Due to the rugged nature of the membrane - domain interface, the minimum distance between oxygen atoms of phosphate moieties of PIP2 and strand β3, β4 is basically identical ~ 2 Å (Figure 84C) rendering a strong binding with the domain though the strands β3 and β4 are in a

vertical plane where β3 is positioned above β4. Moreover, the inositol ring remained localized within the <P> atoms plane and <C> atoms plane (Figure 86).

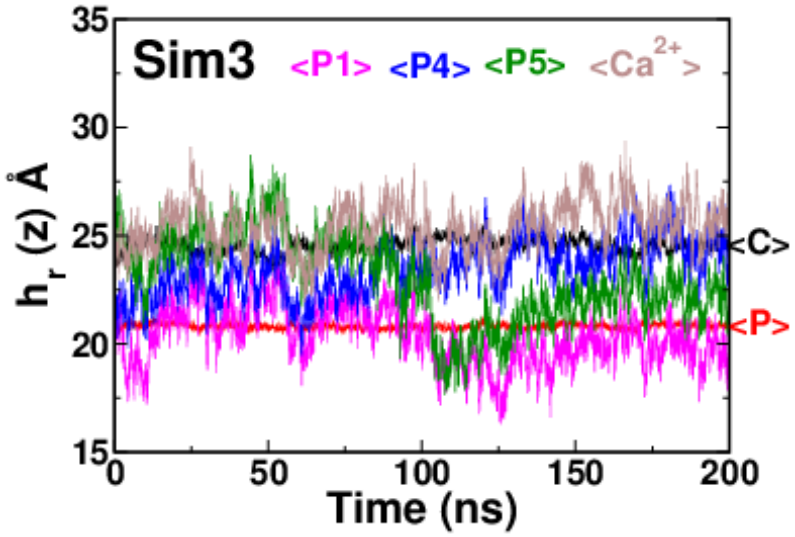

Figure 86: Relative heights for phosphorous atoms of PIP2 in Sim3
The relative heights $h_r(z)$ of phosphorous atom P1 (magenta), P4 (blue) and P5 (green) of inositol ring is shown with respect to the C-atom plane of COO^- moieties (<C> black) and P-atom plane of PO_4^- moieties (<P> red).

5.4 Conclusion

MD simulations employing a full molecular membrane model (FM) were used to determine the effect of PIP2 on the configuration of PKCα-C2 domain bound to a mixed PC + PS + PIP2 membrane. Our simulations show that the final state of PKCα-C2 domain binding to a lipid membrane with lipid area per molecule of ~ 61 $Å^2$ is an open-faced configuration. Introduction of the large headgroup PIP2 lipid reinforces the binding. All of the phosphate moieties ($P1O_4^-$, $P4O_4^-$ and $P5O_4^-$) interact and contribute to the membrane binding in a way that does not alter the membrane bound configuration. Within the MD protocol scheme it is very hard and computer time consuming to achieve a spontaneous binding of a domain in bulk water to an isolated lipid PIP2

embedded in the membrane. We performed test MD simulations, totaling more than 2000 ns, of several PC + PS + PIP2 systems and clues obtained thereafter have been incorporated in successive simulations, including Sim1, Sim2 and Sim3 model systems. The results presented in this chapter are from these three model systems. Through insightful initial positioning of the inositol ring, we achieved our results as presented in this chapter. Such that Sim1 showed that the PIP2 eventually get bound to the domain rendering it an open-faced configuration. Also, in spite of an initially favorable positioning of the inositol ring and orientation in Sim2 system, we do not observed the pushing or the pulling of the domain due to the presence of PIP2 as predicted in literature (29, 30, 32) and that the crystallographic structure representing the docked inositol ring to the PKCα-C2 domain (27) is not stable. Finally, the Sim3 system conclusively showed that an open-faced configuration is a stable and robust final state for the membrane bound PKCα-C2 domain in the presence of the PIP2. Moreover, our simulations of PIP2 bound PKCα-C2 domain configuration at the plasma membrane can provide physical insight regarding the role of DAG in the activation of the PKCα enzyme. Recently, Egea-Jimenez et al (103) has shown that for 5% molar concentration of the PIP2, the PKCα enzyme could be activated even in the absence of DAG, contrary to previous considerations that DAG is required to bind the C1 domain of PKCα to the membrane (74). Our simulations show that the presence of PIP2 increases the number of contacts of the C2 domain to the membrane, without substantially changing its orientation. This, presumably, increases the binding strength. Whether or not this increase in binding strength from the presence of PIP2 can substitute for DAG binding the C1 domain in the activation process is unknown, but would be an interesting avenue to pursue.

CITE LITERATURE

1. Wang, Y.-C., S. E. Peterson, and J. F. Loring. 2014. Protein post-translational modifications and regulation of pluripotency in human stem cells. Cell research 24:143-160.

2. Ubersax, J. A., and J. E. Ferrell Jr. 2007. Mechanisms of specificity in protein phosphorylation. Nat Rev Mol Cell Biol 8:530-541.

3. Cohen, P. 2001. The role of protein phosphorylation in human health and disease. . European Journal of Biochemistry 268:5001-5010.

4. Manning, G., G. D. Plowman, T. Hunter, and S. Sudarsanam. 2002. Evolution of protein kinase signaling from yeast to man. Trends in biochemical sciences 27:514-520.

5. Manning, G., D. B. Whyte, R. Martinez, T. Hunter, and S. Sudarsanam. 2002. The Protein Kinase Complement of the Human Genome. Science 298:1912-1934.

6. Pearce, L. R., D. Komander, and D. R. Alessi. 2010. The nuts and bolts of AGC protein kinases. Nat Rev Mol Cell Biol 11:9-22.

7. Velculescu, V. E. 2008. Defining the blueprint of the cancer genome. Carcinogenesis 29:1087-1091.

8. Endicott, J. A., M. E. M. Noble, and L. N. Johnson. 2012. The Structural Basis for Control of Eukaryotic Protein Kinases. Annual review of biochemistry 81:587-613.

9. Johnson, L. N., and R. J. Lewis. 2001. Structural Basis for Control by Phosphorylation. Chemical Reviews 101:2209-2242.

10. Cohen, P. 2000. The regulation of protein function by multisite phosphorylation–a 25 year update. Trends in biochemical sciences 25:596-601.

11. Pinna, L. A., and M. Ruzzene. 1996. How do protein kinases recognize their substrates? Biochimica et Biophysica Acta (BBA) - Molecular Cell Research 1314:191-225.

12. Martin, D. M. A., D. Miranda-Saavedra, and G. J. Barton. 2009. Kinomer v. 1.0: a database of systematically classified eukaryotic protein kinases. Nucleic acids research 37:D244-D250.

13. Eswaran, J., and S. Knapp. 2010. Insights into protein kinase regulation and inhibition by large scale structural comparison. Biochimica et Biophysica Acta (BBA) - Proteins and Proteomics 1804:429-432.

14. Hanks, S. K., and T. Hunter. 1995. Protein kinases 6. The eukaryotic protein kinase superfamily: kinase (catalytic) domain structure and classification. FASEB J 9:576-596.

15. Hanks, S. K., A. M. Quinn, and T. Hunter. 1988. The protein kinase family: conserved features and deduced phylogeny of the catalytic domains. Science 241:42-52.

16. Rosse, C., M. Linch, S. Kermorgant, A. J. M. Cameron, K. Boeckeler, and P. J. Parker. 2010. PKC and the control of localized signal dynamics. Nat Rev Mol Cell Biol 11:103-112.

17. Bossemeyer, D., R. A. Engh, V. Kinzel, H. Ponstingl, and R. Huber. 1993. Phosphotransferase and substrate binding mechanism of the cAMP-dependent protein kinase catalytic subunit from porcine heart as deduced from the 2.0 A structure of the complex with Mn2+ adenylyl imidodiphosphate and inhibitor peptide PKI (5-24). EMBO J. 12.

18. De Bondt, H. L., J. Rosenblatt, J. Jancarik, H. D. Jones, D. O. Morgant, and S.-H. Kim. 1993. Crystal structure of cyclin-dependent kinase 2. Nature 363:595-602.

19. Jeffrey, P. D., A. A. Russo, K. Polyak, E. Gibbs, J. Hurwitz, J. Massague, and N. P. Pavletich. 1995. Mechanism of CDK activation revealed by the structure of a cyclinA-CDK2 complex. Nature 376:313-320.

20. Knighton, D. R., S. M. Bell, J. Zheng, L. F. Ten Eyck, N. H. Xuong, S. S. Taylor, and J. M. Sowadski. 1993. 2.0 A refined crystal structure of the catalytic subunit of cAMP-dependent protein kinase complexed with a peptide inhibitor and detergent. Acta Crystallographica Section D: Biological Crystallography 49:357-361.

21. Knighton, D. R., J. Zheng, L. F. T. Eyck, V. A. Ashford, N.-H. Xuong, S. S. Taylor, and J. M. Sowadski. 1991. Crystal Structure of the Catalytic Subunit of Cyclic Adenosine Monophosphate-Dependent Protein Kinase. Science 253:407-414.

22. Lowe, E. D., M. E. M. Noble, V. T. Skamnaki, N. G. Oikonomakos, D. J. Owen, and L. N. Johnson. 1997. The crystal structure of a phosphorylase kinase peptide substrate complex: kinase substrate recognition. EMBO J. 16:6646-6658.

23. Verdaguer, N., S. Corbalan-Garcia, W. F. Ochoa, I. Fita, and J. C. Gómez-Fernández. 1999. Ca(2+) bridges the C2 membrane-binding domain of protein kinase Calpha directly to phosphatidylserine. EMBO J. 18:6329-6338.

24. Xu, W. H., S.C.; Eck, M. J. . 1997. Three-dimensional structure of the tyrosine kinase c-Src. Nature 385.

25. Zhang, F. S., A.; Robbins, D.; Cobb., M.H.; Goldsmith E. J. . 1994. Atomic Strucutre of the MAP kinase ERK2 at 2.3 A resolution. Nature 367:704-711.

26. Gomperts, B. D., I. M. Kramer, and P. E. R. Tatham. 2009. Chapter 9 - Phosphorylation and Dephosphorylation: Protein Kinases A and C. In Signal Transduction (Second Edition). B. D. Gomperts, I. M. Kramer, and P. E. R. Tatham, editors. Academic Press, San Diego. 243-272.

27. Guerrero-Valero, M., C. Ferrer-Orta, J. Querol-Audi, C. Marin-Vicente, I. Fita, J. C. Gomez-Fernandez, N. Verdaguer, and S. Corbalan-Garcia. 2009. Structural and mechanistic insights into the association of PKCalpha-C2 domain to PtdIns(4,5)P2. Proc. Natl. Acad. Sci. U. S. A. 106:6603-6607.

28. Malmberg, N. J., and J. J. Falke. 2005. USE OF EPR POWER SATURATION TO ANALYZE THE MEMBRANE-DOCKING GEOMETRIES OF PERIPHERAL PROTEINS: Applications to C2 Domains. Annual review of biophysics and biomolecular structure 34:71-90.

29. Landgraf, K. E., N. J. Malmberg, and J. J. Falke. 2008. Effect of PIP2 Binding on the Membrane Docking Geometry of PKCα C2 Domain: An EPR Site-Directed Spin-Labeling and Relaxation Study. Biochemistry 47:8301-8316.

30. Lai, C.-L., K. E. Landgraf, G. A. Voth, and J. J. Falke. 2010. Membrane Docking Geometry and Target Lipid Stoichiometry of Membrane-Bound PKCα C2 Domain: A Combined Molecular Dynamics and Experimental Study. Journal of Molecular Biology 402:301-310.

31. Chen, C.-H., S. Malkova, S. V. Pingali, F. Long, S. Garde, W. Cho, and M. L. Schlossman. 2009. Configuration of PKCα-C2 Domain Bound to Mixed SOPC/SOPS Lipid Monolayers. Biophysical Journal 97:2794-2802.

32. Ausili, A., S. Corbalán-García, J. C. Gómez-Fernández, and D. Marsh. 2011. Membrane docking of the C2 domain from protein kinase Cα as seen by polarized ATR-IR. The role of PIP2. Biochimica et Biophysica Acta (BBA) - Biomembranes 1808:684-695.

33. Karplus, M. 2002. Molecular Dynamics Simulations of Biomolecules. Accounts of Chemical Research 35:321-323.

34. Karplus, M., and J. Kuriyan. 2005. Molecular dynamics and protein function. Proc. Natl. Acad. Sci. U. S. A. 102:6679-6685.

35. Karplus, M., and G. A. Petsko. 1990. Molecular dynamics simulations in biology. Nature 347:631-639.

36. Frenkel, D., and B. Smit. 2001. Understanding Molecular Simulation : From Algorithms to Applications. Academic Press, Amsterdam, NLD.

37. Swope, W. C. 1982. A computer simulation method for the calculation of equilibrium constants for the formation of physical clusters of molecules: Application to small water clusters. The Journal of Chemical Physics 76.

38. Chandler, D. 1987. Introduction To Modern Statistical Mechanics. Oxford University Press.

39. Phillips, J. C., R. Braun, W. Wang, J. Gumbart, E. Tajkhorshid, E. Villa, C. Chipot, R. D. Skeel, L. Kalé, and K. Schulten. 2005. Scalable molecular dynamics with NAMD. Journal of Computational Chemistry 26:1781-1802.

40. Izaguirre, J. s. A., D. P. Catarello, J. M. Wozniak, and R. D. Skeel. 2001. Langevin stabilization of molecular dynamics. The Journal of Chemical Physics 114.

41. Feller, S. E., Y. Zhang, R. W. Pastor, and B. R. Brooks. 1995. Constant pressure molecular dynamics simulation: the Langevin piston method. The Journal of Chemical Physics 103:4613-4621.

42. Martyna, G. J., D. J. Tobias, and M. L. Klein. 1994. Constant pressure molecular dynamics algorithms. The Journal of Chemical Physics 101:4177-4189.

43. Miyamoto, S., and P. A. Kollman. 1992. SETTLE: an analytical version of the SHAKE and RATTLE algorithm for rigid water models. Journal of computational chemistry 13:952-962.

44. Ryckaert, J.-P., G. Ciccotti, and H. J. C. Berendsen. 1977. Numerical integration of the cartesian equations of motion of a system with constraints: molecular dynamics of< i> n</i>-alkanes. Journal of Computational Physics 23:327-341.

45. Darden, T., D. York, and L. Pedersen. 1993. Particle mesh Ewald: An N· log (N) method for Ewald sums in large systems. The Journal of chemical physics 98.

46. Becker, O. M. 2001. Computational biochemistry and biophysics. M. Dekker, New York.

47. Klauda, J. B., R. M. Venable, J. A. Freites, J. W. O'Connor, D. J. Tobias, C. Mondragon-Ramirez, I. Vorobyov, A. D. MacKerell, and R. W. Pastor. 2010. Update of the CHARMM All-Atom Additive Force Field for Lipids: Validation on Six Lipid Types. The Journal of Physical Chemistry B 114:7830-7843.

48. MacKerell, A. D., D. Bashford, M. Bellott, R. L. Dunbrack, J. D. Evanseck, M. J. Field, S. Fischer, J. Gao, H. Guo, and S. a. Ha. 1998. All-atom empirical potential for molecular modeling and dynamics studies of proteins. The Journal of Physical Chemistry B 102:3586-3616.

49. Vanommeslaeghe, K., E. Hatcher, C. Acharya, S. Kundu, S. Zhong, J. Shim, E. Darian, O. Guvench, P. Lopes, I. Vorobyov, and A. D. Mackerell. 2009. CHARMM general force field: A force field for drug-like molecules compatible with the CHARMM all-atom additive biological force fields. Journal of Computational Chemistry:NA-NA.

50. Humphrey, W., A. Dalke, and K. Schulten. 1996. VMD: visual molecular dynamics. Journal of molecular graphics 14:33-38.

51. Berendsen, H. J. C., D. van der Spoel, and R. van Drunen. 1995. GROMACS: A message-passing parallel molecular dynamics implementation. Computer Physics Communications 91:43-56.

52. Cooper, G. M. H., Robert E.,. 2013. The cell : A Molecular Approach.

53. Ly, H. V., and M. L. Longo. 2004. The Influence of Short-Chain Alcohols on Interfacial Tension, Mechanical Properties, Area/Molecule, and Permeability of Fluid Lipid Bilayers. Biophysical Journal 87:1013-1033.

54. Koenig, B. W., H. H. Strey, and K. Gawrisch. 1997. Membrane lateral compressibility determined by NMR and x-ray diffraction: effect of acyl chain polyunsaturation. Biophysical journal 73:1954-1966.

55. Israelachvili, J. N., S. Marčelja, and R. G. Horn. 1980. Physical principles of membrane organization. Quarterly reviews of biophysics 13:121-200.

56. Rawicz, W., K. C. Olbrich, T. McIntosh, D. Needham, and E. Evans. 2000. Effect of chain length and unsaturation on elasticity of lipid bilayers. Biophysical Journal 79:328-339.

57. Vilchèze, C., T. P. W. McMullen, R. N. McElhaney, and R. Bittman. 1996. The effect of side-chain analogues of cholesterol on the thermotropic phase behavior of 1-stearoyl-2-oleoylphosphatidylcholine bilayers: a differential scanning calorimetric study. Biochimica et Biophysica Acta (BBA) - Biomembranes 1279:235-242.

58. Brzustowicz, M. R., and A. T. Brunger. 2005. X-ray scattering from unilamellar lipid vesicles. Journal of Applied Crystallography 38:126-131.

59. Petrache, H. I., S. Tristram-Nagle, K. Gawrisch, D. Harries, V. A. Parsegian, and J. F. Nagle. 2004. Structure and fluctuations of charged phosphatidylserine bilayers in the absence of salt. Biophysical journal 86:1574-1586.

60. Mattai, J., H. Hauser, R. A. Demel, and G. G. Shipley. 1989. Interactions of metal ions with phosphatidylserine bilayer membranes: effect of hydrocarbon chain unsaturation. Biochemistry 28:2322-2330.

61. MacKerell, A. D., D. Bashford, Bellott, R. L. Dunbrack, J. D. Evanseck, M. J. Field, S. Fischer, J. Gao, H. Guo, S. Ha, D. Joseph-McCarthy, L. Kuchnir, K. Kuczera, F. T. K. Lau, C. Mattos, S. Michnick, T. Ngo, D. T. Nguyen, B. Prodhom, W. E. Reiher, B. Roux, M. Schlenkrich, J. C. Smith, R. Stote, J. Straub, M. Watanabe, J. Wiórkiewicz-Kuczera, D. Yin, and M. Karplus. 1998. All-Atom Empirical Potential for Molecular Modeling and Dynamics Studies of Proteins. The Journal of Physical Chemistry B 102:3586-3616.

62. Yeagle, P. 2011. Structure of Biological Membranes (3rd Edition). CRC Press, London, GBR.

63. Ohkubo, Y. Z., Taras V. Pogorelov, Mark J. Arcario, Geoff A. Christensen, and E. Tajkhorshid. 2012. Accelerating Membrane Insertion of Peripheral Proteins with a Novel Membrane Mimetic Model. Biophysical Journal 102:2130-2139.

64. Cheek, S., H. Zhang, and N. V. Grishin. 2002. Sequence and Structure Classification of Kinases. Journal of Molecular Biology 320:855-881.

65. Hunter, T., Sefton, Bartholomew M., eds. . 1991. Protein Phosphorylation. Part B, Analysis Of Protein Phosphorylation, Protein Kinase Inhibitors, And Protein Phosphatases. San Diego : Academic Press, 1991.

66. Cheng, H.-C., R. Z. Qi, H. Paudel, and H.-J. Zhu. 2011. Regulation and Function of Protein Kinases and Phosphatases. Enzyme Research 2011:1-3.

67. Johnson, L. N. 2009. The regulation of protein phosphorylation. Biochemical Society transactions 37:627-641.

68. Salazar, C., and T. Höfer. 2009. Multisite protein phosphorylation--from molecular mechanisms to kinetic models. FEBS J. 276:3177-3198.

69. Woodgett, J. R., eds. . 2000. Protein Kinase Functions. . Oxford University Press, 2000.

70. Steinberg, S. F. 2008. Structural Basis of Protein Kinase C Isoform Function. Physiological Reviews 88:1341-1378.

71. Farah, C. A., and W. S. Sossin. 2012. The role of C2 domains in PKC signaling. Advances in experimental medicine and biology 740:663-683.

72. Webb, B. L. J., S. J. Hirst, and M. A. Giembycz. 2000. Protein kinase C isoenzymes: a review of their structure, regulation and role in regulating airways smooth muscle tone and mitogenesis. Br J Pharmacol 130:1433-1452.

73. House, C., and B. E. Kemp. 1987. Protein Kinase C Contains a Pseudosubstrate Prototope in its Regulatory Domain. Science 238:1726-1728.

74. Corbalán-García, S., and J. C. Gómez-Fernández. 2013. Classical protein kinases C are regulated by concerted interaction with lipids: the importance of phosphatidylinositol-4,5-bisphosphate. Biophysical Reviews 6:3-14.

75. Ochoa, W. F., S. Corbalán-Garcia, R. Eritja, J. A. Rodríguez-Alfaro, J. C. Gómez-Fernández, I. Fita, and N. Verdaguer. 2002. Additional binding sites for anionic phospholipids and calcium ions in the crystal structures of complexes of the C2 domain of protein kinase calpha. Journal of Molecular Biology 320:277-291.

76. Newton, A. C. 2009. Protein kinase C: poised to signal. AJP: Endocrinology and Metabolism 298:E395-E402.

77. Bolsover, S. R. 2003. Role of the Ca2+/Phosphatidylserine Binding Region of the C2 Domain in the Translocation of Protein Kinase Calpha to the Plasma Membrane. Journal of Biological Chemistry 278:10282-10290.

78. Cho, W., and R. V. Stahelin. 2006. Membrane binding and subcellular targeting of C2 domains. Biochimica et Biophysica Acta (BBA) - Molecular and Cell Biology of Lipids 1761:838-849.

79. Conesa-Zamora, P., M. J. Lopez-Andreo, J. C. Gómez-Fernández, and S. Corbalán-García. 2001. Identification of the Phosphatidylserine Binding Site in the C2 Domain that Is Important for PKCα Activation and in Vivo Cell Localization. Biochemistry 40:13898-13905.

80. Medkova, M., and W. Cho. 1999. Interplay of C1 and C2 domains of protein kinase C-α in its membrane binding and activation. Journal of Biological Chemistry 274:19852-19861.

81. Stahelin, R. V., J. D. Rafter, S. Das, and W. Cho. 2003. The Molecular Basis of Differential Subcellular Localization of C2 Domains of Protein Kinase C-α and Group IVa Cytosolic Phospholipase A2. Journal of Biological Chemistry 278:12452-12460.

82. Corbalán-García, S., J. García-García, J. A. Rodríguez-Alfaro, and J. C. Gómez-Fernández. 2003. A New Phosphatidylinositol 4,5-Bisphosphate-binding Site Located in the C2 Domain of Protein Kinase Cα. Journal of Biological Chemistry 278:4972-4980.

83. Evans, J. H., D. Murray, C. C. Leslie, and J. J. Falke. 2006. Specific translocation of protein kinase Cα to the plasma membrane requires both Ca2+ and PIP2 recognition by its C2 domain. Mol. Biol. Cell 17:56-66.

84. Guerrero-Valero, M., C. Marín-Vicente, J. C. Gómez-Fernández, and S. Corbalán-García. 2007. The C2 Domains of Classical PKCs are Specific PtdIns(4,5)P2-sensing Domains with Different Affinities for Membrane Binding. Journal of Molecular Biology 371:608-621.

85. Marín-Vicente, C., F. E. Nicolás, J. C. Gómez-Fernández, and S. Corbalán-García. 2008. The PtdIns(4,5)P2 Ligand Itself Influences the Localization of PKCα in the Plasma Membrane of Intact Living Cells. Journal of Molecular Biology 377:1038-1052.

86. Sánchez-Bautista, S., C. Marín-Vicente, J. C. Gómez-Fernández, and S. Corbalán-García. 2006. The C2 Domain of PKCα Is a Ca2+-dependent PtdIns(4,5)P2 Sensing Domain: A New Insight into an Old Pathway. Journal of Molecular Biology 362:901-914.

87. Lipp, P., and G. Reither. 2011. Protein Kinase C: The "Masters" of Calcium and Lipid. Cold Spring Harb Perspect Biol 3:a004556-a004556.

88. Stensman, H., and C. Larsson. 2007. Identification of acidic amino acid residues in the protein kinase C alpha V5 domain that contribute to its insensitivity to diacylglycerol. J Biol Chem 282:28627-28638.

89. Corbalan-Garcia, S., and J. C. Gomez-Fernandez. 2010. The C2 domains of classical and novel PKCs as versatile decoders of membrane signals. Biofactors 36:1-7.

90. Conesa-Zamora, P., J. C. Gómez-Fernández, and S. Corbalán-García. 2000. The C2 domain of protein kinase Cα is directly involved in the diacylglycerol-dependent binding of the C1 domain to the membrane. Biochimica et Biophysica Acta (BBA) - Molecular and Cell Biology of Lipids 1487:246-254.

91. Kohout, S. C., S. Corbalán-García, J. C. Gómez-Fernández, and J. J. Falke. 2003. C2 Domain of Protein Kinase Cα: Elucidation of the Membrane Docking Surface by Site-Directed Fluorescence and Spin Labeling†. Biochemistry 42:1254-1265.

92. Kohout, S. C., S. Corbalán-García, A. Torrecillas, J. C. Goméz-Fernandéz, and J. J. Falke. 2002. C2 Domains of Protein Kinase C Isoforms α, β, and γ: Activation Parameters and Calcium Stoichiometries of the Membrane-Bound State†. Biochemistry 41:11411-11424.

93. Manna, D., N. Bhardwaj, M. S. Vora, R. V. Stahelin, H. Lu, and W. Cho. 2008. Differential roles of phosphatidylserine, PtdIns(4,5)P2, and PtdIns(3,4,5)P3 in plasma membrane targeting of C2 domains. Molecular dynamics simulation, membrane binding, and cell translocation studies of the PKCalpha C2 domain. J. Biol. Chem. 283:26047-26058.

94. Marín-Vicente, C., J. C. Gómez-Fernández, and S. Corbalán-García. 2005. The ATP-dependent membrane localization of protein kinase Cα is regulated by Ca2+ influx and phosphatidylinositol 4, 5-bisphosphate in differentiated PC12 cells. Mol. Biol. Cell 16:2848-2861.

95. Medkova, M., and W. Cho. 1998. Mutagenesis of the C2 Domain of Protein Kinase C-α DIFFERENTIAL ROLES OF Ca2+ LIGANDS AND MEMBRANE BINDING RESIDUES. Journal of Biological Chemistry 273:17544-17552.

96. Pérez-Lara, Á., A. L. Egea-Jiménez, A. Ausili, S. Corbalán-García, and J. C. Gómez-Fernández. 2012. The membrane binding kinetics of full-length PKCα is determined by membrane lipid composition. Biochimica et Biophysica Acta (BBA) - Molecular and Cell Biology of Lipids 1821:1434-1442.

97. Rodríguez-Alfaro, J. A., J. C. Gomez-Fernandez, and S. Corbalan-Garcia. 2004. Role of the Lysine-rich Cluster of the C2 Domain in the Phosphatidylserine-dependent Activation of PKCα. Journal of Molecular Biology 335:1117-1129.

98. Torrecillas, A., J. Laynez, M. Menéndez, S. Corbalán-García, and J. C. Gómez-Fernández. 2004. Calorimetric Study of the Interaction of the C2 Domains of Classical Protein Kinase C Isoenzymes with Ca2+ and Phospholipids. Biochemistry 43:11727-11739.

99. Scott, A. M., C. E. Antal, and A. C. Newton. 2013. Electrostatic and Hydrophobic Interactions Differentially Tune Membrane Binding Kinetics of the C2 Domain of Protein Kinase C. Journal of Biological Chemistry 288:16905-16915.

100. Murray, D., and B. Honig. 2002. Electrostatic control of the membrane targeting of C2 domains. Molecular cell 9:145-154.

101. Nalefski, E. A., and A. C. Newton. 2001. Membrane Binding Kinetics of Protein Kinase C βII Mediated by the C2 Domain. Biochemistry 40:13216-13229.

102. Nalefski, E. A., M. M. Slazas, and J. J. Falke. 1997. Ca2+-signaling cycle of a membrane-docking C2 domain. Biochemistry 36:12011-12018.

103. Egea-Jimenez, A. L., A. Perez-Lara, S. Corbalan-Garcia, and J. C. Gomez-Fernandez. 2013. Phosphatidylinositol 4,5-bisphosphate decreases the concentration of Ca2+, phosphatidylserine and diacylglycerol required for protein kinase C alpha to reach maximum activity. PLoS One 8:e69041.

104. Corbin, J. A., J. H. Evans, K. E. Landgraf, and J. J. Falke. 2007. Mechanism of Specific Membrane Targeting by C2 Domains: Localized Pools of Target Lipids Enhance Ca2+ Affinity†. Biochemistry 46:4322-4336.

105. Baylon, J. L., I. L. Lenov, S. G. Sligar, and E. Tajkhorshid. 2013. Characterizing the Membrane-Bound State of Cytochrome P450 3A4: Structure, Depth of Insertion, and Orientation. Journal of the American Chemical Society 135:8542-8551.

106. Mackerell, A. D., M. Feig, and C. L. Brooks. 2004. Extending the treatment of backbone energetics in protein force fields: Limitations of gas-phase quantum mechanics in reproducing protein conformational distributions in molecular dynamics simulations. Journal of Computational Chemistry 25:1400-1415.

107. Malkova, S., F. Long, R. V. Stahelin, S. V. Pingali, D. Murray, W. Cho, and M. L. Schlossman. 2005. X-ray reflectivity studies of cPLA2{alpha}-C2 domains adsorbed onto Langmuir monolayers of SOPC. Biophys J 89:1861-1873.

108. Málková, Š., R. V. Stahelin, S. V. Pingali, W. Cho, and M. L. Schlossman. 2006. Orientation and Penetration Depth of Monolayer-Bound p40phox-PX. Biochemistry 45:13566-13575.

109. Honigmann, A., G. van den Bogaart, E. Iraheta, H. J. Risselada, D. Milovanovic, V. Mueller, S. Mullar, U. Diederichsen, D. Fasshauer, H. Grubmuller, S. W. Hell, C. Eggeling, K. Kuhnel, and R. Jahn. 2013. Phosphatidylinositol 4,5-bisphosphate clusters act as molecular beacons for vesicle recruitment. Nature structural & molecular biology 20:679-686.

110. Ziemba, B. P., J. Li, K. E. Landgraf, J. D. Knight, G. A. Voth, and J. J. Falke. 2014. Single-molecule studies reveal a hidden key step in the activation mechanism of membrane-bound protein kinase C-alpha. Biochemistry 53:1697-1713.

111. Corbalán-García, S., M. Guerrero-Valero, C. Marín-Vicente, and J. C. Gómez-Fernández. 2007. The C2 domains of classical/conventional PKCs are specific PtdIns(4,5)P2-sensing domains. Biochemical Society Transactions 35.

112. Corbalán-García, S., and J. C. Gómez-Fernández. 2010. The C2 domains of classical and novel PKCs as versatile decoders of membrane signals. Biofactors 36:1-7.

113. Farah, C. A., and W. S. Sossin. 2012. The Role of C2 Domains in PKC Signaling. In Calcium Signaling. M. S. Islam, editor. Springer Netherlands. 663-683.

114. Nalefski, E. A., M. M. Slazas, and J. J. Falke. 1997. Ca2+-Signaling Cycle of a Membrane-Docking C2 Domain†. Biochemistry 36:12011-12018.

115. Lupyan, D., M. Mezei, D. E. Logothetis, and R. Osman. 2010. A molecular dynamics investigation of lipid bilayer perturbation by PIP2. Biophys J 98:240-247.

VITA

NAME: Lalit Dubey

EDUCATION: M.S., 2008, Physics, University of Illinois at Chicago, Chicago IL
Ph.D., 2014, Physics, University of Illinois at Chicago, Chicago IL

EXPERIENCE: Research and teaching assistant, Department of Physics, department of bioengineering and department of medicinal chemistry UIC (08/2002-onwards)

HONORS: Board of Trustee, UIC, Tuition waiver, 2013-14.

PUBLICATIONS: *A molecular dynamics study: Membrane bound configuration of PKCα-C2 domain to a mixed PC:PS lipid bilayer*
Lalit Dubey, Y. Zenmei Ohkubo, Emad Tajkhorshid, Mark L. Schlossman *(manuscript in preparation)*

Role of phosphatidylinositol 4,5-biphosphate in membrane bound configuration of PKCa-C2 domain: A molecular dynamics study
Lalit Dubey, Y. Zenmei Ohkubo, Emad Tajkhorshid, Mark L. Schlossman *(manuscript in preparation)*

The influence of lipid density on Membrane bound configuration of PKCα-C2 domain: A molecular dynamics study
Lalit Dubey, Mark L. Schlossman *(manuscript in preparation)*

Orientation and penetration of KIF16B-PX domain as driven by Phosphatidylinositol 3-phosphate *at mixed SOPC/SOPS lipid bilayer: A molecular dynamics study*
Lalit Dubey, Mark L. Schlossman *(data analysis in progress)*

Monte Carlo Simulation Study of Spin Transport in Multilayer Graphene with Bernal Stacking
Soumya Mishra, Bahniman Ghosh, Vikas Nandal, and Lalit Dubey
Journal of Applied Physics 112, no. 2 (2012)

Mechanical signaling on the single protein level studied using steered molecular dynamics
Georgi Z Genchev, Morten Källberg, Gamze Gürsoy, Anuradha Mittal, Lalit Dubey, Ognjen Perisic, et al.
Cell Biochemistry and Biophysics (2009)